Fundamental aspects of intumescent systems for fire protection of steel structures

Nittaya Hansupo

N °:

PhD Thesis

FUNDAMENTAL ASPECTS OF INTUMESCENT SYSTEMS FOR FIRE PROTECTION OF STEEL STRUCTURES

PhD defended at

UNIVERSITE LILLE 1 SCIENCES ET TECHNOLOGIES

Ecole doctorale Sciences de la Matière, du Rayonnement et de l'Environnement, UFR de chimie

To obtain the grade of

DOCTEUR

Specialty: Materials Chemistry (Chimie des Matériaux)

By

Nittaya HANSUPO

Graduated engineer of Ecole Nationale Supérieure de Chimie de Clermont-Ferrand

Master of research in materials for energy from Blaise Pascal University

PhD thesis supervised by

Prof. Serge BOURBIGOT and Dr. Fabienne SAMYN

The defense was held on February 22, 2018 in front of the following dissertation committee:

Prof. Jenny ALONGI	University of Milan	Referee
Prof. Abdelghani LAACHACHI	Luxembourg Institute of Science and Technology	Referee
Mr. Pere CATALA	Hempel	Examiner
Dr. Véronique GEORGES	Centre Scientifique et Technique du Bâtiment	Examiner
Prof. Sophie DUQUESNE	ENSCL	Examiner
Prof. Maude JIMENEZ	Université Lille I	Examiner
Prof. Serge BOURBIGOT	ENSCL	Thesis director
Dr. Fabienne SAMYN	ENSCL	Co-supervisor

For Hansupo family

Positive thoughts will bring positive experiences to your life…'Law of attraction'
Rhonda Byrne

Preface

This dissertation is the results of the three years PhD program at University of Lille I Sciences and Technologies, France. It is the collaborative project between the Unité Matériaux et Transformations (UMET) laboratory (a part of University of Lille I Sciences and Technologies) and the research center of Hempel Company (Barcelona, Spain) who provided the financial support for the project. The work deals with the study of the fundamental aspects of intumescent systems for fire protection of steel structures. The goal of this work is to get insights into the mechanism of action of intumescent coating formulations to be able to develop novel systems of higher efficiency.

Acknowledgement

First, I would like to thank Prof. Alexandre Legris, director of the UMET laboratory, and Prof. Serge Bourbigot, director of the group Ingénierie des Systèmes Polymères (ISP) and Reaction and Resistance to Fire (R2F) team for giving me the opportunity to join the laboratory and work on this project.

Gratefully, I would like to express my deepest appreciation to Prof. Serge Bourbigot, Dr. Fabienne Samyn, Prof. Sophie Duquesne and Prof. Maude Jimenez, who gave me the chance to work with them and achieve this PhD work in the R2Fire team. Thanks a lot for their advice, encouragement and support. I really appreciate what I learnt and acquired throughout these three years.

I would like to thank Prof. Jenny Alongi, Prof. Abdelghani Laachachi, Mr. Pere Catala and Dr. Véronique Georges who accepted to be the jury, for bringing their expertise and time to assess this thesis research.

I would like to acknowledge my industrial partner, 'Hempel company, Spain' for the work we achieved together and for the technical and material support throughout the project. In particular, I would like to thank Michael Hollman, Pere Catala and Joseph Palasi who started and set-up the project and placed the trust in me to lead the project; especially Michael for his kindness, help and co-operation. Then, I thank Hector Farras and Jose Fernandes for giving me a basic training about the intumescent coatings, preparation methods, analysis methods, fire tests… at the beginning of the project. That gave me an excellent experience and provided me a necessary background to conduct this project. I also appreciate the valuable discussions and suggestions that we made together during the regular meetings. Thanks also to all members of passive fire protection team for their kindness and welcoming ambience during my training in Hempel research laboratory. Oh Yep, I learnt some Spanish cultures and words... It was awesome!

I would like to thank all of the technical experts for the training and instructions on how to use specific equipment. First, the NMR team, Grégory Tricot, Bertrand Revel and Bertrand Doumert for their help in designing experiments and discussing the results. I really appreciate

their superb expertise in NMR, availability and kindness. Thanks as well to Laurence Burylo and Pascal Roussel for the work in XRD analysis and Séverine Bellayer for the work in microscopic techniques. Moreover, I thank JoJo and Ben D. for their kindness, availability and technical support to everyday problems. Thanks especially to the big men of the lab, 'Anil' and 'Pierre' for the help, genuine suggestions and kindness from the beginning until the end.

I also sincerely thank all current and former members of the R2F team for all the moments we shared. First, thanks to all the lab's permanent members: Gaëlle, Mathilde, Séverine, Michel, Charafeddine and Fouad for a hospitality and welcoming ambience during these three years. Big thanks to 'une grande femme' of the lab 'Brigitte' for all supports and facilities. Thanks to Agnès for her kindness, friendship and all the moments (in or outside the lab) that we shared together, Ben (Mr. Toutounet) and Nicoloo for sharing 'des conneries' and teaching me the French jargons, Berthy (petit berbère) for being my universal translator, Laurie and Sarah for sharing their fascinating lifestyle. Thanks also to Chi, Hirakooo, Tatendoo, Rololo and Aditya for a friendship and their gentleness (maybe :p), Maryem for funny talks and amity, Katja (craziest labmate ☺) for crazy and joyous moments we made, Audrey and Gizem for joyful coffee times, candies and support during the hardest moment of this thesis. Thanks also to Renault, Mathieu, Pauline, Jonathan (Peruvian jojo), Sawsen, Elodie, Sophie K., Sayed, Charlotte, Morgan, Oscarlosss, Xiadonggg, Regis, Martin, Laura, Anne-lise, Imane and Kaiyuan for the easy-going atmosphere, friendship and many memorial events we shared. I deeply appreciate and enjoy working with them. I would like also to thank my internship students Natalia, Camille and Laura.

Finally and most importantly, I express my greatest gratitude to my lovely family, especially my dad, mom and lovely sister. I thank them so much for their support and love. I could not have reached this milestone without them. Thanks to my best friends (Vassana, Zozo, Yupin, Ying, Katja, Ting, Por, May, Jumpoon, Giftzy) for their never-ending support and encouragement during the bad and good moments during these three years. Last but not least, I really thank all of youcopainspotescolleaguesfriends for being a part of my wonderful memories in this charming city 'Lille'.

Table of contents

Abbreviations

APP	Ammonium Polyphosphate
APB	Ammonium Pentaborate
ATH	Aluminum trihydroxide
BA	Boric acid
CMR	Carcinogenic, Mutagenic, Reprotoxic
DGEBA	Diglycidyl Ether of Bisphenol A
DSC	Differential Scanning Calorimetry
EBA	Ethylene-acrylate copolymer
EMMA	Ethylene-co-methacrylic acid
EPMA	Electron Probe Micro analyzer
FR	Flame Retardant
FTIR	Fourier Transform Infrared Spectroscopy
HMC	Hydrocarbon Modified Curve
HRR	Heat Release Rate
HT	Heat Treatment
HTT	Heat Treatment Temperature
kW	kilowatt
MAS	Magic Angle Spinning
mm	Millimeter
NMR	Nuclear Magnetic Resonance
PER	Pentaerythritol
PFP	Passive Fire Protection
PVC	Polyvinyl Chloride
REACH	European Union regulation concerning the Registration, Evaluation, Authorization and Restriction of Chemical
rpm	Revolutions Per Minute
RWS	Rijkst Water Staat curve

SDS	Safety Data Sheet
SEM	Scanning Electron Microscopy
SEM-EDX	Scanning Electron Microscope associated with Energy Dispersive X-ray Spectrometer
TCPP	Tris (2-chloroisopropyl) phosphate
TEM	Transmission Electron Microscope
TGA	Thermogravimetric Analysis
TPS	Transient Plane Source
TSR	Thermal Scanning Rheometer
THEIC	Tris (hydroxyethyl) isocyanurate
Wt.	Weight
XPS	X-ray Photoelectron Spectroscopy
XRD	X-ray diffraction
ZB	Zinc borate
ZHS	Zinc hydroxystannate
ZS	Zinc stannate

General introduction

Steel is a material used worldwide in the construction of bridges, sport arenas, buildings, offshore platforms etc. It is today the most appreciated building material all over the world because of its numerous benefits. The advantages of using steel structures are both economic (speed of construction, low project costs and ready availability) and ecologic (green construction and recycled materials) approaches. Moreover, it allows a maximum flexibility in design and better load bearing strength.

Steel is a non-combustible material. It does not contribute to a fire but its strength and stiffness are detrimentally reduced when the temperature surpasses 500 ^{o}C [1]. The structural steel should thus be protected to maintain its integrity and to extend the evacuation time in the case of an unexpected fire. Moreover, fire safety of steel structure, especially for building regulations, is a prime requirement in many countries. An example of big disaster related to steel loss of strength is the catastrophic collapse of the World Trade Centre Twin Towers in New York City, 2001 (Figure 1).

Figure 1 World Trade Center collapse, 11 September 2001 [2]

Since this incident occurred, the concern about the protection of lives and assets against fire has been more and more highlighted. Two types of fire protection exist: active and passive fire protections [3]. The active fire protections (e.g. sprinklers, alarms or gas release systems) are immediately activated in a fire. Passive fire protection systems exist in both non-reactive (e.g.

board encasement, concrete, gypsum, mineral fiber and cementitious spray) and reactive (i.e. intumescent coating) forms [4, 5]. The drawback of using active fire protective systems is linked to the fact that they need time to respond (a very short delay will lead to a huge damage). Passive fire protections and in particular non-reactive systems are built as a part of the whole structures. No requirement of operation by people or automatic controls is needed, it can be thus considered as a protector of choice with instant response to a fire. Nevertheless, non-reactive passive fire protections show some limitations. They are heavy, limited in design, hard to apply and needed plenty of space. From this point of view, reactive passive fire protection such as intumescent coatings appears as a solution of choice for fire protection since it does not only provide the efficient fire protection but can also be used as a conventional coating without affecting the aesthetic of the structural framework. Upon exposure to a fire, these intumescent coatings swell to form a multi-cellular insulative barrier which limits mass and heat transfers between the underlying materials and the flame.

Intumescent coatings are highly complex systems. The complete formulation usually contains more than ten ingredients to reach all required specifications [6, 7]. In particular, they usually contain three major active ingredients dispersed in a binder: a carbon source (e.g. pentaerylthritol, isocyanurate or a binder itself), a blowing agent (e.g. evolving ammonia from phosphate and/or borate salts, melamine) and an acid source (e.g. borate and/or phosphate) [8]. These additives have to be chosen carefully. Indeed, the formation of an intumescent fire barrier is a dynamic process; additives should thus degrade and react at the right time and right temperature to provide an appropriate char structure.

Few recent scientific papers are devoted to the fundamental studies of intumescent coatings, but the full understanding of the mode of action of some ingredients is still lacking. In this context, this PhD thesis deals with the fundamental study of the mechanism of action of epoxy based intumescent coatings containing as main ingredients ammonium polyphosphate (APP), borates, calcium carbonate ($CaCO_3$), silicate fibers and titanium dioxide (TiO_2).

Relating to the literature, it is recognized that epoxy based intumescent coatings containing borates such as boric acid or zinc borate are highly efficient fire protective systems,

especially for hydrocarbon fire. However, REACH (European Union regulation concerning the Registration, Evaluation, Authorization and Restriction of Chemical) has reported that some borates, especially boric acid, are suspected to be CMR (Carcinogenic, Mutagenic, Reprotoxic) and should be banned in the future. On the other hand, the mode of action of boron as flame retardant is still ambiguous. **Consequently, the first aim of this work is to understand the mode of action of boron and to provide some outlooks for alternative solutions.**

Although boron is a critical element, the reactivity/interaction of other additives present in the formulation must be considered since the chemical reactivity in such a complex formulation can occur in various ways. The mode of action of phosphorous compounds (e.g. APP), of silicate fibers and of TiO_2 in fire protective intumescent coatings have been extensively studied and reported in the literature [6, 9, 10]. $CaCO_3$ is one of the components among all ingredients. It is generally used as a filler, its flame retardant effects have been investigated but its role in intumescent coatings is still controversy. **Hence, the second objective of this project is to investigate the effect of $CaCO_3$ on fire protective properties and its mode of action in intumescent coating.**

The PhD thesis is organized in four chapters.

The ***first chapter*** gives a recent state of the art about intumescent materials emphasizing the definition of intumescence, intumescent coatings and main ingredients of intumescent coatings. Then, the fire scenarios and intumescent coating formulations are described. Afterwards, the review specifically focuses on epoxy based intumescent coatings and on the chemical reactivity between the ingredients, which are the main interests of this project. Finally, the methods of characterization which have been used in the field of fire protective materials, are described. It focuses concisely on those implemented in this study

The ***second chapter*** presents the materials used, preparation of the coatings, fire tests as well as characterization methods for chemical, thermal and physical modifications. It describes all methods used. The aim is to describe how the research work was experimentally performed.

The ***third chapter*** details the study of the mode of action and role of borates in epoxy based intumescent coatings. First, the effects of different borates were assessed. Afterwards,

boric acid and zinc borate, which provide the most outstanding and interesting result among all, were selected to elucidate in more detail the role of borates. This chapter aims at drawing the mode of action of borates to provide some outlooks for substituting borates and to design alternative solutions.

The fourth chapter is dedicated to the investigation of the effect of carbonates on fire protection. First, the effect of calcium carbonate on fire protection was examined when it is combined with other additives (i.e. APP, borates). The mechanisms of action of the calcium carbonate were also investigated. Afterwards, the effects of various carbonates (i.e. $MgCO_3$, $ZnCO_3$, K_2CO_3, Na_2CO_3) on fire protective properties were examined.

At the end of the dissertation, a general conclusion is given and outlook for future works is proposed, especially the development of **boron free epoxy based intumescent coatings.**

Chapter I: State of the art

First, a literature review regarding intumescent coatings is necessary. The aim of this chapter is to provide a background on the context and the purpose of the thesis research. Hereafter, the concept of intumescence, intumescent coatings and its main ingredients are described. Then, the fire scenarios and conventional intumescent coating formulations are presented. Afterwards, the epoxy based intumescent coatings are detailed. In particular, the mechanism of action of intumescent coatings and the chemical reactivity of the main ingredients of the formulation are fully depicted. Lastly, the characterization methods usually used to study different aspects of intumescent coatings including char properties (e.g. thermal conductivity, viscosity, expansion & expansion rate, char strength, morphology) and chemical analyses of char (e.g. solid state NMR) are presented and fully commented.

1.1 Intumescent coatings

In this section, the definition of intumescence, intumescent coatings and ingredients of intumescent coatings are first given. The fire scenarios are then detailed. Finally, the intumescent coating formulations for specific fire scenarios are reviewed.

1.1.1 What is an intumescent material?

Definition of intumescence

The word ''intumescence'' comes from Latin, it means ''to swell up'' [11]. In the field of materials science, this term refers to a thermally reactive material that can swell up to several times its original thickness to form a multi-cellular insulative barrier (Figure 2). The formed structure, generally referred to as ''char'', slows down the heat and mass transfers acting as a protective layer for the underlying material.

The protection is consequently obtained mainly thanks to an action in the condensed phase. The concept of intumescence to fireproof a substrate is not a new concept. It can be traced back to 1821. Indeed, this year, Gay-Lussac reported that coating hemp and flax woven fabrics by a mixture of borate and ammonium phosphate could retard the burning of these materials thanks to the formation of a swollen char layer [4, 12]. However, the word 'intumescence' was not stated in the text.

Almost one century later, in 1938, Tramm claimed the wood protection against ignition and burning using a mixture of diammonium phosphate (or sulfate), dicyandiamide and formaldehyde via the same kind of expanded barrier. Here, the word intumescence was explicitly mentioned for the first time [13]. Since that time, numerous studies have been performed on the development of intumescent formulations for both fire resistant and fire retardant applications.

Figure 2 Intumescent material (before and after heating)

Intumescent coatings

Intumescent coatings are a particularly successful application of this intumescent concept and are mainly used for the protection of steel and wood structures against fire [14]. They preserve the functionality of substrates as long as possible in case of accidental fire. For structural steel, it means to keep the temperature below its critical temperature, usually defined as the temperature at which only 60 % of the original strength remains, point at which the failure is imminent under full design loads. Intumescent coatings are classified as 'passive reactive fireproofing materials' in opposition to active fire protections such as fire detection and fire suppression systems. Passive fireproofing materials mean insulating systems designed to decrease the heat transfers between a fire and the structure that need to be protected [15]. It is built as a part of the buildings and acts instantaneously in case of fire. Other types of passive fireproofing materials can be used, for example board encasement, concrete, mineral fiber, cementitious spray… [5, 16].

The market share between 2001 and 2016 in Great Britain of different passive fireproofing materials is reported on Figure 3. Intumescent coating market is growing up rapidly as compared to other passive fire protection systems (i.e. broads, sprays). The significant increase over the last decade is due to the development of on-site intumescent coatings that provide better performance with cost effectiveness, the use of off-site application of intumescent coatings is slightly decreasing [17].

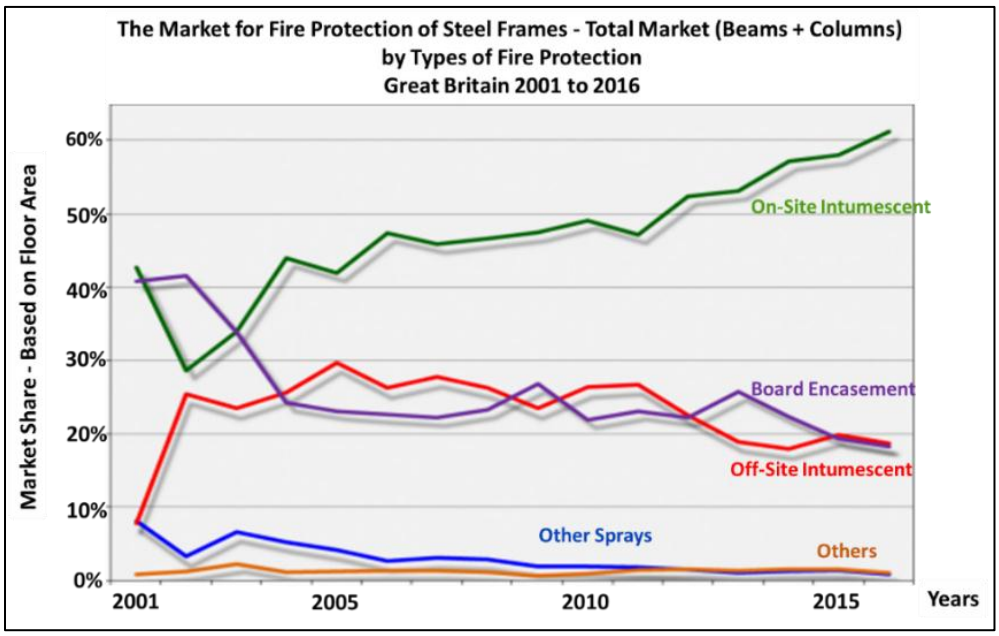

Figure 3 Market share of passive fire protection [17]

Main ingredients of intumescent coatings

To develop intumescence, the presence of three main ingredients namely an acid source, a carbon source and a swelling agent are required as pointed out by Vandersall [8] in the early 1970s. The intricate process that takes place upon heating and that leads to the formation of the intumescent barrier can be described as follows: the acid source (inorganic acid) is released typically between 150 ^{o}C and 250 ^{o}C depending on its chemistry. Then, the acid esterifies the carbon-rich components (carbon source) at temperature slightly above the acid release temperature. The mixture of the materials melts/softens prior or during esterification. The ester decomposes via dehydration resulting in the formation of a carbon-inorganic residue. The release of gases during these reactions and degradation products of blowing agent lead to the foaming of the carbonizing material. At the end, gelation and solidification result in a multicellular foam [11, 18]. The schematic representation of intumescent process is shown in Figure 4. The char formation is usually modelled in three zones: i) a pyrolysis zone close to the substrate, ii) a pre-pyrolysis zone and iii) an upper char layer close to the heat source [19, 20].

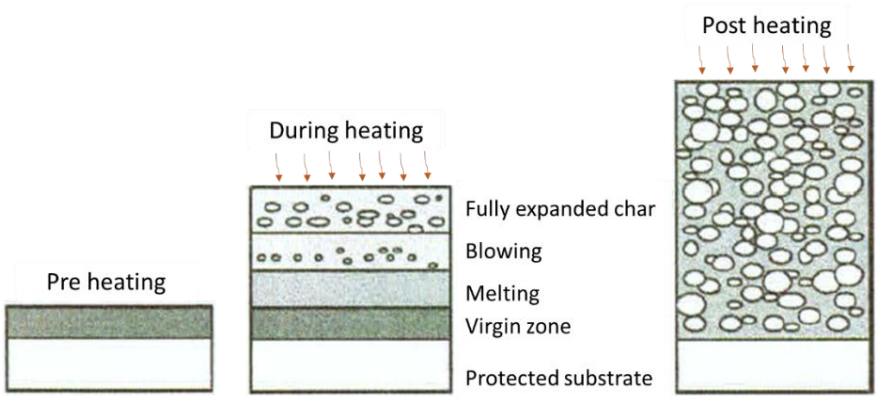

Figure 4 Schematic representation of the intumescent process [3, 19, 20]

The used ingredients will only be effective if they decompose at the right temperature and in the suitable sequence. They have to be chosen and combined accordingly. Examples of main components identified in the literature are given in Table 1. However, some of them can play several roles: for example, ammonium polyphosphate (APP) can act as both acid source and blowing agent. In specific formulations, two acid sources (e.g. APP/boric acid [6, 21]) can be combined to obtain better performances. The use of two blowing agents with slightly different decomposition temperatures has also been reported to obtain greater foam heights (extend the length of gas release) [22]. Concerning the carbon source, it is noticeable that the number of carbon will influence the amount of char formed whereas the number of hydroxyls will determine the rate of char formation [23].

Table 1 Examples of chemicals used as acid source, blowing agent and carbon source for intumescent systems [18, 24]

Inorganic acid source	Acid (e.g. boric, phosphoric, sulphuric) Ammonium salts (e.g. phosphates, polyphosphates, borates, polyborates) Amine/amide phosphate (e.g. melamine phosphate)
Blowing agent	Melamine Ammonium polyphosphate Dicyandiamide
Carbon source	Polymer (e.g. epoxy, acrylic, polypropylene) Tris (hydroxyethyl) isocyanurate (THEIC) Pentaerythritol monomer, dimer, trimer Starch, polysaccharides

Apart from these ingredients, the use of functional additives such as *inorganic fillers, synergistic agents and pigments* can be pointed out. They are generally needed to improve the properties of intumescent coatings and charred layer.

Inorganic fillers such as ***minerals*** (e.g. calcium carbonate, talc, mica, kaolin, clay, silica, carbon black, titanium dioxide…) and ***fibers*** (e.g. natural fibers, glass fibers, silicate fibers…) are primarily used in intumescent coatings because of their inherent benefits concerning the mechanical properties of foamed char. They are mainly hydrophilic and immiscible with the polymer matrix leading to various morphologies [25]. They can also bring additional performances (density reduction, thermal insulation, surface properties…) and can act as a synergist. The presence of such fillers can modify the chemistry of intumescence through ***synergistic*** and/or ***catalytic*** effects as well as the physical properties of the protective char (expansion, char strength, thermal conductivity…).

For exemple, Duquesne et al. [9] studied the influences of two inorganic fillers (i.e. titanium dioxide, mineral fibers) on the fire protection behavior of acrylic based intumescent coatings. They reported that both fillers improve the fire protective behavior of the coating. Ahmad and Ullah research group have extensively studied the effects of fillers (i.e. wollastonite, zirconium silicate), synergists (i.e. kaolin clay) and new additives to enable to enhance fire protective properties of intumescent fire protective coatings [26-29].

Depending on the fire scenarios, the formulations of the intumescent coating can be very different. The next paragraph presents the different existing fire scenarios, followed by the different types of intumescent coatings which are used in those scenarios.

1.1.2 Fire scenarios

Intumescent coating formulations are developed depending on the targeted applications. Such coatings are widely used to protect substrates in three main categories of fire scenarios: cellulosic, hydrocarbon and jet fire.

Cellulosic fires correspond to a general fire scenario when the fuel sources are predominantly cellulose (e.g. wood, paper, cotton). Cellulosic fire curve (standard ISO 834) is characterized by a relatively slow temperature rise to around 927 ^{o}C in 1 hour [30].

Hydrocarbon fires are mentioned when hydrocarbon fuels (e.g. oil, gas, chemical) are present in the fire situation. It is well known as hydrocarbon test curve (UL 1709) [31, 32]. It corresponds to a rapid temperature rise up to 1093 ^{o}C in 5 minutes. Various scenarios presenting a modified hydrocarbon fire curve and specifying a time/temperature curve have been set up by different international organizations/companies: hydrocarbon modified curve (HMC) [33] and EN 1363-2 Hydrocarbon curve [34]… The examples of the standard fire curves are shown in Figure 5.

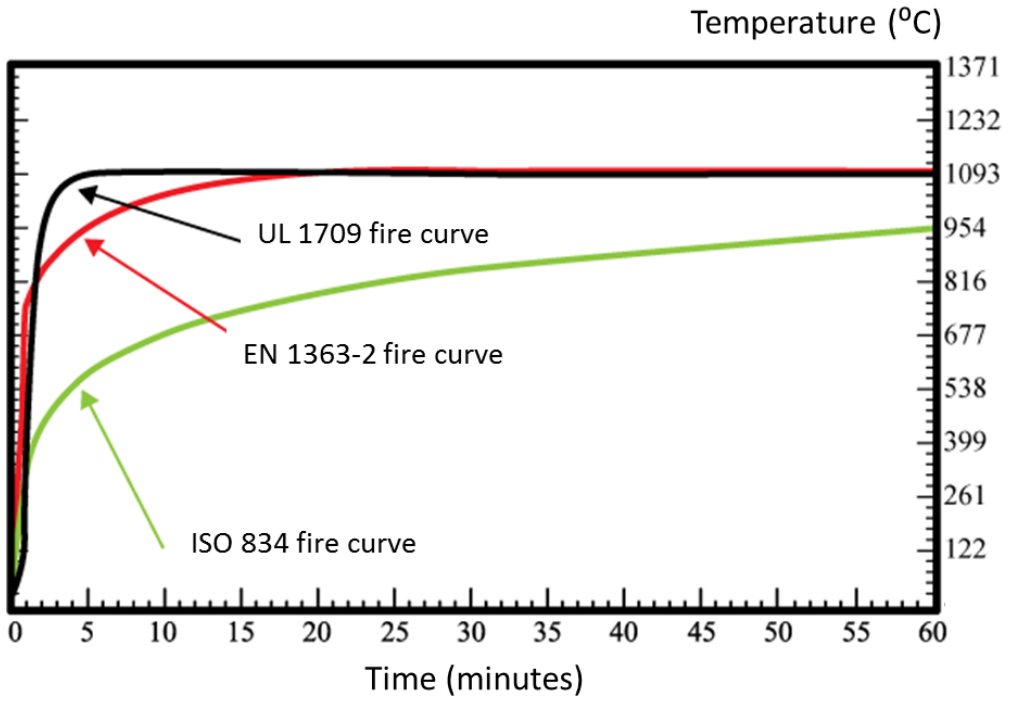

Figure 5 Standard fire test curves [35]

Jet fires are a particular group of hydrocarbon-fueled fire expelled from an orifice under pressure of two bar or greater and give rise to high convective and radiative heat fluxes as well as erosive forces. It reproduces very severe fire condition combining extremely high heating and high velocity of the jet. It is the most severe fire scenario, which mimics fire risks in offshore installations [36]. The standard condition of jet fire test is described under ISO 22899 [37, 38].

Depending on the fire scenario, intumescent coating composition and thickness will vary. They are usually classified either as thin or thick film coatings [1, 11] and the specific formulations versus applications are described hereinafter.

1.1.3 Intumescent coating formulations

Thin film intumescent coatings are usually used in the case of cellulosic fires. They are generally available as waterborne or solvent-based systems. Waterborne intumescent coatings are very efficient but are more sensitive to humidity than solvent-based coatings. They can be applied by spray or brush-roller up to 3 mm thickness. Thermoplastic acrylic or poly (vinyl acetate) resins are typically used as binders. This kind of coating responds and intumesces quickly when exposed to a cellulosic fire. The advantages of these products include their low cost and relatively easy application and that is the reason why they are mostly used in buildings. However, they are unsuitable for exterior use without topcoat due to the lack of weather resistance and durability. Intumescent thin films are often referred as ‘fire retardant coatings’ rather than ‘fireproofing materials’ due to their inferior fire resistance compared to thick film intumescent coating.

Thick film intumescent coatings are widely based on epoxy, vinyl or other elastomeric resins. They are solvent-free systems that allow application of 3 to 30 mm thickness per coat; they are particularly efficient in the case of hydrocarbon fires. They provide an excellent weather resistance, anti-corrosion, resistance to impact and vibration damage. However, they are quite expansive. In addition, these coatings have more stringent surface preparation requirements and smoke produced in fires makes them unsuitable for certain applications, such as enclosed living areas.

To obtain a wide range of fire performances with intumescent coating formulations, complex combinations of binder, of intumescent additives as well as of co-additives are used. This explains the large number of patents on this subject. Some academic research can also be found on particular aspects, such as on the mechanisms of reaction between the ingredients and on the fire protection mechanisms involved in the intumescent coatings. The research groups of Camino [39, 40] and Bourbigot [41, 42] have been particularly active on this research topic and have extensively studied intumescent systems.

To remain competitive and compliant with the standards in terms of performances as well as environmental and safety issues, over the last two decades extensive developments of formulations have been recorded (many patents have been granted). Evolutions have also been observed in terms of additives and of matrix used.

Interestingly, a distinctive proposition has been arisen during the last decade. A silicone based intumescent coating [43, 44] which shows advantages compared to the conventional thermoplastic acrylic or thermoset epoxy based coatings has been developed and patented. This silicone based coating releases less toxic organic gases, which makes it a noteworthy and attractive choice for the future. It was shown in some academic studies that it provides excellent fire resistance in both cellulosic and hydrocarbon fire scenarios and that reaches better performances than commercial acrylic or epoxy based coatings [30, 45]. It is noticeable that silicone resins possess excellent thermal stability and better resistance to oxidation than conventional organic polymers but such kind of coatings has not yet been commercialized.

In this dissertation, the work particularly deals with the fundamental study of thick film epoxy based intumescent coatings. This thick film epoxy based coating is a special type of such coatings that is extensively used in multi-story buildings and offshore installations to provide a protection of steelwork against hydrocarbon fire. ***UL1709*** is used as a standard fire scenario to evaluate the fire protective properties of the coatings in this study.

1.1.4 Conclusion

Intumescent materials are not recent materials, but they still drive a lot of research and development in both universities and companies. The market share of these reactive passive fire protection materials is extending due to their noteworthy benefits over other fire protection materials. The trend is now to obtain thinner products with lower toxicity and lower smoke production. Various kinds of intumescent coatings exist (waterborne, solvent borne, solvent-free…), which have to be defined mainly depending on the fire scenario (cellulosic, hydrocarbon…) and the application (inside, outside). Among all coatings, epoxy based intumescent coatings are of prime interest because of their efficiency against hydrocarbon fire which is the fire scenario of interest in this project. As this work deals with the fundamental study of epoxy based intumescent coatings, the next part of the state of the art especially focuses on this kind of coatings.

1.2 Epoxy based intumescent coatings

What about epoxy resins

Epoxy resins are thermoset polymers obtained either through catalytic homopolymerisation of epoxy prepolymers containing epoxide rings or from the reaction between the latter and a hardener through a polyaddition mechanism. Depending on their functionality, different types of epoxy prepolymers can be distinguished. The most common one is diglycidyl ether of bisphenol A (DGEBA) obtained through the reaction between epichlorhydrin and bisphenol A in the presence of sodium hydroxide [46]. Apart from DGEBA, other prepolymers can be listed (Table 2) such as diglycidyl ether of bisphenol F (DGEBF), tetraglycidyl methylene dianiline (TGMDA) or triglycidyl ether of p-aminophenol (TGAP) etc.

Table 2 Chemical structures of epoxy resins

Epoxy resin	Structure
Diglycidyl ether of bisphenol A (DGEBA)	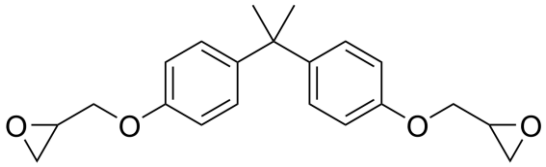
Diglycidyl ether of bisphenol F (DGEBF)	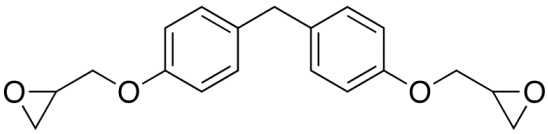
Tetraglycidyl methylene dianiline (TGMDA)	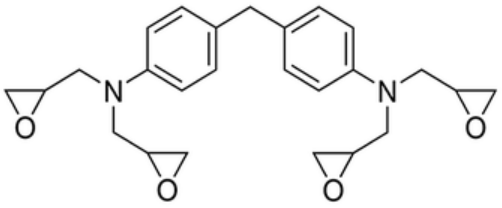

Triglycidyl ether of p-aminophenol (TGAP)	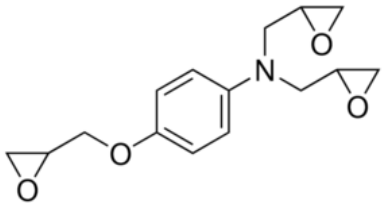

The most commonly used curing agents for epoxy resins are ***amines, amine derivatives, anhydrides, phenols, alcohols, and thiols***. The polymerization process, referred as crosslinking or curing of the resin, is exothermic and irreversible. An infusible three-dimensional network is obtained. The choice of the epoxy prepolymer, of the hardener and of their ratios can lead to a large number of resin presenting various properties (stability, kinetics of polymerisation, glass transition temperature, mechanical performance, chemical resistance,…) [46]. Interesting properties such as high strength, excellent adhesion, chemical and heat resistance can thus be obtained [47]. These result in a large variety of applications of epoxy that go from coatings to adhesives as well as composite materials.

In terms of fire performances, the nature of the monomers of the epoxy resin has a great impact on the performance: for example, the molecular weight of the epoxy resin can control the char expansion and formation of an uniform foamed structure. Wang and Yang [48] studied the influences of molecular weight of epoxy binder (Mn = 446, 568, 1025 and 1739 g/mol) on fire protection of waterborne intumescent fire resistive coating. It was found that a high molecular weight epoxy binder improves thermal stability of the coating and enhances the anti-oxidation of char at high temperature. Moreover, its melt viscosity rises with an increase of molecular weight. Usually, a too low melt viscosity leads to an easy diffusion of gases in the melting matrix. These gases are thus not be trapped but will escape to feed the flame inhibiting char expansion and significantly decreasing the expected fire protection of the coating [49]. An increase in melt viscosity slows down the expansion speed leading to an increase of the cell size. However, a molecular weight of 1739 g/mol seems to be excessive since it leads to the formation of a loose and uneven foam structure.

Moreover, in the case of intumescent coatings, epoxy resin acts not only as a binder but also as a source of carbon, which is converted into a char in a fire. However, a major drawback of epoxy based coatings is the large emission of corrosive and toxic smokes during a fire [50, 51], that makes them unsuitable for indoor application.

Epoxy based intumescent coating formulations

Conventional thin film epoxy based intumescent formulations use APP as acid source, pentaerythritol (PER) as char former and melamine as blowing agent, typically at a weight ratio of 3:1:1 as flame retardant package. Formulations based on these or similar components are reviewed in the paper of Vandersall [8]. However, current commercial formulations can be much more complex. In addition to these three necessary elements, functional additives such as mineral fibers, TiO_2, $CaCO_3$, carbon black, fumed silica... are also incorporated to obtain highly efficient systems.

Regarding thick film intumescent coatings based on epoxy resin used for a protection against hydrocarbon fire, up to now, the patent literature reveals that the efficiency was achieved by combining APP with another acid source in the form of borates (e.g. boric acid, zinc borate or ammonium pentaborate) [6, 52]. The more recent patent from International Paints is based on alternative chemistry without boron but with modified resins or combination of resins [37].

Some examples of epoxy based intumescent coating formulations are given in Table 3.

Table 3 Examples of intumescent coating formulations

Name	Formulation	Ref.	Year
PPG (PITTCHAR)	Epoxy-based mastic/ Versamid 150 (curing agent) Additives: ***boric acid***, **zinc borate**, APP, wollastonite, tris(2-chloroethyl) phosphate, tall oil fatty acid, melamine and attapulgite gallant, aerosol, silica, talc	[53]	1985
PPG	Flexible epoxy resin (polyester chain-extended epoxy) Additives: **APB**, APP, **zinc borate**, silica, talc….	[54]	1991

Textron Systems Corporation (CHARTEK 7)	Epoxy resin/Ancamide 903 (curing agent) Additives: **boric acid**, APP coated with THEIC, triaryl phosphate, black pigment, antifoaming siloxane surfactant, amorphous hydrophobic fumed silica, expanded perlite, amorphous mineral fiber, wetting agent, milled limestone, TiO_2, high surface area Al_2O_3/SiO_2	[21]	2000
Chance and Hunt Limited	Epoxy resin combined with aldehyde resin or ketone thermoplastic resin/phenolic (curing agent) Additives: APP, TiO_2, hydrogenated castor oil viscosity modifier	[55]	2002
International Paints	Epoxy prepolymer (DER 331 and 736), polysulfide polymer (Thioplast G4 and Morton LP3), polysiloxane (DC200 silicone fluid), Ancamine K54 (curing agent) Additives: APP, melamine resin, PER, fibers (carbon, glass and aramid) * Low level of smoke generation and a good weather ability compared to the currently available products on the market	[37]	2012
International Paints	Silicate modified-epoxy resin/polyamide (curing agent) Additives: APP, melamine, metal oxides and/or metal hydroxides (e.g. Aluminium hydroxide) * Enhance the char strength of the intumescent coating with no diminishing of the fire performance, resulting in a surprisingly superior char foam with respect to both strength and fire performance	[56]	2016

For intumescent systems, the design of formulations is a dedicate stage. A random selection of the ingredients does not ensure an intumescent behavior. The components should degrade in an appropriate sequence to provide an effective fire protection. Thus, chemistry of the formulation plays a crucial role. Epoxy based intumescent coatings are very complex systems containing a huge number of ingredients. The patent literature for hydrocarbon fire applications have highlighted that borate and phosphate are used concurrently as acid source in these formulations and this indicates that these ingredients may play a major role resulting in an efficient intumescent behavior. Therefore, the next part of this chapter is dedicated to the review of the chemical reactivity between ingredients present in intumescent coatings such as phosphorus-based compounds, borates, carbonates, fibers and titanium dioxide.

1.3 Chemical reactivity between intumescent ingredients

As already explained in the previous sections, intumescent coating formulations are complex systems. The decomposition pathway of such system is very complicated. In addition to the reaction leading to intumescence, side reactions can occur concurrently between the three intumescent ingredients and the other components of the formulation. Yet the knowledge of the decomposition pathway and of the species formed during the development of protective layer is a key to understand how fire performances are obtained and how to design new efficient formulations. However, some parameters such as the kinetic of these reactions or the stoichiometry between additives can greatly impact the composition of an expanded char. This section thus reviews the decomposition and reactivity of typical ingredients of intumescent formulations (i.e. APP, borates, carbonates, fibers, titanium dioxide) alone or mixed together.

1.3.1 Phosphorus based compounds

Phosphorus based ingredients, and in particular phosphates, are essential components in classical and efficient intumescent formulations. Phosphates are indeed multifunctional; most of them can play the role of both acid source and blowing agent in the intumescent process. They are known to be involved in cross-linking of decomposition products, inducing charring and preventing char oxidation [57, 58]. As they can also react at high temperature with numerous chemicals, their role in the formation of inorganic glassy residue is also well documented [59]. Various phosphorus flame-retardants have attracted intensive interests due to their high reactivity, for example ammonium polyphosphate (APP), ammonium diphosphate (ADP), melamine phosphate, etc. Among them, APP is the most commonly used phosphorous-based compound in both fire retardant and fire resistant intumescent materials. It is also used in the studied formulation. The following section reports general information about APP.

APP is an inorganic salt of polyphosphoric acid and ammonia with the following formula: $(NH_4PO_3)_n$. It is a stable and non-volatile material. It slowly hydrolyzes in contact with water to produce monoammonium phosphate (orthophosphate). The decomposition temperature of APP is related to the length of the polymer chain. A short chain APP decomposes at about 150 ^oC ($n < 100$) while a long-chain APP starts to decompose at temperature above 300^oC [25]; APP degrades

into polyphosphoric acid and ammonia (eq.1) which act respectively as catalyst and spumific in intumescent systems. In general, only a long chain APP is used in fire protective coatings [60].

$$(NH_4PO_3)_n \xrightarrow[T \sim 280\ ^0C]{} (HPO_3)_n + nNH_3 \quad ; n \approx 700 \ [61] \qquad \text{(eq. 1)}$$

In presence of a carbon source, the phosphoric acid formed can react with hydroxyl or other groups of a carbon source to form an unstable phosphate ester (eq. 2) followed by its dehydration. A phospho-carbonaceous foamed structure is formed acting as an insulation layer protecting the underlying substrate [25].

$$(HPO_3)_n + \text{carbon source} \rightarrow \text{Carbon char} + H_3PO_4 + H_2O \qquad \text{(eq. 2)}$$

Un-reacted polyphosphoric acid (degradation product of APP) can dehydrate between 550 and 770 ^oC to yield phosphorous oxide (P_2O_5), which can further sublimate (eq. 3).

$$2(HPO_3)_n \rightarrow nP_2O_{5\ (sublimate)} + n\,H_2O \qquad \text{(eq. 3)}$$

Thermogravimetric analyses of sole APP under air or nitrogen show that it yields a residue of about 5 - 18 wt. % at 800 ^oC [60, 62]. This high variation of residual weight is due to the sublimation of P_2O_5, which may be affected by the experimental conditions.

Due to its high reactivity, APP usually reacts during heating with other chemicals present in the formulation. The following part introduces these other chemicals (borates, carbonates, fibers and titanium dioxide) and their reactivity with APP.

1.3.2 Borates

Borates are used in several applications and one of them flame retardant additive. Different borates have already been tested in intumescent coatings such as ***melamine borate, borax, ammonium pentaborate, boric acid*** or ***zinc borate.*** They are generally used in combination with other additives. Some examples of combinations reported in intumescent coatings are shown in Table 4.

Table 4 Uses of borates in intumescent coatings

Borates	**Co-additives**	**Substrates**	**Ref.**
Melamine borate	Melamine phosphate	Wood and Steel	[63]
Borax	A water-soluble sodium silicate, aluminum trihydroxide (ATH) and kaolin	Steel	[64]
Ammonium pentaborate	Zinc, boron and phosphorus containing compounds	Steel	[65]
Boric acid	APP, triaryl phosphate, THEIC, silica, perlite and ceramic fibers	Steel	[21]
	APP, expandable graphite and melamine	Steel	[66]
Zinc borate	APP and melamine	Steel	[65]
	APP, melamine and expandable graphite, ATH, alumina and talc	Steel	[67]
	Sb_2O_3	Steel	[68]

Usually, boric acid and zinc borate exhibit the highest performance. In the following sections, their decomposition pathways are described and then, their chemical reactivity with other components of intumescent formulations and in particular with APP are reported.

1.3.2.1 Boric acid

Boric acid or orthoboric acid (H_3BO_3), a weak acid, is a white **triclinic** crystal that is soluble in water (5.64 %), alcohols, and glycerin [69, 70]. Triclinic crystal of boric acid found naturally in volcanic fumaroles, hot springs, …is called ***Sassolite*** [71, 72].

Decomposition of H_3BO_3

When heated, boric acid decomposes in two steps [73, 74]: a first step between 100 °C and 140 °C corresponding to a weight loss of about 30 wt. % and a second step in the temperature range 140 °C to 200 °C leading to a thermally stable material (55 wt. % of the initial mass). The first step corresponds to the dehydration of boric acid into metaboric acid (HBO_2) which in the second step further dehydrates into boron oxide (B_2O_3) undergoing endothermic reaction (eq. 4 - 5). Figure 6 shows the phase diagram of B_2O_3 - H_2O system presenting the transformation of boric acid into boron oxide.

$$H_3BO_3 \xrightarrow[T \sim 100-140\ ^0C]{} H_2O + HBO_2 \qquad \text{(eq. 4)}$$

$$2HBO_2 \xrightarrow[T \sim 140-200\ ^0C]{} H_2O + B_2O_3 \qquad \text{(eq. 5)}$$

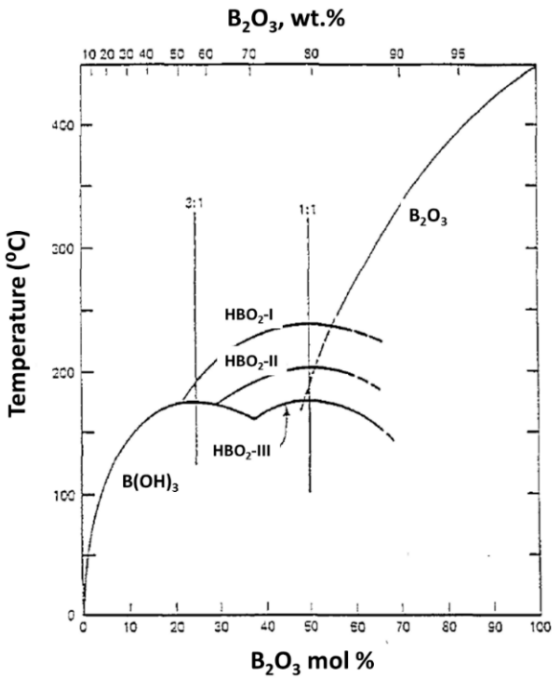

Figure 6 Phase diagram of B_2O_3 - H_2O system [75]

Boron oxide is a white and hard glassy solid. It can be found in both amorphous and crystalline form. Crystalline boron oxide exists in two forms: hexagonal and monoclinic (Table 5). The glassy and commercial form of boron oxide begins to soften at about 325 ^{o}C. It is prepared in large quantity by fusing refined boric acid in a furnace followed by a rapid cooling [76]. The crystalline forms of B_2O_3 melts at about 450 ^{o}C - 465 ^{o}C for hexagonal and 510 ^{o}C for monoclinic [77, 78]. A slow dehydration of boric acid followed by a slow cool down tends to yield the crystalline forms of boron oxide [79, 80].

Table 5 Physical properties of boron oxides [77, 78]

Properties	Vitreous form	Crystalline forms	
		α - form or B_2O_3 (I)	β - form or B_2O_3 (II)
Mp (°C)	Softens 325	450 - 465	510
Density (g/ml)	1.84	2.46	2.95
Crystal form	-	Hexagonal	Monoclinic

Reactivity of H_3BO_3 in presence of APP

The reactivity of boric acid with APP (the most commonly used phosphate) was already reported [74]. The mechanism of reaction was investigated on a mixture of boric acid and APP coated with THEIC. The mixtures were heated at different temperatures in a furnace to elucidate their reactions as a function of temperature. It was found that the reaction between the degradation product of H_3BO_3 (i.e. boron oxide) with the degradation product of coated APP (i.e. polyphosphoric acid) occurs at about 250 ^{o}C leading to the formation of borophosphate (BPO_4), white infusible solid that vaporizes at 1450 ^{o}C - 1462 ^{o}C without decomposition. It is believed that the formation of such thermally stable compound can stabilize the char and increase its mechanical resistance [81, 82]. The equations below (eq. 6 - eq. 8) described the formation of borophosphate.

$$2H_3BO_3 \xrightarrow[T \sim 100-200\ ^{0}C]{} \boldsymbol{B_2O_3} + 3H_2O \qquad \text{(eq. 6)}$$

$$(NH_4PO_3)_n \xrightarrow[T \geq 250\ ^{0}C]{} nNH_3 + \boldsymbol{(HPO_3)_n} \qquad \text{(eq. 7)}$$

$$B_2O_3 + 2(HPO_3)_n \xrightarrow[T \sim 250-400\ ^0C]{} 2n(BPO_4) + nH_2O \qquad \text{(eq. 8)}$$

It was reported that the formation of borophosphate could explain the development of a hard intumescent char. When H_3BO_3 and coated APP are mixed together, the borates provide a hard and mechanically resistant char, while the presence of phosphorous allows promoting a good adhesion of the char to the steel plate.

Ullah et al. [66] also emphasized the interests of adding boric acid in epoxy based intumescent coatings containing APP, expandable graphite and melamine. As a result, the addition of boric acid provides longer fire resistant time and a better adhesion to steel. The presence of borophosphate, boron oxide, sassolite (H_3BO_3) and graphite which are high thermal stability, are claimed to be partly responsible for a better fire resistance of the protective char. It was also reported that the structure of the residual char became more porous when the weight percentage of boric acid was increased with respect to that of melamine improving fire performances of the coatings.

1.3.2.2 Zinc borate

Zinc borates have found industrial, with $2ZnO.3B_2O_3.7H_2O$ and $3ZnO.5B_2O_3.14H_2O$ primarily utilized in 1940s. The most important commercial zinc borate today is ***$2ZnO.3B_2O_3.3.5H_2O$*** (***Firebrake ZB)***. It is produced by the reaction between zinc oxide and boric acid, or between zinc and borate salts, in hot water (> 65°C) [69].

Decomposition of zinc borate

The mechanism of decomposition of Firebrake ZB was reported [83, 84]. The first step consists in the condensation of the B-OH groups between 290 °C and 420 °C with release of water. The zinc borate degrades to yield an amorphous product with corresponds to its dehydrated form (eq. 9). Then, $2ZnO.3B_2O_3$ decomposes totally or partially to yield $ZnO.2B_2O_3$ and another non-identified phase in the temperature range 420 °C to 580 °C (eq. 10). Between 580 °C and 800 °C, other reactions take place leading to the formation of two different compounds ($ZnO.2B_2O_3$ and $4ZnO.3B_2O_3$) (eq. 11).

$2ZnO.3B_2O_3.3.5H_2O \xrightarrow[290\ °C < T < 420\ °C]{} 2ZnO.3B_2O_3$ (amorphous phase) + $3.5H_2O$ (eq. 9)

$2ZnO.3B_2O_3 \xrightarrow[420\ °C < T < 580\ °C]{} ZnO.2B_2O_3$ + non-identified phase (eq. 10)

$ZnO.2B_2O_3$ + non-identified phase $\xrightarrow[580°C < T < 800\ °C]{} ZnO.2B_2O_3 + 4ZnO.3B_2O_3$ (eq. 11)

ZB decomposes by releasing water, which dilutes the gas phase, thus reducing the temperature. After decomposition, the residual borates typically form a vitreous-like layer (amorphous phase) that could improve the thermal insulation and durability of char [85, 86].

Reactivity of zinc borate in presence of APP

The reactivity between zinc borate and APP was described in literature [83]. It was reported that the degradation product of zinc borate ($2ZnO.3B_2O_3$, amorphous phase) reacts with the decomposition product of APP (polyphosphoric acid and/or phosphoric acid) between 300 °C and 415 °C, leading to the formation of BPO_4 specie. Two possible reactions are proposed to explain their formation (eq. 12 and eq. 13).

$10(HPO_3)_n + 2ZnO.3B_2O_3 \xrightarrow[300\ °C < T < 415\ °C]{} 6BPO_4 + (n-6)/4P_4O_{10} + 2ZnO + n/2H_2O$ (eq. 12)

$10H_3PO_4 + 2ZnO.3B_2O_3 \xrightarrow[300\ °C < T < 415\ °C]{} 6BPO_4 + P_4O_{10} + 2ZnO + 15H_2O$ (eq. 13)

Between 415 °C and 580 °C, zinc orthophosphate ($Zn_3(PO_4)_2$) is formed, which results from the reaction between zinc oxide (ZnO) and phosphorus oxide (P_2O_5) (eq. 14) which are by products of the reaction of formation of BPO_4 (eq. 13).

$3ZnO + P_2O_5 \xrightarrow[T \sim 580\ °C]{} Zn_3(PO_4)_2$ (eq. 14)

Between 580 °C and 800 °C, a decrease of the amount of BPO_4 specie is observed. This decrease could be explained by its reaction with zinc orthophosphate to yield zinc pyrophosphate and boron oxide as shown in equation 15.

$2Zn_3(PO_4)_2 + 2BPO_4 \rightarrow B_2O_3 + 3Zn_2P_2O_7$ (eq. 15)

At higher temperature (at about 1050 °C), zinc orthophosphate then decomposes to yield zinc oxide (ZnO) and phosphorus oxide (P_2O_5), these two degradation products can then possibly react together to yield zinc pyrophosphate ($Zn_2P_2O_7$) (eq. 16 - 17).

$$Zn_3(PO_4)_2 \xrightarrow[T \sim 1050\,^{\circ}C]{} 3ZnO + P_2O_5 \qquad \text{(eq. 16)}$$

$$2ZnO + P_2O_5 \xrightarrow[T \sim 1050\,^{\circ}C]{} Zn_2P_2O_7 \qquad \text{(eq. 17)}$$

As a conclusion, the degradation pathway and chemical reactivity of boric acid and zinc borate are different. They decompose at different temperatures and their reactions with APP (binary mixture of APP with borates) lead to different products. In an intumescent system, which is much more complex than a binary mixture, their chemical reactivity can also be very different. The next par detailed another types of fillers widely used in intumescent coatings: the carbonates.

1.3.3 Carbonates

1.3.3.1 Calcium carbonates

Calcium carbonate ($CaCO_3$) is widely used in several industries due to its abundance and low cost. It is generally used as a filler for polymers to reduce the cost of materials and to improve the impact strength [25]. It is a thermally stable compound up to 680 °C. Its decomposition occurs in a single step in a temperature range from 680 °C to 900 °C [87, 88]. It corresponds to the conversion of $CaCO_3$ (eq. 18) into calcium oxide (CaO) releasing carbon dioxide (CO_2). A residue of 53 wt. % is observed after the decomposition of $CaCO_3$ corresponding to the expected amount of CaO.

$$CaCO_3 \xrightarrow[T \geq 680\ °C]{} CaO + CO_2 \qquad \text{(eq. 18)}$$

Calcium carbonate has been reported to have effects on rheology, processing and morphology depending on considered polymeric systems [25]. Its effect on flame retardant properties has also been investigated by different authors [89, 90].

For example, the flame retardant effect of $CaCO_3$ on modified polyolefin was reported [87]. Compared to the pure polymer, the addition of 30 % of $CaCO_3$ in an ethylene - acrylate copolymer (EBA) leads to a dramatic decrease in the heat of combustion since the flammable polymer is diluted with an inert material that does not contribute to the fire. This effect is seen with any inorganic filler. In addition to this, $CaCO_3$ could have a more active contribution as CO_2 can be released via an endothermic reaction.

Another study showed that the complex viscosity of poly(ethylene-co-methacrylic acid) (EMMA) modified with calcium carbonate and silicone elastomer increases above a critical temperature (250 °C) due to ionomer formation between acidic groups of the polymer and calcium ions. This has a great impact on the fire performance by reducing the transportation rate of gases in and out of the material [91].

From a general point of view, $CaCO_3$ seems to improve the flame retardant effects of polymeric materials. However, the effect of calcium carbonate may differ when combined with flame-retardants. As an example, Almeras et al. [92] reported that the addition of $CaCO_3$ in

intumescent polypropylene blends deteriorates its fire retardancy. Apart from that, the function of $CaCO_3$ in passive fire protection (PFP) material was pointed out by Ciudad et al. [93] who reported the endothermic effect of $CaCO_3$ at high temperature with a rich heat-absorbing profile.

Reactivity of $CaCO_3$

The literature review shows that a reaction between $CaCO_3$ with components such as APP or borates can occur as well as reaction with silicone matrix.

Relating to the article reported by Deodhar et al. [94], the possible reactions between $CaCO_3$ and APP are reported in equations below (eq. 19 - 20).

$$(NH_4PO_3)_n \xrightarrow{T \sim 300\ ^0C} (HPO_3)_n + nNH_3 \quad \text{(eq. 19)}$$

$$2(HPO_3)_n + CaCO_3 \xrightarrow{T \sim 300\ ^\circ C} Ca(PO_3)_2 + CO_2 + H_2O \quad \text{(eq. 20)}$$

Calcium carbonate, because of its basic nature, can react at low temperature (≈ 300 °C) with polyphosphoric acid (degradation product of APP) releasing carbon dioxide (CO_2) and water vapor leading to the early decomposition of $CaCO_3$. From this reaction, a thermally stable compound (β-calcium metaphosphate ($Ca(PO_3)_2$) is formed. In-situ formation of $Ca(PO_3)_2$ was reported to increase the flame retardant properties while the addition of $Ca(PO_3)_2$ as an inorganic filler does not seem to improve FR properties (e.g. in polypropylene) [95].

Another work by Baykal et al. [96] proposed a reaction between BPO_4 and $CaCO_3$. As mentioned in the previous part, BPO_4 can be formed by the reaction between borates and phosphates contained in the formulation. In presence of $CaCO_3$, they could react together leading to the formation of $CaBPO_5$. The reaction can occur at around 900 °C (eq. 21).

$$CaCO_3\ (s) + BPO_4\ (s) \xrightarrow{T \sim 900\ ^\circ C} CaBPO_5\ (s) + CO_2\ (g) \quad \text{(eq. 21)}$$

In case of fire protective coatings, the interests of adding $CaCO_3$ to a silicone based coating containing expandable graphite have also been demonstrated by Gardell et al. [30]. It was reported that the addition of $CaCO_3$ in this coating provides a good fire protective effect resulting from the reaction between the degradation products of the silicone based compounds (i.e. SiO_x) and of $CaCO_3$ (i.e. CaO) yielding thermally stable compounds (i.e. calcium silicate). The interaction

occurs between 650 °C and 750 °C leading to the stabilization of the system. The successive reactions of the formation of calcium silicate are shown in equation 22 - 24.

$$\text{Silicone matrix} \xrightarrow[T > 500\,^{\circ}C]{} SiO_x \qquad \text{(eq. 22)}$$

$$CaCO_3 \xrightarrow[T > 600\,^{\circ}C]{} CaO + CO_2 \qquad \text{(eq. 23)}$$

$$CaO + SiO_x \xrightarrow[T > 600\,^{\circ}C]{} \text{Calcium silicate} \qquad \text{(eq. 24)}$$

For epoxy based intumescent coatings, a small amount of $CaCO_3$ is usually added [21] as a filler. Nevertheless, its flame retardant effects have never been detailed in this kind of coatings.

1.3.3.2 Other types of carbonates

The effect of other carbonate species including calcium magnesium carbonate (Dolomite, $CaMg(CO_3)_2$) on a traditional intumescent flame retardant system (Epoxy-APP- H_3BO_3-expandable graphite-melamine) has been studied by Gillani et al. [97]. The char morphology of the coating without dolomite compared to that containing 8 % wt. of dolomite is very different. With dolomite, homogeneous with small pores, compact and uniform char structure without cracks were obtained while big holes and cracks, which can cause failure in heat shielding, were observed in the absence of dolomite. It was suggested that the incorporation of dolomite clay enhances the fire performance and significantly affects the formation of dense and continuous char.

1.3.4 Fibers

Fibers are mainly used as reinforcing materials. Numerous types of fibers exist, which can be classified as shown in Figure 7 [98]. Most of them (except natural fibers) are stable up to very high temperatures (T ≥ 1000 °C).

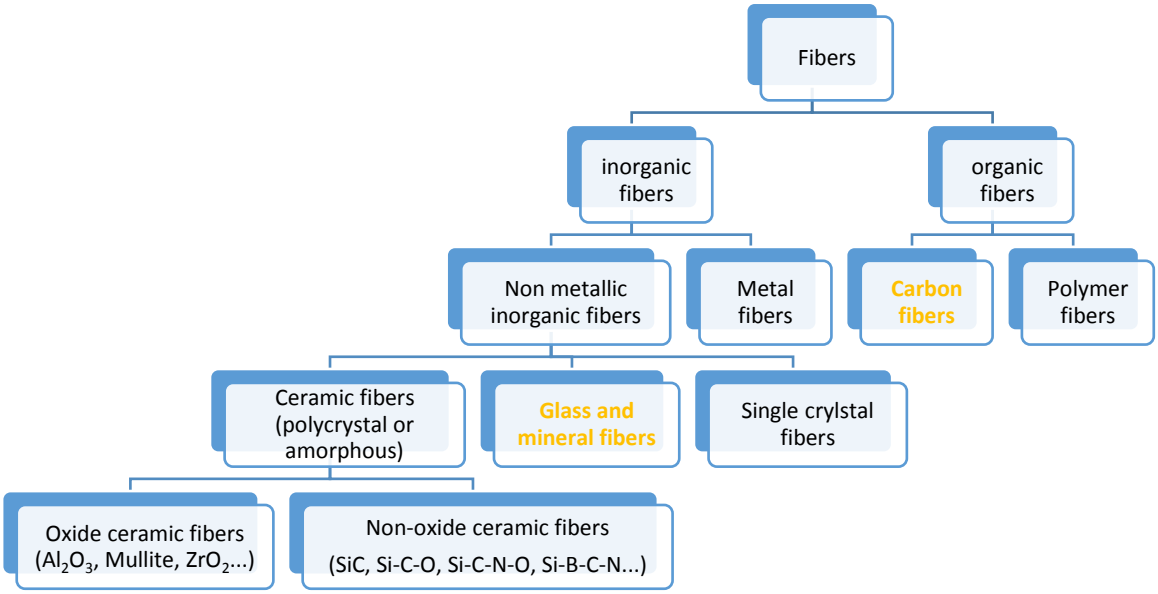

Figure 7 Classification of fibers [98]

Fibers, such as glass, mineral and carbon fibers, are incorporated in intumescent coatings to strengthen and improve the mechanical properties of the protective char obtained in case of fire (e.g. increase char strength), which affects positively the fire protective performance of the coatings (e.g. longer fire protection time) [99]. The incorporation of the fibers is very useful, especially for hydrocarbon and jet fires [100]. Another benefit of adding fibers into the intumescent coating is to adjust the viscosity of the coating as well as the melt viscosity of the intumescent matrix, which could improve the charring process and the subsequent char morphology [101].

As an example, Amir et al. [29] investigated the effects of fiber reinforcement on the char characteristics of epoxy based intumescent coatings. It was reported that long carbon fibers and glass fibers improve char structure, char height and char strength.

Another study demonstrated the benefits of adding silicate based mineral fibers (Rockforce® MS603-Roxul 1000) in an acrylic-based intumescent coating [9]. It was shown that the incorporation of either 2 % or 5% of fibers leads to a better fire resistance. These fibers improved the fire protective behavior and helped maintaining the protective performance for longer time without a collapse of charred structure

1.3.5 Titanium dioxide

Titanium dioxide (TiO_2) is an inorganic filler widely used in intumescent coatings for various purposes. Traditionally, it is used as a white pigment in intumescent coating formulations. It is chemically inert at room temperature. The beneficial contribution of TiO_2 on fire resistance of different intumescent coatings has been demonstrated. As an example, the addition of 4 % wt. of TiO_2 into epoxy based intumescent fire retardant coating composed of APP, expandable graphite, melamine and boric acid provides a better thermal insulation to the substrates [102].

TiO_2 can indeed react with APP or with its degradation products to form a ceramic like protective layer of titanium pyrophosphate (TiP_2O_7) at high temperature [103]. The reaction stage is shown below (eq. 25).

$$TiO_2 + P_2O_5 \xrightarrow[T \sim 600\ ^0C]{} TiP_2O_7 \qquad \text{(eq. 25)}$$

Gu et al. drew another stoichiometric reaction [104] as described in eq. 26.

$$2TiO_2 + (NH_4)_4P_4O_{12} \rightarrow 2TiP_2O_7 + 4NH_3 + 2H_2O \qquad \text{(eq. 26)}$$

The effects of different atomic ratios between titanium and phosphorous in an acrylic based intumescent coating have also been investigated [9]. Three ratios were considered: Ti/P= 0.5, 1, and 2; the best performance was obtained for the atomic ratio 0.5, corresponding to the Ti/P ratio in TiP_2O_7. On the contrary, Mariappan et al. [105] suggested that a slightly excess atomic ratio of Ti/P (0.9) provides better thermal insulation properties for a vinyl acetate based intumescent coating since TiO_2 in excess can act as radiative heat reflector and heat resistant filler.

On the other hand, the attempt to synthesize TiP_2O_7 by the reaction of TiO_2 with BPO_4 (specie formed when APP and borate are mixed together) has been reported by Bamberger and Begun [106]. TiP_2O_7 is obtained at around 1000 °C and further decomposes at around 1150 °C into tinanyl pyrophosphate ($(TiO)_2P_2O_7$). The latter decomposes into TiO_2 and phosphorus oxide (P_2O_5) around 1200 °C. The reaction scheme is presented in eq. 27- 29.

$$TiO_2 + 2BPO_4 \xrightarrow[T \sim 1000\ ^0C]{} TiP_2O_7 + B_2O_3 \qquad \text{(eq. 27)}$$

$$TiP_2O_7 \xrightarrow[T \sim 1150\ ^0C]{} (TiO)_2P_2O_7 + P_2O_5 \qquad \text{(eq. 28)}$$

$$(TiO)_2P_2O_7 \xrightarrow[T \sim 1200\ ^0C]{} 2TiO_2 + P_2O_5 \qquad \text{(eq. 29)}$$

The incorporation of nano-TiO_2 was also reported in some intumescent coatings. For example, Aziz et al. [107] reported that the incorporation of nano-TiO_2 into epoxy based intumescent coating comprising APP, melamine, boric acid and barite ($BaSO_4$) allows increasing the residual weight of the coating and provides longer protection time compared to conventional fire retardant coatings. Another paper [108] reported synergistic effects of nano-TiO_2 and eggshell micro powder on the improvement of fire protective properties of an acrylic based intumescent coating by increasing the residual weight of the chars and enhancing the anti-oxidation properties of the char at high temperature.

1.3.6 Conclusion

As a conclusion, the reactivity of intumescent additives in the condensed phase is a complex phenomenon. Various ingredients are present and numerous reactions can occur in many ways. Phosphorous can easily react with almost all of the elements present in the formulation such as boric acid, zinc borate, $CaCO_3$, fibers, TiO_2… The literature reports its chemical reactivity in simple systems, in flame retardant materials or outside the scope of intumescent materials. This reactivity is usually reported as an advantage. Indeed, it is widely reported that the species formed from APP or its degradation products stabilize the char, modify its sensitivity to oxidation and affect the morphology of the char which is a key aspect when dealing with heat transfer in intumescent coatings.

To investigate all those aspects, methodologies have been developed and the next part of this chapter is dedicated to the review of the characterization methodologies applied to intumescent materials. It first gives a general review and then emphasizes the ones which are implemented in the present study.

1.4 Characterization methodologies

The intumescent process is a very complicated process involving chemical, rheological, morphological, dimensional and thermo-physical modifications. To have insights of the mechanism of action, it is crucial to characterize the properties and chemical compositions of the coatings before burning, during burning and after burning (char). This section proposes a critical review of the different techniques usually used to characterize intumescent coatings. As a general comment, it can be noticed that there are different ways to characterize intumescent coatings [109, 110]: (i) characterizations performed at ambient temperature on the char residue collected at characteristic time or temperature of the intumescent process namely ex-situ measurement (ii) characterizations performed during the degradation versus either time or temperature referring to in-situ measurements (iii) characterizations through numerical approach.

1.4.1 Determination of the char properties

The properties of the intumescent protective layer, a foamed residual structure widely referred as ''char'' are key parameters to understand the fire performances of the intumescent materials. Many characterization techniques exist to investigate different properties of char such as thermal conductivity, viscosity, expansion, strength, structure, etc. Next section reviews the most widely reported techniques.

1.4.1.1 Thermal conductivity

The aim of using the intumescent approach to protect substrates is to build a thermal barrier on their surfaces. Consequently, it means that the char developed during the intumescent process should exhibit the smallest conductivity value. To determine this parameter, numerical or experimental methodologies have been reported [111, 112].

Staggs [113] calculated heat conductivity of intumescent char containing 60 % of fillers by numerical simulation. It was reported that heat conductivities vary from 0.1 to 0.4 W/mK from ambient temperature to 600 ^{o}C. This study gives the approximate range of the heat conductivity of an intumescent char. A few years ago, the estimation of equivalent thermal conductivity of intumescent coatings has been carried out by Calabrese et al. [114]. The equivalent thermal

conductivity of the intumescent layer produced under the action of a cone calorimetric apparatus has been assessed based on the inverse heat conduction problem approach. The values at the backside of steel were obtained as a function of temperature; they were well consistent with the heat conductivity values reported by Staggs.

Muller et al. [115] measured the heat conductivity of two intumescent polyurethane (PU) based systems (PU/30wt. % APP and PU/28wt.%APP/2wt.%nanoMgO) at different temperatures using the Transient Plane Source (TPS) method [116] (Figure 8). The heat conductivity values obtained in this study are also in the range of those reported by Staggs. The changes observed in terms of thermal conductivity have been attributed to modifications in the morphology. The expanded materials exhibit the lowest values at around 400 ^{o}C with 0.13 W/mK for PU/APP and 0.05 W/mK for PU/APP/nano-MgO. The TPS method seems an appropriate and reliable technique for the measurement of the thermal conductivity of intumescent materials. Nevertheless, this technique has some limitations. The sensor used is expensive and it can be used only one time to ensure the reliability of the measurements (sensor can be deteriorated/oxidized at high temperature). Another drawback is linked with that fact that this technique is time consuming since it takes a day or more for one measurement.

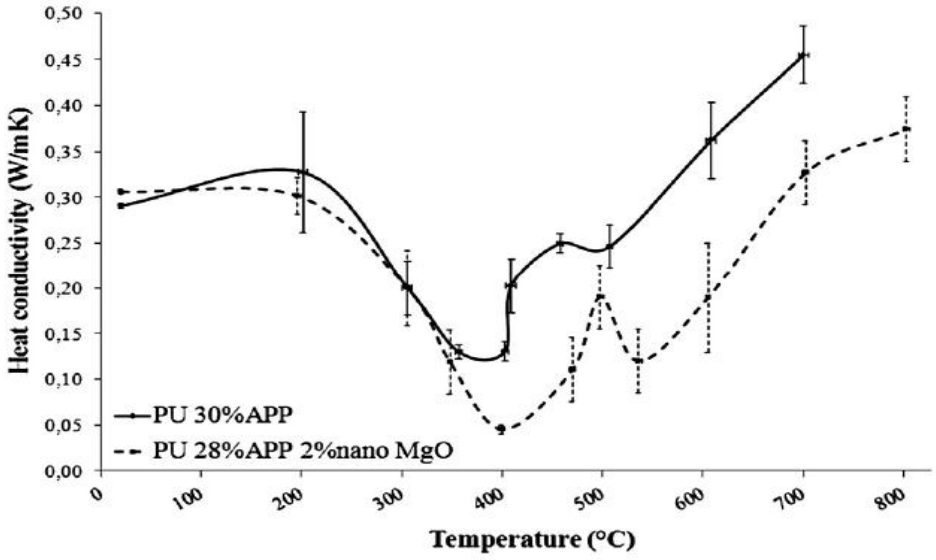

Figure 8 Evolution of heat conductivity as a function of temperature for intumescent polyurethane systems (PU30%APP and PU28%APP2%nano MgO) [115]

1.4.1.2 Viscosity, expansion and expansion rate

The viscoelastic behavior of an intumescent system during the expansion phase significantly affects the char morphology and thus the fire protection of intumescent coating [117, 118]. The formation of a multicellular char layer occurs via a semi-liquid phase that coincides with gas emission and expansion. Gases released from the degradation of the intumescent material and of a blowing agent, have to be trapped and to diffuse slowly in the highly viscous melt degraded matrix to create a char layer with an appropriate morphology as shown in Figure 9.

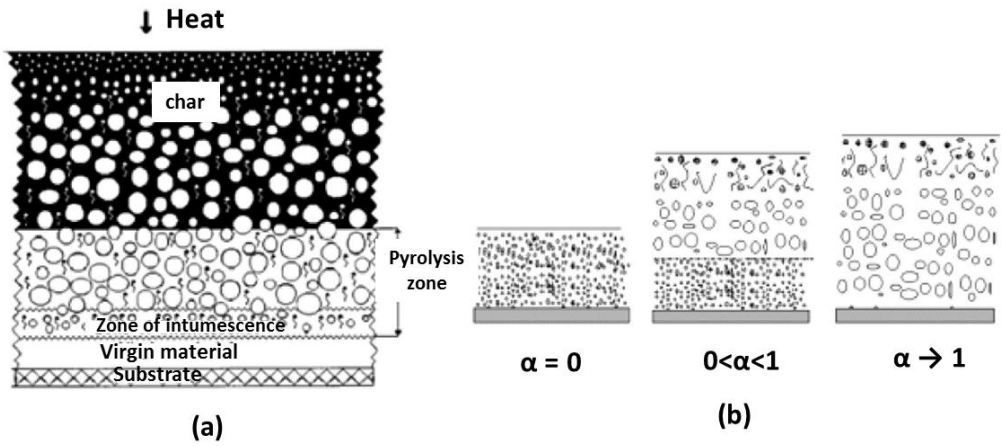

Figure 9 Schematic view of an intumescent coating with different zones (a) and intumescent development as a function of the conversion degree α (b) [18]

The control of the structure of the foamed residue relates not only to the gas formation process but also to the viscosity of the semi-liquid degraded matrix. Indeed, if the degraded matrix is too liquid, then the gases are not trapped but escape to feed the flame [20, 119] or dilute the gas phase. If on the contrary, the viscosity is too high, the expansion will be prevented. When the char structure is formed, if the shield becomes too hard, the creation and propagation of cracks may lead to a rapid degradation of the material [120].

Therefore, the viscoelastic properties of intumescent materials in the range of temperature corresponding to the development, stabilization and destruction of the protective char have to be investigated. Measurements of viscosity versus temperature at low heating rate (10 ^{o}C/min) can be done using a Rheometer in a parallel configuration as proposed by Bugajny et

al. in 1999 [119]. Duquesne et al. [20], in early 2002, proposed to follow simultaneously the change in viscosity and expansion using the same characterization tool by introducing an auto-adjustment of the gap between the plates during the measurements in order to keep the normal force at a set constant value. Jimenez et al. [81] implemented this method on epoxy based intumescent coatings and highlighted the interest of combining APP and H_3BO_3 in an epoxy resin both from the expansion and viscosity points of view (Figure 10).

This kind of measurements gives useful pieces of information to understand the behavior of different intumescent materials. However, this technique is not suitable for all materials, as it requires a char having a reasonable mechanical resistance when a normal force is applied. Moreover, the normal force applied might affect the expansion and the expansion under constraint is consequently measured. However, the heating rate used for such measurement is quite low and is not representative of a real fire scenario.

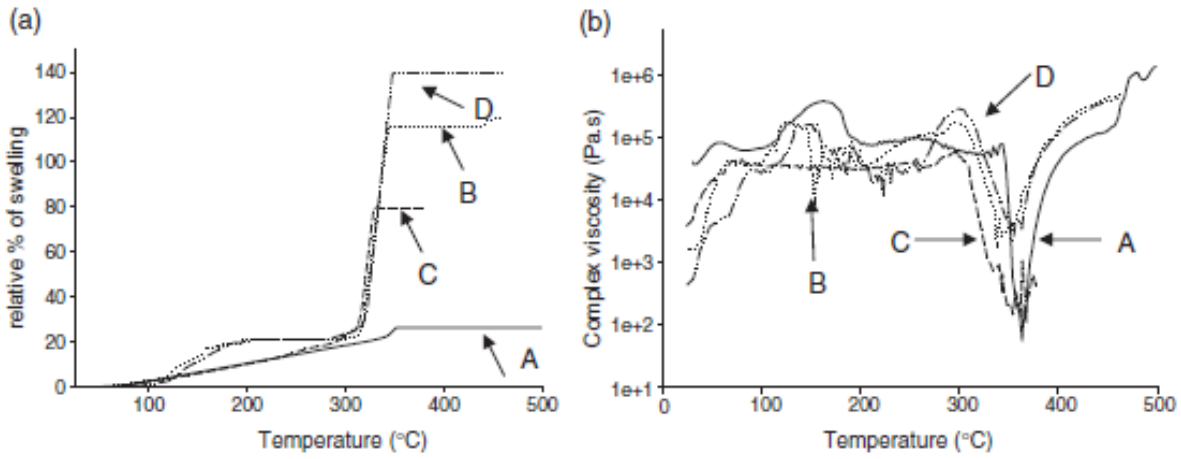

Figure 10 (a) Relative expansion (b) complex viscosity [81] of intumescent epoxy-based coatings (A: epoxy resin, B: epoxy resin+APP, C: epoxy resin+H_3BO_3, D: epoxy resin+APP+H_3BO_3)

Another approach to follow the ***dynamic expansion*** and ***expansion velocity*** was thus developed to perform measurement during fire tests (cone calorimeter or furnace test). Gardelle et al. [121] used two methods to quantify the expansion and expansion velocity of intumescent char. For the first one called 'static state', the furnace test mimicking UL1709 was stopped at different times and the thickness of the char was measured (ex-situ measurement). In a second approach, an infrared camera monitored the development of the char during a cone calorimeter

experiment. This allowed measuring the swelling versus time during a cone calorimeter experiment (in-situ measurement). Using these two methods, swelling of silicone-based coatings containing expandable graphite versus time could be obtained (Figure 11) and the velocity of expansion was calculated from the slope of the curve during the expansion step. It reached 18%/s in static method and 19%/s using dynamic method. The same authors also used the second approach (dynamic measurement using an infrared camera) to investigate the expansion rate of silicone based coatings for the fire protection of carbon fiber reinforced composites during a jet fire bench [122].

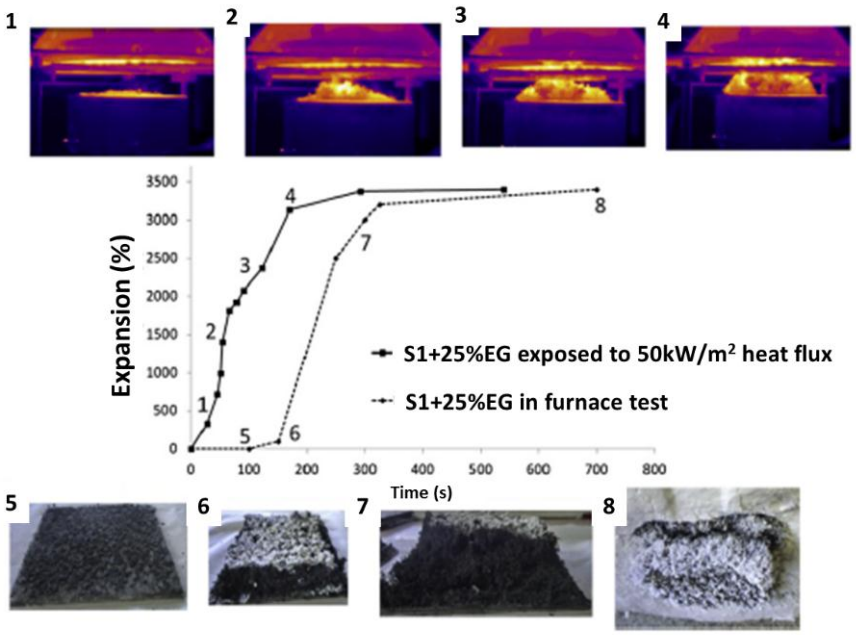

Figure 11 Expansion of silicone-based coatings versus times in dynamic (1-4) and static (5-8) state

Such measurements enable to follow the expansion versus time and are consequently very interesting. However, each of these tests presents different limitations. On the one hand, in the case of ex-situ measurement, each point of the curve requires the use of one sample and the repeatability of each measurement has to be checked at least by doing the experiment twice. Therefore, to be accurate, a great number of samples is required. Moreover, sometimes for the same formulation, the intumescence process and the creation of the foamed structure vary significantly from one sample to another. Consequently, for each measurement, the uncertainty

can be relative high. The measurements done on one sample by image analysis during a fire test, on the other hand, can be difficult to applied to other fire scenario (furnace test for example).

1.4.1.3 Char strength

Another important aspect of intumescent formulations is the strength of the char. Indeed, in case of jet fire scenario for example, the intumescent char is exposed to high pressure and erosion and thus its mechanical stability is highly important. The term 'strength' associated with char is used as a general term covering resistance to external mechanical constraints such as mechanical ablation by the flame application, influence of wind,… [18, 123]. The strength of char depends on both the structure and porosity of the foamed intumescent material as well as on the chemical composition of the char. Different methodologies are mentioned in the literature to evaluate this parameter.

In early studies, Reshetnikov et al. [124, 125] used various techniques to assess the mechanical strength of char of coatings designed for either buildings or space aircraft protection. These methods are in both hot and cold states. One described method was to find the minimum force necessary to destroy the char by inserting a rod through the heated sample at a temperature up to 1200 ^{o}C. Another method is used to measure the shear strength of the char at high temperature. The principle is to spin the sample at a controlled rate (1000 rounds/min), until the chars break at the weakest point. Both of these high temperature techniques are reported to perform well only in the case of low expansion factors (1.5 - 2).

Afterwards, Duquesne et al. [20] developed a dynamic measurement using 'a parallel plate configuration Rheometer'. Within this technique, the mechanical strength against compression as a function of temperature is obtained. The sample is heated with a desired ramp (up to 20 ^{o}C/min) to a specific temperature without any constraint. Then, maintaining the temperature at the chosen level, the upper plate is brought on the sample at a constant rate. The compression force linked to the mechanical properties of the char can then be measured as a function of the gap between lower and upper plates.

In 2013, an alternative method to investigate the mechanical stability of an intumescent char has been proposed by the Technical University of Denmark [19]. Samples were heated in a

muffle oven in atmosphere air (1100 °C) for 10 min. Char was then moved and placed on an aerated concrete stone next to the muffle oven to cool to 150 °C, before placing it in a desiccator. After cooling, the mechanical stability of the char was measured with a Texture Analyzer (Figure 12) recording the work necessary to move a cylindrical piston to a certain depth of the char. Note that an important limitation of this method is that the results are obtained at room temperature. This investigation is important for intumescent coating applied where objects may fall down on the coating during a fire and damage the char.

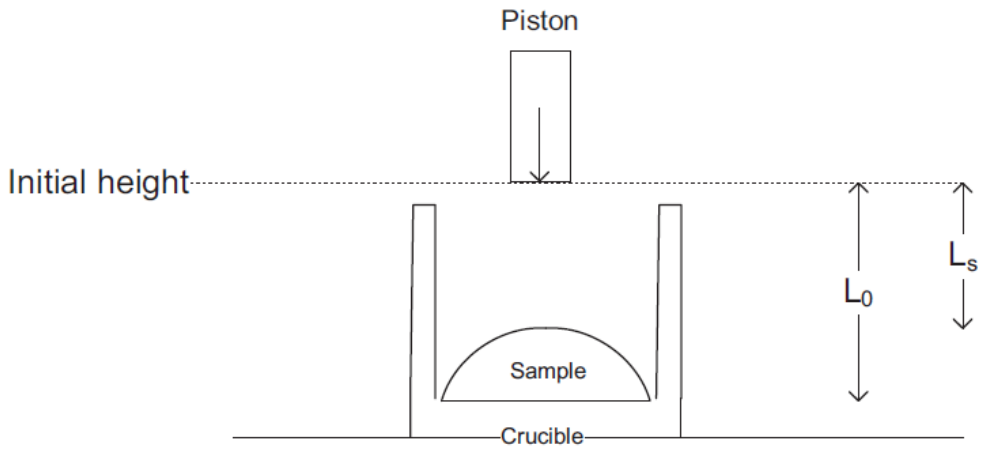

Figure 12 Schematic illustration of the Texture Analyzer used to determine the strength of an intumescent char. L_s and L_0 are the distance to the sample top and sample bottom from a selected initial height respectively. The height of the sample is the difference given by L_0 - L_s [19]

Recently, an in-situ experimental protocol was developed by Naik et al. [123] to evaluate the char strength of intumescent coatings on steel panel during hydrocarbon fire test. In that case, an air or nitrogen jet flow was used to impact the char and evaluate its stability regarding this stress. During the test, it is thus possible to monitor at the same time the physical integrity, mechanical stability, and thermal insulation capacity of intumescent coating. The system was applied to compare silicone-based products and a commercial epoxy based coating. It was shown that silicone based char exhibits higher strength than the epoxy one.

Muller et al. [126] investigated and compared several methods to demonstrate the effect of the preparation method of the char on its strength. They reported that the presence of a flame, heating type (convective or radiative heating), and quenching temperature do not modify the

mechanical properties of the resulting intumescent char. On the contrary, the critical parameters involved in the formation of a resistant char are the heating temperature and heating rate. Moreover, they show that the modification of the temperature at which the mechanical test is performed (in-situ vs. ex-situ measurement) leads to different results.

1.4.1.4 Morphology

The morphology of a char is one of the prime factors governing the fire protective properties of intumescent char (e.g. thermal insulation, mechanical resistance of char). The chemical composition of the degrading system as well as its physical properties (i.e. viscosity, expansion) will directly influence the morphology of the resulting charred structure [109]. Wang et al. [127] demonstrated, through a numerical approach, that the pore size should be small (within 50 µm) to obtain a good insulation of charred layer. Big, open and unevenly distributed holes with low strength of charred layer could damage the fire protective properties.

Characterization of the foamed char layer (e.g. cell size, closed or open cells, number of cells) with adapted techniques appears as an indispensable way to better understand the reaction between ingredients and fire performance obtained. However, it is not an easy task.

The morphology of intumescent char can be visualized at various scales depending on the scale of interest. It includes visual observation, digital photography, optical microscopy, scanning electron microscopy (SEM), transmission electron microscopy (TEM) as well as 3D X-ray tomography.

As an exemple, Gérard et al. [128] observed the char morphology of intumescent epoxy resins using a digital photographer. In that case, it is necessary to cut off the char without damaging the sample to obtain a cross-sectional image. This can provide a visual observation on how char looks like and allows comparing the char aspects of different samples. The same researchers [129] used an optical microscope to characterize the morphology of the surface or cross-sectional cut of the charred residue after heat treatments. It also allows observing the char surface (e.g. cell size). This technique can provide a clearer view of char residues compared to a numeric photographer. It can also scale the dimension of porous structure.

The well-known and commonly used microscopies such as SEM and TEM are also widely used in the field of research and development of flame retardant systems particularly in the case of fire protective materials [130-132]. They provide information on the microstructures of the studied char, dispersion of additives, crystallinity of species, dimensions of the fibers...

To study the morphology of the char, samples have to be cut off to observe the cross section of samples but the integrity of the inner structure cannot be guaranteed during the preparation of samples. To overcome this issue, X-ray computed tomography (non-destructive technique) appears as a technique of choice. Muller et al. [115] used this technique to acquire 3D images of charred structure of intumescent polyurethane containing FR additives (i.e. APP and nano-MgO). Interestingly, they correlated the obtained morphology with the thermal conductivity of the formed char. By using this technique, the intumescent process can be more precisely characterized. The application of X-ray computed tomography was also appeared in the work of Morys et al. [133] who used this technique to study the intumescent process and char properties of different intumescent coatings. This superior research tool was also combined with SEM and mechanical testing to investigate the char obtained after exposition to a standard time temperature muffle furnace. Apart from the precious information provided by X-ray computed tomography, it however has some limitations including a long scanning time and difficult treatment of data to obtain quantitative information [134]. Moreover, this technique, at the present time, does not permit to make an in-situ measurement.

1.4.2 Chemical analyses

In addition to the char thermo-physical properties (i.e. thermal conductivity, viscosity, expansion, expansion rate, char strength, morphology) which are described in the previous section, chemical composition of char is also an important factor among all. When intumescent coatings degrade, the carbon and organic materials originally present in the intumescent formulation react with the other ingredients of the formulation. The resulting residues generally consist in a mixture of carbonaceous char and inorganic compounds, which are formed during the intumescent process by the reactivity between ingredients. The chemical composition of the char is reported to influence significantly the fire protective performances of intumescent coatings [66, 109] and thus need to be investigated. Since charred structures are poorly soluble in traditional organic solvents, most of the techniques used are solid-state analyses.

Various analytical techniques have been used for the chemical analyses of intumescent char residues. The techniques widely reported in the literature include Fourier Transform Infrared Spectroscopy (FTIR), Raman Spectroscopy, X-ray Photoelectron Spectroscopy (XPS), Scanning Electron Microscope associated with Energy Dispersive X-ray Spectrometer (SEM-EDX), Electron Probe Micro-Analysis (EPMA), X-Ray Diffraction (XRD) and solid state Nuclear Magnetic Resonance (NMR).

FTIR can be a first choice for a char analysis due to its simple use [59, 62, 135, 136], it can indicate bonding types and functional groups but it cannot provide information on the fine structures. Raman spectroscopy is also useful to investigate the ordered level of carbonaceous structure (from well-ordered graphite to a disordered carbon structure) [137]. XPS is used to elucidate the elements present in a sample in a semi-quantitative way. In addition, the XPS spectrum of specific element can be used to investigate the chemical structure [30, 138]. It can be a good complement to other techniques. As an example, the ^{15}N solid state NMR requires a long scanning time for a measurement because of the low isotropic abundance of ^{15}N (0.4 %). XPS can thus be used in this case instead of solid-state NMR to investigate the structure of nitrogen. Nevertheless, it allows analyzing only the extreme surface of the sample. EPMA allows elucidating the distribution of interesting elements on char surface or cross-section of char [138, 139]

similarly to SEM-EDX [140]. XRD is a conventional technique, which allows identifying the formation of crystalline compounds. The use of XRD in this research field is extensively implemented [83, 94, 141] but is limited to crystalline compounds. Finally, solid state NMR is a technique of choice to characterize intumescent structure and this technique has been widely used [59, 137].

Solid state NMR is a very useful technique for char analyses. It provides not only the chemical composition but also the structures of studied materials. The measurements can be performed with elements having a non-zero spin of nuclei and can be considered as an advanced analytical tool depending on the nuclei and techniques (e.g. 2D NMR). The main advantage of NMR spectroscopy is its selectivity on specific nucleus. Furthermore, quantitative measurements can be performed, when the parameters are chosen correctly (importance of the time of spin relaxation). On the other hand, experiment can be time consuming. As an example, when dealing with ^{13}C NMR studies, the low natural abundance of ^{13}C isotope (1.1 %) [142] coupled with the weak interactions between each ^{13}C nucleus and important distances between isolated ^{13}C spins and nearest unpaired electron result in long spin relaxation time causing long time experiments.

Since two decades, our laboratory in Lille has used quite intensively 1D solid state NMR to characterize fire protected samples [59, 137, 143]. Solid state 1D NMRs of various nuclei (e.g. ^{11}B, ^{13}C, ^{27}Al, ^{29}Si, ^{31}P,) were realized, which provide for example information on the evolution of carbonaceous structure of char residue (^{13}C NMR) [136], of phosphorus and of boron containing species in the condensed phase versus temperature (^{31}P and ^{11}B NMR) [83] etc…

Recently, with advanced tools and methods, solid state NMR has become more and more performant. Advanced NMR techniques are widely applied in various research fields such as 2D NMR sequences. In the field of flame retardancy, Karrasch et al. [144] studied flame retardant mechanisms in the condensed phase of bisphenol A polycarbonate and silicone acrylate rubber blends after pyrolysis. $^{31}P\{^{1}H\}$ and $^{13}C\{^{31}P\}$ Rotational Echo Double Resonance (REDOR) were used to estimate the distance between P atoms in different structural units and the surrounding protons and the distance between the various C atoms and the surrounding P atoms respectively. 2D Heteronuclear Correlation (2D HECTOR) was also used to investigate the various types of

protons present. Another work by Sut et al. [58] used double resonance NMR technique including REDOR and Transfer of Population in Double Resonance (TRAPDOR) to deeply elucidate the chemistry behind the interactions in multicomponent flame-retardant polymers. Such techniques provide additional information which were not given when using 1D NMR.

1.4.3 Conclusion

To conclude, this section described the most common and recent characterization methods that have been used to investigate char properties; it includes the thermo-physical properties and chemical composition of char. To explore the chemical reactivity and draw the mechanism of action of intumescent systems, it is very important to use different methods and to compare the obtained results.

1.5 Conclusion

In this chapter, the basic knowledge and current state of the art on intumescence in general and on intumescent coatings in particular were reported. Concept of intumescence, intumescent process and mechanism, as well as main ingredients of intumescent coatings and associated fire tests were reviewed. A focus was made on epoxy based intumescent coatings. It was concluded that, even if some literature deal with the reactivity between two or three ingredients, the reactivity of these ingredients inside the complex intumescent formulation is rarely reported. Systematic approaches in the case of boron based flame retardant and carbonate systems are still missing.

In this context, this work focuses on the investigation of ***the mechanism of action of epoxy based intumescent coatings with a particular attention dedicated to boron-based compounds and carbonates***. The studied formulation contains phosphorus-based compounds (i.e. APP), borates, fibers, titanium dioxide and calcium carbonate as main ingredients. Referring to the literature, borates (and especially boric acid) are mentioned as crucial ingredients in intumescent coatings providing specific properties to a protective char to pass hydrocarbon fire test. However, no systematic approach is reported and the environmental concern related to boric acid should lead to mandatorily substitute it. ***The first goal of this work*** is thus to better understand the role of borates inside a complete intumescent formulation that can be used to protect steel against hydrocarbon fire. These results will be presented in chapter III of this dissertation. Not only borates but also other components react and play a significant role in intumescent formulations. From this point of view, the comprehension of the reactivity between the intumescent ingredients should be taken into consideration. In this fire protective coating, the mode of action of carbonates has been reported but is still controversy. Therefore, ***the second objective of this work is to identify the mode of action of carbonate compounds***, which are used as fillers in the coating. The results are detailed in chapter IV of this dissertation. Before going into details regarding the results, chapter II details the materials and methods which were used in this project. It provides information on how the experimental research work was realized.

Chapter II: Materials and methods

This PhD thesis focuses on the mechanisms of action of intumescent coatings in a fire: questions remain on how the charred layer is formed, on the role and interactions of each component of the formulation. The materials and methods used in this study are detailed in this chapter. First, the preparation methods of the epoxy based intumescent coatings are described. The sample preparation is specific for each analysis, so they are fully described. Then, the furnace test used to assess fire protective performance of the coatings and heat treatment conditions are presented. Finally, the characterization methods used to assess thermal, physical and morphological properties of the coatings and char are described.

2.1 Materials

The study was performed on an intumescent coating. The formulation hereafter called IF(BA) which is formulated by the industrial partner is used as a reference; it is a conventional and efficient intumescent formulation. The compositions as well as the commercial names and suppliers of the different ingredients are summarized in Table 6. The formulation is divided into two parts: part A based on the epoxy resin and part B based on the curing agent (aliphatic polyamide amine).

Table 6 Compositions of IF(BA) formulation

Description	Commercial name (supplier)	Part B (%w/w)	Part A (%w/w)
Aliphatic polyamide amine	Ancamide 903 MAV (Air Products)	17.59	
Calcium Carbonate or Dolomite	Micral 5 (Reverté)	1.91	
Based on ammonium polyphosphate	Exolit AP 755 (Clariant)	2.20	8.54
Titanium dioxide, rutile	Tronox CR-826 (Huntsman)	0.37	
Natural, expanded silicate	Rotocell 0,5 mm (Rotec)	1.07	0.57
Composite reinforcement, Man-made vitreous (silicate) fibers	Rockforce MS603-Roxul1000 (Lapinus)	2.64	1.28
Composite reinforcement, Man-made vitreous (silicate) fibers	Rockforce MS605-Roxul1000 (Lapinus)	3.16	1.28
Bisphenol A diglycidylether epoxy	Epikote 828 (Momentive)		31.20
Tris(2-chloroisopropyl)phosphate (TCPP)	Fyrol PCF (ICL)		8.03
Carbon black	Lamp Black 101 (Orion engineered carbons)		0.06
Fumed silica	AEROSIL R 8200 (Evonik)		0.85
Boric acid	Optibor (20 Mules team)		19.25
Total (% w/w)		**28.94**	**71.06**

One objective of this work is to compare systematically the effects of different borates (i.e. boric acid, zinc borate, borax and Ammonium pentaborate (APB)). To follow this purpose, boric acid in the reference formulation was substituted by another borate (i.e. zinc borate, borax or APB). It was made by maintaining the molar content of boron (B) constant. The corresponding formulations are called IF(ZB)m, IF(borax)m and IF(APB)m respectively. The formulation details are presented in Appendix I.

Table 7 describes the properties, chemical structures and suppliers of the different borates used in this study.

Table 7 Suppliers, properties and chemical structures of boric acid, zinc borate, borax and APB

Properties	Boric acid	Zinc borate	Borax	APB
Formula	H_3BO_3	$2ZnO.3B_2O_3.3.5H_2O$	$Na_2B_4O_7{\cdot}10H_2O$	$NH_4B_5O_8.4H_2O$
Commercial name	Optibor	Firebrake ZB	Borax decahydrate	Ammonium pentaborate
Supplier	20 Mule team	20 Mule team	20 Mule team	20 Mule team
Molecular weight (g/mol)	61.8	434.5	381.4	272.2
Density (g/cm^3)	1.51	2.60	1.73	1.58
Decomposition (Dehydration Temp)	100 °C	290 °C	75 °C	110 °C
Wt. % of boron (B)	17.5	14.9	11.3	19.9
Water release (wt. %)	44	14	46	37
Chemical structure	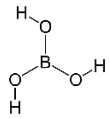	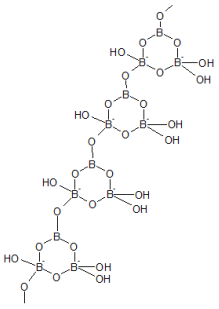	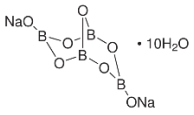	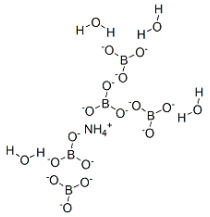

Instead of molar substitution, another approach consists in weight substitution. This approach was however only performed in the formulation containing zinc borate. Boric acid was thus substituted by zinc borate in weight ratio. The formulation is named IF(ZB)wt, it is also presented in Appendix I.

Another objective of the work is to study the role of carbonates including calcium carbonate. In a first step, the formulations were simplified to be able to investigate precisely the influence of calcium carbonate ($CaCO_3$) on fire protective performances. The compositions of the studied formulations are presented in Table 8. First, formulations containing only APP and borate were formulated and were used as reference formulations (IF-APPBA and IF-APPZB). $CaCO_3$ was then added into these two formulations leading to IF-APPBACa and IF-APPZBCa formulation. Another formulation without boron was also studied. It consists of a mixture between the binder, APP and $CaCO_3$ and it is referred as IF-APPCa. For all those formulations, the ratios between the additives are similar to those of IF(BA) formulation (molar ratio).

Table 8 Compositions of IF-APPCa, IF-APPBA, IF-APPBACa, IF-APPZB and IF-APPZBCa

	IF-APPCa	IF-APPBA	IF-APPBACa	IF-APPZB	IF-APPZBCa
Epoxy	31.97	31.97	31.97	31.97	31.97
Curing agent	18.03	18.03	18.03	18.03	18.03
APP	38.7	12.68	11.8	12.68	11.8
H_3BO_3 or BA		37.32	34.75		
ZB				37.32	34.75
$CaCO_3$	11.3		3.45		3.45

In a second step, the influence of various carbonates (including magnesium, zinc, sodium and potassium carbonates) on the fire protective performances of the intumescent coatings was also investigated. The formulations were made by substituting $CaCO_3$ in **IF-APPBACa** by another carbonate compound, the substitution is made by maintaining the weight ratio. The formulations were named IF-APPBA$MgCO_3$, IF-APPBA$ZnCO_3$, IF-APPBANa_2CO_3, and IF-APPBAK_2CO_3 respectively.

The properties of the studied carbonates are presented in Table 9.

Table 9 Suppliers and properties of $CaCO_3$, $MgCO_3$, $ZnCO_3$, Na_2CO_3 and K_2CO_3

Properties	$CaCO_3$	$MgCO_3$	$ZnCO_3$	Na_2CO_3	K_2CO_3
Commercial name	Micral 5	Magnesium carbonate	Zinc carbonate	Sodium carbonate	Potassium carbonate
Suppliers	Reverté	Acros	Prolabo	Carbo Erba	Sigma Aldrich
Molecular weight (g/mole)	100	84.3	125.4	106	138.2
Density (g/cm^3)	2.71	2.96	4.44	2.54	2.43
Decomposition temperature (^oC)	680-900 [87, 88]	620-650 [145]	300-452 [146, 147]	850 (SDS)	890 (SDS)
CO_2 release (% wt.) by calculation	44	52	35	41.5	31.8

2.2 Methods

2.2.1 Sample preparations

2.2.1.1 Fabrication of the coatings

The coatings were prepared using a DISPERMAT mixer (VMA Getzman GMBH, D-51580 Reichshof). The epoxy part (part A) and curing agent part (part B) were prepared separately. First, the liquid components (e.g. epoxy resin and TCPP for part A/curing agent for part B) were stirred for about 3 - 5 minutes with a low rotational speed (300 - 400 rpm, Ø = 50 mm). Then, all solid ingredients (e.g. ammonium polyphosphate (APP), boric acid, zinc borate, TiO_2, fumed silica) were added into the mixture. They were then mixed together for 30 - 50 minutes at high rotation speed (1800 - 2200 rpm) until the temperature of the mixture reached 55 - 60 ^oC. The rotation speed was then decreased before adding the mineral silicate fibers, in order to avoid shortening the fiber length. After finishing the preparation, part A and part B were stored separately and mixed together in the recommended ratio by a mixing device. The mixing ratio in weight was 3.44 of part A/1.00 of part B for all formulas.

2.2.1.2 Preparation of the coatings for fire test

100 x 100 x 3 mm^3 steel plates (S235) were blasted with steel grits of 75 - 100 microns to clean the surface, increase its roughness profile and improve the adhesion of the coatings. The industrial partner prepared the steel plates. The blasted steels were kept in a tightly closed container with silica gel to avoid the rust formation during the shipment and storage. Moreover, to improve the adhesion, a primer (Epodux Zinc 57 - 35, zinc epoxy primer: Maestria) was applied with a thickness of 50 - 100 µm on top of the steel plate before applying the coatings.

The mixture of part A and part B with the recommended ratio was applied on the steel plate and the coating was cured at ambient temperature over a 48 hours period (Figure 13). The thickness of the coating was in the range of 4 ± 0.2 mm. To control the thickness, the cured coatings were polished with a belt sander (Scheppach bts 800) to get the required thickness. The thickness was measured using an ultrasonic thickness gauge (Elcometer 456).

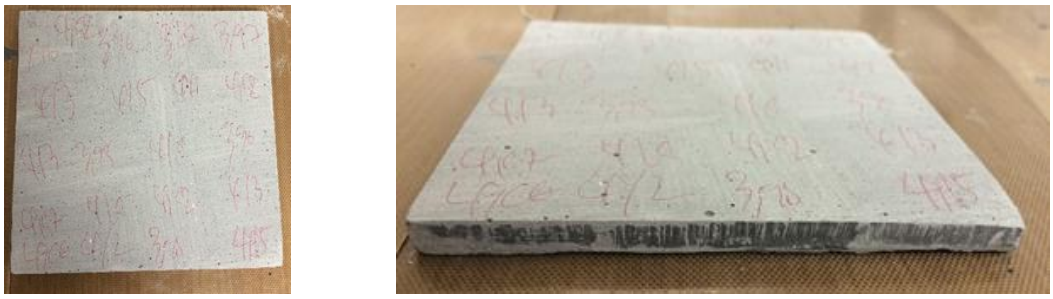

Figure 13 Photos of 100 x 100 x 3 mm^3 steel plate coated with 4 mm of intumescent coating

2.2.1.3 Preparation of the coatings for thermal analyses, heat treatments and chemical analyses

To perform thermal analyses, heat treatments and chemical analyses, part A and part B were mixed in the mentioned ratio. The mixture was deposited in a plastic bag and cured at ambient temperature over a 48 hours period. The cured material was then ground using an ultra-centrifugal mill to produce a fine powder.

2.2.1.4 Preparation of the coatings for Rheometer test

Part A and part B were mixed in the mentioned ratio and deposited in Teflon mold to obtain disks of 25 mm of diameter and 1 mm of thickness (Figure 14). Those disks were used for rheological, expansion and mechanical measurements. The coatings were also cured for at least 48 hours before performing measurements.

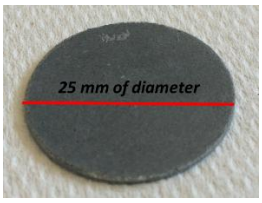

Figure 14 Sample of 25 mm of diameter and 1 mm of thickness for Rheometer test

2.2.1.5 Preparation of the coatings for thermal conductivity measurements

The samples prepared for Hotdisk measurements (see the section 2.2.3.2) correspond to a disk of 25 mm of diameter. A mixture of part A and part B in the previously defined ratio was put into two Teflon mold having a diameter of 25 mm. A mica sensor was then placed between two disks and the coatings were cured at ambient temperature for at least 48 hours. This ensures a good contact between the sample and the sensor during the measurement. The thickness of the sample was adjusted to have enough material to give the heat impulsion during the test and to avoid an overflow of the char formed in the sample holder. The setup of the sample in the specific device to perform measurements at high temperature is presented in Figure 15.

Figure 15 Sample installation for thermal conductivity measurement

2.2.1.6 Char preparation for chemical analyses

Cured coatings were exposed to various heat treatments (see section 2.2.2.2) to obtain a char. The collected char or the residue obtained after furnace tests (see section 2.2.2.1) was ground using a mortar to obtain fine and homogeneous powder for chemical analyses. The powder as well as char residue were kept in a desiccator before any analyses to avoid the modification of chemical species due to the humidity.

2.2.2 Furnace test and heat treatment

2.2.2.1 Furnace test (UL 1709)

To avoid an expensive and time-consuming experiment in a large industrial furnace test, a small-scale furnace test was developed in the laboratory to evaluate the fire performance of intumescent coatings mimicking the UL1709 hydrocarbon fire scenario.

The lab scale furnace (Figure 16) exhibits an internal volume of 26 dm^3. Refractory fibers (stable up to 1300 ^oC) cover the sides of the furnace. The furnace is equipped with two 20 kW propane burners. The gas pressure was fixed at 1.8 bars and the gas flow was controlled in order to mimic the UL1709 curve. The furnace is equipped with a quartz window allowing an observation of the intumescent event during the test. The sample is placed into the sample holder, which is located in the midst of the front gate of the furnace. The sample is mounted in a vertical position; the adhesion and cohesion of a foamed char during the fire test are evaluated simultaneously. The backside of the steel plate is insulated by a mineral wool (ECOSE® Technology) which is put on four borders.

To obtain the time-temperature curve, a thermocouple is welded on the backside of steel plate. To ensure the repeatability of the experiments, each formulation was tested at least twice.

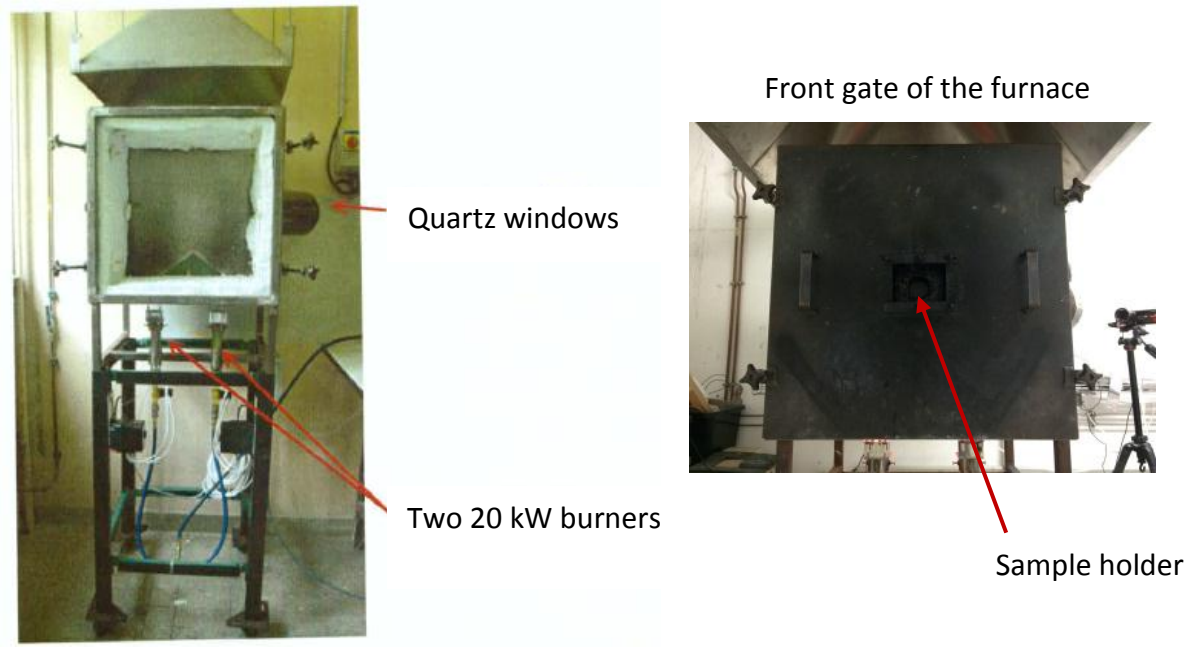

Figure 16 Small-scale furnace test

2.2.2.2 Heat treatments

Thermal treatments consist in heating a sample in a furnace (Figure 17) at a defined temperature. To perform heat treatments (HT), powder sample (≈ 2 g) was placed in a porcelain rectangular crucible (45 mm x 25 mm) and then inserted in a tubular furnace. Before heating, the sample was maintained at 30°C under inert atmosphere (nitrogen flow, 60ml/min) for 1 hour in order to purge air. The temperature was increased with a heating rate of 10 °C/min from 30 °C up to a chosen heat-treatment temperature (HTT). The sample was maintained at this temperature for 2 hours under nitrogen flow and then cooled down to ambient temperature without any defined cooling rate (still under nitrogen). Only the upper part of the sample was collected and analyzed to avoid any potential interaction between the intumescent coating and the porcelain. After heat treatments, the residue was kept in a desiccator to avoid its hydrolysis until analyzing. The samples were weighted before and after heat treatment to calculate the residual weight percentage.

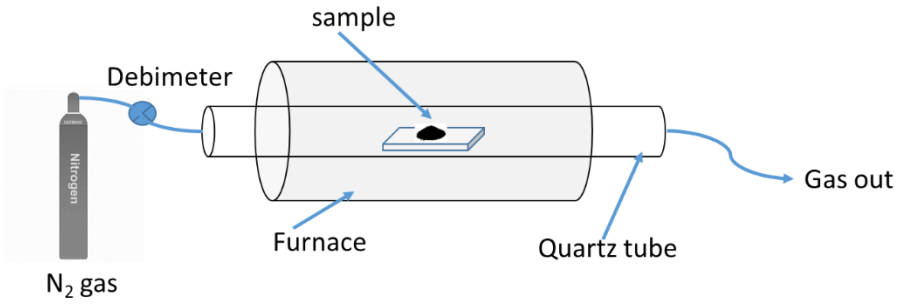

Figure 17 Schematic representation of heat-treatment

2.2.3 Thermal characterizations

2.2.3.1 TG analyses

Thermo-Gravimetric Analyses (TGA) were carried out using TGA Discovery (TA instrument). Samples of 10 ± 0.3 mg were put in an alumina plan covered with a gold sheet to avoid the interaction between alumina pan and phosphorus-based compounds. Samples were underwent an isothermal at 30 ^{o}C for 30 minutes followed by a heating ramp of 20 ^{o}C/min from 30 ^{o}C to 800 ^{o}C or 1000 ^{o}C under air or nitrogen flow to mimic thermo-oxidative or pyrolytic decomposition respectively. The balance purge flow was set to 15 ml/min whereas the sample purge flow was set to 50 ml/min.

To determine if there is or not some reactions occurring between the components, the weight difference curves between the experimental and theoretical data can be computed as follows:

- M_i (T): TG curve of the component i,
- x_i is the content of component I in the formulation
- M_{exp} (T): TG curve of the intumescent coating
- M_{cal} (T): calculated TG curve computed by linear combination between the values of weight given by TG curves of the component i, ii,…, n: M_{cal} (T) = $\sum_i^n xi\ Mi(T)$
- Weight difference curve: Δ(T) = M_{exp} (T) – M_{cal} (T)

The Δ(T) curve shows a potential increase or decrease in the thermal stability of a mixture. When the experimental curve is higher than the theoretical one (or when the difference weight loss curve is positive), it indicates that the reactivity leads to a thermal stabilization of the materials. If the experimental curve is lower than the theoretical one (negative difference weight loss), the reactivity leads to a thermal destabilization of the systems.

2.2.3.2 Thermal conductivity measurements

The thermal conductivity of a material describes the transport of energy in form of heat through a material. In this work, the thermal conductivity was measured using Hot Disk thermal constant analyzer (Hot Disk TPS 2500S, Thermoconcept). The used technique is the so-called

transient plane source method equipped. The systems can be used in a furnace that has been designed for our research area, allowing measuring the thermal conductivity as a function of temperature up to 700 °C. The data are acquired by using the Hot Disk Thermal Analyzer software. The sensor, which acts as both a heater and a thermocouple, is placed in the middle of the samples (Figure 18; see section 2.2.1.5 for details concerning the preparation of the sample). The sensor typically consists in a thin layer of an electrically conducting material. During the experiment, a current passes through a nickel spiral which leads to an increase in temperature. Then, the generated heat dissipates through the sample depending on the thermal characteristic of the tested material.

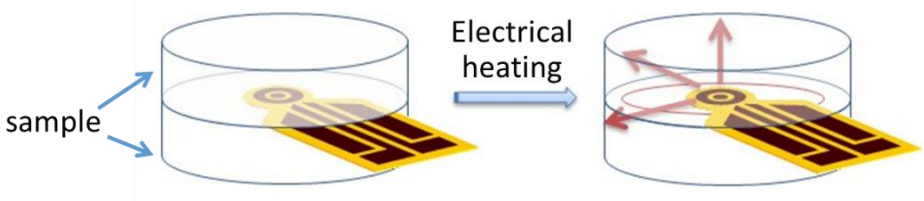

Figure 18 Experimental setup of transient plane source method

To be able to perform a measurement as a function of temperature, the furnace is directly connected to Hot Disk instrument. The furnace is purged under nitrogen flow and all experiments were carried out in an inert atmosphere to prevent the oxidation of the sensor. Mica sensor with a diameter of 3.2 mm was used for these measurements (the smallest diameter exists).

Measurements have been carried out at the following temperatures: 25, 100, 200, 300, 400, 500, 600 and 700 °C (with a precision of around ± 0.1 °C). The thickness of the coating has to be adjusted depending on the temperature since the relative expansion varies. To perform a measurement in the temperature range 25 °C to 300 °C, the thickness was fixed at 8 mm. From 300 °C, the thickness is decreased to 2.5 mm to eliminate the constraint between expanded char and sample holder due to an expansion and to avoid an overflow of char in the sample holder. The heat pulse power and measurement time were adjusted for each sample and at each temperature to be optimized. Power varies between 10 - 70 mW and measurement time is comprised between 5 and 40 s, thus insuring the reliability of the measurements. To ensure a good repeatability, each measurement was performed twice.

2.2.4 Physical characterizations

2.2.4.1 Rheological measurement

Rheological measurements were carried out using a Rheometric scientific ARES 20A thermal scanning rheometer (TSR) in a parallel plate configuration (Figure 19). The change of viscosity as a function of temperature was monitored up to a maximum temperature of 500 °C.

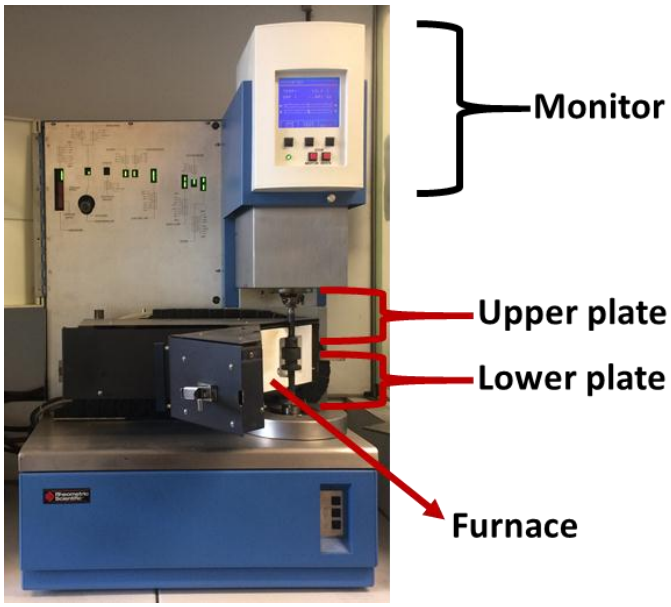

Figure 19 Rheometer in a parallel plate configuration

To perform a measurement, a disk of coating (25 mm of diameter and 1 mm of thickness) was placed between the two plates. A hollow cylindrical sample holder of 32 mm internal diameter (20 mm height) and an upper plate of 25 mm diameter were used for this study. A constant normal force of 10 ± 2 g was systematically applied to obtain a good contact between the sample and the plates. The heating program used was a 'dynamic temperature ramp test' with a heating rate of 10 °C/min in the range 25 - 500 °C and a strain of 1 % was applied. The experimental scheme is shown in Figure 20.

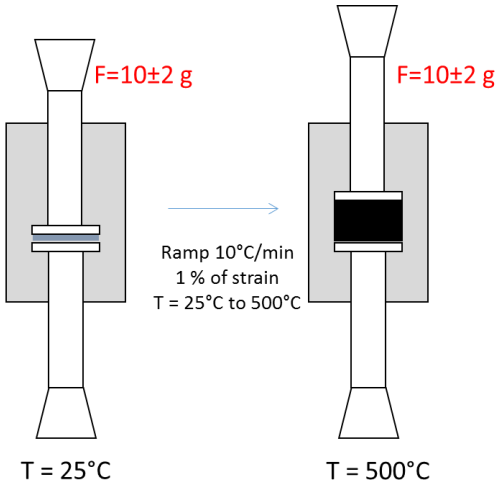

Figure 20 Measurement of viscosity

2.2.4.2 Expansion measurements

To measure the expansion of char, two approaches can be followed: i) to use the Rheometer and ii) to measure the expansion of the foamed char after the furnace test. The details are described in the following part.

2.2.4.2.1 Rheometer test

The first method consists in the use of the Rheometer test. The expansion can be recorded at the same time as viscosity (previously described). The gap variation between the upper and lower plates was registered as a function of temperature during the test using the same experimental parameters. The relative expansion is calculated referring to the gap increase (I) versus an initial thickness (l_0) of the dry coating (eq. 30).

$$\text{Expansion} = l/l_0 \times 100 \qquad \text{(eq. 30)}$$

2.2.4.2.2 Furnace test (UL 1709)

The relative expansion can also be calculated by comparing the thickness of the dry coating (before the furnace test) and of the foamed char (after the furnace test). The foamed char thickness was measured using a ruler and the thickness of the dry coating was measured using an ultrasonic thickness gauge (Elcometer 456). At least six measures were taken over a char surface and dry coating to determine an average of the values.

2.2.4.3 *Char strength measurements*

The mechanical strength of intumescent coatings was determined by measuring the char compression resistance using Rheometric scientific ARES 20A thermal scanning rheometer (TSR) in a parallel plate configuration (the same as used for the measurements of viscosity and expansion but with a different protocol). This method allows measuring online the mechanical strength of char in function of temperature. First, the sample of 25 mm of diameter and 1 mm of thickness was put into the Rheometer furnace and was heated with a heating rate of 10 °C/min up to 500 °C without applying any strain (the upper plate is not in contact with the sample). This allows the sample to expand without any constraint.

The temperature was then maintained at 490 °C. At this temperature, the upper plate was then brought into contact with the intumescent char, and the gap between the plates was reduced at a fixed rate (0.02 mm/s). The compression force required to destroy the char was registered as a function of the distance between the two plates and corresponds to the char strength. The sample holder is the same as that used for expansion and viscosity measurements. The upper plate used in this experiment has however a diameter of 5 mm in order to increase the pressure on the whole sample and ensure a complete destruction of the char. The experimental scheme is shown in Figure 21.

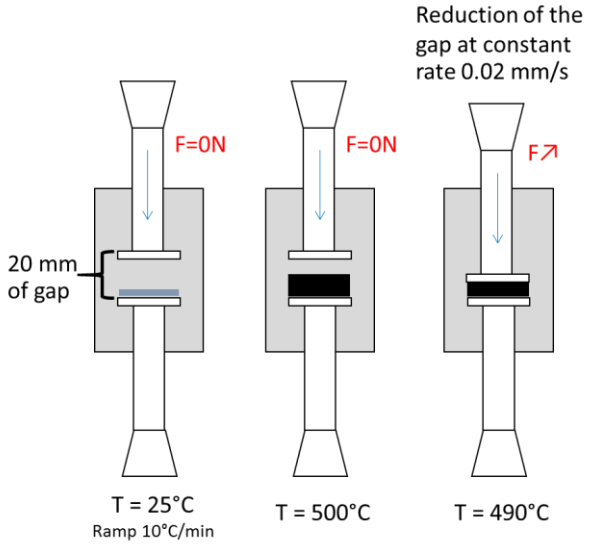

Figure 21 Protocol to measure mechanical resistance of char

2.2.5 Chemical characterizations

2.2.5.1 X-ray diffraction

XRD spectra were recorded in the 5° - 60° 2θ range using a Bruker Advance D8-A25 diffractometer ($\lambda_{Cu\text{-}K\alpha}$ = 1.5418 Å, 40 kV, 40 mA) in configuration θ/θ. The acquisition parameters used were the followings: a step of 0.02 °, a step time of 0.5 s. The data were analyzed using the diffraction patterns of Inorganic Crystal Structure Database (ICSD).

2.2.5.2 Solid state NMR

Solid state NMR is a powerful technique for structural analyses. The conditions used for the analyses are detailed hereafter. All NMR data were obtained at room temperature.

When performing solid-state NMR measurements, the large number of protons in the sample interferes with decay of the isolated nucleus due to weak interactions of the spins. The dampening of the signal can be removed by a strong radio frequency signal, which holds the protons in a highly resonating state so that they are not capable of absorbing resonance from the nuclei. This is called ^{1}H dipolar decoupling (DD). On the other hand, in a solid state, the chemical shift anisotropy (CSA) has a severe effect on the spectra resulting in broadened peaks. This effect is worsened when the mobility of the chains or molecules decreases. Through a tensoral analysis of the magnetic moments in a molecule, it is possible to demonstrate that a ''Magic Angle'' exists with respect to the applied magnetic field at which rapid spinning of the solid sample minimizes an absorption line broadening due to chemical shift anisotropy. This angle is called 'magic angle spinning or MAS'.

1D ^{13}C solid-state NMR measurements were performed on a Bruker Avance 400 at 100.8 MHz (9.4 T) with MAS (magic angle spinning), high power 1H decoupling (DD) and ^{1}H - ^{13}C cross polarization (CP) using 4 mm standard probe. For all samples, a recycle delay (d1) is set at 3 s, a contact time at 1 ms and a spinning speed at 12.5 kHz. All spectra were acquired as the result of 2048 scans. Tetramethylsilane (TMS) was used for the calibration.

1D ^{31}P solid-state NMR measurements were performed on a Bruker Avance 400 at 162 MHz (9.4 T) with MAS (magic angle spinning) and high power ^{1}H decoupling (DD) using 4 mm standard probe. For all samples, a recycle delay is set at 120 s (^{31}P has a long relaxation time, T_1) and a spinning speed at 12.5 kHz. All spectra were acquired as the result of 8 or 16 scans. H_3PO_4 in aqueous solution (85%) was used for the calibration.

1D ^{11}B solid-state NMR measurements were performed on Bruker Avance III 800 at 256.6 MHz (18.8 T) with MAS (magic angle spinning) using 3.2 mm probe. In this study, MAS ^{11}B NMR at high magnetic field (18.8 T) was used in order to eliminate the quadrupolar interaction and separate the peaks of BO_3 and BO_4 units. ^{11}B spectra were obtained through direct observation. The recycle delay of 10 s or 30 s (depending on the relaxation time) and a spinning speed of 20 kHz were used. All spectra were acquired as the result of 128, 64 or 32 scans. Before measuring, the calibration was done using $NaBH_4$ (characteristic peak is - 42.06 ppm). The deconvolution of the spectra has been carried out using the software DMFIT [148], assuming Gaussian/Lorentzian and Q MAS ½ (quadrupolar lineshape). The simulation allows distinguishing different boron structures. An example of the simulated curves is shown in Figure 22a. By visual observation, it is not obvious to differentiate BO_4 units whereas two types of BO_4 units can be clearly differentiated by simulation as shown in Figure 22b.

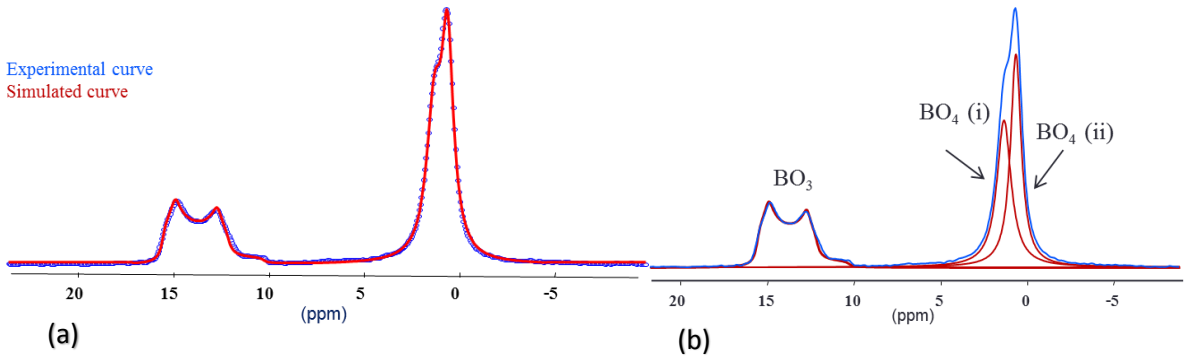

Figure 22 Example of simulated ^{11}B NMR spectrum (18.8 T) using the software DMFIT (i.e. neat IF(ZB)wt coating)

2.2.5.3 Elemental analysis

Elemental analysis was performed by the external laboratory (Institut des Sciences Analytiques, Villeurbanne - France).

The determination of the amount of carbon was made by burning the sample in an excess of oxygen at 1050 ^{o}C. The quantity of the evolved CO_2 was then determined by carbon dioxide infrared gas detectors and was proportional to the total quantity of carbon in the sample.

For boron and phosphorous, their amount was determined by Inductively Coupled Plasma Optical Emission Spectrometry ((ICP-OES), Agilent-Varian) after dissolution of the sample in the acid mixture (HCl/HNO_3).

2.2.6 Char morphology

A 3D optical microscope was used to investigate char morphology, which uses optic and a charge coupled device (CCD) camera to output a digital image to a monitor. In this work, Keyence VHX 1000 digital microscope was used. The lens used is 20z - 200z lens. The images were captured with 3D stitching mode to increase the resolution of the images.

2.3 Conclusion

In chapter II, the studied formulations were presented in the first part. Afterwards, methods to prepare the coatings for different tests were detailed. Experimental techniques used to perform the fire test and heat-treatment were then described. Furthermore, methods to characterize the thermal, physical and chemical properties of the intumescent coatings were depicted.

The selection of the methodologies are based on our knowledge and on the literature (review detailed in chapter I). They are implemented in combination to be able to achieve the thesis objectives. The strategy used in chapter III and IV are quite similar. First, the furnace test was used to assess the fire protective properties of the formulations. The char residues collected after the furnace test were then fully characterized to investigate the chemistry in the condensed phase, char morphology, expansion rate… The thermal and physical properties were also investigated using adapted techniques in order to elucidate the intumescent behavior/process. The heat treatments were implemented when required to investigate the chemical reactivity between the ingredients of the intumescent formulations at defined temperatures.

Chapter III: Mode of action of borates on the fire protection of epoxy based intumescent coatings

The use of different borates in intumescent coatings as well as its efficiency have been recognized in the literature and described in chapter I. Boric acid and zinc borate are the most commonly used borates. Borax and APB were also claimed to be used in some intumescent formulations. However, comprehensive work detailing the exact roles of borates in intumescent coatings has never been done so far. This chapter deals with the investigation of the role of borates in epoxy based intumescent coating used as a protection against hydrocarbon fire. It aims at systematically examining the effects of different borates including boric acid (BA), zinc borate (ZB), borax and ammonium pentaborate (APB) on fire protective properties of complex intumescent formulations. Other goals are to characterize the evolution of chemical species formed in the condensed phase under different conditions (under pyrolytic condition at defined temperature or when submitted to a fire test) and to examine the thermo-physical properties of the intumescent char. It is then expected to determine the mode of action of borates in intumescent formulations.

3.1 Influence of borates on the fire protection

In this section, intumescent coatings containing different borates namely BA, ZB, borax and APB (respectively called IF(BA), IF(ZB)m, IF(borax)m and IF(APB)m) with constant P/B molar ratio (1/3.3) were evaluated in terms of fire protective performances using a small-scale furnace test mimicking UL1709 hydrocarbon fire scenario. At the end of the tests, char expansion, adhesion, cohesion and general aspects of char were observed. The collected char residues were then analyzed to elucidate the chemical reactions taking place in the condensed phase.

3.1.1 Fire protective properties

Figure 23 shows the evolution of temperature as a function of time on the backside of the steel plates coated with the different intumescent formulations during hydrocarbon fire test. 500 ^{o}C was chosen as the failure temperature since it corresponds to the temperature at which steel begins to lose its structural properties [19, 149]. Thus, time to reach 500 ^{o}C is considered as a critical point to compare the fire protective performance of the studied formulations. The longer the time to reach the failure temperature, the better the fire protection.

When comparing the fire protective performance at the failure temperature, it was shown that IF(ZB)m exhibits an excellent fire protection among all formulations. It takes 29.8 minutes to reach the failure temperature while IF(BA), IF(borax)m and IF(APB)m reach this temperature in 17.2, 20.2 and 15 minutes respectively. In the case of IF(BA)m and IF(APB)m, a drastic temperature increase can be observed at about 14 and 13 minutes assigned to the detachment of char. It is noteworthy that the formulation containing zinc borate exhibits a sharp temperature increase in the first five minutes of the test. Then, the temperature slowly increases. In this zone, the curve shape looks like ‘a plateau’ up to 18 minutes. After this time, the temperature increases smoothly to 500 ^{o}C, which is reached at about 30 minutes. Whereas IF(borax)m has no problem of adhesion, the increasing rate of temperature is significantly higher than the others and 500 ^{o}C is reached after 20 minutes.

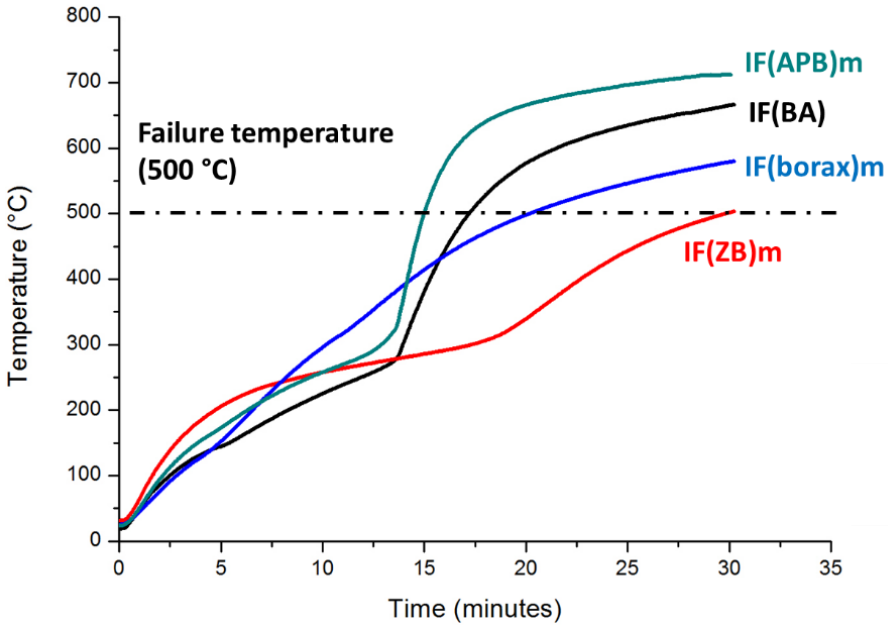

Figure 23 Time – temperature curves of IF(BA), IF(ZB)m, IF(borax)m and IF(APB)m

Table 10 shows the char aspects of the four formulations after burning for 30 minutes in the furnace test. For IF(ZB)m, the char exhibits an expanded structure constituted of an homogeneous layer with small pores through its thickness. The relative expansion is of about 650%. Globally, this layer is hard, cohesive and well adhesive to the steel plate.

For IF(borax)m, there is almost no expansion (only 170 %) and the obtained char is compact, dense and hard. Several cracks can be observed on the surface of the structure. However, the formed char presents a good adhesion to the steel plate during the test.

IF(BA) and IF(APB)m have similar chars which differ greatly from the one of IF(ZB)m. At the point of collection, only a small part of char still sticks to the steel plate whereas the majority of the char falls off. For IF(BA), char falls two times: the biggest part (1) first falls at 14 minutes and another part (2), which is about half of the steel plate, falls off at the end of the test when the sample was removed. Both IF(BA) and IF(APB)m chars are light and brittle, and some shrinkage has occurred. The observation of the fallen part of the char indicates that during the test the decomposition gasses should accumulate to form big holes in the middle of the structure resulting in their detachments. For IF(BA) and IF(APB)m, the expansion has not been measured due to a detachment of char residues.

Table 10 Char aspects and relative expansions of IF(ZB)m, IF(borax)m, IF(BA) and IF(APB)m (30 minutes)

Formulation	% Relative expansion	Global view	Cross sectional view
IF(ZB)m	650 ± 30 %		
IF(borax)m	170 ± 10 %		

Formulation	% Relative expansion	Part of the char on the substrate	Fallen part of the char	
			top	rear
IF(BA)	-			 (1)
				 (2)
IF(APB)m	-	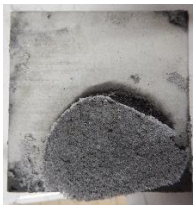		

Conclusion

For the studied formulations, the formulation containing zinc borate leads to a good adhesion and good char characteristics resulting in the best fire resistance. The formulations containing boric acid or ammonium pentaborate exhibit similar fire protective behaviors and char aspects. A different result is obtained when borax is incorporated; a low expansion is obtained while fire protective performance is intermediate between the formulation containing zinc borate and these containing boric acid or ammonium pentaborate. To try to understand the fire protective behaviors obtained when different borates were incorporated, further investigations have to be made. It is of interest to investigate the chemical species formed in the condensed phase that relates to its mechanism of action/protection. The next part thus aims at understanding the fire protective behavior and char aspects obtained when the different borates were incorporated. For all formulations, the tests were stopped at 30 minutes and the char residues were collected and characterized. Elemental analysis, XRD, solid state ^{13}C, ^{31}P and ^{11}B NMR have been used as characterization tools.

3.1.2 Characterization of the char residues of complex formulations collected after a furnace test

First, ***elemental analysis*** has been carried out to determine the phosphorus (P), boron (B) and carbon (C) contents remaining in the char residues. The quantities of P, B and C in the non-degraded coatings were also calculated from the composition of the formulation.

P/C and B/C ratios of the non-degraded coatings and char residues of IF(BA), IF(ZB)m, IF(APB)m and IF(borax)m are shown in Figure 24. The P/C and B/C ratios of the non-degraded coatings of four formulations are the same (P/C = 0.07 and B/C = 0.08) since these formulations were formulated by keeping constant the molar ratio of the additives.

P/C ratios of the char residues for all formulations increase when compared to these of the non-degraded coatings. This means that the stabilization of the phosphorous species is favored compared to the carbonaceous species. When looking at the B/C ratio, the similar tendency was obtained suggesting the stabilization of the boron species as well. Between the four formulations, the carbon species in the formulation containing zinc borate are more stabilized compared to the others. The formulations containing boric acid or APB contain less carbon content than the previous one and the formulation containing borax has the value between them.

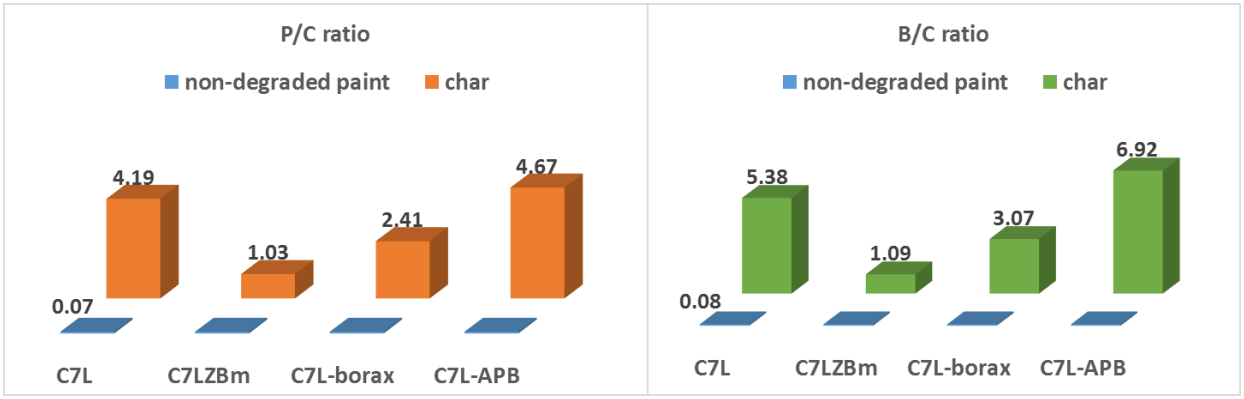

Figure 24 P/C ratio and B/C ratio in non-degraded coatings (by calculation) vs. in char residues (by elemental analysis)

Based on these results, it can be mentioned that the addition of zinc borate stabilizes the carbonaceous char (increasing the remaining carbon in the residue) when compared to the other borates.

To go further in the investigations, XRD was used to characterize the crystalline chemical species formed in these samples.

Figure 25 shows the XRD diffractograms of the char residues of the four formulations and the diffractograms of boron oxide (B_2O_3) and boric acid (H_3BO_3). The residues present various crystalline species and certain peaks are common to different residues such as B_2O_3 and borophosphate (BPO_4).

Indeed, the XRD patterns of IF(BA) and IF(APB)m residues clearly suggest the presence of B_2O_3. In the case of IF(borax), only the main signal of the B_2O_3 specie is observed (28.1 °) but the presence of this specie can be assumed nevertheless. Whereas for IF(ZB)m residue, B_2O_3 is not detected. The thermal decompositions of boric acid, ammonium pentaborate and borax at temperature between 100 °C and 450 °C, is reported to produce boron oxide as described in the eq. 31, 32 and 33 ([150-152]). In the same range of temperature on the other hand, zinc borate does not decompose into B_2O_3. Its decomposition yields rather to the formation of amorphous $2ZnO.3B_2O_3$ ([83, 84]) as shown in eq. 34.

$$2H_3BO_3 \xrightarrow[T \sim 100-250\ ^0C]{} 3H_2O + B_2O_3 \quad \text{(eq. 31)}$$

$$2NH_4B_5O_8.4H_2O \xrightarrow[T \sim 100-450\ ^0C]{} 2NH_3 + 9H_2O + 5B_2O_3 \quad \text{(eq. 32)}$$

$$Na_2B_4O_7{\cdot}10H_2O \xrightarrow[100\ ^\circ C < T < 250\ ^\circ C]{} 2NaBO_2 + B_2O_3 + 10H_2O \quad \text{(eq. 33)}$$

$$2ZnO.3B_2O_3.3.5H_2O \xrightarrow[290\ ^\circ C < T < 420\ ^\circ C]{} 2ZnO.3B_2O_3 \text{ (amorphous phase)} + 3.5H_2O \quad \text{(eq. 34)}$$

Borophosphate peaks are observed on the diffractograms of IF(BA), IF(APB)m and IF(ZB)m char residues. It is a highly stable compound [153] which can be found in both crystalline and amorphous forms [154, 155]. It was already reported to be found in the char residues of intumescent coatings when the formulations contain boric acid and APP [26, 66]. It is obtained by the reaction between the degradation products of these reactants (i.e. polyphosphoric acid and B_2O_3). Such reaction could explain the formation of BPO_4 in IF(APB)m residue however it does not seem to occur for IF(Borax)m as no crystalline BPO_4 is detected in this case. The reaction between

APP and zinc borate to form borophosphate, already reported in a publication [83], could explain the formulation of BPO_4 in IF(ZB)m char.

For IF(BA), IF(APB)m and IF(borax)m, the detection of B_2O_3 at the end of the experiment can be due to the stoichiometry of the reactants. Indeed, in the formulations, borate is in excess compared to phosphorous (P/B molar ratio = 1/3.3). There is consequently more B_2O_3 formed by decomposition of BA, APB and borax than APP present in the formulation. Consequently, it makes sense to get 'unreacted B_2O_3' in the char residue. On the other hand, when looking precisely at the peak at the 2Θ value of 15° (split signal-like), the presence of H_3BO_3 in the char residue may be suspected, especially in IF(BA). Boron oxide being hygroscopic [76], it can absorb water under atmospheric conditions and revert back to boric acid as shown in eq. 35 [156, 157]. In our case, two assumptions can be drawn. First, during the degradation, water is released from the combustion reaction and thus the reaction can occur during the test. A second assumption consists in considering that the reaction of boron oxide with water occurs after the test (cooling phase or storage). Indeed, even if the char was conserved under dried atmosphere, this assumption cannot be dismissed.

$$B_2O_3 + 3H_2O \rightarrow 2H_3BO_3 \qquad \text{(eq. 35)}$$

For IF(BA), IF(APB)m and IF(borax)m, $Ca_3(PO_4)_2$ is also detected. This specie was reported [158] to be formed by reaction between calcium carbonate and phosphoric acid as shown in eq. 36 [159]. $CaCO_3$ is one of the ingredients of the formulations and phosphoric acid comes from the degradation of the APP, $Ca_3(PO_4)_2$ can thus be formed in these formulations.

$$3CaCO_3 + 2H_3PO_4 \xrightarrow[950\ ^\circ C < T < 1150\ ^\circ C]{} Ca_3(PO_4)_2 + 3H_2O + 3CO_2 \qquad \text{(eq. 36)}$$

For IF(borax)m formulation, the diffractogram shows that the residue is not highly crystalline. Apart from the peaks of B_2O_3 and $Ca_3(PO_4)_2$, the main signal is a broad band lying between the 2Θ value of 18 ° and 35 ° indicating a disordered structure (amorphous) of the char residue. This can probably be partly attributed to the formation of pregraphitic carbon [83] as usually observed in intumescent char. Moreover, Na/Na_2O is a known fluxing agent [160], which

can decrease the glass forming temperature that may consequently produce a vitrified char at lower temperature as observed in IF(borax)m formulation.

For IF(ZB)m, in addition to BPO_4, other crystalline compounds are detected: zinc orthophosphate (α-$Zn_3(PO_4)_2$), zinc pyrophosphate (α- and γ-$Zn_2P_2O_7$), and zinc metaborate ($Zn_4B_6O_{13}$). $Zn_4B_6O_{13}$ is a degradation product of zinc borate, which is formed when zinc borate is heated above 800 ^oC [83]. Interestingly, most of the crystalline compounds formed are zinc-based compounds. It highlights the important role of zinc from zinc borate that reacts with other components (especially phosphorous-based compounds). In the opposite to other three formulations, $Ca_3(PO_4)_2$ is not formed. With the presence of Zn, the formation of Zn-P compounds is probably favored rather than the one of Ca-P compounds, that is occurred in the IF(ZB)m formulation.

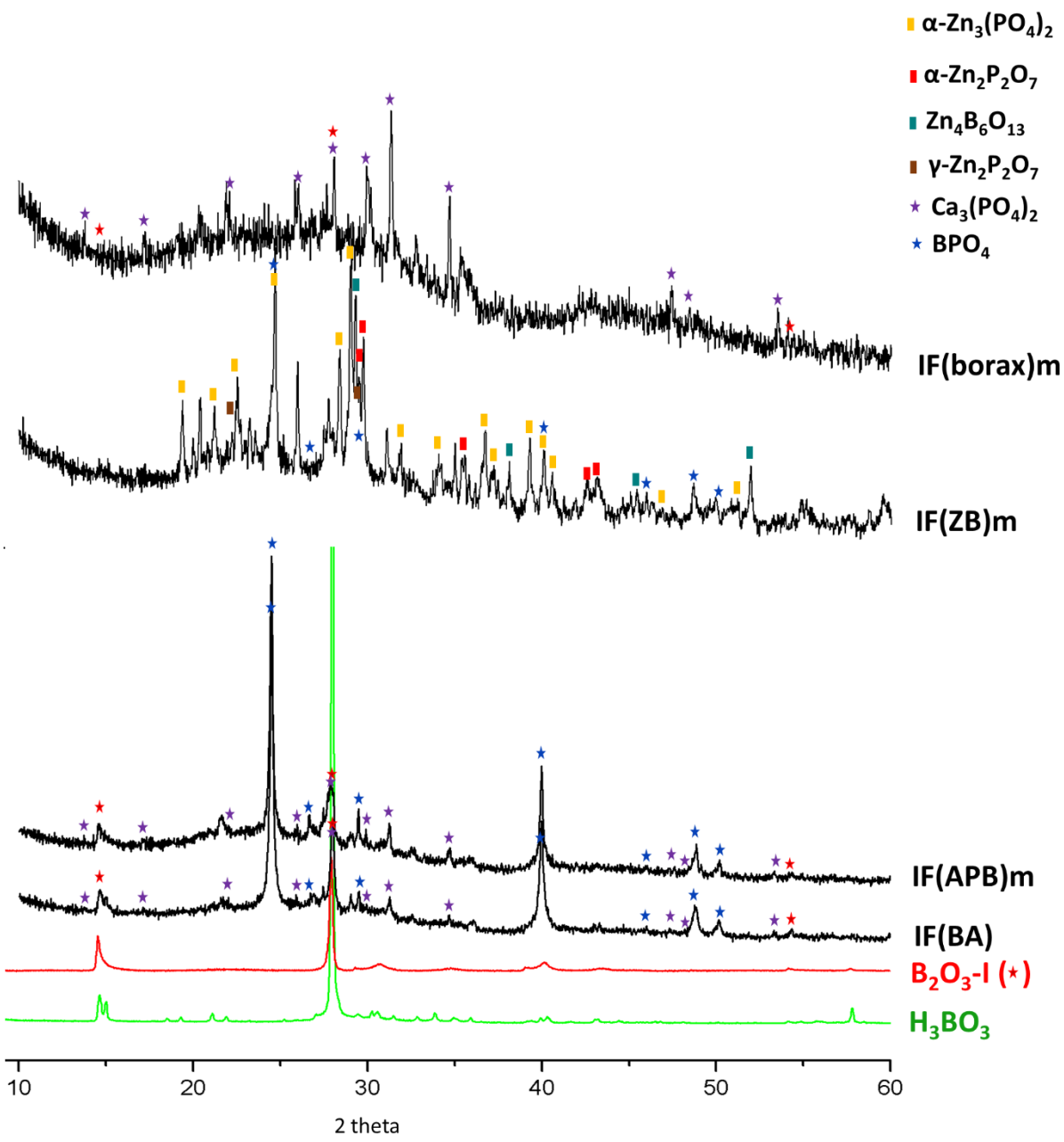

Figure 25 XRD diffractograms of IF(BA), IF(ZB)m, IF(borax)m and IF(APB)m char residues (30 minutes) and of H_3BO_3 and B_2O_3

Figure 26 shows the ^{13}C NMR spectra of the char residues of the four formulations. For all formulations, there is a broad signal appearing between 0 and 90 ppm (with low intensity), which is assigned to aliphatic carbons. A broad band lying between 110 and 150 ppm is also observed in the case of IF(BA), IF(ZB)m and IF(borax)m. It is assigned to several types of aromatic and/or polyaromatic carbon species [136, 137]. This band exhibits a tail up to 160 ppm which is assigned

to oxidized species linked to polyaromatic structure [161]. The signal for IF(ZB)m and IF(Borax)m is more intense when compared to the others but no quantification can be made because the signal was acquired using cross polarization (CP). It means that the efficiency of the magnetization transfer between ^{1}H and ^{13}C should be known precisely to make any quantification. Nevertheless, it is reasonable to explain this higher resolution of the spectra by the higher carbon content in the two formulations as already shown by elemental analysis.

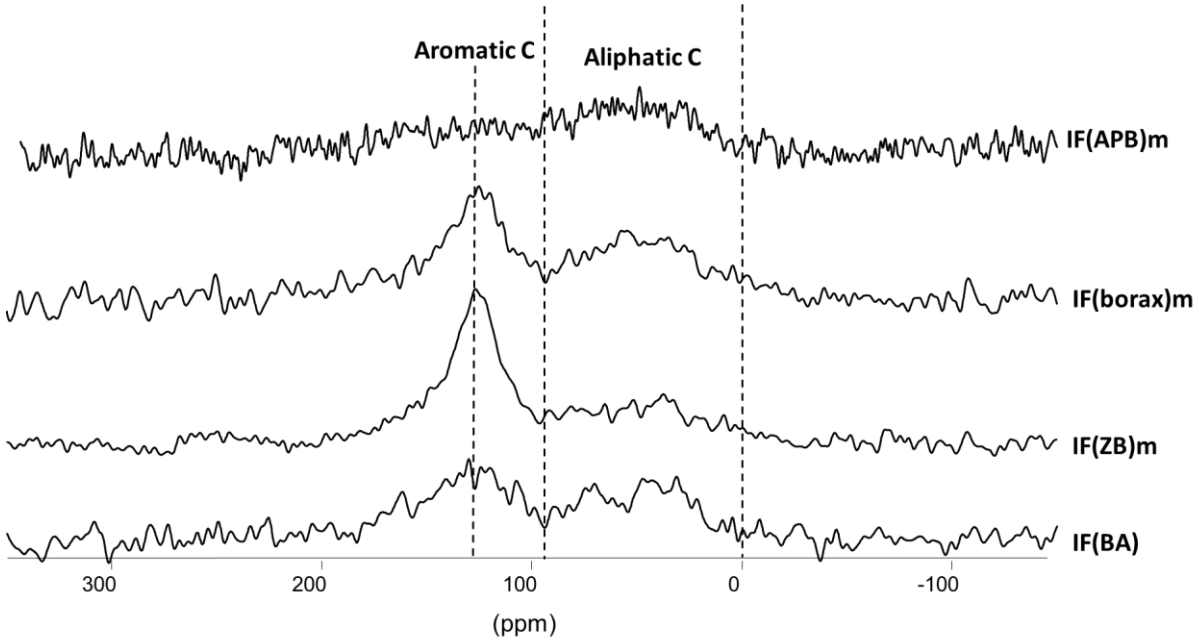

Figure 26 ^{13}C NMR spectra (9.4 T) of IF(BA), IF(ZB)m, IF(borax)m and IF(APB)m char residues

To investigate the evolution of the phosphorus species in the char residues, ***^{31}P solid state NMR*** was performed on the char samples. In ^{31}P solid state NMR, the Q^n terminology is used to classify the structures of phosphate. Q represents a phosphorous tetrahedron and n the number of bridging oxygen atoms in this tetrahedron (Figure 27). For example, Q^2 structure contains two bridging and two non-bridging oxygen atoms and is the so-called metaphosphate [162-164]. In such structure, the higher the number of bridging oxygen atoms attached to a phosphorous atom, the lower the ^{31}P isotropic chemical shift. The peak position is an indicator of PO_4 tetrehedra with varying degree of condensation/polymerization.

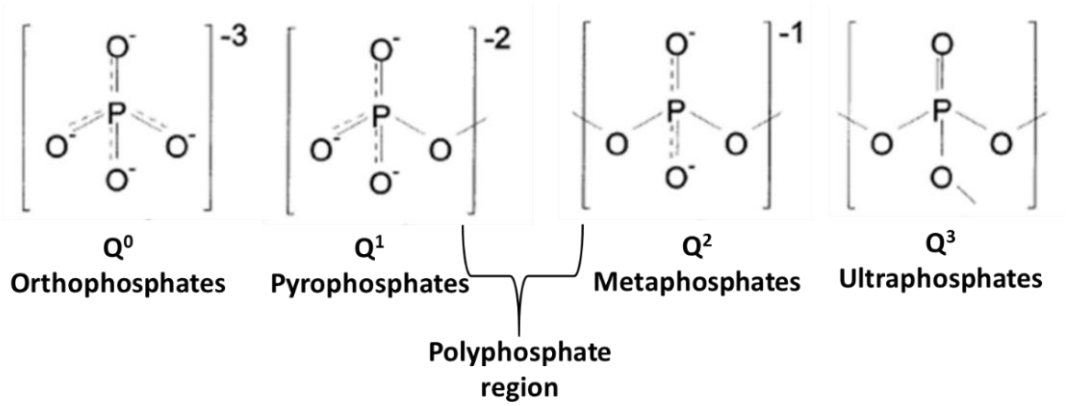

Figure 27 Q structure of phosphate: Q^0 isolated units (ortho-P), Q^1 end units (pyro-P), Q^2 middle units (meta-P) and Q^3 crosslinking units (ultra-P)

^{31}P NMR spectra of the char residues of IF(BA), IF(ZB)m and IF(APB)m (Figure 28) show a sharp peak at -30 ppm, which is assigned to crystalline BPO_4 [74, 165]. It is consistent with the XRD results. The quantity of BPO_4 in IF(ZB)m is obviously lower compared to the other formulations when considered the peak height. For IF(BA) and IF(APB)m, there are low intensity signals between -6 and -10 ppm (in zoom area on Figure 28). These features are assigned to Q^1 phosphate sites (pyrophosphate).

In IF(ZB)m char residue, besides BPO_4, additional signals appear at 3.9, -1.3, -5.3, -7.1, -10.1, -15.9, -18.8 and -21.1. The attributions can be made as follows. The sharp peak at 3.9 ppm is assigned to zinc orthophosphate (α-$Zn_3(PO_4)_2$) [144, 165], the triple peak appearing at -15.9,-18.8 and -21.1 is assigned to α-zinc pyrophosphate (α-$Zn_2P_2O_7$) [83, 166] and the peaks at -5.3, -7.1 and -10.1 ppm can be assigned to γ-$Zn_2P_2O_7$ [59, 167]. The identification of these species is in good agreement with XRD results. A low intensity signal appearing at -1.3 ppm is also observed. That is assigned to Q^0 phosphate site.

^{31}P NMR spectra of IF(borax)m char residue exhibits a broad signal lying between 10 and -30 ppm, which can be assigned to amorphous phosphates. In this range of ^{31}P chemical shift, these phosphate structures could be composed of Q^2, Q^1 and Q^0 phosphate structures. Additional peaks are observed at 10.2 and 11.4 ppm, these sharp peaks suggest the formation of crystalline species. They can be attributed to $(RO)_2PO$-H, i.e. phosphonate structures [168, 169] and could be formed through the reduction of phosphate (+V) in phosphonates (+III).

$Ca_3(PO_4)_2$ which is suggested by XRD exhibits a signal lying between 5 and -2 ppm [170]. This signal does not appear in the ^{31}P NMR spectrum of IF(BA), IF(APB)m and IF(Borax)m. Its absence may be explained by its low quantity in the char sample (there is only 1.91 wt. % of $CaCO_3$ in the initial formulation).

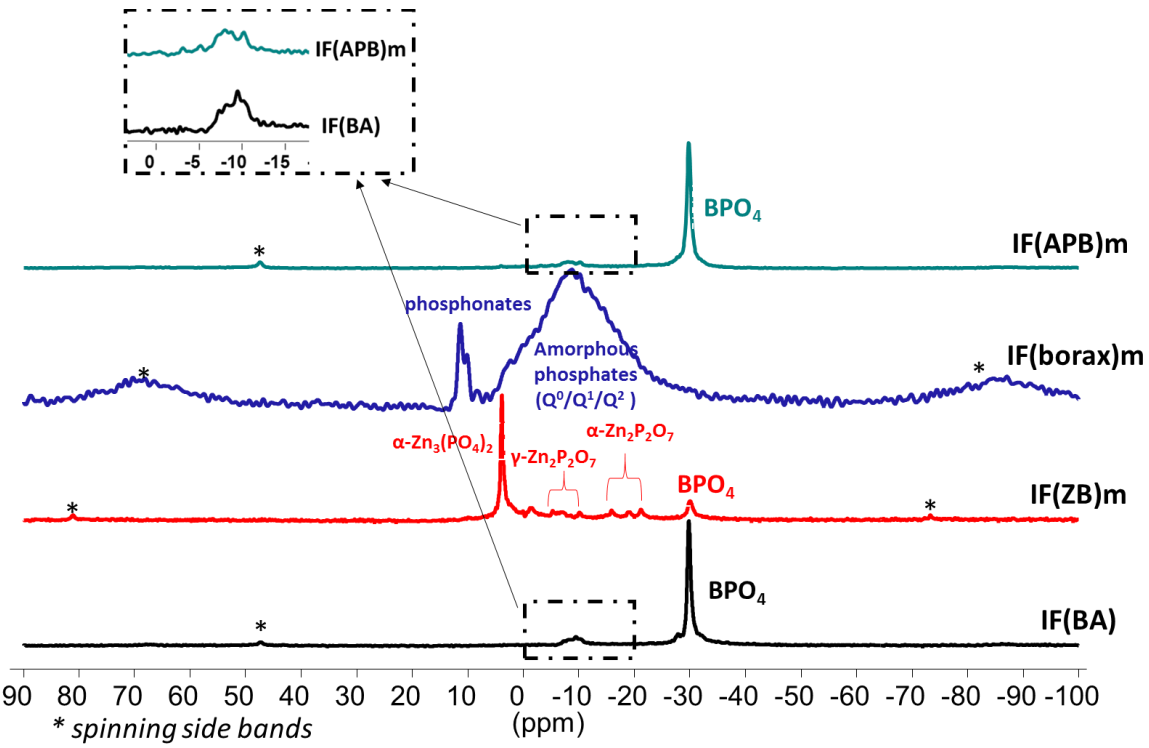

Figure 28 ^{31}P NMR spectra (9.4T) of the IF(BA), IF(ZB)m, IF(borax)m and IF(APB)m char residues

To complement the results obtained by elemental analysis, XRD, ^{13}C and ^{31}P solid state NMR, ***^{11}B solid state NMR*** was used. Borates contain trigonal BO_3 and/or tetrahedral BO_4 units, which can form a wide number of different structures going from isolated orthoanions to chains, rings, layers, and frameworks. These types of structures are found in crystalline alkali metal borates, mineral borates as well as borate glasses. In ^{11}B solid state NMR, two types of boron environments can be distinguished by the ^{11}B isotropic chemical shift (δ_{iso}): (i) BO_3 units resonate in the range $12 \leq \delta_{iso} \leq 25$ ppm and (ii) BO_4 groups exhibit chemical shifts in the approximate range $-4 \leq \delta_{iso} \leq 6$ ppm. Furthermore, BO_3 and BO_4 units can be distinguished by their ^{11}B quadrupolar coupling parameters. Generally, BO_4 tetrahedra in borates exhibit quadrupolar coupling constant

(C_Q) values less than 1 MHz whereas BO_3 groups possess quadrupolar coupling constant in the range of $2.4 \leq C_Q \leq 3.0$ MHz [171]. In our study, thanks to high magnetic fields NMR (18.8T) used to acquire the ^{11}B solid-state NMR spectra of the char residues (Figure 29), BO_3 and BO_4 units can be clearly distinguished.

On the one hand, three different BO_4 units are detected in the samples. The first one corresponds to a sharp and intense signal appearing at -3.8 ppm on the spectra of IF(BA), IF(ZB)m and IF(APB)m char residues. It is assigned to crystalline BPO_4 [58, 74]. This peak is not observed for IF(borax). These results are consistent with XRD and ^{31}P NMR results. Another BO_4 unit appearing at 0.5 ppm ($BO_{4\,(i)}$) can be observed in the four formulations. Here, the broad signal indicates a low crystallinity of this unit; this signal is highly intense in IF(borax)m. Additional BO_4 unit appearing at 1.9 ppm ($BO_{4\,(ii)}$) can be distinguished in IF(ZB)m char residue. $Zn_4B_6O_{13}$ identified in XRD pattern has no ^{11}B NMR spectrum reported in the literature. It possesses a cage structure in which 24 tetrahedron (BO_4) construct a closed truncated octahedron ($B_{24}O_{48}$) by sharing the corner oxygen atoms [172, 173]. This signal at 1.9 ppm may be the characteristic signal of BO_4 unit in $Zn_4B_6O_{13}$. Unfortunately, this assumption could not be proved since this zinc borate is not commercially available.

On the other hand, the broad signal lying between 5 and 20 ppm attributed to BO_3 units (typical second-order quadrupolar line shape) is observed for the four samples. At least two BO_3 units are overlapping in this broad signal. Indeed, according to the XRD results (Figure 25), crystalline B_2O_3 should be observed in all samples except IF(ZB)m. To clearly identify the B_2O_3 contribution on the ^{11}B NMR spectrum, its spectrum was acquired as a reference. The superimposition of the spectrum line shape of B_2O_3 with those of the char samples (Figure 29, IF(APB)m as an example) confirms the presence of B_2O_3 in IF(BA), IF(APB)m and IF(borax)m char samples. The presence of at least another BO_3 unit in IF(BA), IF(APB)m and IF(borax)m is also suggested. In IF(ZB)m char, the presence of BO_3 unit in amorphous $2ZnO.3B_2O_3$ is also suspected. High magnetic fields NMR (18.8T) can clearly distinguish BO_3 and BO_4 units but the differentiation of various BO_3 units needs the advanced NMR to be possible.

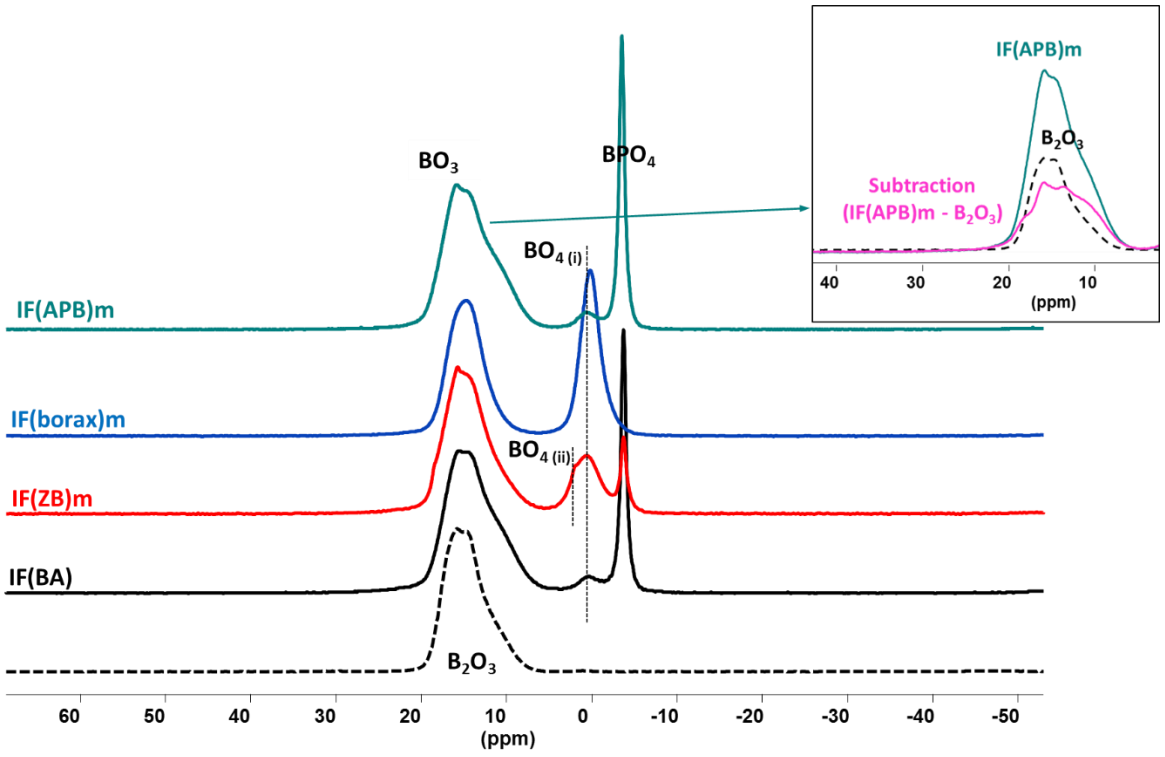

Figure 29 ^{11}B NMR spectra (18.8T) of the IF(BA), IF(ZB)m, IF(borax)m and IF(APB)m char residues and of B_2O_3

Conclusion

In this part, the char residues were characterized to elucidate the chemical modifications in the condensed phase in presence of the different borates. A clear influence of borates on chemical species formed is evidenced. The use of zinc borate as a boron source leads to form various crystalline compounds (e.g. BPO_4, $Zn_3(PO_4)_2$, $Zn_2P_2O_7$, $Zn_4B_6O_{13}$), many of them are zinc-based compounds. The stabilization of the carbonaceous char (e.g. increasing the remaining carbon in the residue) when zinc borate is incorporated is evidenced by elemental analysis and ^{13}C NMR. These indicate the contribution of zinc borate on the stabilization of the carbonaceous char. The addition of boric acid or of APB shows the formation of similar species in the char residues (i.e. BPO_4, B_2O_3, $Ca_3(PO_4)_2$). The carbon content and carbonaceous species in these two samples are also similar. Borax exhibits some common crystalline species to the others (i.e. B_2O_3, $Ca_3(PO_4)_2$). It is however different, amorphous products are the main components in its char residue.

3.1.3 Conclusion

In this part, the effects of four borates namely boric acid, zinc borate, borax and APB on fire protective properties were studied. Additionally, their interactions with the other additives of the formulation in the condensed phase after testing were elucidated. As a result, it was shown that the formulation containing zinc borate exhibits the best fire protection among all (longer time to reach the failure temperature). The formation of various crystalline compounds in the formulations, which are thermally stable, are suspected to be responsible of the good fire protection. They may stabilize and strengthen the carbonaceous char. To go further in the investigation, it is of interest to investigate in more detail the decomposition pathway (as a function of temperature or exposed time in the furnace) of those formulations as well as their thermo-physical properties. For these purposes, the formulations containing either boric acid (IF(BA)) or zinc borate (IF(ZB)) were chosen. IF(ZB) was chosen because it provides promising results in the fire protection and char characteristics. IF(BA) was selected because BA is commonly used as intumescent ingredient in commercial systems [6, 52, 81]. Moreover, as boric acid is mentioned to be CMR by REACH, the comprehension of the role of boric acid is of interest since it might give information on how to substitute it. Thus, the next part is dedicated to the investigation of the thermal decomposition and thermo-physical properties of the selected intumescent coatings during charring process.

3.2 Insight into the mechanism of action of boric acid and zinc borate in complex formulations

The previous part showed the interesting fire protective performance of the formulation containing zinc borate. The chemical species formed in the condensed phases were identified giving some clues on its mode of action. Nevertheless, the mechanism of action of intumescent material is a hugely complex and dynamic process. The characterization of the chemistry in the char residues collected at one point does not provide enough information to understand this complex process. In this part, the mechanism of action will be fully investigated. Two formulations including the formulations containing either zinc borate or boric acid were selected for a full characterization (chemical and thermo-physical modifications).

First, the thermal decompositions of the two selected coating formulations were investigated under pyrolytic condition or under a real fire test (UL 1709). The aim is to elucidate the evolution of chemical species formed in the condensed phase during the decomposition process to understand their mechanism of reaction, which occurs in the condensed phase. In the following part, the study deals with the measurements of the thermo-physical properties. It includes the investigation of the complex viscosity, relative expansion, char morphology, thermal conductivity, and char strength. Char morphology was assessed (at room temperature) as a function of the exposed times after the fire test while the thermal conductivity, complex viscosity, relative expansion and char strength were dynamically measured as a function of temperature. Finally, the mechanisms of protection of borates, are commented.

3.2.1 Thermal decomposition of IF(BA) and IF(ZB) coatings

3.2.1.1 Pyrolysis of IF(BA) and IF(ZB) coatings

3.2.1.1.1 Thermogravimetric analyses of IF(BA) and IF(ZB) coatings

During the furnace test, it is admitted that most of the oxygen is consumed by the combustion leading to only 3 - 4 % of oxygen left [73, 174]. The decompositions were thus examined under pyrolysis conditions (i.e. under nitrogen) by TGA. TG curves of IF(BA) and IF(ZB)wt coatings are presented in Figure 30. In the following part, the characterizations were made on the IF(ZB)wt formulation due to the practical reason since IF(ZB)m and IF(ZB)wt exhibit the similar results in fire protective properties and thermal degradation pathway (superimposed TGA curves).

IF(BA) exhibits four successive degradation steps. The first step (between 90 ^{o}C and 140 ^{o}C) corresponds to a weight loss of about 6 % and the second one (between 140 ^{o}C and 198 ^{o}C) corresponds to a weight loss of 3 %. These two steps can be attributed to the dehydration of boric acid, which is one of the ingredients in IF(BA) coating. This attribution can be confirmed by a theoretical calculation. In IF(BA) formulation, there is 19.3 wt.% of boric acid which degrades in two steps between 100 ^{o}C and 250 ^{o}C leading to a total weight loss of 44 % [73, 141]. This should lead to 8.5 % of total weight loss of the coating formulation. Theoretical and experimental results are thus well correlated (8.5 vs. 9 wt. %). The third step of degradation (between 198 ^{o}C and 280 ^{o}C) corresponds to a weight loss of about 8 % and the fourth one (main degradation step) leads to a total weight loss of 46 %. The third and fourth steps are assigned to the degradation of the epoxy resin and of the other components in the formulation. From 600 ^{o}C, there is a slight weight loss of 2 % until 800 ^{o}C. The residue at 800 ^{o}C is about 35 wt. %.

IF(ZB)wt degrades into two steps. The first one (between 200 ^{o}C and 275 ^{o}C) corresponds to 10 wt. %. The second one (between 275 ^{o}C and 550 ^{o}C) is the main degradation step corresponding to 48 wt. %. There is a slight weight loss of 2 % from 600 ^{o}C similar to that occurring for IF(BA). The degradation pathway of IF(ZB)wt is different from the one of IF(BA). It has a slightly higher residual weight than IF(BA) (40 vs. 35 %); this difference could be due to the nature of

borates (i.e. residual weight at 800 °C of zinc borate and of boric acid are 88 and 56 wt. % respectively).

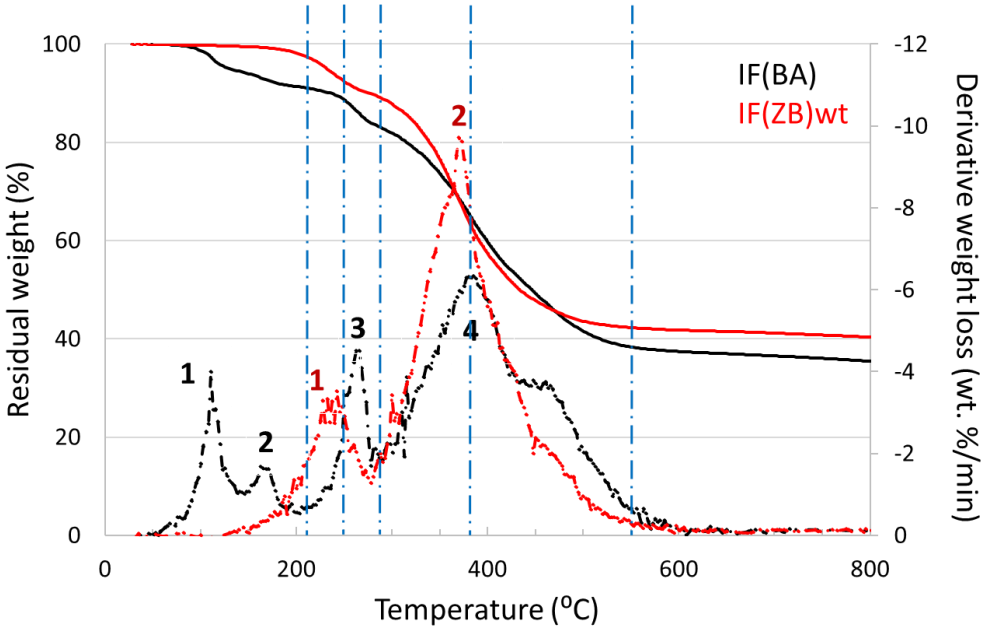

Figure 30 TG curves of IF(BA) and of IF(ZB)wt

Consequently, both IF(BA) and IF(ZB)wt decompose in multi-steps. The formulation containing zinc borate possesses higher char residue at high temperature and the decomposition pathways between the two formulations are different. To study the decomposition pathway and mechanism of reaction occurring in the condensed phase, the coatings were heat treated at different characteristic temperatures (Table 11). Regarding the TG curves of the studied coatings, five temperatures were selected (blue dot lines visualized on Figure 30).

Table 11 Selected heat treatment temperatures of IF(BA) and of IF(ZB)wt

HTT (°C)	IF(BA)	IF(ZB)wt
210	After the first and second step of degradation	-
250	Maximum weight loss of the third step	Maximum weight loss of the first step
280	After the third step of degradation	End of the first step of degradation
380	Maximum weight loss of the main step	Maximum weight loss of the main step
550	After the total degradation and stabilization of the residue	

The chars collected for each heat-treatment temperature were then analyzed using XRD, ^{31}P and ^{11}B solid state NMR. Hereafter, it is of interest to identify the chemical species formed at defined temperature under pyrolytic conditions, which can suggest what could occur in a real fire test. The results are presented in the following section.

3.2.1.1.2 Identification of the chemical species formed

In this part, the decomposition pathway of IF(BA) is first discussed and that of IF(ZB)wt is examined afterwards.

a) IF(BA) formulation

Figure 31 shows the diffractograms of IF(BA) coating at ambient temperature in comparison with the residues after heat-treatment at different characteristic temperatures. XRD pattern of the coating at ambient temperature shows the presence of ammonium polyphosphate (APP), boric acid, $CaCO_3$ and TiO_2. It is consistent with the composition of the coating. The signals of Si based compounds (from fumed silica, expanded silicate or silicate fibers) were also expected but they are not identified in XRD. It is probably due to their low crystallinity.

In the residue heat treated at 210 °C, three components including APP, $CaCO_3$ and TiO_2 are still identified. According to TGA result, boric acid degrades between 100 °C and 200 °C to yield B_2O_3, it should thus degrade at this temperature. On the XRD pattern, the most intense peak of boron oxide at 2theta value of 28 ° appears (with a low intensity) and it evidences the presence of boron oxide. At 250 ° C, APP is decomposed. B_2O_3 is identified but no additional species are detected. At 280 ° C, in addition to B_2O_3, the formation of borophosphate (BPO_4) is detected. It implies that the formation of BPO_4 occurs between 250 ° C and 280 ° C by reaction between the decomposition products of APP and boron oxide. The XRD pattern of the char residue after heat treatment at 380 ° C is the same as that of 280 ° C; it means no evolution of chemical crystalline species between these two temperatures. At 550 ° C, it is surprising to identify boric acid instead of B_2O_3. It could be due to the hydration of B_2O_3 reverting back to boric acid (we suspect rehydration of B_2O_3 during fire test or cooling phase similar to what was described in 3.1.2). Interestingly, the XRD pattern of $CaCO_3$ and TiO_2 are visualized at all heat-treatment temperatures. It points out that $CaCO_3$ and TiO_2 do not decompose nor react with other

ingredients in the formulation up to 550 ^{o} C. The coating at ambient temperature as well as the char residues at different characteristic temperatures exhibit a convex lying between 2Θ values of 15 ^{o} and 30 ^{o} assigned to amorphous phases (e.g. disordered graphitic carbon [83]).

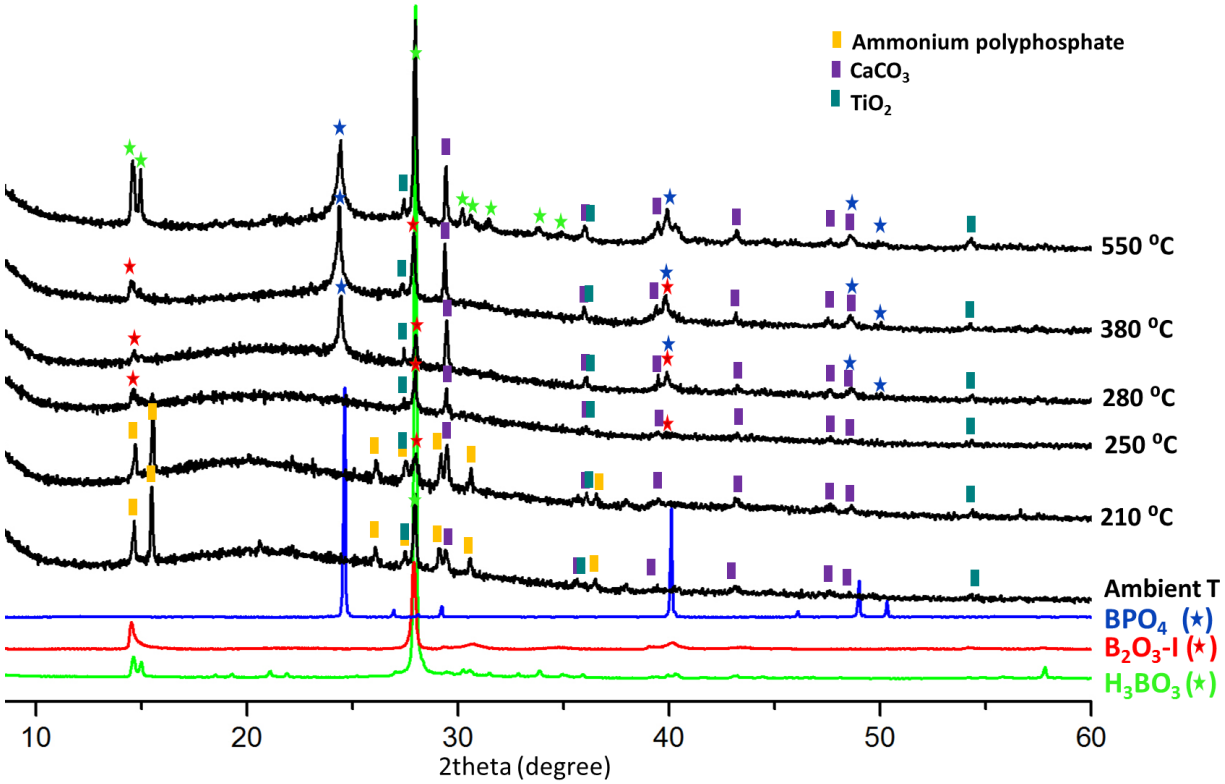

Figure 31 XRD diffractograms of IF(BA) char residues versus temperatures

To investigate more precisely the evolution of phosphorous species versus temperatures, ^{31}P NMR was performed on the non-degraded coating and char residues (Figure 32).

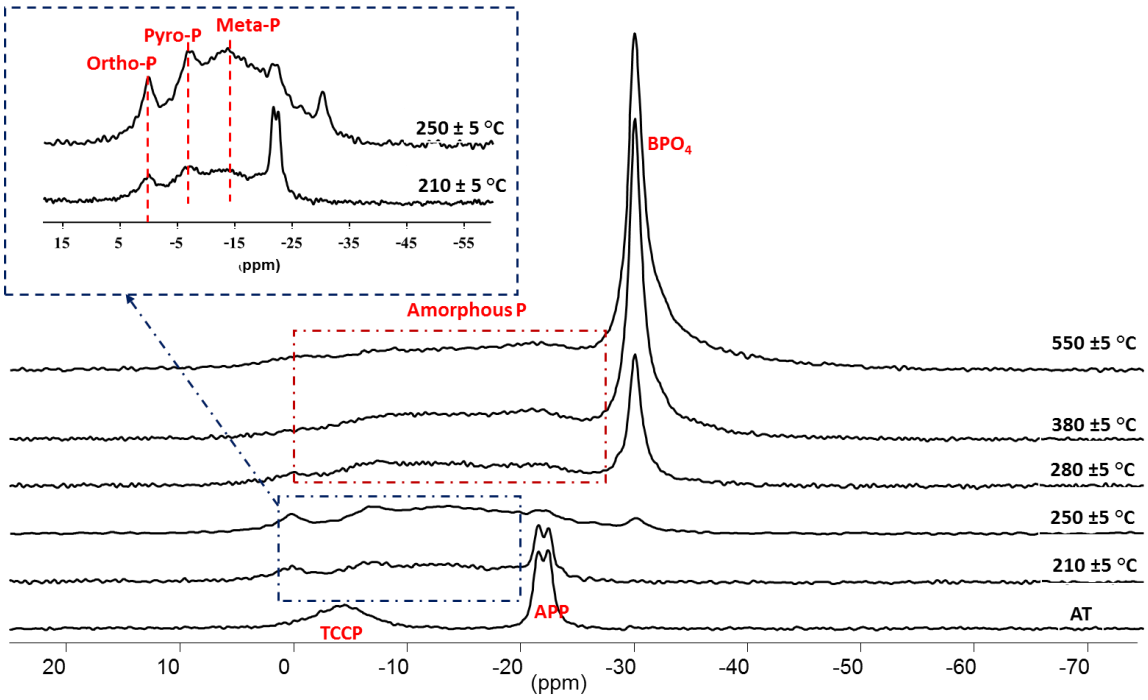

Figure 32 ^{31}P NMR (9.4T) of IF(BA) char residues versus temperatures and the zoom out of the spectra at 210 °C and 250 °C (in the blue dotted line)

For the coating at ambient temperature, ^{31}P NMR spectrum is characterized by a split signal at -22 and -24 ppm, which correspond to a crystalline structure of Q^2 phosphorus units contained in polyphosphate chains [161, 175]. The broad band centered at -4.4 ppm corresponds to an orthophosphate group, which is attributed to orthophosphate in tris (2-chloroisopropyl) phosphate (TCPP) (Figure 33a), an additive used as flame retardant and/or plasticizer in the studied formulation. Indeed, the comparison of the spectrum of pure TCPP and IF(BA) coating (Figure 33b) enables to identify the presence of this compound. The widening of the peaks of IF(BA) compared to the reference TCPP is linked to the fact that TCPP was analyzed in solution whereas the coating was characterized in solid state (structural effect). In powdered samples, the lack of rapid molecular tumbling corresponds to a static distribution of crystallite, molecular or orientations. This leads to a broadening of the NMR line shape [176].

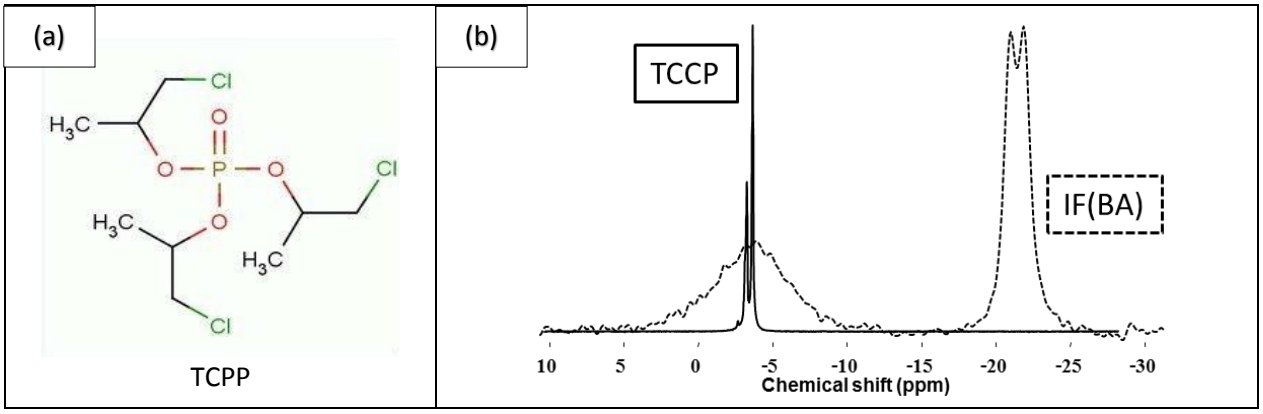

Figure 33 Chemical structure of TCPP (a) and ^{31}P NMR spectra (9.4T) of TCPP and of neat IF(BA) coating (b)

For a HTT of 210 °C (Figure 32), the spectrum is modified compared to the coating at ambient temperature. At this temperature, APP begins to degrade leading to the release of NH_3 and H_2O and to the formation of a highly cross-linked polyphosphoric acid (a broad band lying between -10 and -18 ppm) [161, 177]. The additional broad peak centered at -7.1 ppm (observed from 210 °C up to 250 °C) is assigned to pyrophosphate (Q^1) and/or terminal phosphate groups [59, 143]. At 210 °C and 250 °C, an additional signal appearing at 1 ppm can also be detected, this can be assigned to Q^1 phosphate structure of orthophosphate [178]. Another broad band lying between -10 and -25 ppm is observed from 210 °C until 550 °C with very low intensity at high temperature (in rectangular dotted line). It is assigned to disordered structures of meta-phosphate (Q^2), which is different from the degradation products of APP.

Characteristic peak of TCPP (-4.4 ppm) disappears at 250 °C which is in agreement with the decomposition temperature of TCPP (244 °C, product data sheet). On the other hand, at high temperatures ($T \geq 280$ °C), a single sharp peak is observed at -30 ppm. This band can be attributed to B-O-P bonds of borophosphate (BPO_4) [74, 179]. It is consistent with XRD results. At 250 °C, the characteristic peak of BPO_4 can also be observed with a very low intensity indicating that the formation of BPO_4 has begun. The ^{31}P NMR spectra can be considered as a semi-quantitative indicator (all samples were performed with the same parameters and respecting the relaxation of the nucleus). It can be mentioned that the concentration of BPO_4 increases as a function of temperature.

^{11}B solid state NMR spectra of IF(BA) residues are presented in Figure 34, ^{11}B NMR spectrum of IF(BA) at ambient temperature exhibits BO_3 and BO_4 units. Their relative concentrations are equal to 92 % and 8 % for the BO_3 and BO_4 units respectively. These signals correspond to the characteristic line shape of boric acid (only one boron source in the formulation). The spectrum of boric acid at ambient temperature shows a second-order quadrupolar line shape, that is typical boron atom in a trigonal bonding configuration [180, 181], which mainly contains trigonal boron atom (BO_3) with small amount of BO_4 as impurity at ambient temperature [74].

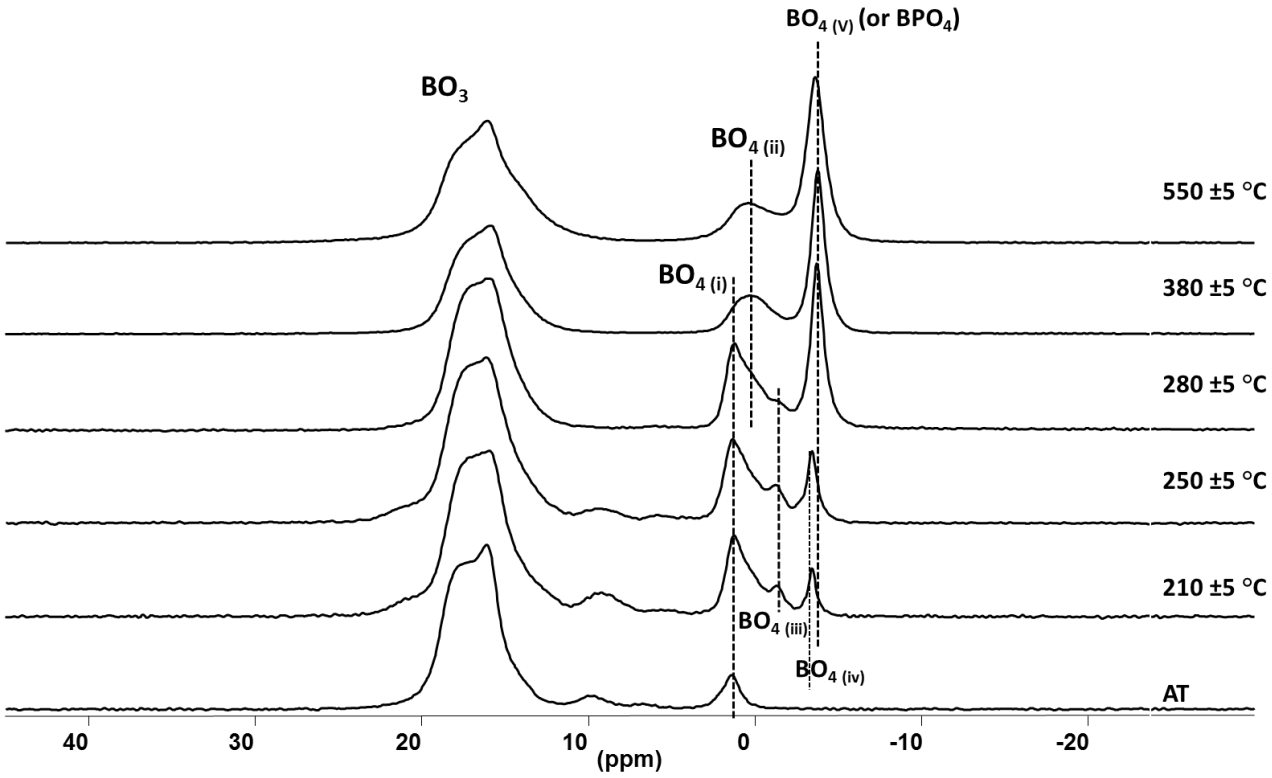

Figure 34 ^{11}B NMR spectra (18.8T) of IF(BA) char residues versus temperatures

A sharp signal appearing at about -3.8 ppm, which is detected from 280 °C up to 550 °C, can be assigned to the characteristic signal of borophosphate (BPO_4) [144, 165]. This is consistent with the results shown by XRD and ^{31}P NMR.

In the samples heat-treated at 210 °C and 250 °C, a low intense peak can be distinguished at -3.4 ppm. Since the chemical shift is very close to that of BPO_4, an assumption was arisen that

it may be the signal of BPO_4 with less crystallinity, (e.g. initial phase of the formation of BPO_4). To justify this assumption, these char residues were carried out to 1D $^{11}B(^{31}P)$ D-HMQC experiment [182] to filter the ^{11}B signal which possesses the spatial proximity with P nucleus. This allows identifying the presence of B-O-P linkage (e.g. B-O-P in BPO_4). The char residues of HT at 250 ^oC and 280 ^oC were measured by D-HMQC experiment. As a result (Figure 35), for char residue at 250 ^oC, no signal in $^{11}B(^{31}P)$ D-HMQC NMR spectrum is observed but the one at 280 ^oC exhibits a signal at -3.8 ppm confirming the presence of B-O-P linking of BPO_4 as expected. Consequently, the signal at -3.4 ppm which appears at the temperature of 210 ^oC and 250 ^oC, is assigned to BO_4 unit in another conformation (not BPO_4) and the formation of BPO_4 at 280 ^oC (sharp peak at -3.8 ppm) is moreover confirmed by 1D $^{11}B(^{31}P)$ D-HMQC NMR.

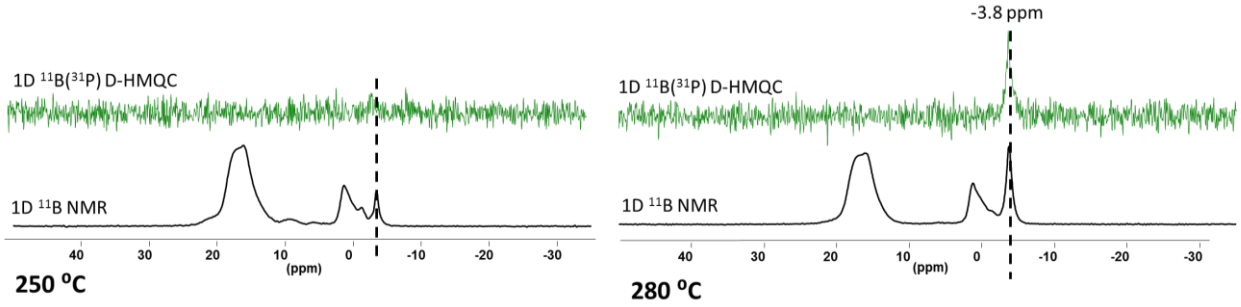

Figure 35 1D $^{11}B(^{31}P)$ D-HMQC NMR (B connected to P nucleus, 18.8T) vs. 1D 11B NMR signal of IF(BA) char residues at 250 ^oC (left) and 280 ^oC (right)

The evolution of BO_3, BO_4 and BO_4 (in BPO_4) conformations (Figure 36) can be estimated (semi-quantitative). It is observed that when the temperature increases from ambient temperature up to 280 ^oC, the BO_3 units of boric acid turn into BO_3 units in different configurations (e.g. B_2O_3) and BPO_4 (formed by the reaction between B_2O_3 and phosphate). In contrast, at high temperature the relative concentration of BO_4 units obviously decreases when the relative concentration of BPO_4 increases and the relative concentration of BO_3 units remains constant. The formation of borophosphate occurs by the reaction of one mole of boron and one mole of phosphorous. The molar ratio of phosphorous to boron in IF(BA) is 1/3.3, boron is thus in excess. The presence of BO_3 units at high temperature could thus be attributed to BO_3 units of B_2O_3; this attribution is further supported by XRD results.

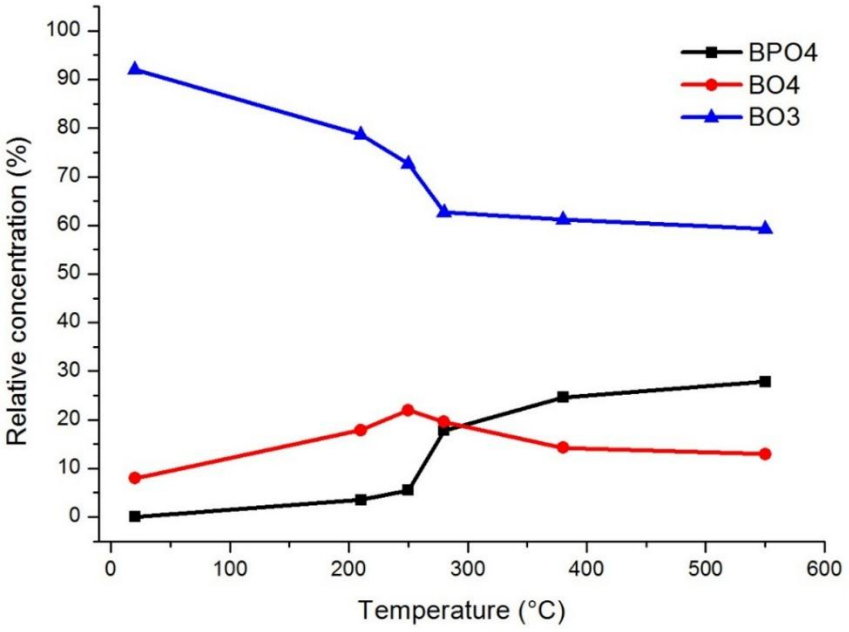

Figure 36 Evolution of the relative concentration of boron species in IF(BA) versus temperatures

Conclusion

The decomposition pathway of the complex intumescent formulation called IF(BA) was investigated as a function of temperature. To summarize, boric acid first degrades in the temperature range of 100 °C and 200 °C yielding boron oxide (B_2O_3). APP then degrades at higher temperature (250 ° C) and its degradation product reacts with boron oxide to form thermally stable materials (i.e. borophosphate (BPO_4)). The formation of BPO_4 occurs at about 250 °C, it is first formed as amorphous borophosphate (detected in ^{31}P NMR but not in XRD) and it then turns to crystalline compound at higher temperature. Its concentration rises as a function of temperature. In this complex formulation, neither $CaCO_3$, TiO_2 nor Si based compounds (from fumed silica, expanded silicate, silicate fibers) evidence interactions with other components of the formulation up to 550 °C. These results emphasize the important role of borate and phosphate in the mechanism of reaction in condensed phase of the complex intumescent formulation.

b) IF(ZB)wt formulation

Figure 37 shows diffractograms of the coating at ambient temperature and the char residues obtained after heat-treatments at different characteristic temperatures. XRD patterns of the coating at ambient temperature and the char residue after the treatment at 250 ^{o}C are similar. It clearly shows the presence of zinc borate and ammonium polyphosphate (APP), which are the raw ingredients in the coating. At 280 ^{o}C, APP decomposes while zinc borate does not decompose at this temperature. At 380 ^{o}C, the formation of additional species are observed. It suggests that the reaction between the additives occurs between 280 ^{o}C and 380 ^{o}C. BPO_4 is detected and it is formed by the reaction between APP and zinc borate like what was described in 3.1.2. Another crystalline phase is boric acid, which can be obtained by hydration of B_2O_3 (a part of degradation product of zinc borate). At 550 ^{o}C, an additional specie, zinc orthophosphate (α-$Zn_3(PO_4)_2$) is detected. The XRD patterns of $CaCO_3$ and TiO_2 are clearly observed in the char residues after the treatment at 380 ^{o}C and 550 ^{o}C. The identification of these two species in the non-degraded coating and in the residue of HTT below 280 ^{o}C are not evident since they are present with low quantity in the coating formulation. Nevertheless, it indicates that these two additives neither decompose nor react with other ingredients in the formulation up to 550 ^{o}C. It also happened in the case of IF(BA). On the one hand, Si based compounds (from fumed silica, expanded silicate, silicate fibers) are not identified in XRD patterns.

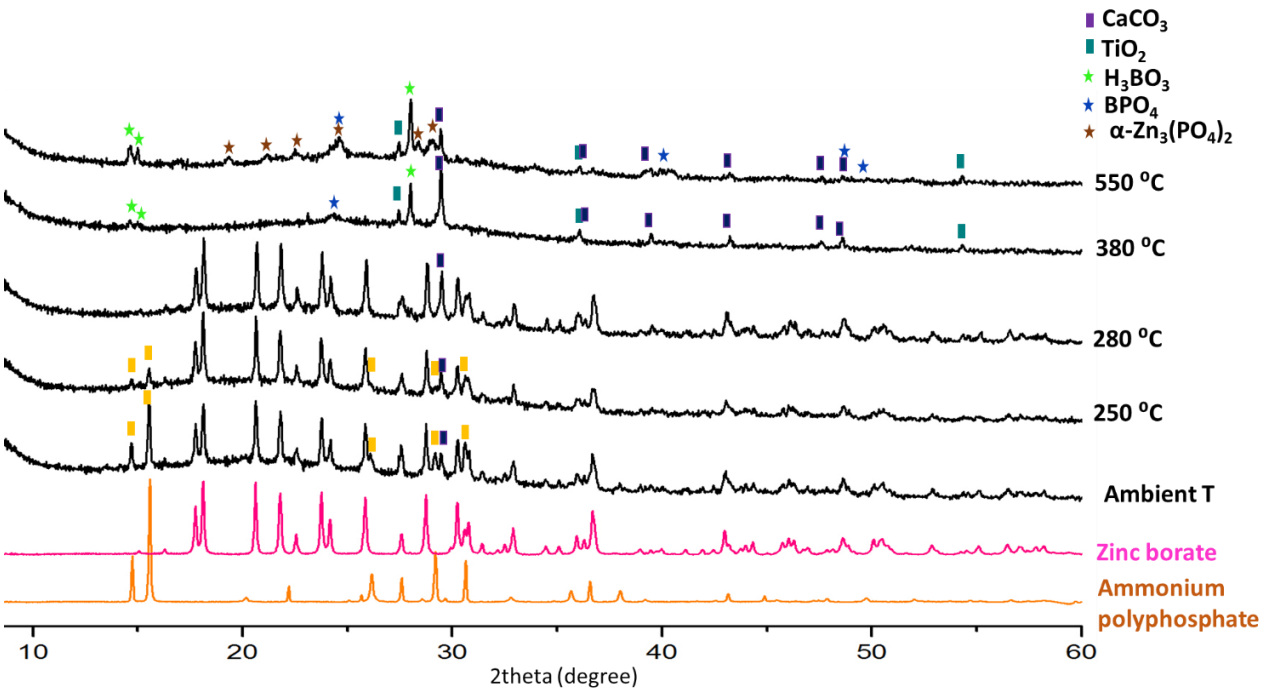

Figure 37 XRD diffractograms of IF(ZB)wt char residues versus temperatures

The resulting materials (crystalline species) are quite similar in IF(BA) and IF(ZB)wt (only one specie different: zinc orthophosphate). XRD only permits to identify the crystalline species in the samples. To go further in the investigation and to detect the potential differences between the two formulations, ^{31}P NMR is used to investigate in more detail the evolution of phosphorous species as a function of temperature.

The ^{31}P NMR spectra of IF(ZB)wt coating and of its residues after heat treatments at different characteristic temperatures are presented in Figure 38. The ^{31}P NMR spectrum of IF(ZB)wt coating at ambient temperature exhibits the same spectrum as IF(BA) with characteristic bands of polyphosphate chains (-22 and -24 ppm) and of TCPP (-4.4 ppm). At 250 °C, the evolution of phosphorus species between IF(ZB)wt and IF(BA) are quite similar. The phosphate degrades and phosphoric acid and/or orthophosphate are detected at 0 ppm [161, 175]. However, on the opposite of what was observed for IF(BA), borophosphate is not observed at 250 °C in the case of IF(ZB)wt.

The evolution of phosphorus species at high temperature (T> 280 °C) is different between IF(ZB)wt and IF(BA) formulations. In the case of IF(ZB)wt, a broad band is observed between 5 and -35 ppm (centered -16 ppm). Such a signal can be due to the formation of a disordered structure containing various bond angles, bond lengths and coordination spheres leading to a continuous distribution of ^{31}P isotropic chemical shift and thus to a widening of the signal [183]. Such structure can be observed in amorphous phosphates. At high temperature (380 °C and 550 °C), the characteristic band of borophosphate at -30 ppm is observed. The borophosphate formed is supposed to have a low crystallinity. This statement is supported by the XRD pattern of BPO_4 shown in Figure 37 (not well-identified peaks). In other words, the line width at half maximum ($LW_{1/2}$) [184] of the characteristic peak of borophosphate at 380 °C and 550 °C are of 620 and 770 Hz respectively, these values are about three times higher than the $LW_{1/2}$ of crystalline BPO_4 found in IF(BA) char residue (($LW_{1/2}$ = 244 Hz). Moreover, for a HTT of 550 °C, an additional sharp band is observed at 3.9 ppm. This peak is assigned to orthophosphate structure of α-zinc orthophosphate (α-$Zn_3(PO_4)_2$) [144, 165].

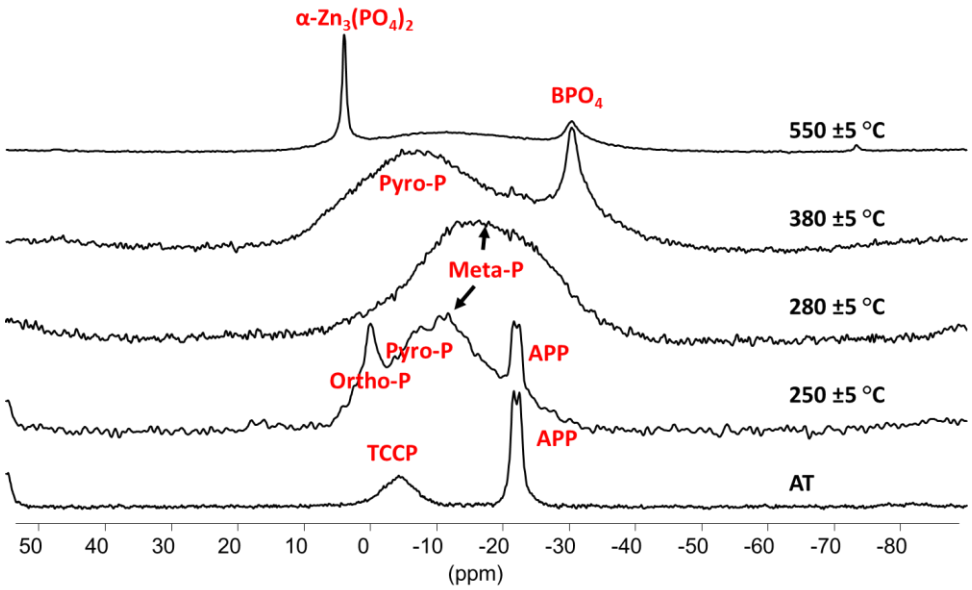

Figure 38 ^{31}P NMR spectra (9.4 T) of IF(ZB)wt char residues versus temperatures

Afterwards, the evolution of boron species was taken into consideration. ^{11}B NMR spectra of IF(ZB)wt residues collected after different heat treatments are presented in Figure 39. The same approach was used; the spectra were simulated to quantity the BO_3 and BO_4 populations (Figure 40). The ratio of BO_3/BO_4 unit obtained by simulating the experimental spectrum of IF(ZB)wt coating at ambient temperature is 1/2.2. This is in agreement with the literature where it was reported that neat zinc borate is composed of 1 BO_3 unit and 2 BO_4 units [83, 84]. At 280 ^oC, the boron spectrum line shape is slightly modified compared to that of ambient temperature: a BO_3 band lying between 16 and 20 ppm and a broad BO_4 signal lying between -2 and -6 ppm appear. Indeed, zinc borate starts to degrade at the temperature of 290 ^oC. Under heat treatment condition, the samples were heat-treated at 280 ± 5 ^oC for 2 hours, zinc borate could partially degrade or modify at this temperature. The characteristic peak of borophosphate at -3.8 ppm are observed from 380 ^oC up to 550 ^oC. These are in good agreement with the results obtained from XRD and ^{31}P NMR.

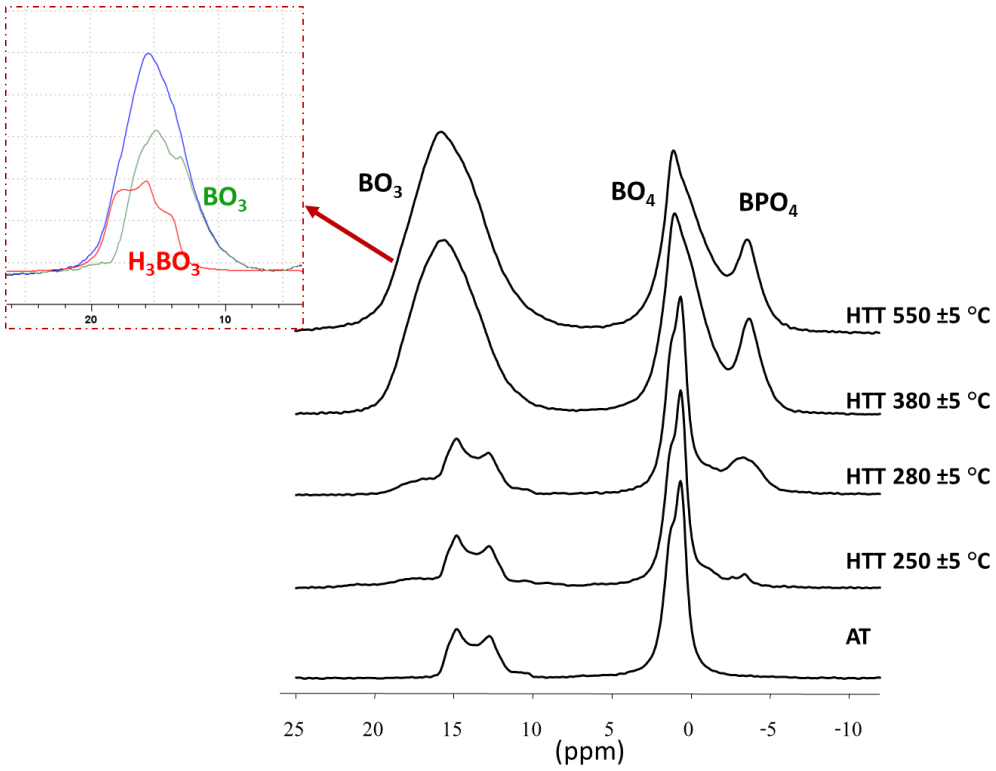

Figure 39 ^{11}B NMR spectra (18.8 T) of IF(ZB)wt char residues versus temperatures

Considering the evolution of the relative concentration of boron species versus temperature (Figure 40), it is observed that the boron species change a little bit from ambient temperature up to 280 °C. Above 280 °C, the relative concentration of BO_4 units decrease whereas the amount of BO_3 units and BPO_4 increase. It is noteworthy that the relative concentration of borophosphate is much lower than that of BO_4 unit whereas the opposite was observed in the case of IF(BA) formulation.

BO_3 in zinc borate changes to BO_3 in a different conformation (280 ^oC to 380 ^oC). This is reasonably attributed to the dehydration of zinc borate leading to the formation of $2ZnO.3B_2O_3$ (as boron is in excess in the formulation, reactions between borates and phosphates cannot consume all boron). A broad signal of BO_3 unit lying between 10 and 20 ppm might be assigned to BO_3 unit in boric acid conformation (identified by XRD) and BO_3 unit in $2ZnO.3B_2O_3$ (degradation product of zinc borate). As this case, it also suggests the reversion of boron oxide to boric acid like it is observed in the case of formulation containing boric acid.

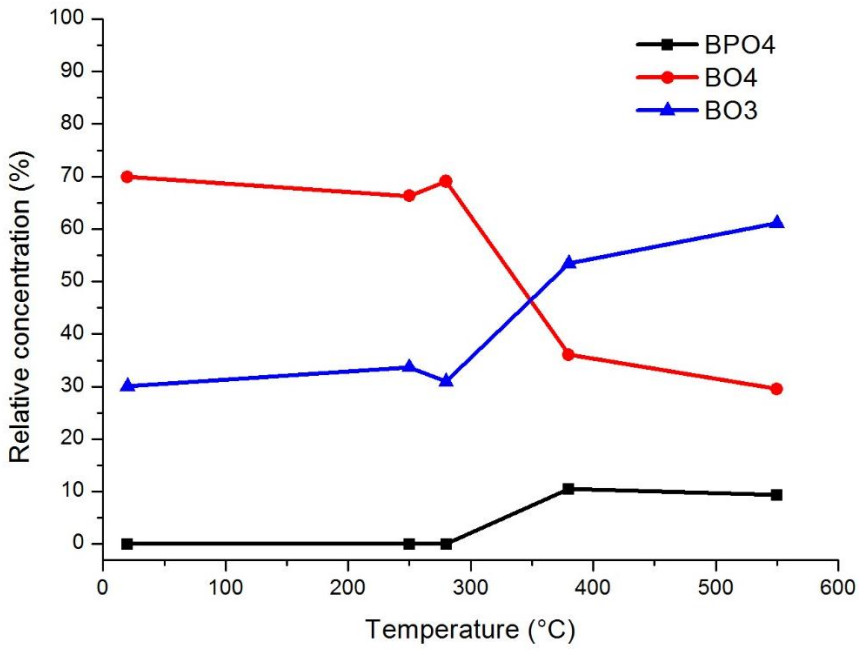

Figure 40 Relative concentrations of boron species in IF(ZB)wt char residues versus temperatures

Conclusion

The decomposition pathway of IF(ZB)wt was investigated using the same approach as in the case of IF(BA) formulation. The decomposition pathway of IF(ZB) is different to IF(BA) due to the different dehydration temperature of borates. The obtained results can be summarized as follows:

i) BPO_4 is formed but it is found at higher temperature (380 ^oC vs. 250 ^oC) when ZB is used instead of boric acid
ii) Formed BPO_4 has a lower crystallinity than that found in IF(BA)
iii) Formation of boric acid (H_3BO_3) by the hydration of boron oxide (B_2O_3) can be found in both cases
iv) Additional compound because of zinc borate (i.e. α-$Zn_3(PO_4)_2$) is found at 550 ^oC
v) $CaCO_3$ and TiO_2 do not decompose nor react with other components in the formulation up to 550 ^oC as similar to IF(BA)
vi) No sign of reactions between Si based compounds (from fumed silica, expanded silicate, silicate fibers) with any components is observed

3.2.1.2 When submitted to a fire test

In the previous part, the chemical species formed in the condensed phase after heat-treatment (at defined temperatures under pyrolytic condition) were identified. It can give information on the decomposition pathway and on how the additives react together. However, it should be noticed that the heating ramp and the studied temperatures are hugely different from real fire test: low temperature with a long heating time (HT) vs. high temperature with a short exposed time (under fire test). Hence, this part investigates the transformation of species formed in the condensed phase when the coatings are exposed to a fire test.

The coated steels were submitted to the furnace test (UL1709) and stopped at different characteristic times. The time-temperature curves of IF(BA) and IF(ZB)wt pointing out the characteristic times are shown in Figure 41. The selected times are 2, 5, 10, 12 and 15 minutes for both formulations. In addition to these, longer exposure time (20 minutes) was also used for IF(ZB)wt. This point is excluded in the case of IF(BA), since for this formulation a detachment of char at about 13 - 14 minutes occurred. Note that the samples continued burning after stopping the burners since the fuel sources (e.g. polymeric contents) were not completely consumed. The burning samples were removed from the furnace and a fire was immediately extinguished.

The same approaches as done in the previous part (3.2.1.1) were used. The char residues were collected after each test to be analyzed. XRD, ^{11}B and ^{31}P NMR were used as the characterization tools for char analyses. In the following part, only the identification of chemical species formed in the condensed phase will be discussed. Meanwhile, the expansion and char morphology were also assessed and will be detailed in the section 3.2.2 (thermo-physical properties).

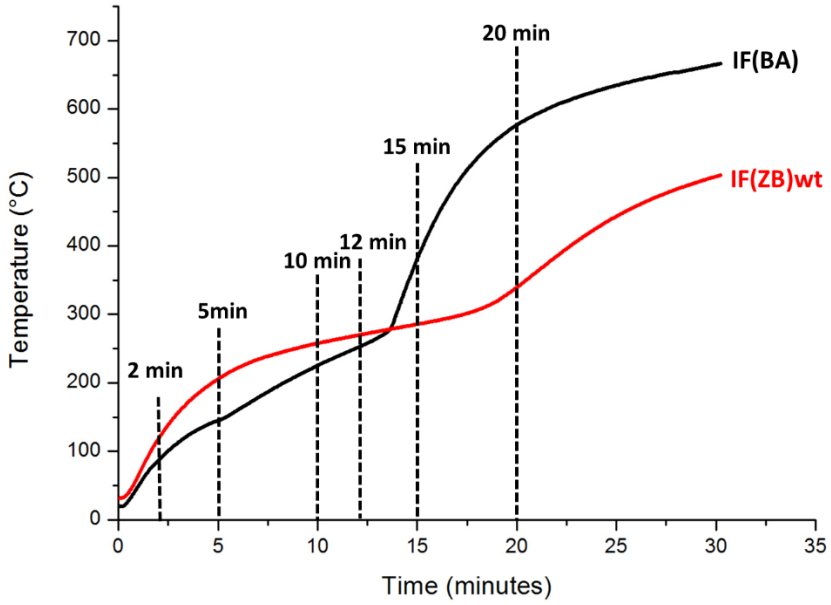

Figure 41 Time-temperature curves of IF(BA) and IF(ZB)wt pointing out the characterisric times

a) IF(BA) formulation

At 2 and 5 minutes of the test, the IF(BA) coating is not completely transformed to an expanded char; non-degraded coating is still observed underneath (Figure 42). The thickness of non-degraded coating after the fire test was measured compared to the initial thickness of the coatings. It was found that only a top thin layer of the coating decomposes yielding a char residue. The thickness of the non-degraded coating decreases averagely of about 0.11 mm and 0.55 mm for the test at 2 and 5 minutes respectively.

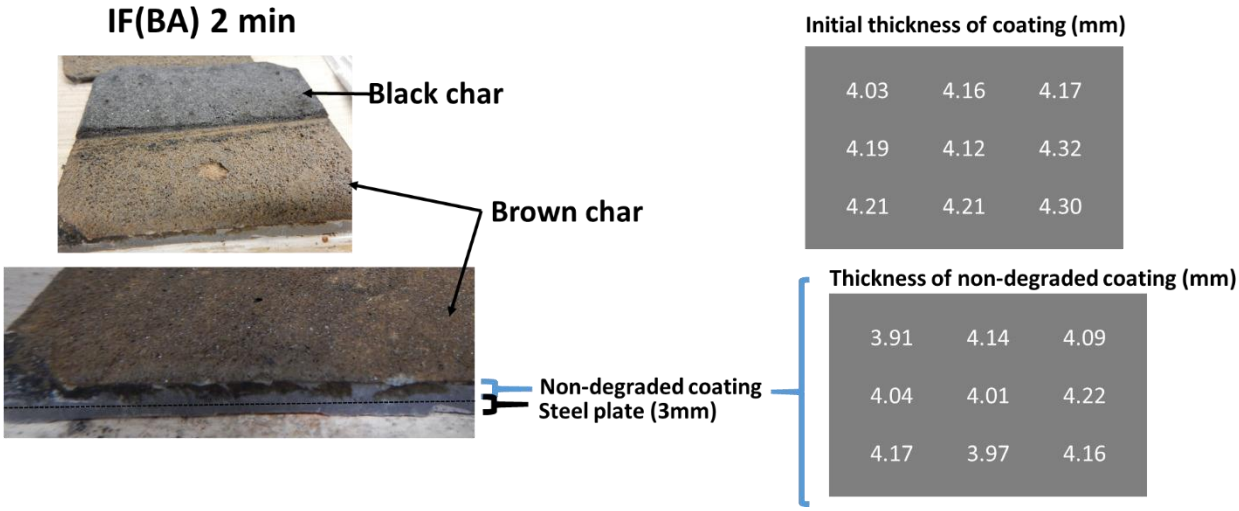

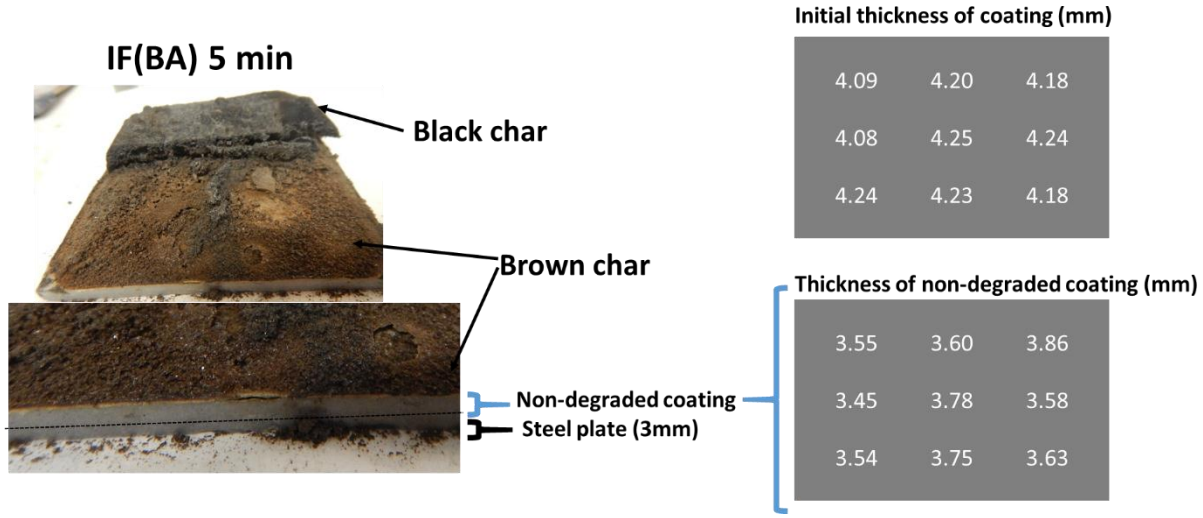

Figure 42 Photos of IF(BA) residual aspects collected after the furnace test (2 and 5 minutes)

Figure 43 shows the diffractograms of IF(BA) coating and of char residues at different characteristic times. For the non-degraded coating, the results are the same as described in the previous part (*3.2.1.1 Pyrolysis of IF(BA) and IF(ZB)*); the XRD pattern shows the presence of APP, boric acid, $CaCO_3$ and TiO_2. The chemical species formed in the char residues at 2, 5, 10, 12 and 15 minutes are the same; it indicates the presence of BPO_4, boric acid, TiO_2 (low intense peaks) and $CaCO_3$. Under a fire test condition, the reversion of boron oxide to boric acid is more plausible compared to the heat treatment under pyrolytic condition. Here, boric acid was found in all samples whereas it was previously identified only in the char residue after heat-treatment of 550 ^oC (in 3.2.1.1). The presence of $CaCO_3$ is surprising; $CaCO_3$ decomposes in one step in the temperature range of 680 ^oC to 900 ^oC [87, 88]. With the furnace test's condition (1100 ^oC in 5 minutes), $CaCO_3$ was expected to decompose. The presence of large heat gradient in intumescent layers has been evidenced in the publication [185] in less severe conditions (ISO 834 vs. UL 1709). These results showed the gradient of temperatures of about 100 to 200 ^oC between different positions in the intumescent layer. In addition, the temperatures measured in the char are much lower than the furnace temperature. This can be the reason of the identification of $CaCO_3$ in these char residues and it suggests that the temperature inside the charred layer stays lower than 680 ^oC. The analyzed samples were prepared by taking all charred layers and they were ground together, it makes sense to detect $CaCO_3$ at all characteristic times. Nevertheless, CaO (or Ca-

based compounds) should be formed too but it was not detected by XRD probably because of too low concentration of these species in the residues or low crystallinity.

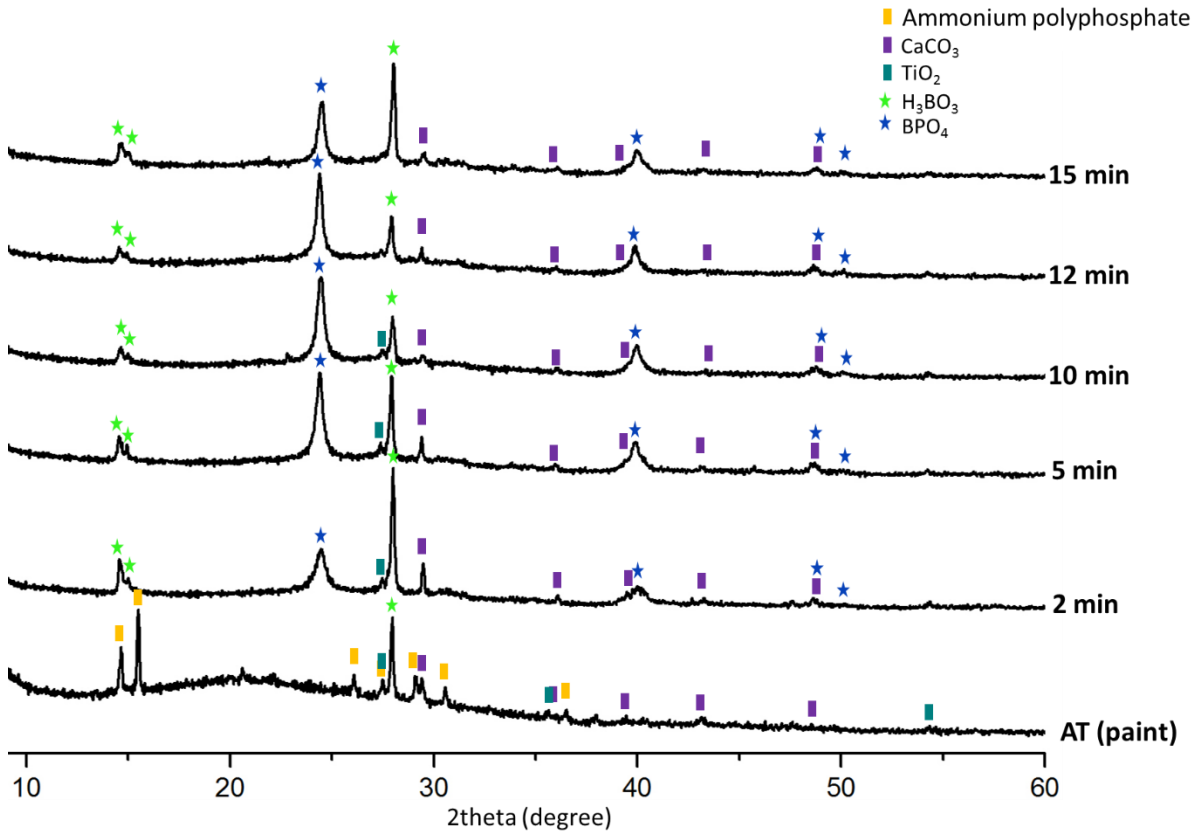

Figure 43 XRD diffractograms of IF(BA) char residues versus times

Afterwards, the residual samples were characterized using ^{31}P NMR (Figure 44). A sharp peak appearing at - 30 ppm, which is a characteristic peak of BPO_4, is observed in all samples (from 2 to 15 minutes). It evidences the formation of BPO_4, which is in good agreement with the results obtained by XRD diffractograms. At 2 min, there is a broad peak lying between 0 and - 25 ppm, which indicates the presence of amorphous phosphate. However, its intensity is very low.

The results show that the formation of BPO_4 occurs immediately after starting the fire test. This observation is consistent with the fact that the formation of BPO_4 occurs at the temperature between 250 ^oC and 280 ^oC that is much lower than the temperature in the furnace test. Note also that APP completely decomposes to yield amorphous phosphate and reacts with boric acid.

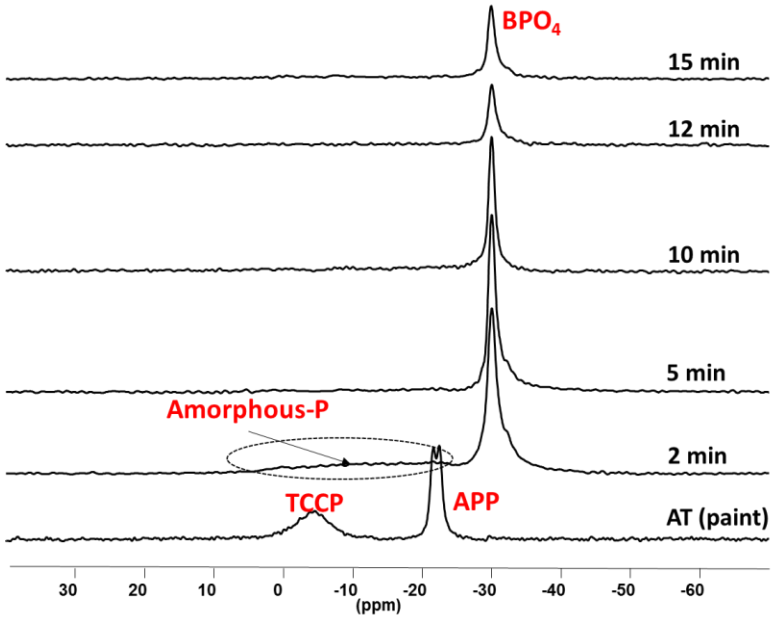

Figure 44 ^{31}P NMR spectra (9.4 T) of IF(BA) char residues versus times

XRD and ^{31}P NMR show no difference in chemical species formed from 2 minutes to 15 minutes. The crystalline compounds and phosphorus species formed are identical as a function of time. As previously remarked, boron is one of the most important elements. ^{11}B NMR is thus taken into account to investigate whether or not boron structure changes versus exposed times in the furnace test. Figure 45 shows the ^{11}B NMR spectra of IF(BA) char residues at different characteristic times. The formation of BPO_4 is obviously identified. An additional signal appears at about 0 ppm, which can be assigned to another boron tetrahedron species (BO_4). It is found in all samples. A signal of BO_3 unit lying between 5 and 20 ppm can be observed. The line shape suggests several BO_3 units overlapping, e.g. BO_3 tetrahedron in boric acid conformation (suggested by XRD). The spectra were then simulated to characterize and to quantify the relative concentration of each boron unit (Figure 46). It was found that the evolution of boron species does not change between 2 and 10 minutes. Afterwards, the relative concentrations of BPO_4 and BO_4 decrease while the relative concentration of BO_3 increases.

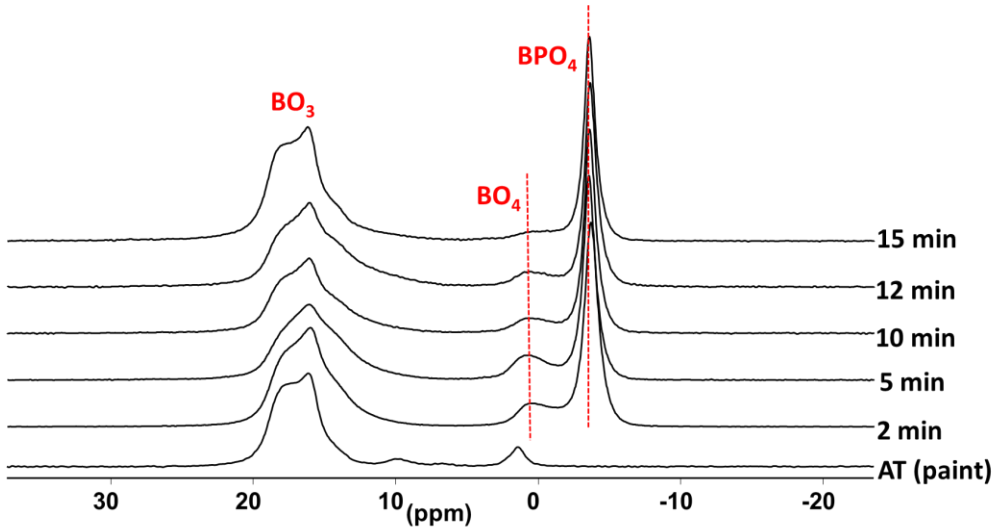

Figure 45 ^{11}B NMR spectra (18.8 T) of IF(BA) char residues versus times

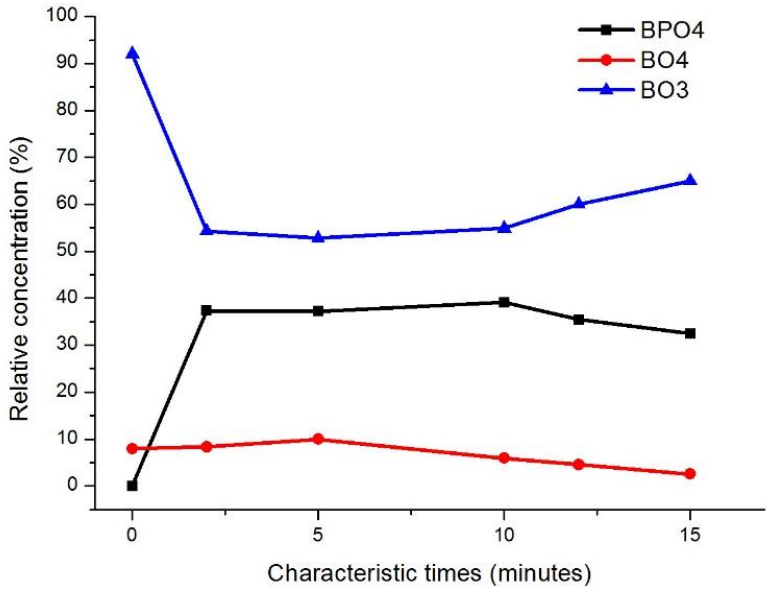

Figure 46 Relative concentration of boron species in IF(BA) char residues versus times

Conclusion

The decomposition pathway of the IF(BA) coating versus the exposed times in the furnace test was investigated. The formation of BPO_4 and of B_2O_3 (in form of boric acid) were evidenced throughout the studied period (between 2 and 15 minutes); no modification of chemical species was observed as a function of time. The resulting species are the same as observed in char residues after heat-treatment under pyrolysis condition at 380 ^oC and 550 ^oC. It was shown that some of $CaCO_3$ does not decompose up to 15 minutes of the test. TiO_2 and Si based compounds (i.e. SiO_2, silicate) were not identified to react with other components (i.e. borate, phosphate).

Note that the experimental conditions between the furnace and HTT conditions are different in terms of heating ramp, heating temperature and duration; i) HT - under low temperature for a long time and ii) furnace test - under high temperature for a short time but it does not change the chemical species formed. The first case (HT) allows elucidating in more detail the beginning stage of decomposition while the second case permits to elucidate the real event occurring under the fire test and characterize the high stable compounds formed at high temperature with a long exposed time. Moreover, these results also highlight the important role of borate and phosphate in the complex formulations.

b) IF(ZB)wt formulation

At 2 and 5 minutes of the test, it is noteworthy that the aspects of the char residues (Figure 47) are similar to the one of IF(BA) char. Only a thin charred layer is formed at the surface of the material. The top charred layer is only analyzed in the following and not the non-degraded material found underneath.

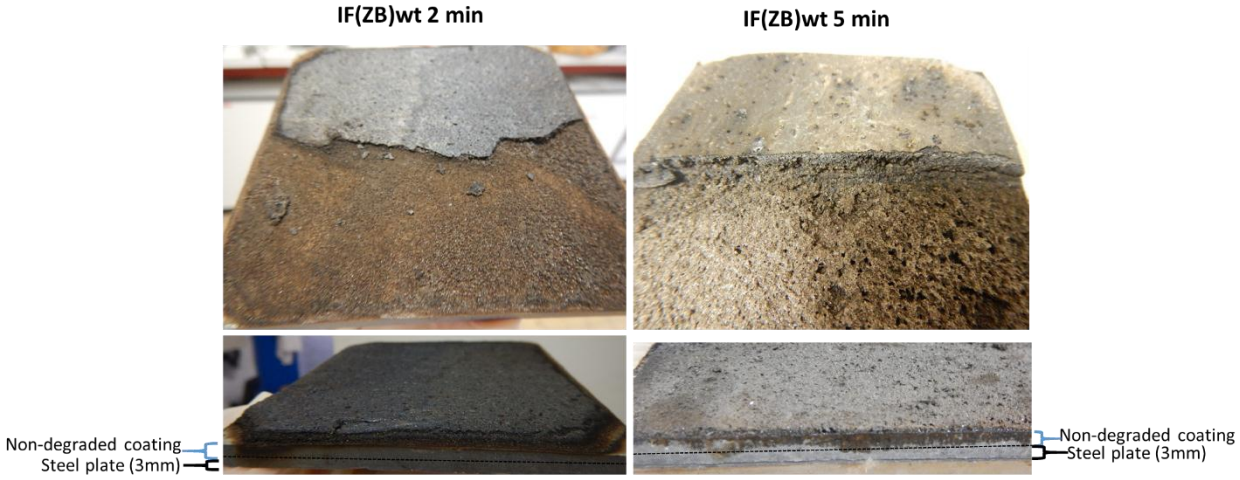

Figure 47 Photos of IF(ZB)wt residual aspects after the furnace test (2 and 5 minutes)

XRD diffractograms of IF(ZB)wt coating and of char residues are shown in Figure 48. In the coating at ambient temperature, it possesses the raw ingredients of the coatings (e.g. zinc borate, APP, $CaCO_3$, TiO_2) as similar to what was described in 3.2.1.1.2. Char residue collected at 2 minutes contains amorphous phase together with the crystalline boric acid, $CaCO_3$ and TiO_2. Note that only the most intense peaks can be distinguished at 2 minutes, it could be due to a high amount of amorphous part. Small and thin characteristic peaks of $CaCO_3$ and TiO_2 are observed up to 10 minutes. From 15 minutes, $CaCO_3$ and TiO_2 are no longer distinguished but no conclusion can be drawn because they could be hidden by other peaks. BPO_4, zinc orthophosphate (α-$Zn_3(PO_4)_2$) and B_2O_3 (in form of H_3BO_3) are detected from 5 minutes up to 20 minutes. In addition to these mentioned species, another zinc-based compound (i.e. α-zinc pyrophosphate (α-$Zn_2P_2O_7$)) is detected. α-$Zn_2P_2O_7$ is formed from about 10 minutes of the test and is still present up to 20 minutes. Note that the chemical species formed in this formulation are very complex, some crystalline species have not been attributed yet.

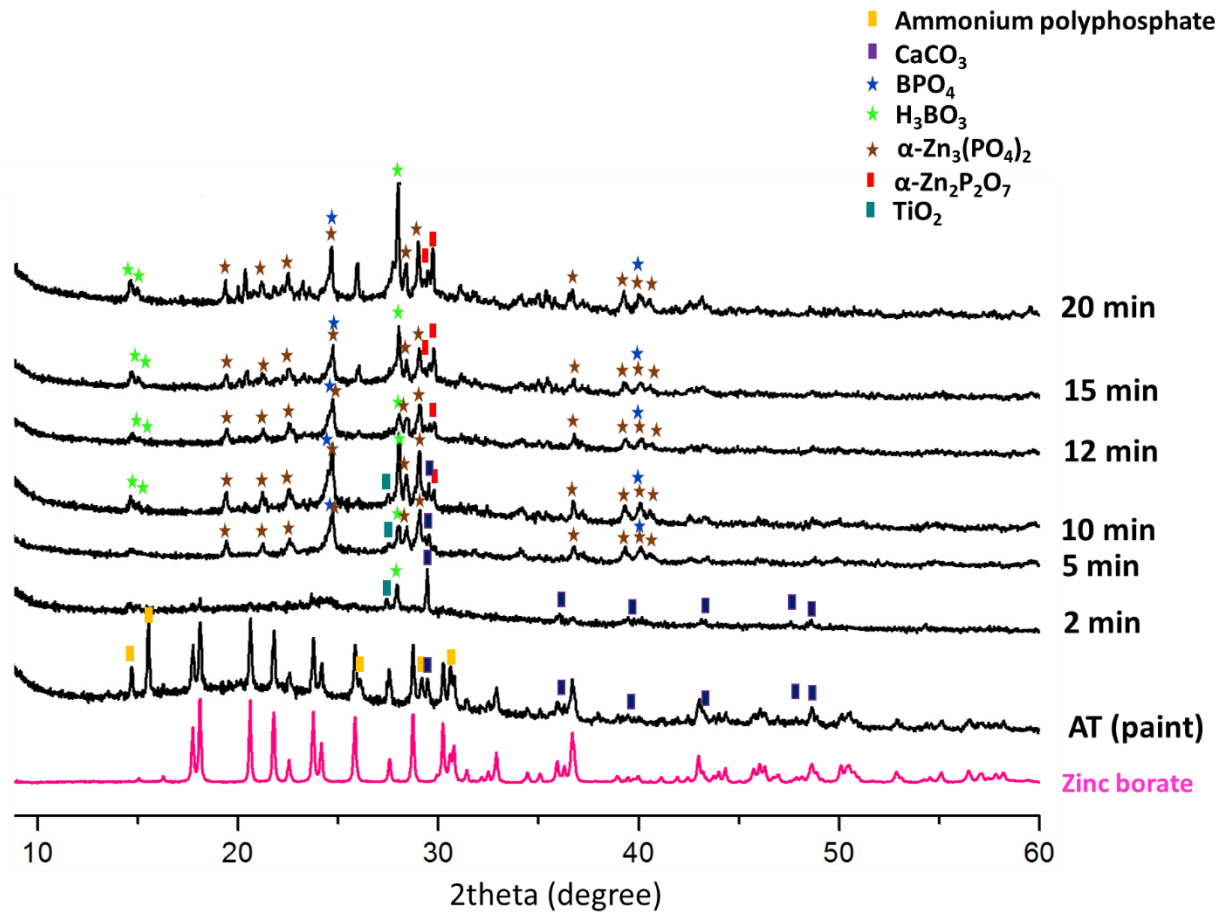

Figure 48 XRD diffractograms of IF(ZB)wt char residues versus times

To identify the evolution of phosphorus species, ^{31}P NMR was performed. Figure 49 shows ^{31}P NMR spectra of the char residues. It shows the formation of BPO_4 (signal at -30 ppm) and α-$Zn_3(PO_4)_2$ (signal at 3.9 ppm), they are formed from 2 minutes of the test. However, these two species were not identified on the XRD diffractogram at 2 minutes, probably because of their poor crystallinity and they are observed up to 20 minutes. At 2 minutes, a broad signal lying between 0 and -30 ppm is moreover observed; this indicates the disordered structure of phosphate which is then vanished (from 5 minutes). This underlines the transformation of amorphous species and/or poorly crystalline species into highly crystalline species.

In the zoom area (left hand side of Figure 49), additional peaks are observed between -5 and -20 ppm (low intense peaks). There are two sets of triple peaks, which can be assigned to the characteristic signals of α- and γ-zinc pyrophosphate (α-$Zn_2P_2O_7$ → -5.2, -7.3, -10 ppm and γ-

$Zn_2P_2O_7$ → -15.9, -19, -21.1 ppm) [59, 83, 167]. These are similar to what were observed in the char residues of IF(ZB)m described in 3.1.2. They are formed from 10 minutes up to 20 minutes of the test. Regarding the peak height, it suggests that these additional species are present at very low concentration. The identification of α-$Zn_2P_2O_7$ is consistent with the XRD results as previously described while γ-$Zn_2P_2O_7$ was not identified in XRD pattern (Figure 48). When looking at the XRD pattern of γ-$Zn_2P_2O_7$ in the database or literature [186] compared to that of the char samples, it is possible to have γ-$Zn_2P_2O_7$ in XRD pattern but their peaks could be hidden by other peaks.

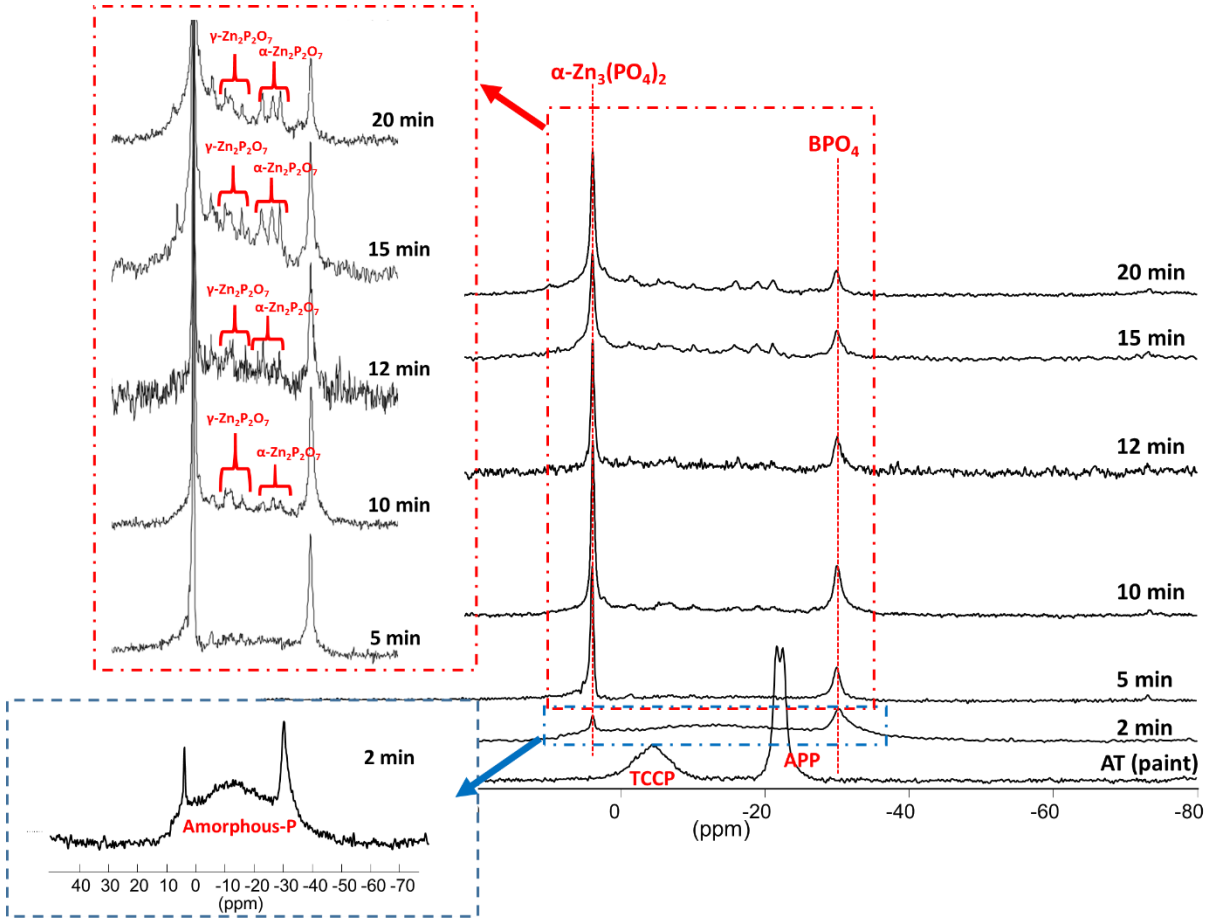

Figure 49 ^{31}P NMR spectra (9.4 T) of IF(ZB)wt char residues versus times

^{11}B NMR spectra of IF(ZB)wt char residues (Figure 50) show the evolution of boron species versus times. It confirms the formation of BPO_4 (-3.8 ppm) from 2 minutes to 20 minutes; it is consistent with the results shown by XRD and ^{31}P NMR. Additionally, a peak of BO_4 unit is distinguished between 0.2 and 0.8 ppm. A broad signal lying between 10 and 20 ppm (BO_3 units)

is observed up to 20 minutes. When considering the ^{11}B NMR spectra of the coating and of char residue collected at 2 minutes, they are completely different; this suggests the total degradation of zinc borate. The relative concentrations of each specie as a function of the characteristic times is shown on Figure 51. When zinc borate decomposes, the BO_4 species decrease exponentially. It is suspected to transform into BO_3 species in different environment (e.g. $ZnO.B_2O_3$). Between 2 and 10 minutes, the relative concentration of BPO_4 slightly increases while BO_4 unit decreases. After 10 minutes of the test, the concentration of BPO_4 decreases gradually up to 20 minutes.

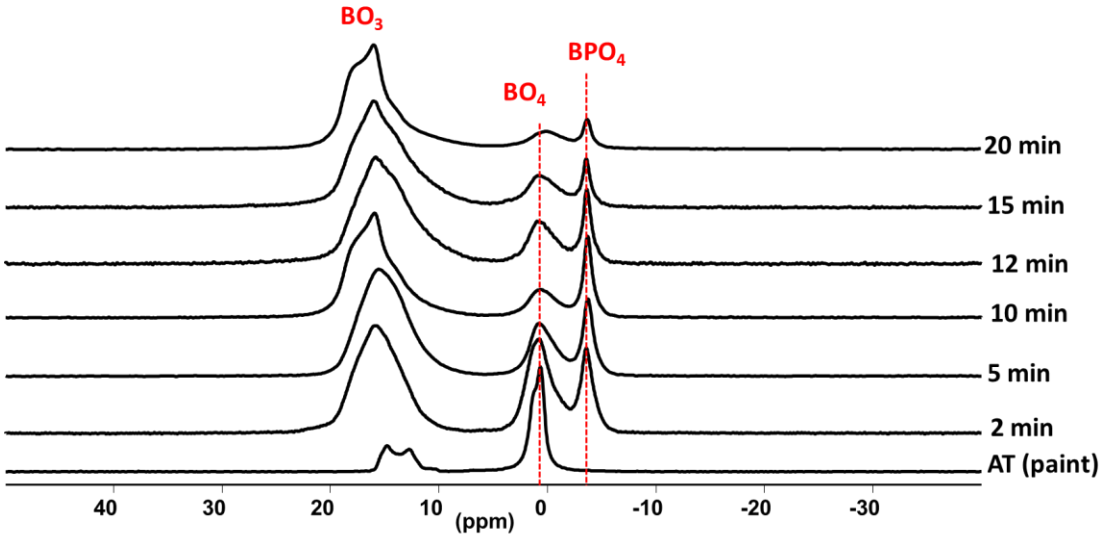

Figure 50 ^{11}B NMR spectra (18.8 T) of IF(ZB)wt char residues versus times

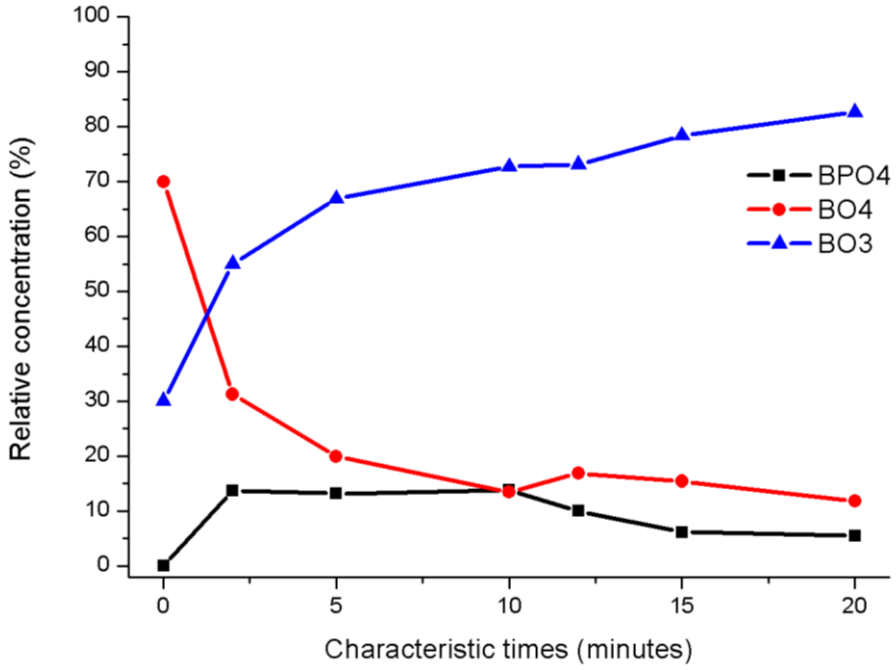

Figure 51 Relative concentration of boron species in IF(ZB)wt char residues versus times

Conclusion

The decomposition pathway of IF(ZB)wt coating was investigated. The evolution of chemical species formed in the condensed phase during the furnace test (between 2 and 20 minutes) was greatly modified. The formation of BPO_4 is identified from 2 to 20 minutes. While the formation of dissimilar specie to the IF(BA) formulation (i.e. $Zn_3(PO_4)_2$) was also identified (2 → 20 minutes). In addition to these, the formation of zinc pyrophosphate (α- and γ- $Zn_2P_2O_7$) were detected from 10 minutes of the test. This highlights the notable role of zinc borate on the formation of crystalline zinc based compounds. However, the quantity of these two latter species are very low compared to the major species such as BPO_4 and $Zn_3(PO_4)_2$. Whereas the reactivity of $CaCO_3$, TiO_2 or SiO_2 in these char residues could not be identified.

3.2.1.3 Proposed mechanisms of decomposition

The summarization of the results are schemed in Figure 52.

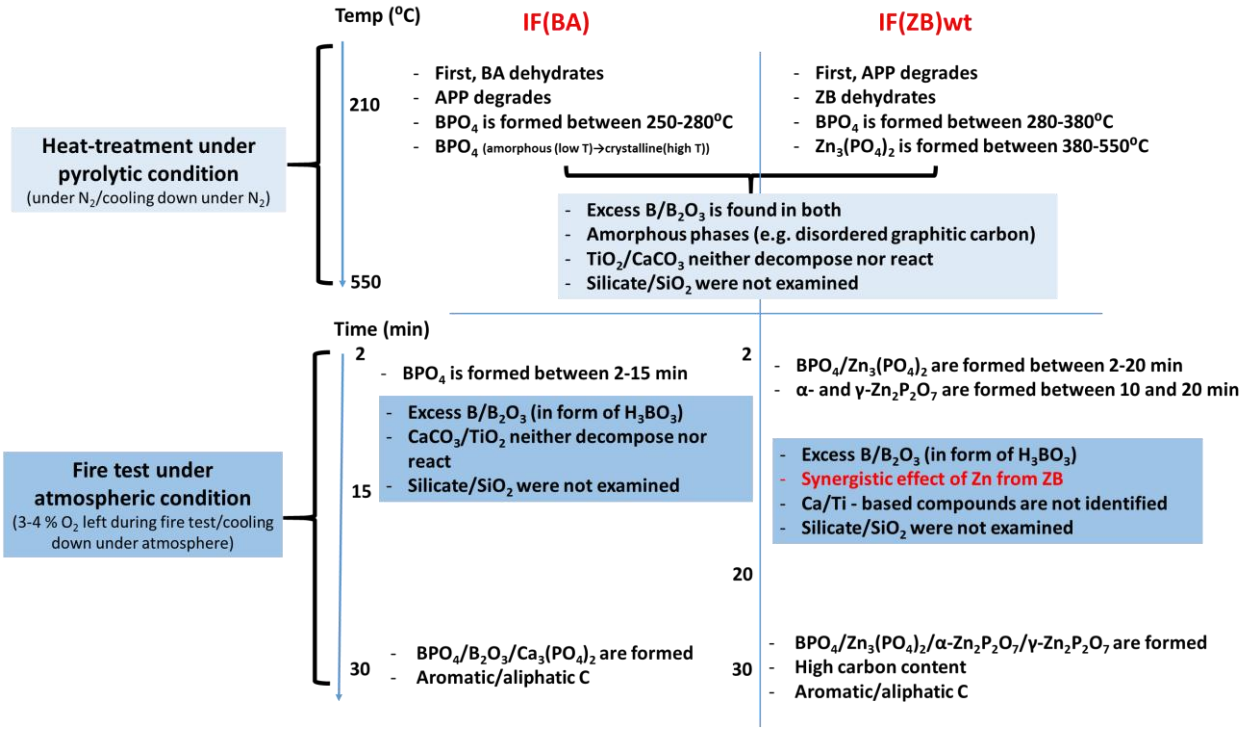

Figure 52 Mechanisms of decomposition of IF(BA) and IF(ZB)wt

In the case of IF(BA), boric acid first degrades yielding boron oxide. APP then degrades at higher temperature. The reaction between boron oxide and decomposition product of APP occurs immediately after degradation. The formation of BPO_4 occurs between 250 °C and 280 °C. B is in excess compared to P, B_2O_3 is thus present in the char residue. BPO_4 and B_2O_3 are highly stable compounds, they are formed and present in the char residues up to 15 minutes of the test (B_2O_3: 210 → 550 °C and 2 → 15 minutes and BPO_4: 250 → 550 °C and 2 → 15 minutes). Surprisingly, $CaCO_3$ was found in char residues of all samples (210 → 550 °C and 2 → 15 minutes), evidencing that it does not decompose nor react with any components. For TiO_2 or SiO_2, there is no evidence of their reaction.

In the case of IF(ZB)wt, APP first degrades. Zinc borate then degrades. The formation of BPO_4 is shown to occur between 280 °C and 380 °C and it is also found under the furnace condition

up to 20 minutes of the test (BPO_4: 380 → 550 °C and 2 → 20 minutes). The additional specie such as α-$Zn_3(PO_4)_2$ is formed at 550 °C, resulting from the contribution of zinc borate. This crystalline specie is also thermally stable compound and is found under the furnace test up to 20 minutes (α-$Zn_3(PO_4)_2$: 550 °C and 2 → 20 minutes). Under the furnace condition, two polymorphs of zinc pyrophosphate were found (α- $Zn_2P_2O_7$: 10 → 20 minutes and γ- $Zn_2P_2O_7$: 10 → 20 minutes).

The formation of inorganic compounds, which are thermally stable, are supposed to be responsible for stabilizing and strengthening the carbonaceous char. BPO_4 and B_2O_3 which were mentioned to enhance the fire protective properties and adhesion of the protective char [74] are found in both formulations. In the case of the formulation containing zinc borate, zinc based compounds, which are thermally stable (i.e. α-$Zn_3(PO_4)_2$, α- and γ-$Zn_2P_2O_7$) are additionally formed. These indicate the high reactivity of zinc from zinc borate reacting with other species in the formulation, especially phosphorous based components. It allows stabilizing phosphorus in the condensed phase, that benefits char formation and char stabilization as described in the state of the art.

3.2.1.4 Conclusion

In this part, the mechanisms of decomposition of the intumescent coatings containing either boric acid or zinc borate were investigated. The study focuses particularly on the mechanisms occurring in the condensed phase. This study highlights the important role of borate and phosphate in the complex formulations. Even if the formulations contain twelve ingredients, the reaction of borate and phosphate are predominant. In both cases, borophosphate and boron oxide are formed. Zinc from zinc borate plays a very important role in the condensed phase, zinc-based compounds (e.g. $Zn_3(PO_4)_2$, $Zn_2P_2O_7$) are additionally formed in IF(ZB)wt char residue.

The intumescent phenomenon is a complex process. Not only chemical modifications in the condensed phase but also thermo-physical properties govern the efficiency of the intumescent char. The next part thus deals with the investigation of the thermo-physical properties of the studied intumescent coatings including IF(BA) and IF(ZB)wt.

3.2.2 Thermo-physical properties of the chars of IF(BA) and IF(ZB) coatings

The goal of this part is to measure the complex viscosity, dynamic expansion, char morphology, thermal conductivity, as well as the char strength of the studied intumescent coatings. The intumescent chars collected in the previous part (3.2.1.2) were analyzed ex-situ while the complex viscosity, thermal conductivity and char strength were dynamically measured as a function of temperature, namely an in-situ way. Only expansion was assessed in two aspects: i) static (cool state after furnace test) and ii) dynamic (as a function of temperature). The results are discussed in the following.

3.2.2.1 Complex viscosity and expansion

The efficiency of the char is related to its ability to expand and form a multicellular structure. One of the main aspect is the physical structure of intumescent char (uniformity and porosity). The type of char depends on the way the intumescent develops, which is closely linked to its chemical transformation during heating [49]. The expansion of intumescent coating is due to the slow diffusion of the evolved degradation gases released into the degraded matrix. The importance of the visco-elastic properties of this layer is crucial because it directly affects the porosity of the obtained char. In the literature [119, 187], good correlations between the different steps of the intumescent process and measurements of the expansion and apparent viscosity were demonstrated. It is consequently of interest to measure in-situ viscosity along with expansion of intumescent coatings and to correlate these data to their degradation behavior obtained by TG analysis.

3.2.2.1.1 Dynamic measurement of complex viscosity and expansion

Complex viscosity, relative expansion and TG curve of IF(BA) are presented in Figure 53. IF(BA) exhibits a slight expansion between 150 ^{o}C and 210 ^{o}C, concurrently to an increase of viscosity from 1.3x10^{5} Pa.s (150 ^{o}C) to 4.3x10^{5} Pa.s (210 ^{o}C). The increase of viscosity can be attributed to the dehydration of boric acid to from B_2O_3. A similar result was observed by M. Jimenez [81]. The viscosity remains steady up to about 260 ^{o}C while a slight expansion is still observed. The highest expansion (180 % of relative expansion) is reached when the viscosity falls

down to about $6.5x10^3$ Pa.s. However, the expansion dramatically decreases when viscosity reached its lower value ($5.0x10^2$ Pa.s). This dramatic decrease in viscosity observed between 300 °C and 460 °C corresponds to the main degradation step of the coatings (see TGA), and in particular to the degradation of the epoxy resin. Indeed, epoxy resin degrades in two main steps: a first step between 220 °C and 380 °C, corresponding to about 84 % weight loss and a second step between 375 °C and 550 °C leading to the total degradation of the resin. Epoxy resin degrades by hemolytic rupture of bonds (e.g. N-C, O-CH_2) producing free radicals which undergo further reactions that are expected to be of complex nature [81, 128]. The negative value of the relative expansion (-100 % of relative expansion) means that (i) there is no char left at this moment or (ii) char is not hard enough (upper plate easily presses the char and is totally destroyed by the upper plate pressure). The second assumption is favored in our study since weight loss is equal to around 50 wt. % at 500 °C. The increase in viscosity after 370 °C can be attributed to a carbonization process, the viscous phase disappears and a highly condensed char structure is produced.

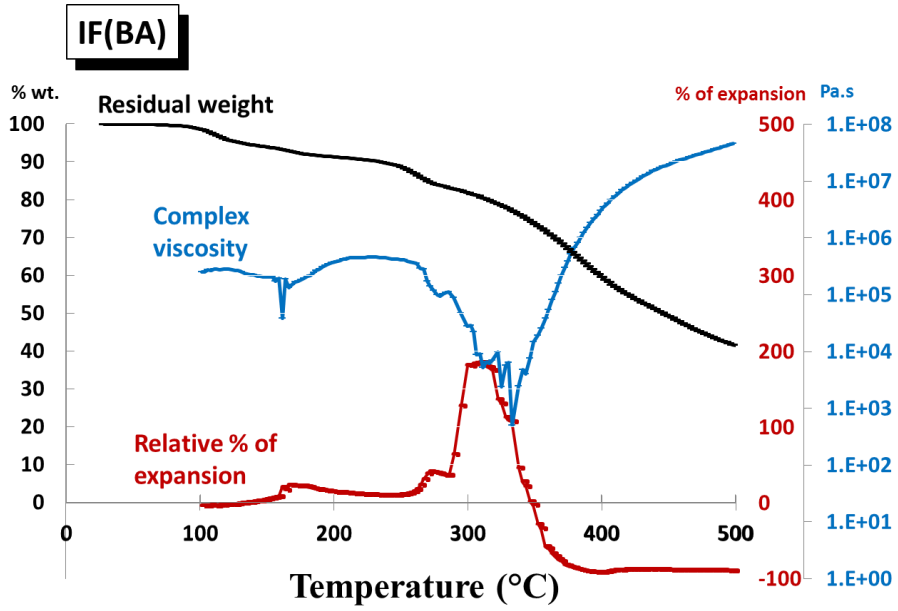

Figure 53 Complex viscosity, relative expansion and TG curve of IF(BA)

The same analyses were carried out on IF(ZB)wt. Complex viscosity, relative expansion and TG curve of IF(ZB)wt are shown in Figure 54. The complex viscosity of IF(ZB)wt remains steady until 265 °C. It then increases from $1.8x10^4$ Pa.s (265 °C) up to $2.6x10^5$ Pa.s (312 °C) but no

expansion is observed in this temperature range. The difference in the behavior of IF(BA) and IF(ZB)wt can be attributed in this temperature range to zinc borate stability compared to boric acid which dehydrates. The viscosity then decreases to $5.0x10^4$ Pa.s while the coating expands up to its maximum value (230 relative % of expansion). A strong decrease of expansion, similar to that observed for IF(BA) is observed around 370 °C. However, the relative percentage of expansion obtained at the end of the test for IF(BA) and IF(ZB)wt are different (-100 vs. 43 % of expansion) suggesting that IF(ZB)wt has a stronger char residue. A carbonization process (an increase of viscosity) at the end of the test is also observed.

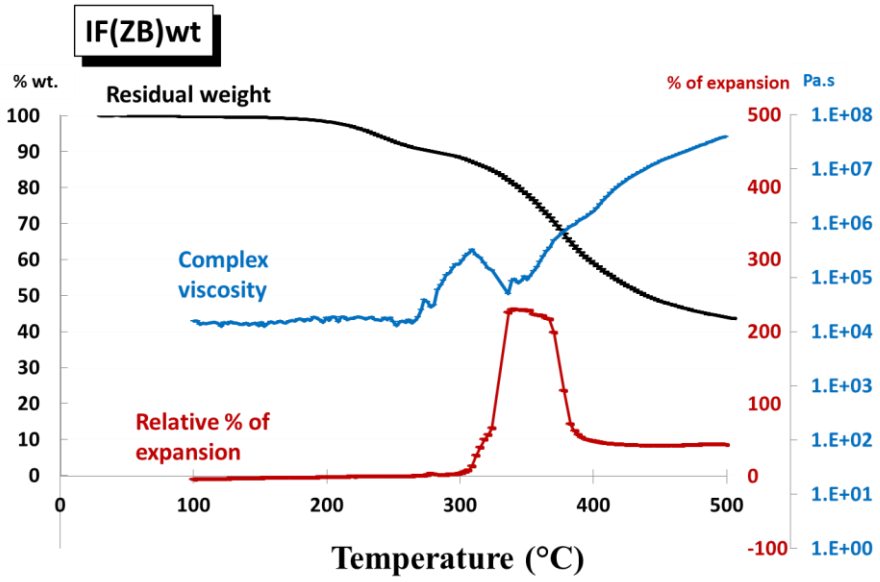

Figure 54 Complex viscosity, relative expansion and TG curve of IF(ZB)wt

Char aspects at ambient temperature obtained after Rheometer tests are presented in Table 12. IF(BA) char divides into two parts after removal of the upper plate. One part sticks to the upper plate and another sticks onto the lower plate. IF(BA) char is not hard enough (upper plate easily presses the char), so the obtained relative percentage of expansion becomes negative value (lower thickness than the initial one). IF(ZB)wt leads to a higher residue remaining on the sample holder compared to IF(BA), that fits with the registered expansion at the end of the test.

Table 12 Residual appearances of IF(BA) and IF(ZB)wt captured after the rheological measurements

IF(BA)	IF(ZB)wt
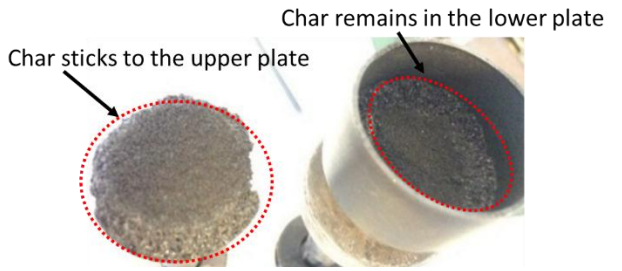	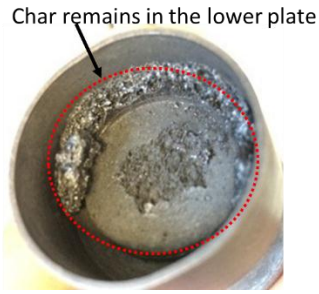

It can be concluded that the addition of either boric acid or zinc borate in the studied formulation shows different effects on the degradation pathway, complex viscosity and expansion of char. When boric acid is present in the formulation, the coating degrades at lower temperature to yield a structure that causes an increase in the viscosity and a slight expansion in the temperature range of 150 ^{o}C to 260 ^{o}C. However, the maximum value of expansion is lower than that of the formulations containing zinc borate.

3.2.2.1.2 Static measurement of expansion

The dynamic measurements of viscosity and expansion, as demonstrated in the previous part, provide valuable information on the mode of action of the intumescent formulations. However, these measurements are limited by the equipment used in terms of the heating ramp (10 ^{o}C/min) and maximum temperature (500 ^{o}C). In parallel to the dynamic approach, static measurements of the expansion of char at characteristic times during the fire test (described in *3.2.1.2 When submitted to a fire test*) were measured.

From these measurements, the expansion versus time curve can be plotted and the expansion rate (velocity of expansion) can be calculated during the expansion step.

Figure 55 shows the relative expansion (%) and expansion rate (%/s) of IF(BA) and IF(ZB)wt. Between 5 and 10 minutes, the two formulations exhibit similar behavior; their relative expansions increases about 100 %. Nevertheless, IF(BA) has a higher expansion compared to

IF(ZB)wt. A huge difference is observed between 10 and 12 minutes, IF(BA) exhibits an extremely high expansion (742 to 1372 % of expansion) while IF(ZB)wt exhibits a lower expansion (565 to 747 % of expansion). Unfortunately, IF(BA) charred layer detaches about 13-14 minutes, no data were collected after 12 minutes. In the case of IF(ZB)wt, the relative expansion continues to increase until 15 minutes and it then decreases from 859 to 687 % of expansion at 20 minutes. The decrease of expansion could be due to the shrinkage and/or collapse of the carbonaceous protective structure.

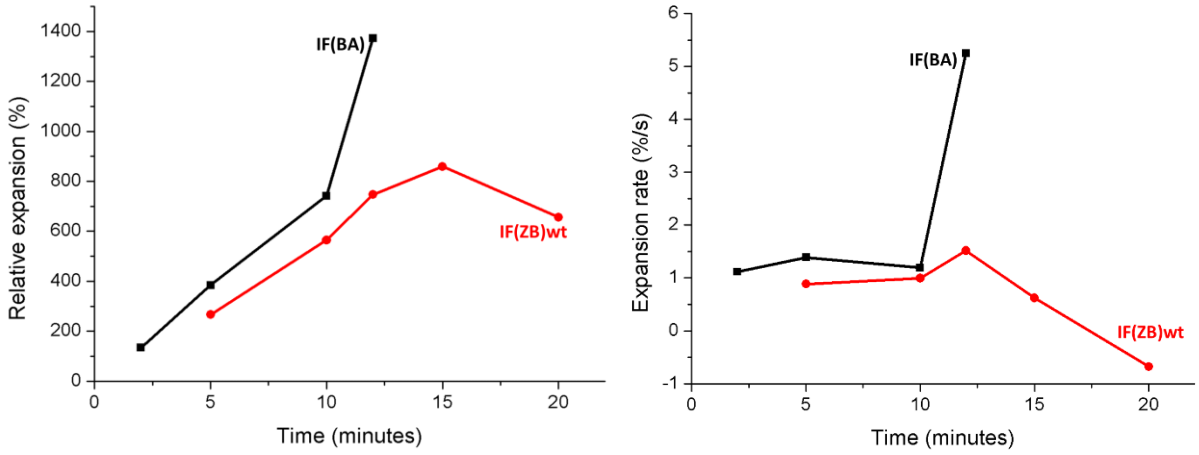

Figure 55 Relatvie expansion (%, left) and expansion rate (%/s, right) of IF(BA)and of IF(ZB)wt

3.2.2.2 Char morphology

The fire protective properties are directly linked to the morphology of the carbonaceous char. The smaller the cell size of the protective char, the better the resistance to a fire [119]. The char appearances of IF(BA) and IF(ZB)wt collected at 30 minutes were shown in *3.1.1 Furnace test* (Table 10). This part intends to look at the evolution of foamed structures through the observation of chars of the fire test obtained at the characteristic times to observe the development of the intumescent structures. Two scales will be considered: first a macroscopic point of view (picture of the char) and then from a microscopic point of view to observe the morphology and the cell size (optical microscopic image).

Pictures of chars of IF(BA) collected at 2, 5, 10, 12 and 15 minutes after the furnace test are shown in Figure 56. At 2 minutes, only the surface of the coating starts to degrade and form

a foamed char. A thin layer of black char forms on the surface and a brown residue was found underneath. Note that the non-degraded coating is still left under the brown residue; similar results were obtained for the furnace test at 5 minutes. Char is homogeneous and crumbly. A huge evolution of morphology occurs between 5 and 10 minutes. The char is expanded and a foamed char structure with different cell sizes (non-homogeneous) is formed. At 12 minutes, the residue is even more heterogeneous with very big holes between char layers together with the small size cells and medium size cells in some parts. At 15 minutes, a part of char still sticks on the steel and another part falls off. At this point, char is crumbly.

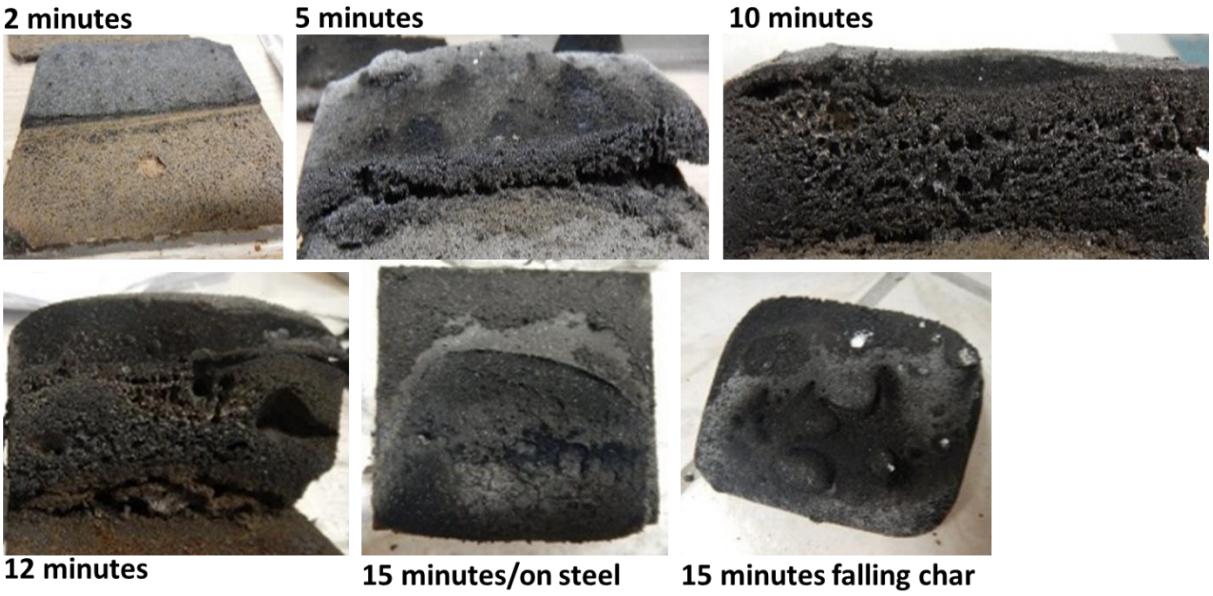

Figure 56 Char appearances of IF(BA) versus times captured by numeric camera

IF(ZB)wt char pictures are shown in Figure 57. It is clear that the char aspects are quite different from these of IF(BA) after 5 minutes exposure time. When the tests were stopped at 2 and 5 minutes, similar results as those observed in the case of IF(BA) are obtained. Only the top layer is exposed to fire and the non-degraded coating is found underneath. Between 5 and 10 minutes, the foamed char is produced. Char is compact, dense and hard; it is well homogeneous. At 12 minutes, the compact and dense char transforms to a different structure, which possesses a different color and different size cells; char in the top is light brown with medium size cells while char in the bottom is dark grey with smaller size cells than the top layer. Between 12 and 15

minutes, the char structure does not change visually. The char structure at 20 minutes is different to that at 15 minutes. A concave-shaped hole is fond at the bottom layer. Two separate layers can be observed: i) a compact layer in the bottom and ii) a spongy char with medium size cells in the top layer.

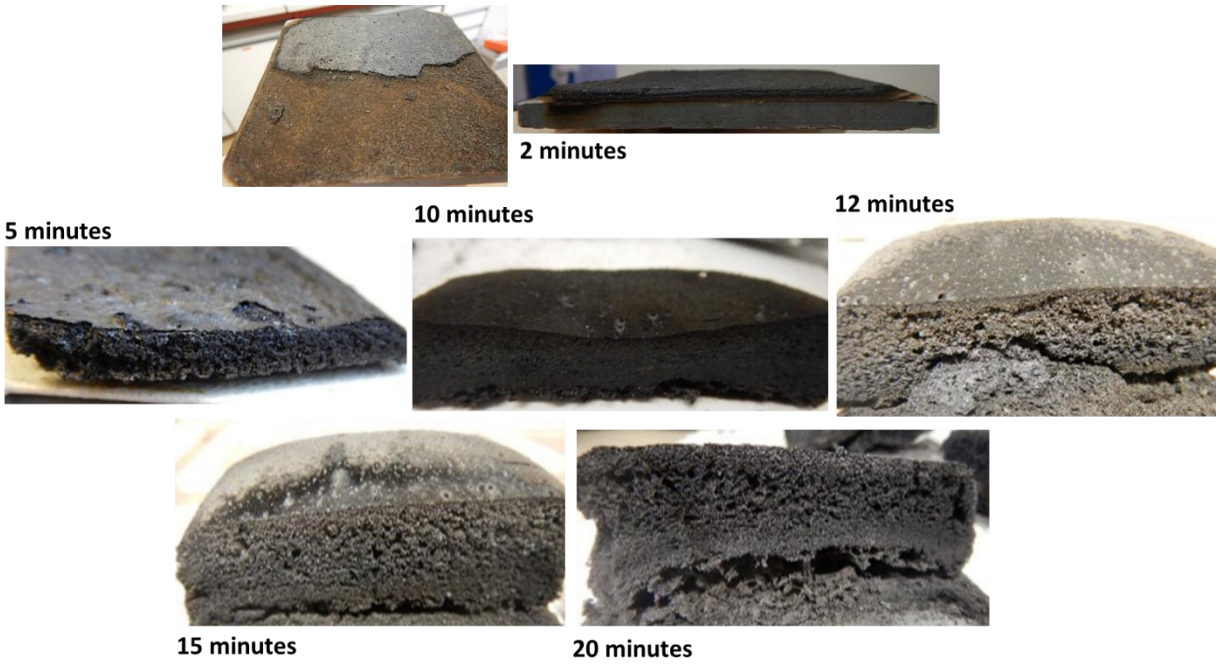

Figure 57 Char appearances of IF(ZB)wt versus times captured by numeric camera

The morphologies of chars were then analyzed by optical microscopy. IF(BA) and IF(ZB)wt char morphologies are shown in Figure 58. An evaluation of the pore size reveals that the mean diameter of pore size in IF(BA) char increases gradually from 5 to 12 minutes. Char at 5 minutes is compact with the pore size estimated at approximately 0.5 mm. It increases to 1-2 mm at 10 minutes. The char collected at 12 minutes has a random pore size, some are about 1-2 mm and the big holes are between 3-4 mm.

For IF(ZB)wt, the char morphologies collected at 5 and 10 minutes have a dense and compact structure with very small size pores. The pore size is averagely about 1-2 mm at 12 and 15 minutes and it is about 1 mm at 20 minutes. Note that for the two formulations, the residues collected at 2 minutes are not presented herein since the foamed chars were not yet developed at this point.

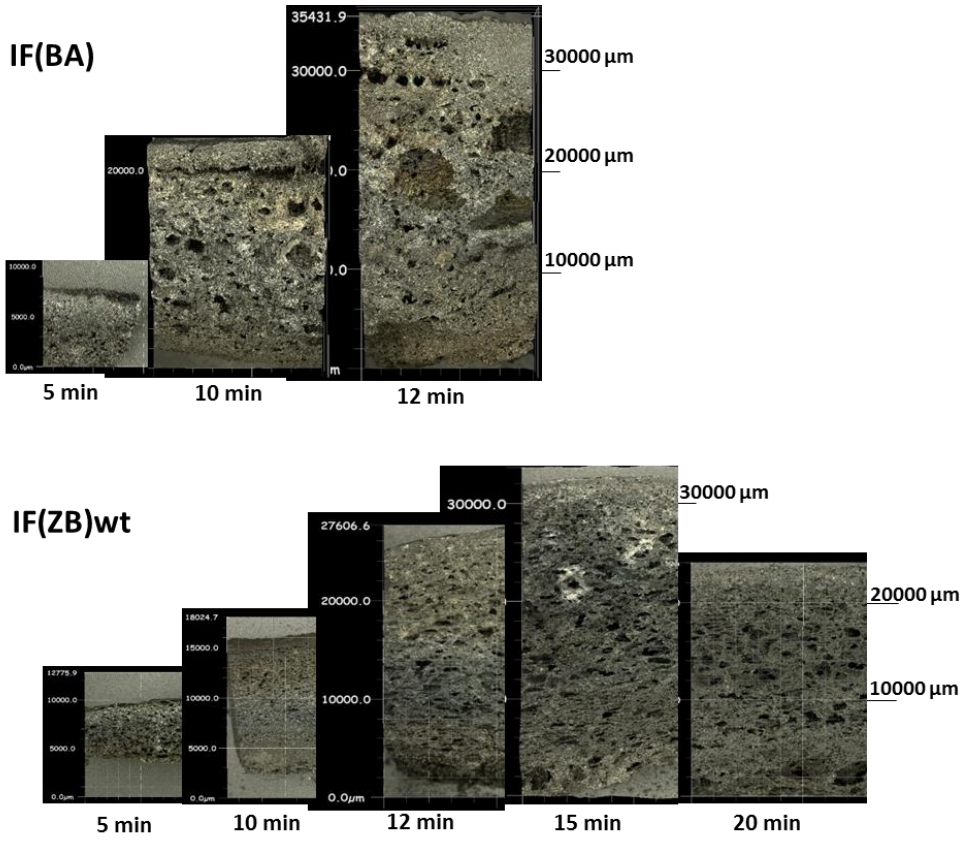

Figure 58 Char morphology of IF(BA) and IF(ZB)wt versus times observed by microscope optic

3.2.2.3 Thermal conductivity

Heat conductivity is one of the key parameters governing the thermal insulation of an intumescent material. It is directly linked to the morphology of the char [115, 129]. The thermal conductivities of IF(BA) and IF(ZB)wt as a function of the temperature are shown in Figure 59.

At room temperature according to the literature, the thermal conductivity of neat epoxy resin is around 0.35 W/mK [188]. The experimental values of the two formulations at 25 °C are close to 0.40 W/mK, and the slight difference with neat epoxy resin is due to the fillers inside the resin. IF(BA) and IF(ZB)wt exhibit similar heat conductivity values as a function of temperature. The heat conductivity is around 0.40 W/mK up to 200 °C and it then drops to a minimum of 0.15 W/mK between 300 °C and 400 °C (related to the modification of the char structure) before increasing again at higher temperature. The increase of thermal conductivity in the temperature range of 400 °C and 700 °C can be due to i) the modification of char structure (e.g. bigger voids), ii) the radiative heat transfers across the char pores [112] or the combination of these two effects.

In this studied formulation, the substitution of boric acid by zinc borate does not influence the heat conductivity of the intumescent char under these conditions.

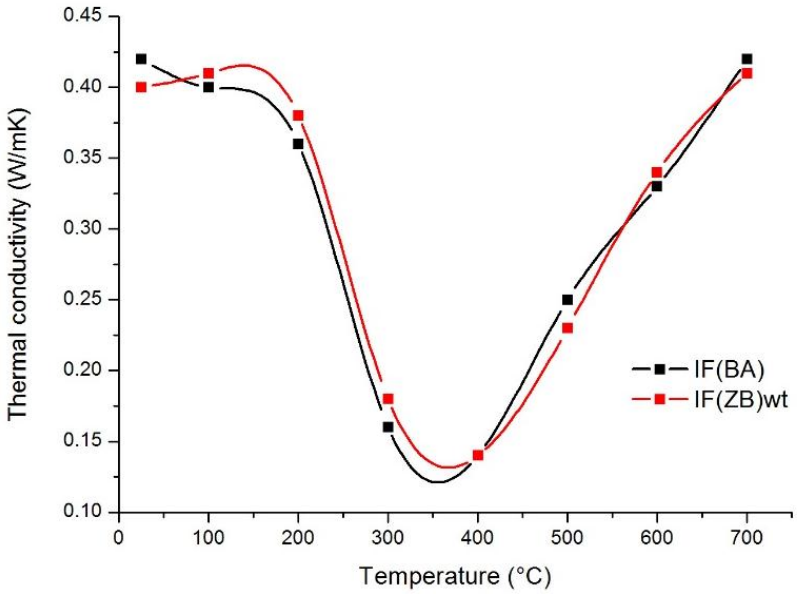

Figure 59 Thermal conductivity (W/mK) of IF(BA) and IF(ZB)wt versus temperatures

Only few papers have reported conductivity values for char materials. J.E.J. Staggs [113] calculated heat conductivity of intumescent char by numerical simulation. It was reported that heat conductivity varies from 0.1 to 0.4 W/mK from ambient temperature to 600 ^{o}C. The experimental values obtained are in the range of these values mentioned by Staggs. However, his simulation does not take into account the changes induced by chemical reactions conducting to the expansion from a certain temperature.

3.2.2.4 Char strength

The mechanical resistance of char is also a key parameter, which permits to ensure the char integrity, especially under severe fire scenarios such as hydrocarbon fire [123, 126]. Therefore, mechanical resistance of the coatings are examined in this section.

The curves related to the mechanical resistance of the IF(BA) and IF(ZB)wt chars are shown in Figure 60. The evolution of force is registered, in situ at 490 ^{o}C versus the gap (mm) between the two plates of the rheometer. A measured strength can be related to a destructive force. When the strength is high, it means that the underlying material resists to the pressure applied on its surface. Two extreme cases can be observed…

i) If a material is extremely hard, the strength recorded will immediately increase until the highest force permitted by the equipment (~1400 g) when the upper plate touches the char

ii) If a material is not resistant at all, the strength recorded will be very low while the upper plate is brought down until the char is destroyed. The char strength always drastically increases at one point of the experiment, but for fragile materials, it is just the consequence of the force exerted by the broken pieces compacted at the bottom of the sample holder. When the measurement of the strength cannot be recorded anymore because of the maximum force reached, the gap is named the 'critical gap'.

The curves (Figure 60) can be divided into two parts: ***part I*** corresponds to the mechanical resistance of the structure and ***part II*** is related to the compression of the residue [189]. The char aspects at the end of the tests are shown in Table 13.

The structure formed at 490 ^{o}C of IF(BA) is quite homogeneous but it shows bad cohesion as one part of the char sticks to the upper plate (similar behavior to that observed during the viscosity and expansion measurements). The force, which is applied to compress the IF(BA) char throughout it thickness, is constant (about 200 g between 13.5 and 17.5 mm of gap). In the case of IF(ZB)wt, the force increases gradually from 0 to 600 g for gap values comprised between 20

and 7.5 mm. It indicates that the char gets stronger from the top to the bottom of the samples. Pictures taken show that IF(ZB)wt char is quite homogeneous, hard and well cohesive.

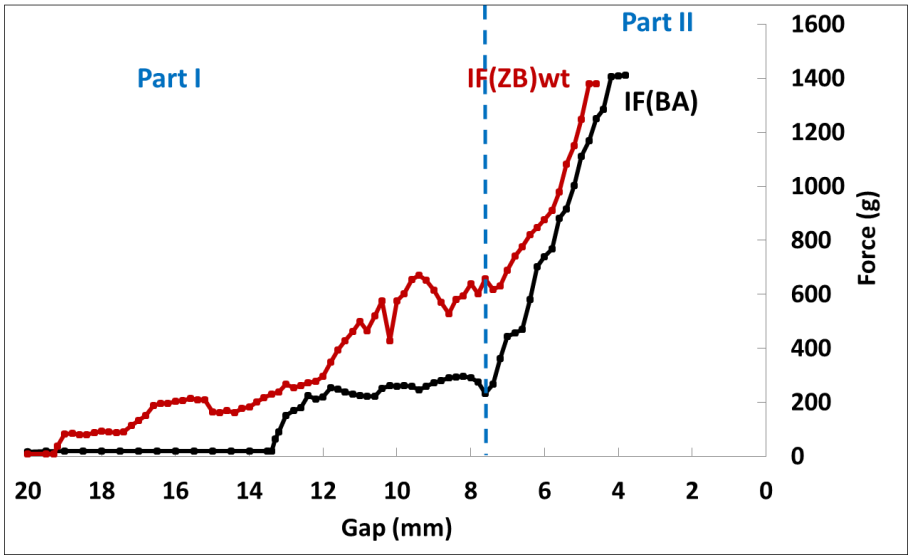

Figure 60 Mechanical resistance of IF(BA) and IF(ZB)wt char

Table 13 Residual appearances of IF(BA) and IF(ZB)wt captured after the mechanical resistance test

IF(BA)	IF(ZB)wt
	

To conclude, the char obtained for the formulation containing zinc borate (IF(ZB)wt) exhibits a higher mechanical resistance and cohesion than that containing boric acid (IF(BA) and the char aspects after the test are different.

3.2.3 Mechanisms of protection of complex intumescent formulations

When crossing the data obtained relating to the thermal decomposition pathway and thermo-physical properties, the different effects provided by boric acid or zinc borate can be detected and their mechanisms of protection can be drawn.

Boric acid due to its low dehydration temperature makes the char to expand at the beginning stage of the fire test. It also leads to the huge expansion for few minutes before the detachment of char. This huge expansion could be probably due to the drastic decrease of the viscosity, which was observed by Rheometer measurement. Those phenomena lead to the higher protective performance at the beginning stage of the fire test (between 0 and 12 minutes) compared to the formulation containing zinc borate. BPO_4 and B_2O_3 are found immediately in the beginning stage of the fire test. These species in addition to the other additives (i.e. $CaCO_3$, TiO_2, SiO_2) are supposed to stabilize and reinforce the carbonaceous structure but it does not promote the char adhesion/cohesion of this formulation.

Zinc borate promotes the effective fire protection tardily compared to the formulation containing boric acid; a slow temperature increase can be obtained after 5 minutes of the fire test. It can be related to the higher dehydration temperature of zinc borate, this may delay the reactivity between the borate with other components of the formulation. Afterwards, this formulation exhibits very interesting behavior: ''a plateau region'' (very low temperature increasing rate between 7 and 18 minutes). It could be due to the formation of a very small, homogeneous and closed-cell foamed structure. A great char adhesion/cohesion could be probably due to the formation of zinc-based compounds (i.e. $Zn_3(PO4)_2$, $Zn_2P_2O_7$). The char strength of the formulation containing zinc borate is obviously higher than the one containing boric acid. This high char strength can also benefit the resistance to fire of such formulation.

3.3 Conclusions

Chapter III was dedicated to the investigation of the role of different borates in epoxy based intumescent coatings. First, the effects of four borates including boric acid, zinc borate, borax and APB on fire protective properties were studied. It was shown that the formulation containing zinc borate exhibits the best fire protection among all. For these four formulations, their chemical modifications in the condensed phase were investigated.

Afterwards, the full characterization including chemical modifications and thermo-physical properties of the formulations containing either boric acid or zinc borate were done. Their mechanisms of protection are very different. When zinc borate is added into the formulation, a high fire protective performance is obtained, that is supposed to be related to the specific char morphology and the high char strength. However, boric acid also provides interesting results in terms of fire protective performance since the reactivity between the components can occur at the beginning stage of decomposition leading quickly to the formation of the protective layer. That leads to a good fire protection at the beginning stage of the fire test. The bad adhesion observed for the formulation containing boric acid may be due to the huge expansion occurring in a short time. The mechanisms of fire protection of borates (especially boric and zinc borate) were drawn in this chapter.

Chapter IV: Influence of carbonates on the fire protection of epoxy based intumescent coatings

In chapter III, it was shown that the mechanisms of fire protection are different when incorporating boric acid (BA) or zinc borate (ZB) in the formulation. In addition to this, the coating formulation is very complex. Not only borates but also other ingredients play important roles. The mechanism of action of the components such as phosphates, silicate fibers, TiO_2…have been extensively studied and they were reviewed and detailed in chapter I but the role of calcium carbonate while in a significant amount in the formulation, remains unclear. To go further in the investigation, this chapter IV intends to study the effect of carbonates (here it is not only limited to $CaCO_3$ to get additional information on the potential role of the cation of the carbonate). First, the effect of a conventional carbonate compound (i.e. $CaCO_3$) on fire protection was investigated. Then, the comprehension of the mode of action of calcium carbonate was undertaken. The second part is dedicated to the assessment of the effect of various carbonates (i.e. $MgCO_3$, $ZnCO_3$, Na_2CO_3, K_2CO_3) on fire protective properties of intumescent coatings.

4.1 Influence of $CaCO_3$ on the fire protection

As detailed in chapter I, different authors studied the roles of calcium carbonate ($CaCO_3$) as flame retardant in some polymeric systems. Negative or positive effects were obtained depending on the studied systems. Its interaction with phosphates (i.e. APP, one of the ingredients of the studied formulation), BPO_4 (product formed in this system) … were also reported. For epoxy based intumescent coatings, $CaCO_3$ was added (i.e. commercial coating [21]) but its exact role has never been investigated. In this part, the effect of $CaCO_3$ on fire protective properties of epoxy based intumescent coatings using against hydrocarbon fire is examined. To investigate the intrinsic effect of $CaCO_3$, the formulation was simplified. It was done by adding $CaCO_3$ into the formulation containing APP and borate since these two latter additives are the main components of the intumescent formulation as shown in chapter III and reviewed in chapter I: state of the art. The studied borates are either boric acid or zinc borate using the same considerations to what were argued in chapter III. Then, the mode of action of $CaCO_3$ in presence of different borates (i.e. APPBA$CaCO_3$ and APPZB$CaCO_3$) was investigated to explain the results obtained.

4.1.1 Fire protective properties

This part aims at investigating the effect of $CaCO_3$ on fire protective properties of the intumescent coatings. Comparison between the performances of the five formulations evaluated using the small-scale furnace test (UL 1709) is made.

These formulations are based on IF(BA) in terms of ratios between additives (see details in chapter II) but the number of components is reduced to a minimum to be able to evidence the potential interactions between the APP, BA or ZB and $CaCO_3$. Three formulations are used as references. They contain two additives; i.e. APP with either borate or $CaCO_3$. They are named IF-APPBA, IF-APPZB and IF-APPCa. The last two formulations called IF-APPBACa and IF-APPZBCa are the formulations of interest as they contain APP/borate/$CaCO_3$. The formulation containing only borate and $CaCO_3$ was not taken into account since its calculated difference weight loss curve based on TG data (mixture ratio refers to IF(BA)) shows no significant thermal stabilization or

destabilization indicating that the reaction between borates and $CaCO_3$ does not occur up to 800 ^oC. The details are shown in Appendix III.

Time-temperature curves of IF-APPCa, IF-APPBA, IF-APPZB, IF-APPBACa and IF-APPZBCa are shown in Figure 61; it presents the evolution of temperature as a function of time at the backside of the coated steel plates. The failure temperature of 500 ^oC is considered as the critical point as mentioned in chapter III.

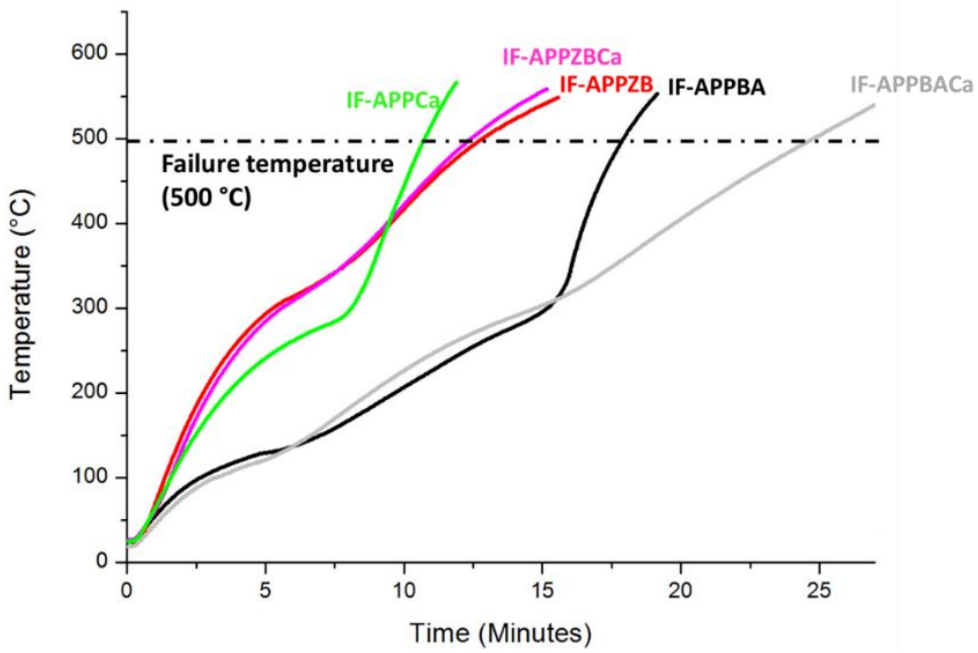

Figure 61 Time-temperature curves of IF-APPCa, IF-APPBA, IF-APPZB, IF-APPBACa and IF-APPZBCa

For the formulations containing two additives, IF-APPCa, IF-APPBA and IF-APPZB show different behaviors on fire protection; times to reach the critical temperature are 10.9, 18.1 and 12.9 minutes respectively. For IF-APPCa, a sharp increase of temperature, which corresponds to the falling of char, is observed at about 6 - 7 minutes of the test. At this point, not all of char falls off from the plate; one part falls and another part remains stuck on the steel plate. IF-APPZB has no detachment problem but its efficiency is not better than IF-APPCa. While IF-APPBA shows a better fire protection than the two mentioned (longer time to reach the failure temperature: 18.1 minutes) even if the char falls off at about 16 minutes (a sharp increase in temperature seen on the curve (black line)).

For the formulations containing three additives, times to reach the failure temperature of IF-APPBACa and IF-APPZBCa are 24.6 and 12.2 minutes respectively. The addition of $CaCO_3$ into the formulation containing APP and BA is beneficial, time to reach the failure temperature is increased about 6 minutes (18.1 → 24.6 minutes) and the adhesion is improved (no more detachment of charred structure). In the opposite, the benefits of $CaCO_3$ were not seen in the formulation containing APP and ZB. The times to reach the failure temperature of IF-APPZB and IF-APPZBCa are identical.

The char aspects and relative expansion, at the end of the furnace test, of the five formulations (IF-APPCa, IF-APPBA, IF-APPBACa, IF-APPZB and IF-APPZBCa) are shown in Table 14.

In the case of IF-APPCa, the charred structure falls off during the test letting only a small residue at the surface of the plate. The main part of char is collected on the bottom of the furnace at the end of the test. This part of the char is multicellular, soft and easy to destroy. The fall of the char can be explained by a rapid and high expansion of char, which were observed via a quartz window during the tests. This high level of expansion could partly be due to the amount of APP added in this formulation to keep constant the ratio of APP/$CaCO_3$. In this formulation, APP amount is thus about 3 times higher than other four formulations (in weight ratio). In addition, as described in the literature, reaction between APP and $CaCO_3$ can occur leading to the decarbonation of $CaCO_3$ at about 300 ^oC [94]. Big amount of evolved gases releasing by APP and $CaCO_3$ may be responsible of a high expansion observed. The expansion in the furnace test is considered as one of the key parameters in the development of fire protective coatings [117]. This parameter is necessary but a very high expansion could lead to the formation of light char with less mechanically resistance as observed in the case of IF-APPCa.

In the case of the formulations containing BA, the behavior of the coating during the test is much contrasted. Without $CaCO_3$ in the formulation (IF-APPBA), the char falls off the plate whereas with $CaCO_3$ (IF-APPBACa) it is maintained on the plate until the end of the experiment. Both residues are expanded but the aspects of the chars differs greatly. The residue collected in the furnace for IF-APPBA presents non-homogeneous cell sizes on the bottom (toward the plate) with very big holes contrary to IF-APPBACa which presents two dense layers: on the bottom layer a black and homogeneous char and on top a grey char with a bigger cell size. These differences

of structures result in different mechanical resistance of the char (evaluated roughly by hand) with on the one hand a crumbly material without $CaCO_3$ and a hard residue in presence of $CaCO_3$.

With ZB, the presence of $CaCO_3$ does not change the char aspect. In both cases, the chars are not much expanded; the relative expansion is about 120 %. Char is very hard, compact and dense.

It was noted that, at the high amount of borates (34 - 37 wt. % in the formulation), zinc borate inhibits the expansion of the coatings. That is not the case for boric acid. In the particular case of boric acid, it dehydrates yielding higher amount of vapor compared to zinc borate (44 vs. 14 wt. %), that may affect the expansion of intumescent formulation. This influence might not be observed with a low amount of borates.

Table 14 Char aspects and relative expansions of IF-APPCa, IF-APPBA, IF-APPBACa, IF-APPZB and IF-APPZBCa

Formulation	% Relative expansion	Global view	Cross-sectional view
IF-APPCa	-Char falls off-		
IF-APPBA	-Char falls off-		 *** *A part of char falls off from the plate*

IF-APPCaBA	929 ± 25 %		
IF-APPZB	118 ± 8 %		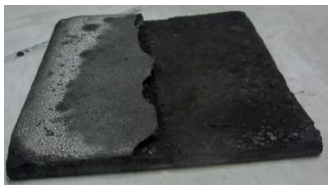
IF-APPCaZB	119 ± 11 %		

Conclusion

This part investigated the effect of $CaCO_3$ on fire protective performances of intumescent coatings. At this studied ratio, it was shown that the formulation containing only APP and $CaCO_3$ without borate does not provide a good fire protective performance. It leads to an extremely high expansion and soft char. The combination of APP and boric acid leads to a good fire protection but the char eventually falls off the plate. The addition of $CaCO_3$ in this formulation (APPBA+$CaCO_3$) improves a fire protective performance and promotes a good char adhesion and/or cohesion that allows keeping the intumescent structure on the steel plate. The opposite results were obtained when the formulation contains APP and zinc borate, it shows much lower fire protection than those containing boric acid. The addition of $CaCO_3$ in this formulation (APPZB+ $CaCO_3$) shows no positive impact on fire performance.

In this work, the contributions of $CaCO_3$ on fire protective properties of intumescence coatings were highlighted in the formulation containing APP/BA but not for the case of APP/ZB. To go further in the investigations, it is of interest to investigate its mechanisms of action, how it improves the fire protective performance of intumescent coatings.

4.1.2 Mode of action of $CaCO_3$ in the fire protection of intumescent coatings

The furnace tests allow assessing the fire protective properties, expansion, char aspects and mechanical property of char (at room temperature after the test) and observing what is happening during the fire test, but they do not give detailed information on the effects of the additives, thermal degradation, possible interactions and rheological properties (i.e. viscosity).

In order to understand why $CaCO_3$ works well when combined with BA/APP but not with ZB/APP, the reactivity between the additives was first investigated. The chemical interactions in binary systems containing APP with BA, ZB or $CaCO_3$ were reported in the literature, respectively by M. Jimenez et al. [74], F. Samyn et al. [83] and S. Deodhar et al. [94] and their results were summarized in details in chapter I. In this manuscript, the work consequently focuses on the ternary systems: APP/borate/$CaCO_3$ (the ratio between the additives is the same as in the IF(BA) coating, i.e. 23.6/69.5/6.9 % w/w). Secondly, the physical properties (i.e. viscosity and expansion) of the five formulations were measured. The results are discussed in the following part.

4.1.2.1 Reactivity of $CaCO_3$ with APP and borates under pyrolysis condition

To study the reactivity between the three additives, the same methodologies as in 3.2.1.1 were used. TG analyses were first performed in order to predict the interaction between the additives. Heat treatments were then carried out on the mixtures of the additives. The collected residues were then characterized by XRD and solid state NMR. All experiments were performed under pyrolytic condition (i.e. under nitrogen). Note that this study was done outside the complex intumescent formulation, which allows elucidating the authentic reactions between them.

4.1.2.1.1 APP/BA/$CaCO_3$

Figure 62 presents the experimental TG curve of the mixture of the three components, calculated one and difference weight loss curve.

The TG curve of the mixture APP/BA/$CaCO_3$ (black line) exhibits three steps of decomposition. The first and second steps are overlapping between 90 °C and 200 °C corresponding to 30 % weight loss. The third step is between 200 °C and 395 °C leading to a weight loss of 6 %. There is a progressive weight loss after 400 °C.

According to the difference weight loss curve, a thermal destabilization can be observed from 100 °C up to 600 °C and then a thermal stabilization from 600 °C up to 800 °C. The char residue obtained experimentally is about 11 wt. % higher than expected. These results consequently indicate that there are potential interactions between APP, BA and $CaCO_3$.

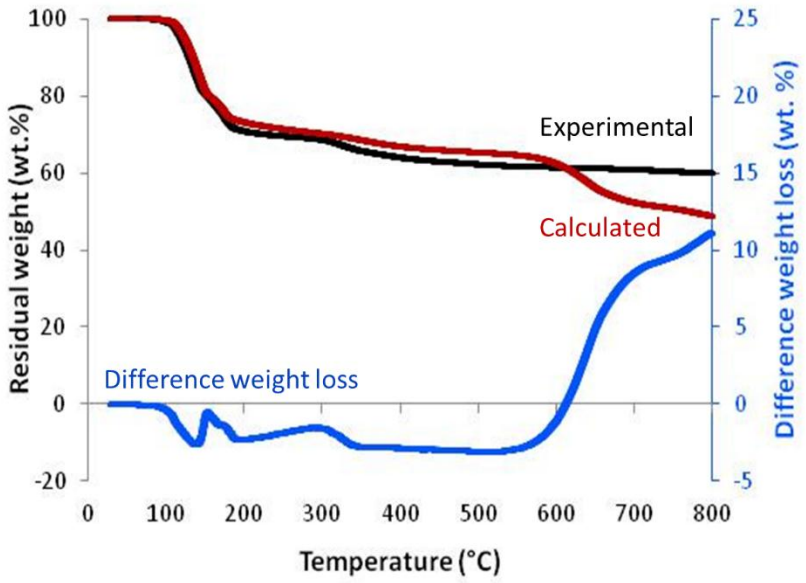

Figure 62 Experimental, calculated TG curves and different weight loss of the mixture of APP/BA/$CaCO_3$

The reaction between APP and BA and reaction between APP and $CaCO_3$ were reported to occur (refer to the literature [74, 94] and see chapter I). Based on this information, the assumption can be made that one part of APP can react with BA and another can react with $CaCO_3$.

To go further in the investigations, the mixture of APP/BA/$CaCO_3$ was heat treated. Three characteristic temperatures including 280 °C, 550 °C and 800 °C were performed:

i) 280 °C: after the massive weight loss and during the destabilization of the systems
ii) 550 °C: after the total degradation (the beginning of stabilization of the systems)
iii) 800 °C: high thermal stabilization of the system (+11 wt. % refers to different wt. loss)

The appearance and weight of the residues after heat treatments (HT) are presented in Table 15. At 280 °C, 550 °C and 800 °C, the residues are white powder. The aspects of the residues do not change much versus the HT temperatures.

Table 15 APPBACa residues at different heat treatment temperatures

HT of 280 °C	HT of 550 °C	HT of 800 °C
 (Residual weight: 65 wt. %)	 (Residual weight: 62 wt. %)	 (Residual weight: 59 wt. %)

The XRD analyses were carried out on the samples and XRD diffractograms are presented in Figure 63. The diffractograms at 280 °C and 550 °C show identical results. Evidently, APP totally degrades after 280 °C. $CaCO_3$, BPO_4 and B_2O_3 are identified. This result highlights the reactivity between APP and BA, which leads to the formation of BPO_4, as previously described. The reaction between APP and $CaCO_3$, which was reported to occur at the temperature about 300 °C leading to the formation of calcium metaphosphate [94], did not occur in this ternary mixture. This could be related to their kinetics of the reaction [190, 191]. Obviously, it can be mentioned that $CaCO_3$ neither degrades nor reacts up to 550 °C. These results are in good agreement with the results of the complex formulation (i.e. IF(BA)) describing in 3.2.1.1. Moreover, it makes sense to get B_2O_3 since it results from the degradation of BA, which is in excess comparing to other additives. At 800 °C, BPO_4 and B_2O_3 are still identified. In addition to these products, calcium borophosphate

($CaBPO_5$) [96, 192, 193] is detected, this product can be formed by the reaction between BPO_4 and $CaCO_3$ as described in chapter I. However, BPO_4 is still present in the char residue at 800 °C; it makes sense since the amount of the APP and BA (precursors of the formation of BPO_4) is much higher compared to $CaCO_3$.

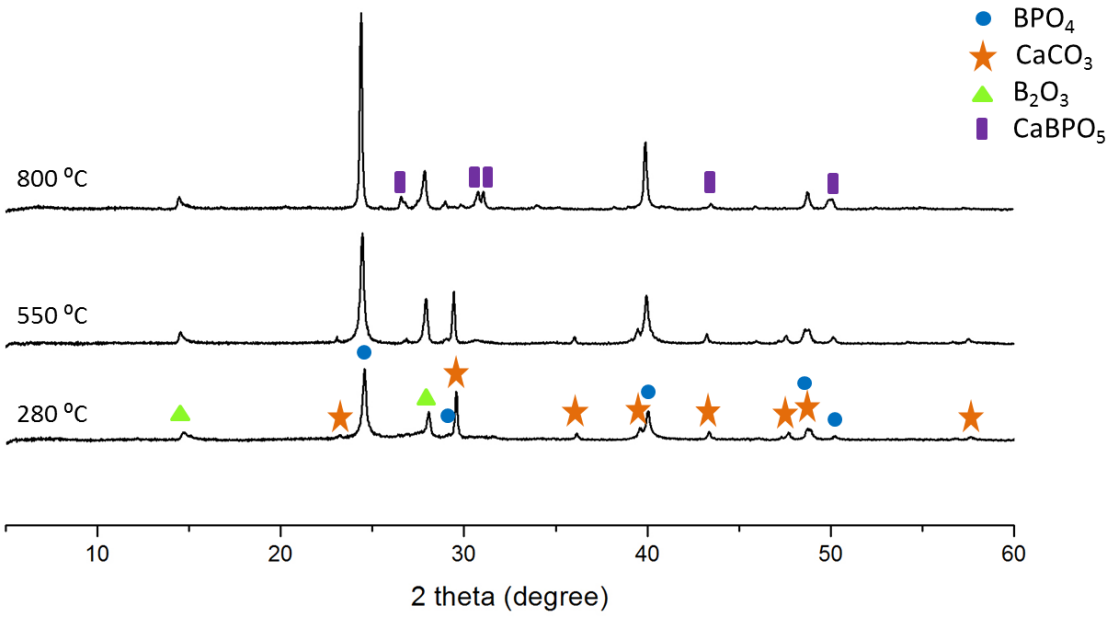

Figure 63 XRD diffractograms of APPBACa residues versus temperatures

To confirm these results, ^{31}P NMR analyses of APP/BA/$CaCO_3$ residues heat treated at 280 °C, 550 °C and 800 °C are performed (Figure 64). A sharp signal at -30 ppm attributed to the characteristic peak of BPO_4 [74, 165] is clearly observed from 280 °C up to 800 °C. These results are consistent with the results obtained by XRD. At 800 °C, three additional peaks appear at 1.2, -7.1 and -9.3 ppm. The signal at 1.2 ppm can be attributed to orthophosphate (Q^0 structure of phosphate). The signals at -7.1 and -9.3 ppm can be attributed to pyrophosphate (Q^1 structure of phosphate) [161]. Refer to the literature [155], another attribution can be given to the signal at -9.3 ppm, the characteristic signal of $CaBPO_5$ was reported to be found in the same region and this attribution is consistent with the result suggested by XRD. $CaBPO_5$ is classified as metal borophosphate compounds ($XBPO_5$, when X= Ca, Sr, Ba…) [192]. This kind of borophosphate possesses Q^2 phosphate structure (Figure 65), its chemical shift is thus different to the well-known

borophosphate (i.e. crystalline BPO_4) and it swops to appear in the higher chemical shifts. This phenomenon may also involve the deshielding effect of phosphorus nucleus, in which the electron density around P nucleus decreases staggering its chemical shift to a higher ppm. This phenomenon may be occurred when P is substituted by a smaller atomic radius (e.g. boron) in the crosslinking network or it can be mentioned as the effect of the second coordination sphere of B in phosphate structures [194, 195].

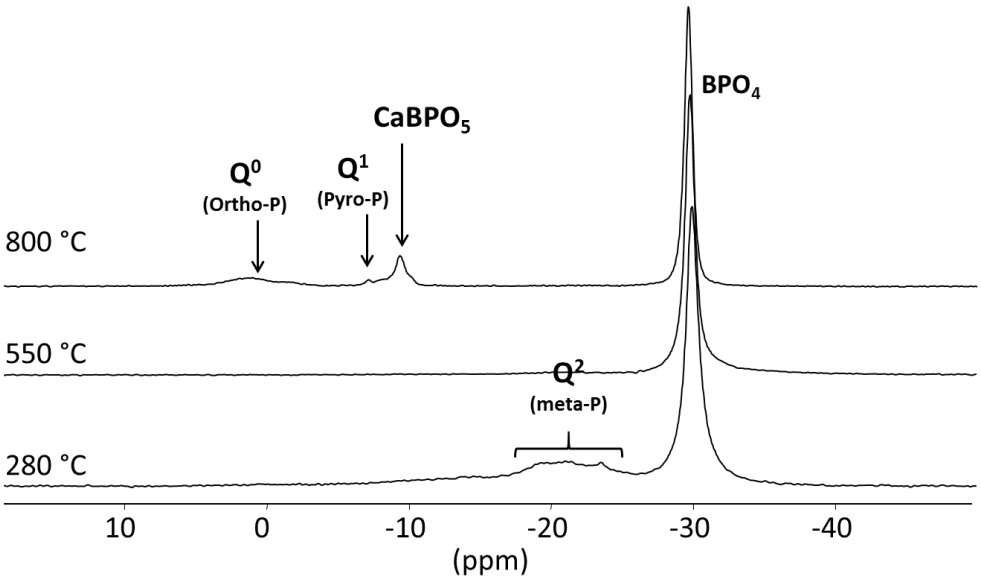

Figure 64 ^{31}P NMR spectra (9.4T) of APPBACa residues versus temperatures

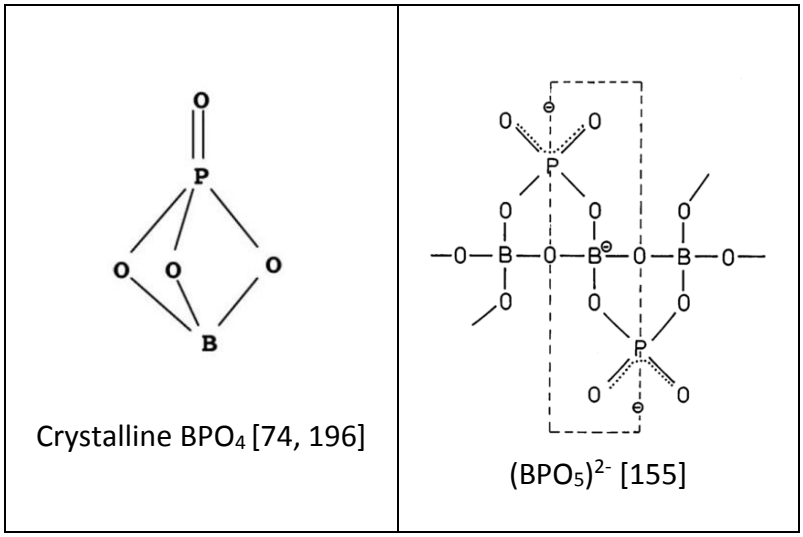

Figure 65 Chemical structures of crystalline BPO_4 and $(BPO_5)^{2-}$ anion

^{11}B NMR spectra of APP/BA/$CaCO_3$ residues heat treated at 280 °C, 550 °C and 800 °C were also collected and the results are presented in Figure 66. The characteristic peak of BPO_4 is detected at -3.8 ppm [165] which is consistent with XRD and ^{31}P NMR results. It confirms the formation of BPO_4 in the mixture APP/BA/$CaCO_3$. The additional signal between -10 and -20 ppm can also be observed for all heat treatment temperatures. Comparison of these spectra with that of boron oxide (B_2O_3) clearly indicates the presence of B_2O_3 in the char residues (especially the one at 800 °C). This signal can be thus attributed to trigonal boron unit (BO_3) in boron oxide (B_2O_3). At 800 °C, a symmetric peak with a low intensity appears at 0.6 ppm. This signal well fits with the characteristic signal of $CaBPO_5$ reported in the literature [155], it can thus be assigned to BO_4 unit in crystalline $CaBPO_5$. This is well consistent with the XRD and ^{31}P NMR results. The presence of $CaBPO_5$ in the char residue after heat treatment of 800 °C is thus confirmed.

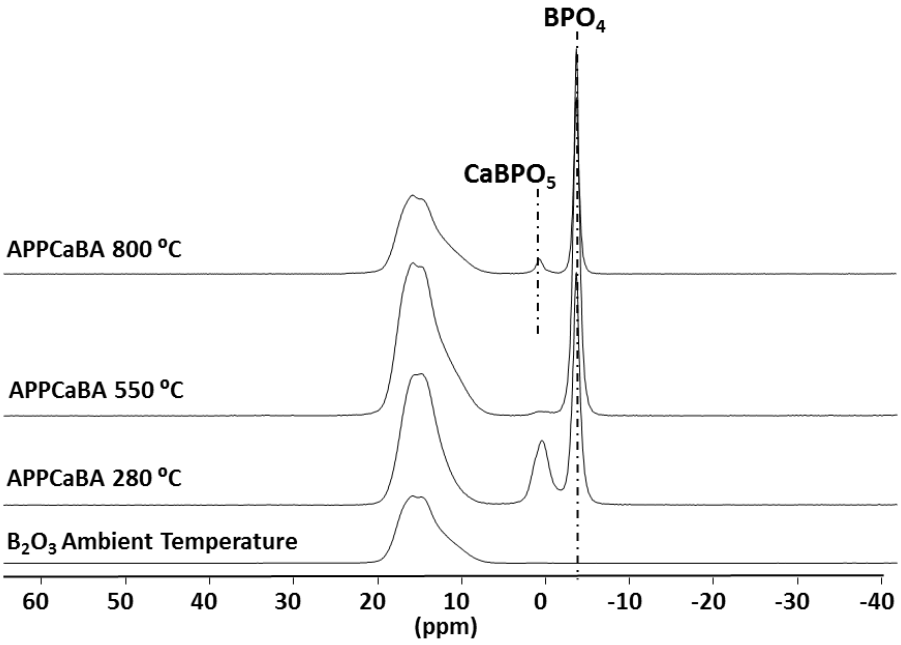

Figure 66 ^{11}B NMR spectra (18.8T) of APPBACa residues versus temperatures

Conclusion

In this part, the mechanisms of interaction between the intumescent additives including APP, BA and $CaCO_3$ (APP/BA/$CaCO_3$ = 23.6/69.5/6.9 % w/w) were investigated. Based on the results obtained together with the literature data [94], their mechanisms of interactions can be

proposed. It is shown that BA first degrades in the temperature range of 100 °C - 200 °C, APP then degrades (T < 280 °C). The degradation products of APP can react with the degradation products of BA (B_2O_3) to yield borophosphate (BPO_4). BPO_4 can be identified from 280 °C up to 800 °C. B_2O_3 was also found in the residues due to the excess of BA in the mixture.

The reaction between the degradation products of APP with $CaCO_3$ due to its acidic-basic nature yielding calcium metaphosphate ($Ca(PO_3)_2$), which was described in the literature, did not occur in this ternary mixture. Instead, calcium borophosphate ($CaBPO_5$) was identified in the char residue after the heat treatment at 800 °C. This evidences the reaction between boron, phosphorous and calcium based compounds. Two possible ways of formation of $CaBPO_5$ can be suggested: i) $CaCO_3$ reacts with BPO_4 (formed in the early stage) releasing CO_2 and ii) it may be occurred by the reaction between P_2O_5, B_2O_3 and $CaCO_3$ yielding the same products as the first reaction ($CaBPO_5$ and releasing CO_2). P_2O_5 comes from the degradation of APP and it general sublimates in the temperature range of 550 °C and 770 °C [60, 135]. If the formation of $CaBPO_5$ is occurred by the latter possibility, this can prevent the sublimation of P_2O_5 and stick phosphorus into the condensed phase favoring the char formation and char stabilization as described in the state of the art. According to this study, the mechanisms of reaction of $CaCO_3$ in condensed phase, when APP and BA are present, can be proposed in the following equations (eq. 37-41).

$$2H_3BO_3 \xrightarrow[T \sim 100^0C]{} 3H_2O + B_2O_3 \quad \text{(eq. 37)}$$

$$(NH_4PO_3)_n \xrightarrow[T < 280^0C]{} nNH_3 + \boldsymbol{(HPO_3)_n} \quad \text{(eq. 38)}$$

$$B_2O_3 + 2(HPO_3)_n \xrightarrow[T < 280\ ^0C]{} 2n(\mathbf{BPO_4}) + nH_2O \quad \text{(eq. 39)}$$

$$BPO_4 + CaCO_3 \xrightarrow[T \sim 550^0C-800\ ^0C]{} \mathbf{CaBPO_5} + CO_2 \quad \text{(eq. 40)}$$

$$P_2O_5 + B_2O_3 + 2CaCO_3 \xrightarrow[T \sim 550^0C-800\ ^0C]{} 2\mathbf{CaBPO_5} + 2CO_2 \quad \text{(eq. 41)}$$

The calcium based compounds (i.e. $CaBPO_5$), which are formed in the char residues, are supposed to be involved to improve fire protective properties and adhesion of intumescent coatings, that was shown in the previous part.

4.1.2.1.2 APP/ZB/$CaCO_3$

Hereafter, the interactions between APP/ZB/$CaCO_3$ are investigated. The same approaches as previously were followed (TGA, HT, XRD and solid state NMR). The experimental and calculated TG curves as well as the difference weight loss curve of APP/ZB/$CaCO_3$ are shown in Figure 67. The experimental TG curve of the mixture APP/ZB/$CaCO_3$ (black line) exhibits two steps of decomposition between 295 °C and 470 °C corresponding to 18 % weight loss. A progressive weight loss after 470 °C is observed (2 % wt. loss up to 800 °C). The difference weight loss curve shows that the interactions between the three additives lead to a thermal destabilization in the temperature range 300 °C to 600 °C. A thermal stabilization appears from 600 °C up to the end of the experiment (+11 wt. % at 800 °C). This suggests the interactions between APP, ZB and $CaCO_3$.

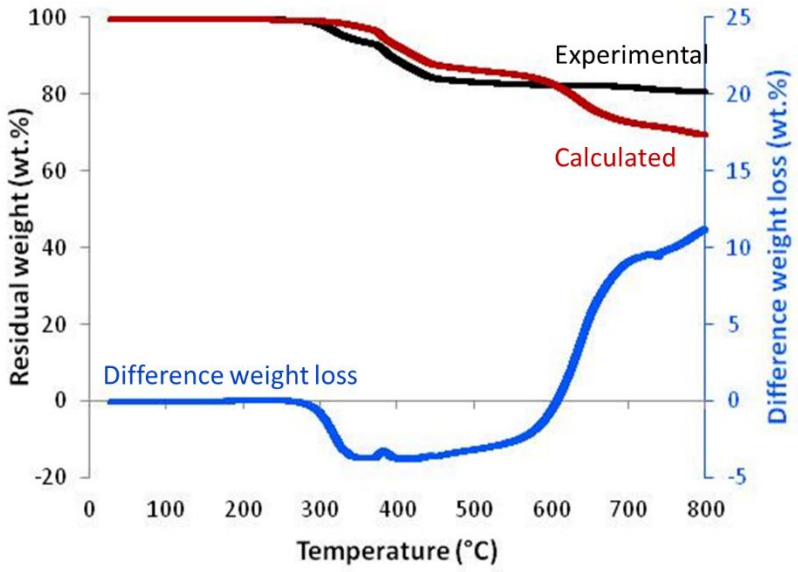

Figure 67 Experimental, calculated TG curves and different weight loss of the mixture of APP/ZB/$CaCO_3$

The samples were heat treated at 280 °C, 550 °C and 800 °C in a similar way as before.

iv) 280 °C: beginning stage of the degradation

v) 550 °C: after the total degradation (destabilization of the system)

vi) 800 °C: high thermal stabilization of the system (+11 wt. % refers to different wt. loss)

Residues (Table 16) do not significantly change depending on the heat treatment temperatures. It remains as a white powder for three heat treatment temperatures.

Table 16 APPZBCa residues at different heat treatment temperatures

HT of 280 °C	HT of 550 °C	HT of 800 °C
		
(Residual weight: 91 wt. %)	(Residual weight: 83 wt. %)	(Residual weight: 81 wt. %)

XRD diffractograms of the APP/ZB/$CaCO_3$ char residues at different heat treatment temperatures are shown in Figure 68. At 280 °C, it is clearly showed that the diffractogram of the mixture looks similar to the superimposition of those of zinc borate and $CaCO_3$. It evidences that ZB and $CaCO_3$ do not degrade at this temperature. It makes sense considering the degradation temperature of those additives ($T_{Decomposition}$ of ZB ≈ 290 °C and of $CaCO_3$ ≈ 680 °C). APP is not identified but at this temperature, APP totally degrades, as similar to what was demonstrated in 3.2.1.1.

At 550 °C, the formation of BPO_4 and of zinc orthophosphate (α-$Zn_3(PO4)_2$) are identified. The formation of zinc boron oxide (ZnB_4O_7) is also found at this temperature. While $CaCO_3$ is still present in the residue, it can be mentioned that the degradation product of APP does not react with $CaCO_3$, being opposite to what was observed in the case of the APP/$CaCO_3$ mixture [94]. This event is similar in both systems (APP/BA/$CaCO_3$ and APP/ZB/$CaCO_3$); there is no reaction between $CaCO_3$ and borates or phosphates up to 550 °C.

BPO_4 is not detected at 800 °C whereas α-$Zn_3(PO4)_2$ and ZnB_4O_7 are still present in the residue. Additionally, the XRD pattern of α-$Zn_2P_2O_7$ and α-$CaZn_2(PO4)_2$ are detected. When looking precisely on the XRD diffractograms, there is no evidence of the formation of $CaBPO_5$, which was found in APP/BA/$CaCO_3$ mixture.

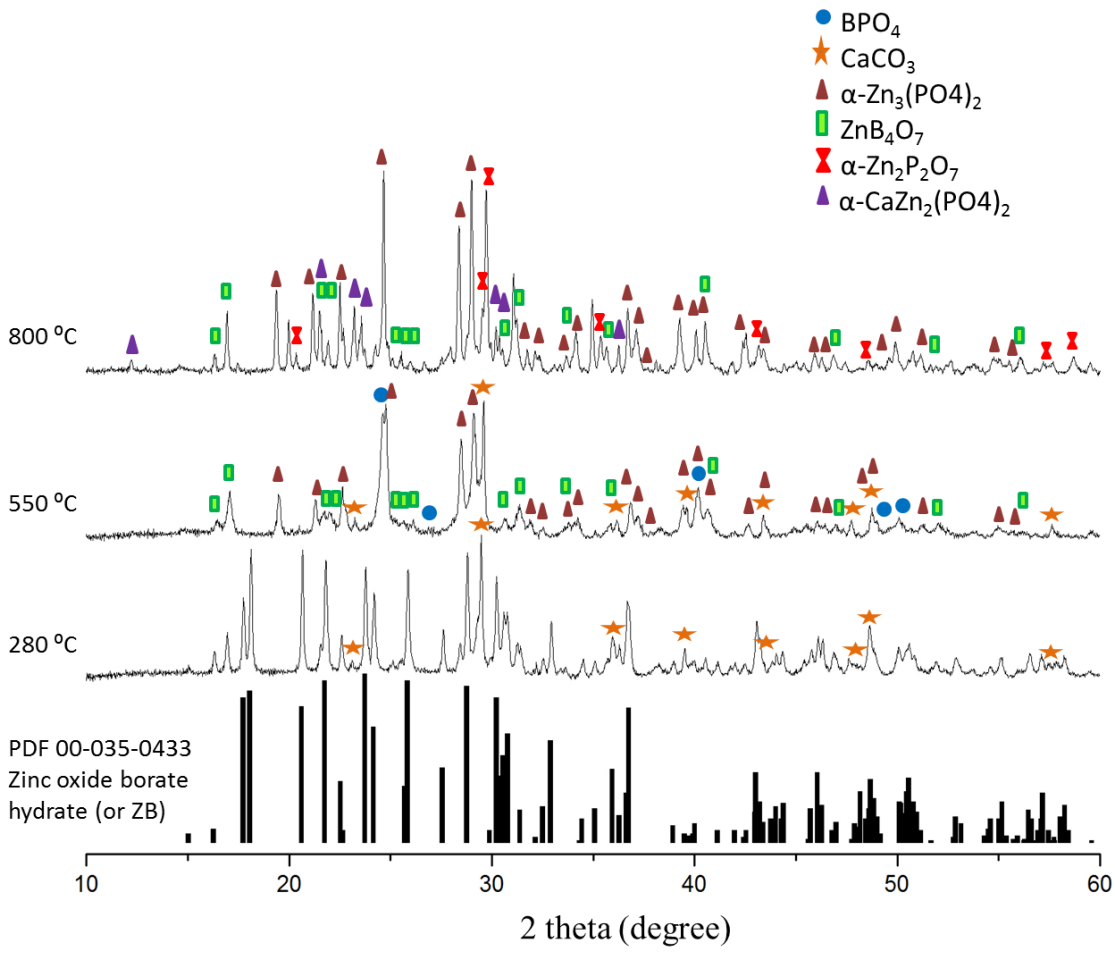

Figure 68 XRD diffractograms of APPZBCa residues versus temperatures

^{31}P NMR spectra of APP/ZB/$CaCO_3$ residues heat treated at 280 °C, 550 °C and 800 °C are shown in Figure 69. At 280 °C, a broad band lying between 0 to -40 ppm appears. Such a broad signal can be due to the formation of a disordered structure of phosphates [183], which is similar to what was observed in the entire formulation (i.e. IF(ZB)wt).

At 550 °C, two sharp signals appear at -30 ppm and 3.9 ppm, which are assigned to the characteristic signal of BPO_4 and of α-$Zn_3(PO4)_2$) [165]. There is a huge evolution of phosphorus species between 550 °C and 800 °C. At 800 °C, the signal of BPO_4 at -30 ppm disappears. The results obtained by NMR are in good agreement with XRD results. The disappearance of BPO_4 at high temperature in similar system was suggested by F. Samyn [83]. It was proposed that $Zn_3(PO4)_2$ reacts with BPO_4 to form zinc pyrophosphate ($Zn_2P_2O_7$) and B_2O_3 as described in the eq. 42.

$$2Zn_3(PO_4)_2 + 2BPO_4 \rightarrow B_2O_3 + 3Zn_2P_2O_7 \quad \text{(eq. 42)}$$

The signal of α-$Zn_3(PO_4)_2$ can still be observed at 800 °C. In addition to this, other sharp signals are observed at 9.9, 2.2, -1.3, -9.3, -14.8, -15.8, -18.8, -21 ppm. Sharp peaks suggest a high crystallinity of the formed products. The triple signals at -15.8, -18.8 and -21 ppm can be attributed to the characteristic signal of α-$Zn_2P_2O_7$ [83]. Additional peaks at 9.9 and 2.2 ppm correspond to the characteristic signals of calcium zinc orthophosphate (α-$CaZn_2(PO4)_2$) [142, 166, 197]. These are consistent with XRD results. Interestingly, the characteristic peak of $CaBPO_5$ at -9.3 ppm can also be observed but the peak intensity is extremely low (it is almost invisible) and this specie is not detected in XRD pattern.

The peaks at -1.3 and -14.8 ppm can be attributed to Q^0 phosphate structure (orthophosphate) and Q^1 phosphate structure (pyrophosphate) respectively. It is very interesting that the presence of zinc borate can change phosphorus species to many crystalline phases compared to the system containing BA.

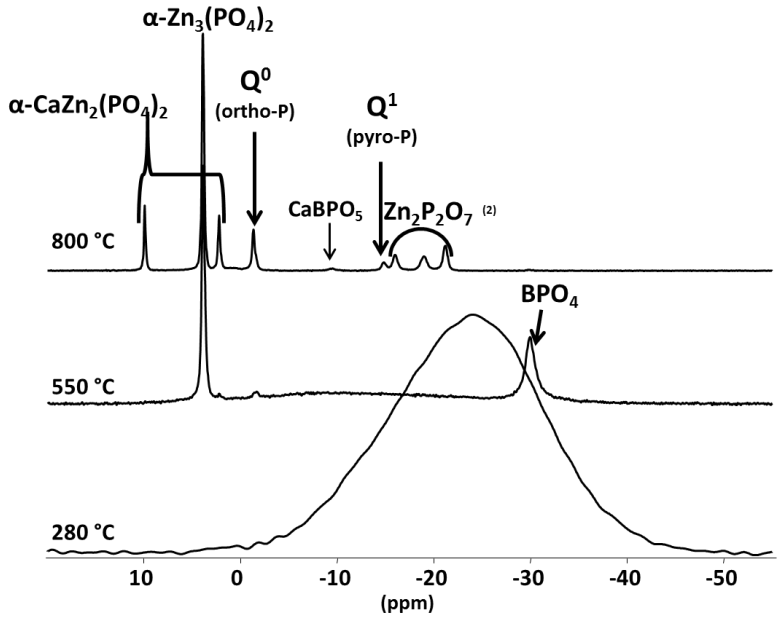

Figure 69 ^{31}P NMR spectra (9.4 T) of APPZBCa residues versus temperatures

^{11}B NMR spectra of APP/ZB/$CaCO_3$ residues heat treated at 280 °C, 550 °C and 800 °C are shown in Figure 70. Boron species at 280 °C change a little bit when comparing to the spectrum of zinc borate. The HTT is close to the dehydration temperature of ZB (290 °C), zinc borate probably starts to degrade. At 550 °C, the formation of BPO_4 is also observed (a sharp signal at -3.8 ppm). At 800 °C, the characteristic signal of BPO_4 still appears with very low intensity but the presence of BPO_4 at this temperature was not identified in neither XRD nor ^{31}P NMR. This can be due to the higher sensitivity of ^{11}B NMR experiment comparing to other techniques.

BO_3 unit of zinc borate lying between 10 and 16 ppm (at ambient temperature) changes to BO_3 in a different conformation at 550 °C to 800 °C, broad and poorly defined line shape suggests the presence of amorphous species. This could be reasonably attributed to the dehydration of ZB leading to the formation of $2ZnO.3B_2O_3$. At 550 °C and 800 °C, there is a sharp signal of BO_4 unit appearing at 1 ppm, this signal is supposed to belong to BO_4 unit in ZnB_4O_7 which was identified by XRD. It is consistent with the network structure of ZnB_4O_7 reported, it is exclusively composed of tetrahedral boron units (BO_4) [198, 199].

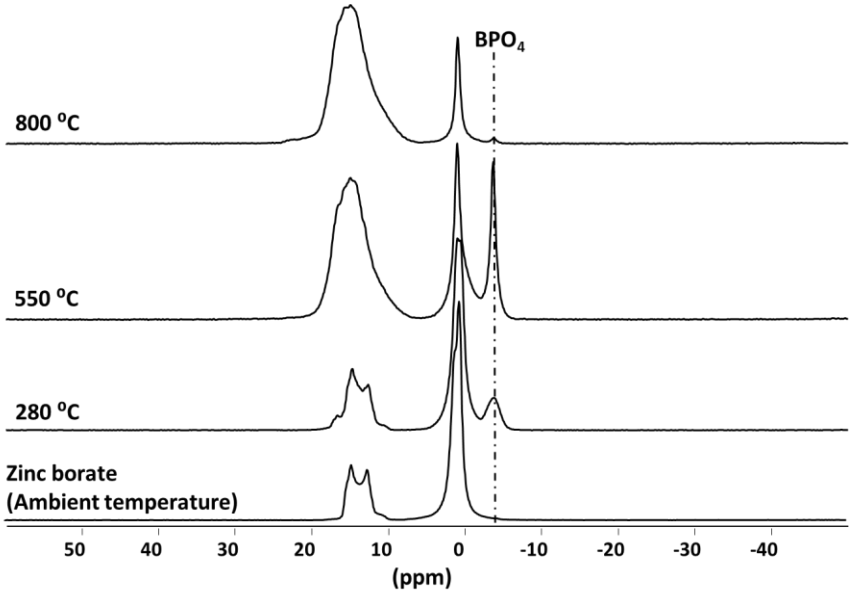

Figure 70 ^{11}B NMR spectra (18.8 T) of APPZBCa residues versus temperatures

Conclusion

In this part, the mechanisms of interaction between the intumescent additives including APP, ZB and $CaCO_3$ (APP/ZB/$CaCO_3$ = 23.6/69.5/6.9 % w/w) were investigated. As a result, borophosphate is formed similar as the system containing BA but its quantity decreases at high temperature (small quantity is left detecting in ^{11}B NMR spectrum). It is supposed that borophosphate reacts with zinc orthophosphate to yield boron oxide and zinc pyrophosphate, this phenomenon is similar to what was observed in the binary system (mixture APPZB) reported in the literature. $CaCO_3$ remains in the char residue and it does not take part in the reaction up to 550 °C. Between 550 °C and 800 °C, calcium based compound (e.g. CaO, degradation product of $CaCO_3$) reacts with zinc and phosphorus based compounds forming calcium zinc orthophosphate ($CaZn_2(PO_4)_2$). This is different to what occurred in the system containing BA. The formation of $CaBPO_5$ is also evidenced in ^{31}P NMR spectrum but its concentration seems to be very low (regarding the peak intensity). In addition to BPO_4, $CaZn_2(PO_4)_2$ and $CaBPO_5$, other crystalline species are formed including zinc orthophosphate ($Zn_3(PO_4)_2$), zinc pyrophosphate ($Zn_2P_2O_7$) and zinc boron oxide (ZnB_4O_7). The mechanisms of reaction occurred in this system is much more complex than the one containing BA.

4.1.2.1.3 Conclusion

In this part, the mechanisms of interaction of the ternary mixture of additives (i.e. APP/BA/$CaCO_3$, APP/ZB/$CaCO_3$) were studied under pyrolytic condition. The results showed that the mechanisms of interactions are different between the systems containing BA or ZB.

For APP/BA/$CaCO_3$ mixture, it was shown that BPO_4 is formed at temperature below 280 ^oC. B_2O_3 (degradation product of boric acid) is present in all heat-treatment temperatures. While $CaCO_3$ does not react with any species up to 550 ^oC, the reactivity of $CaCO_3$ leading to the formation of $CaBPO_5$ was remarked between 550 ^oC and 800 ^oC. The formation of $CaBPO_5$ is supposed to occur by the reaction between $CaCO_3$ and BPO_4 or between $CaCO_3$, B_2O_3 and P_2O_5. These reactions, especially the second possibility are supposed to be highly beneficial to the intumescent phenomenon since phosphorous species can be more stabilized in the condensed phase.

For APP/ZB/$CaCO_3$ mixture, the formation of BPO_4 was found at higher temperature (between 280 ^oC and 550 ^oC) and it then decreases at 800 ^oC. Other species, especially zinc and calcium based compounds (i.e. $Zn_3(PO_4)_2$, $Zn_2P_2O_7$, ZnB_4O_7, $CaZn_2(PO_4)_2$, $CaBPO_5$) were found in this system. Interestingly, in this system, calcium based compound tends to react with both Zn-P compounds and B-P based compounds. However, it is more favorable to react with Zn-P rather than B-P based compounds.

As previously described, not only chemical but also physical properties are also important parameters to understand the mechanisms of action of intumescent system. The fire test results present in 4.1.1 showed the huge difference in char aspect and char expansion between the five formulations: i) promising expansion (IF-APPBA and IF-APPBACa), ii) high expansion (IF-APPCa), and iii) very low expansion (IF-APPZB and IF-APPZBCa). Relating to the fact that the viscosity is a key parameter governing the char aspect and char expansion. This arises an interest in investigating the viscosity of the five formulations. Moreover, the expansion of the five studied formulations cannot be compared after the furnace test due to a detachment of some formulations. Thus, the measurements of expansion using a lab scale test (i.e. Rheometer) were also taken into account. The results will be discussed in the following part.

4.1.2.2 Complex viscosity and expansion

The aim of this part is to investigate the complex viscosity and expansion of the five studied formulations to be able to understand their behaviors in a fire, which were reported in the previous part (4.1.1).

Figure 71 shows the complex viscosity, relative expansion and TG curve of ***IF-APPCa*** measured as a function of temperature. The viscosity is steady up to 300 ^{o}C. It is consistent with TG curve of this formulation. This formulation shows no decomposition up to 300 ^{o}C. Afterwards, the viscosity decreases drastically to the lowest value of about 2 x 10^2 Pa.s (340 ^{o}C), this is called the critical point, which corresponds to the decomposition of epoxy matrix [200]. Then, the viscosity increases slightly until 400 ^{o}C before a drastic increase up to the end of the test, that can be attributed to a carbonization process of the intumescent char [20]. The viscous phase disappears and a highly condensed char structure is produced. It was stated [127] that a low viscosity of melted coating results in the formation of many open holes in charred layer deteriorating fire protective performance of the charred layer. This is consistent with that occurred in this case. It can be mentioned that the formulation containing only APP and $CaCO_3$ leads to a very low viscosity at the critical point (degradation of the epoxy resin), which causes a huge expansion, which was observed during the furnace test.

When looking at the relative expansion, it has no expansion up to 300 ^{o}C, which is well consistent with TG curve (no degradation before 300 ^{o}C). An expansion occurs when the viscosity decreases promptly (at about 305 ^{o}C). Then, the expansion drops to a minus value (-80 % of expansion). At the end of the test, the char aspect was observed, it was found (Table 17) that IF-APPCa coating has a huge expansion and the lower plate is overflowing with the char. This is well consistent with what observed during the furnace test (very high expansion). When taking out the upper plate, it was remarked that char was very fragile and was totally ruined. The minus value was recorded because all material blew up and no char remained in the lower plate.

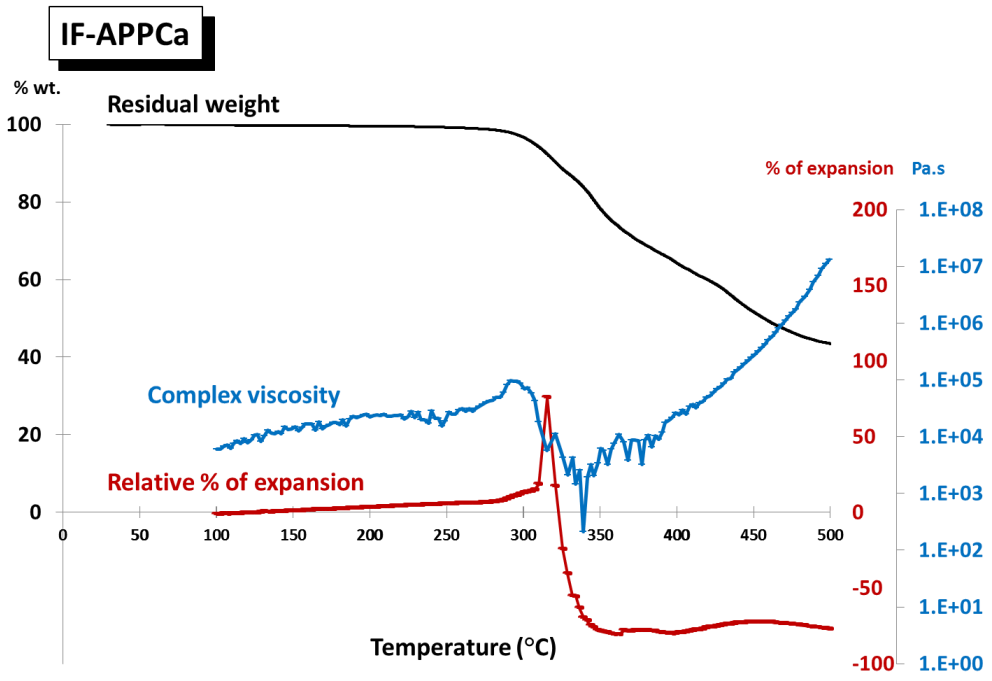

Figure 71 Complex viscosity, relative expansion and TG curve of IF-APPCa

Table 17 Char aspect of IF-APPCa after the rheological measurement

		
End of test (cool state)	Upper plate	Lower plate

The complex viscosity, relative expansion and TG curves of ***IF-APPBA and IF-APPBACa*** are shown in Figure 72. Their viscosities in a temperature range of 100 ^{o}C and 500 ^{o}C are similar. It is pointed out that the addition of $CaCO_3$ into IF-APPBA has no effect on viscosity of the melting matrix. The viscosity increases from about 1 - 2 x 10^5 Pa.s (170 ^{o}C) to 8 - 9 x 10^5 Pa.s (230 ^{o}C). This phenomenon can be attributed to the dehydration of boric acid to form B_2O_3, which increases the viscosity of the matrix [81]. It is similar to what observed for the complex formulation IF(BA) described in chapter III. The viscosity then decreases to the lowest value about 3.5 x 10^4 Pa.s (330 ^{o}C), which is much higher than that of IF-APPCa. Afterwards, it increases sharply (carbonization process) and slowly increases from 420 ^{o}C to the end of the measurement (500 ^{o}C).

When looking at their relative expansion, IF-APPBA and IF-APPBACa exhibit a small expansion between 150 ^{o}C and 290 ^{o}C, which corresponds to the dehydration of boric acid. It then swells to reach the maximum expansion of 113 and 130 relative % for IF-APPBA and IF-APPBACa respectively. The results show that the addition of low amount of $CaCO_3$ has no particular effect on the expansion of the formulation containing APP and boric acid. When looking at the curves, it is noteworthy that the maximum expansion corresponds to the lowest viscosity. The expansions of IF-APPBA and IF-APPPBACa measured using a Rheometer are much lower than these obtained after a furnace test. The difference can be related to the experimental conditions (e.g. heating ramp, temperature, thermal constraint, sample dimension) [126].

To do so, the viscosity and expansion of IF-APPZB and IF-APPZBCa were also measured. The similar results were obtained. The addition of $CaCO_3$ has no significant effect on the viscosity and expansion of the coatings (up to 500 ^{o}C). The results are presented in Appendix IV.

The decarbonation of $CaCO_3$ as a blowing agent is not effective in the case of IF-APPBACa and IF-APPZBCa since the decarbonation occurs outside the region of the significant modification of the viscosity (300 ^{o}C - 400 ^{o}C). Since $CaCO_3$ takes place in the reaction between 550 ^{o}C and 800 ^{o}C as shown in the previous part. This is opposite to the case of IF-APPCa, in which the decarbonation occurs at lower temperature (≈ 300 ^{o}C) by the interaction between APP and $CaCO_3$, that enhances the expansion of intumescent coating.

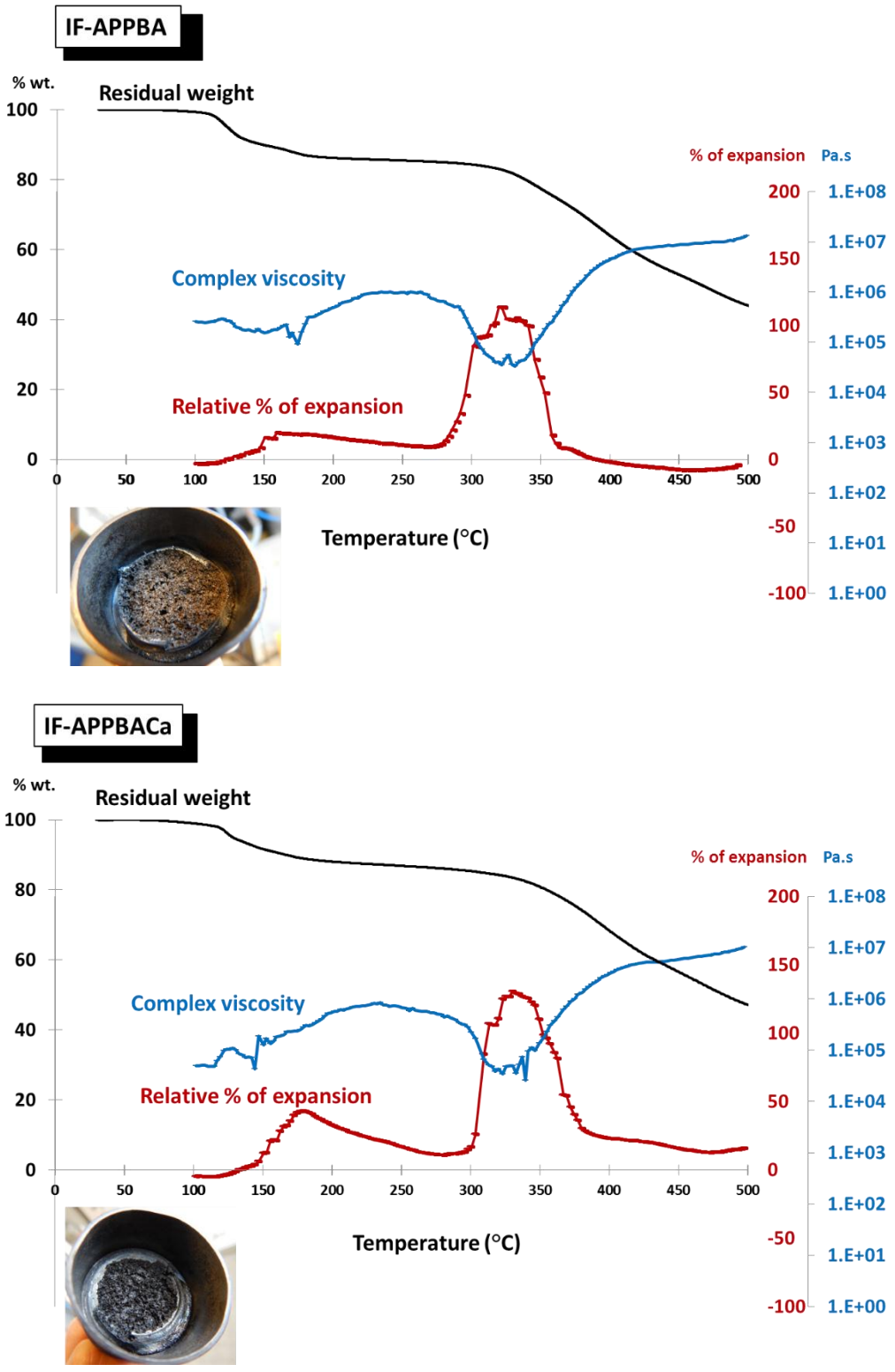

Figure 72 Complex viscosity, relative expansion and TG curves of IF-APPBA and IF-APPBACa

4.1.2.3 Conclusion

To investigate in detail the mode of action of $CaCO_3$ and to explain the results observed during the furnace test, the interactions between the additives as a function of temperature and physical properties (i.e. viscosity and expansion) were investigated. It was shown that $CaCO_3$ reacts with other components of the formulation to form the thermally stable compounds that could stabilize the charred structure. The reactions occur in different way depending on the incorporated components:

- ***i)*** APP+ $CaCO_3$: $CaCO_3$ stabilizes APP by forming Ca-P compounds (i.e.$Ca(PO_3)_2$ [94]).
- ***ii)*** APP+BA+$CaCO_3$: $CaCO_3$ or Ca based compounds (e.g. CaO) reacts with B-P compounds leading to the formation of $CaBPO_5$
- ***iii)*** APP+ZB+$CaCO_3$: $CaCO_3$ or Ca based compounds (e.g. CaO) reacts with B-P and Zn-P compounds leading to the formation of $CaBPO_5$ and $CaZn_2(PO_4)_2$. In this case, its reaction with Zn-P compounds is more favorable than the one of B-P compounds
- For the case (i), the reaction occurs at low temperature (≈ 300 ^oC) leading to the release of CO_2, that enhances the expansion of intumescent char
- For the case (ii) and (iii), the decarbonation of $CaCO_3$ (occur by the decomposition (≈680 ^oC) or its reaction with other components (between 550 ^oC and 800 ^oC)) does not enhance the expansion of intumescent char because it occurs outside the region of the significant modification of the melt viscosity

No beneficial effect of $CaCO_3$ in the mixture of APP/ZB is supposed to be due to the additive ratio, high amount of zinc borate exhibits the expansion and changes the properties of the molten matrix (e.g. too high viscosity). This may be the reason why the incorporation of $CaCO_3$ into APP+ZB does not improve/change any intumescent properties. However, the benefits of $CaCO_3$ in the fire protection of epoxy based intumescent coatings were highlighted (i.e. improvement of fire protection and adhesion, stabilization of B and P in the condensed phase). Consequently, $CaCO_3$ plays an important role in the condensed phase by reacting with other components to form the thermally stable compounds (i.e. $CaZn_2(PO_4)_2$, $CaBPO_5$) stabilizing the

other components of the formulation but the decarbonation of $CaCO_3$ in the case of IF-APPBACa and IF-APPZBCa does not benefit the expansion of the intumescent char.

4.1.3 Conclusion

In this part, the effects of $CaCO_3$ on fire protective properties of intumescent coatings and its mode of action were investigated. The graphic conclusion of this part is shown in Figure 73.

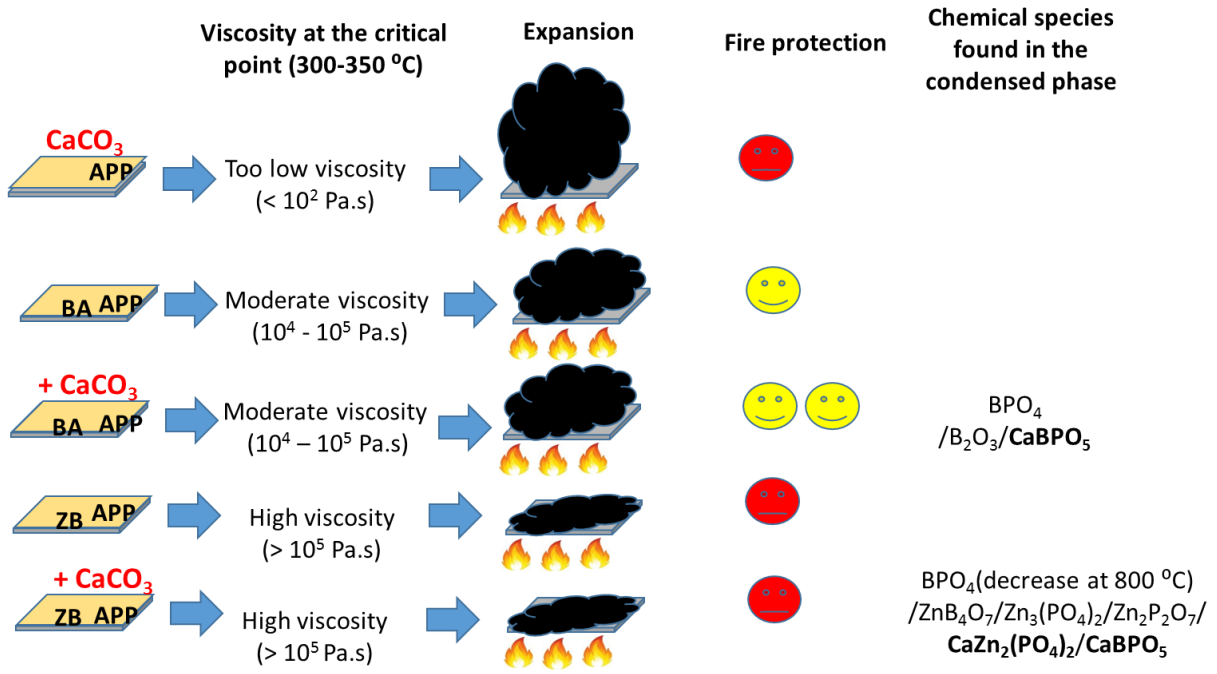

Figure 73 Graphic conclusion of the study of the effect of $CaCO_3$ on intumescent coatings

The addition of $CaCO_3$ into the formulation containing APP and borate was proven to be beneficial for the epoxy based intumescent coatings enhancing the fire protective properties and char adhesion/cohesion of intumescent coatings (when the additive ratio between APP and borate is optimized). $CaCO_3$ or its degradation products react with other components of the formulation (e.g. P, B, Zn based compounds), that forms inorganic species which are thermally stable enhancing the stabilization of the char residues. The combination of $CaCO_3$ and high amount of APP was not recommended since this combination exhibits a too low viscosity and extremely high expansion, which lead to a detachment of charred layer deteriorating fire protective properties of intumescent coatings. Based on these results, the effect of other carbonates on fire protection of intumescent coatings is also of interest. To follow this purpose, IF-APPBACa formulation was chosen to study the effects of carbonates in the next part since it exhibits promising results.

4.2 Influence of different carbonates on fire protection

In the previous part, it was demonstrated that the addition of $CaCO_3$ in the formulation containing APP and BA improves the fire protective performance and adhesion/cohesion of intumescent char. For this reason, other carbonates as ingredient of intumescent formulation were examined.

To study the effects of different carbonates, the IF-APPBACa formulation was chosen. Four carbonate compounds including $MgCO_3$, $ZnCO_3$, K_2CO_3 and Na_2CO_3 were considered in this part.

$MgCO_3$ was reported to use as a flame retardant additive in poly(vinyl chloride) [201] and in polypropylene [202]. $ZnCO_3$ was mentioned to improve the flame retardant properties of polymeric materials forming protective inorganic glasses and limiting the release of combustible gases [203, 204]. K_2CO_3 was used as a flame retardant additive in polymeric materials (e.g. polymethylmethacrylate, polypropylene, nylon) and it was reported to reduce the heat release rate without significantly increasing smoke or carbon monoxide during the combustion [205]. And Na_2CO_3 was used as an ingredient of coating formulation for fire retardancy of cotton textile [206]. However, the use of these four carbonates as intumescent ingredients in epoxy based intumescent coating has never been investigated.

Four carbonate compounds were added into IF-APPBACa formulation instead of $CaCO_3$ with the same weight ratio (3.45 % w/w of carbonate in the formulation). The formulations are named IF-APPBA$MgCO_3$, IF-APPBA$ZnCO_3$, IF-APPBANa_2CO_3, and IF-APPBAK_2CO_3. The coatings were carried out to the small-scale furnace test to assess its fire protective properties and the char collected after the furnace test were characterized to investigate the chemistry in the condensed phase and so, to determine the influence of each carbonate.

4.2.1 Fire protective properties

Time - temperature curves of the studied formulations are shown in Figure 74. The results showed that the addition of $MgCO_3$ exhibits good fire protective properties as similar to those of $CaCO_3$. Their time - temperature curves are almost superimposed. For IF-APPBACa and IF-APPBA$MgCO_3$, times to reach the failure temperature are 24.6 and 25.3 minutes respectively. The addition of $ZnCO_3$ exhibits an interesting result from the beginning of the fire test up to about 14 minutes but after this time, the intumescent falls off leading to a sharp increase of temperature. IF-APPBA$ZnCO_3$ takes 16.6 minutes to reach the failure temperature. For IF-APPBANa_2CO_3 and IF-APPBAK_2CO_3, the fire protective behaviors are quite similar, times to reach the failure temperature are of 20.3 and 19.3 minutes respectively. Afterwards, for both Na_2CO_3 and K_2CO_3, a sharp temperature increase which corresponds to a detachment of char, was observed after passing the failure temperature (≈ 22 - 23 minutes of the test). When compared to the reference formulation IF-APPBA, which takes 18.1 minutes to reach the failure temperature, it was found that the formulations containing Na_2CO_3 or K_2CO_3 exhibit a better fire protective performance than the reference one (IF-APPBA).

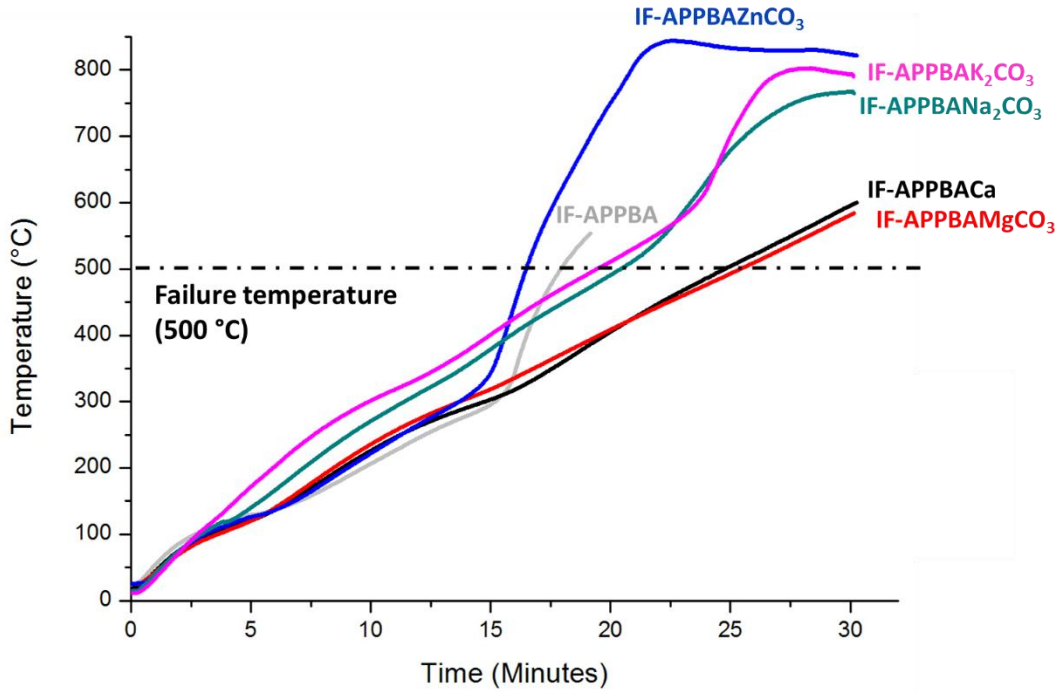

Figure 74 Time-temperature curves of IF-APPBACa, IF-APPBA$MgCO_3$, IF-APPBA$ZnCO_3$, IF-APPBAK_2CO_3 and IF-APPBANa_2CO_3

Table 18 shows the char aspects and expansions of IF-APPBACa, IF-APPBAMgCO_3, IF-APPBAZnCO_3, IF-APPBANa_2CO_3, and APPBAK_2CO_3. At first, the tests were stopped at 30 minutes. It evidenced that three formulations including IF-APPBAZnCO_3, IF-APPBANa_2CO_3, and APPBAK_2CO_3 have no char left on the steel plate due to a detachment of char as previously described. Thus, it is not evident to compare the char aspects of the five formulations at this point. Therefore, 18 minutes after exposing in the furnace test was chosen to be able to compare the char aspects and to elucidate the chemical modifications in the condensed phase affecting by different carbonates.

The char aspects (18 minutes) are obviously different between the five formulations. IF-APPBACa has a hard and compact char structure, some big holes are found between the char layers. The char aspect shown in this part is a bit different to that shown in *4.1 Influence of CaCO3 on the fire protection* because the exposed times in the furnace are different (18 vs. 24 minutes).

IF-APPBAMgCO_3 char is hard and compact. A grey char was formed on the surface. The char is quite homogeneous, holes between the char can also be observed but they are smaller than those of IF-APPBACa. For IF-APPBAZnCO_3, the char is brittle and crumbly. Then, there are big boles between the char structure. For IF-APPBANa_2CO_3, the char is compact and dense with a medium size pores. Glassy and hard char is found on the surface. For IF-APPBAK_2CO_3, the char is fragile, it is not possible to cut at the middle since it splits and breaks into small pieces. Three distinct layers are observed. It includes the dark grey char on top, light grey char in the middle and black char underneath.

When looking at the relative % of expansion after cooling down the samples, IF-APPBACa exhibits the highest expansion. It expands to 898 %, while IF-APPBAMgCO_3 has 484 % of expansion, which is the lowest expansion among all. Low expansion but high fire protective performance in the case of IF-APPBAMgCO_3 is probably due to its charred structure (dense and compact). IF-APPBANa_2CO_3 and IF-APPBAK_2CO_3 expand to 508 and 610 % of relative expansion respectively; they provide an intermediate expansion between the highest and lowest ones.

Table 18 Char aspects and relative expansions of IF-APPBACa, IF-APPBAMgCO$_3$, IF-APPBAZnCO$_3$, IF-APPBANa$_2$CO$_3$, and IF-APPBAK$_2$CO$_3$ (18 minutes)

Formulation	% Relative expansion	Global view	Cross sectional view
IF-APPBACa	898 ± 30 %	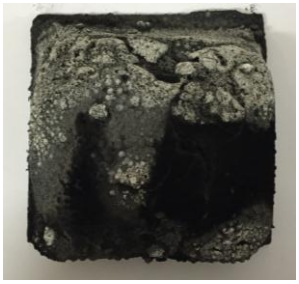	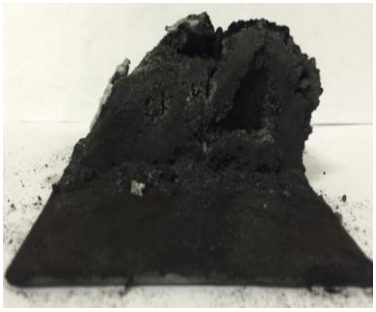
IF-APPBAMgCO$_3$	484 ± 20 %	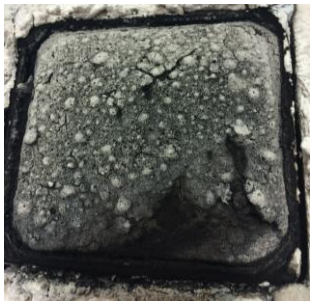	
IF-APPBAZnCO$_3$	-Char falls off-		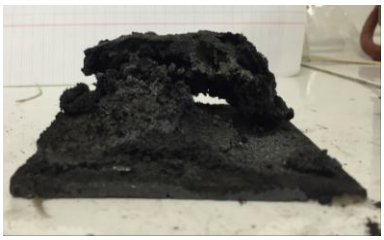
IF-APPBAK$_2$CO$_3$	508 ± 23 %		

IF-APPBANa_2CO_3	610 ± 20 %		

Conclusion

In this part, the effects of five carbonates on fire protective properties, char aspects and char expansion were investigated. It was shown that the incorporation of carbonates into epoxy based intumescent coatings improves the fire protective performances compared to the reference without carbonates, except the formulation containing zinc carbonate which possesses a bad adhesion leading to a shorter time to reach the failure temperature. Among all, the addition of calcium or magnesium carbonates exhibits the best results. For the char aspects, the formulation containing magnesium carbonate forms a dense and homogeneous char without big holes between the charred layers while the one containing calcium carbonate has similar char aspect but some big holes are produced. Char aspects of zinc, potassium and sodium carbonates are different from the two mentioned above. To try to understand the different fire protective behaviors obtained, the char residues collected after the furnace test were characterized and the results will be discussed in the next part.

4.2.2 Chemical composition analyses

This part aims at analyzing the chemical compositions formed in the condensed phase influenced by the different carbonates. It is expected to understand the mechanisms of protection, in particular in the condensed phase. The char residues of the five formulations collected after 18 minutes of the tests were characterized using XRD and solid state NMR. In addition to this, the char residues of IF-APPBACa and IF-APPBA$MgCO_3$ collected after 30 minutes were also analyzed since these two latter formulations do not have a detachment problem.

XRD is used to characterize the presence of crystalline phases in the char residues. Figure 75 shows the XRD diffractograms of IF-APPBACa, IF-APPBA$MgCO_3$, IF-APPBA$ZnCO_3$, IF-APPBANa_2CO_3 and IF-APPBAK_2CO_3 char residues collected after 18 minutes of the tests. The XRD diffractograms of the char residues of the five formulations are identical. It demonstrates the presence of crystalline BPO_4 and B_2O_3. In addition to these, there is a convex signal lying between the 2Θ value between 20 and 33 ° indicating the presence of amorphous phase. XRD patterns show no effect of cations (e.g. Ca^{2+}, Mg^{2+}, Zn^{2+}) on the formation of crystalline species. However, the influence of cation on the formation of amorphous species may be occurred; this cannot be distinguished by XRD.

When looking at the XRD diffractograms of the char residues of IF-APPBACa and IF-APPBA$MgCO_3$ (Figure 76) collected for a longer time after the furnace test (30 minutes), additional crystalline phases in addition to BPO_4 and B_2O_3 are identified. It shows the presence of calcium borophosphate ($CaBPO_5$) in IF-APPBACa char residue and magnesium pyrophosphate (α-$Mg_2P_2O_7$) in IF-APPBA$MgCO_3$ char residue.

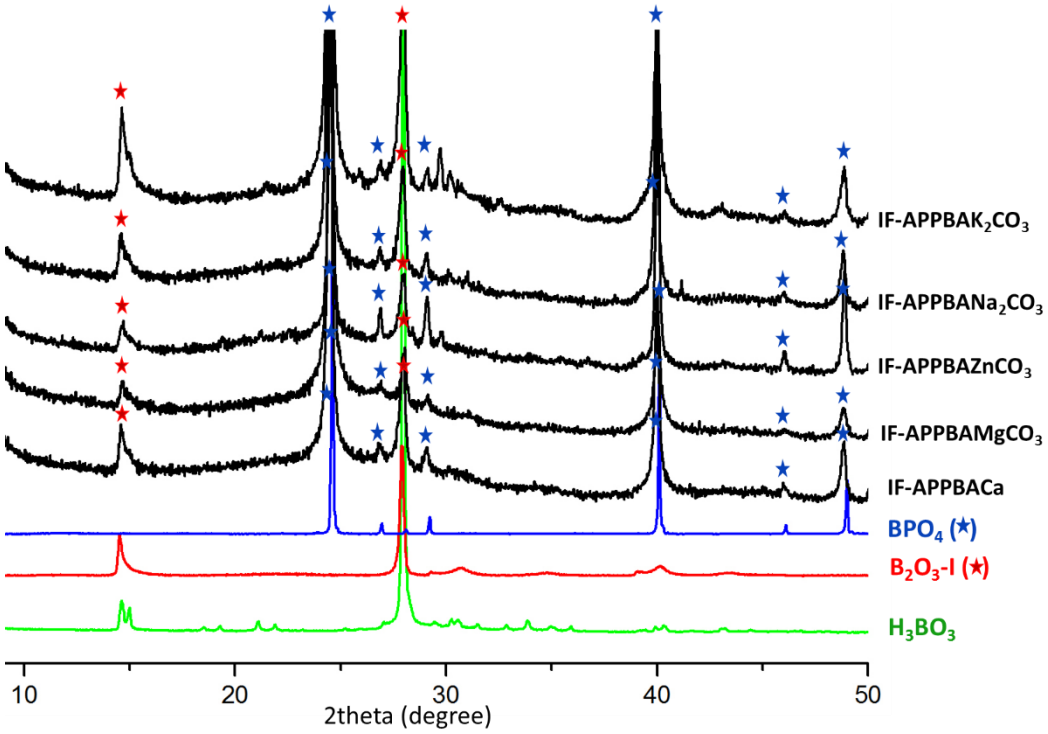

Figure 75 XRD diffractograms of IF-APPBACa, IF-APPBAMgCO₃, IF-APPBAZnCO₃, IF-APPBAK₂CO₃ and IF-APPBANa₂CO₃ char residues (18 minutes)

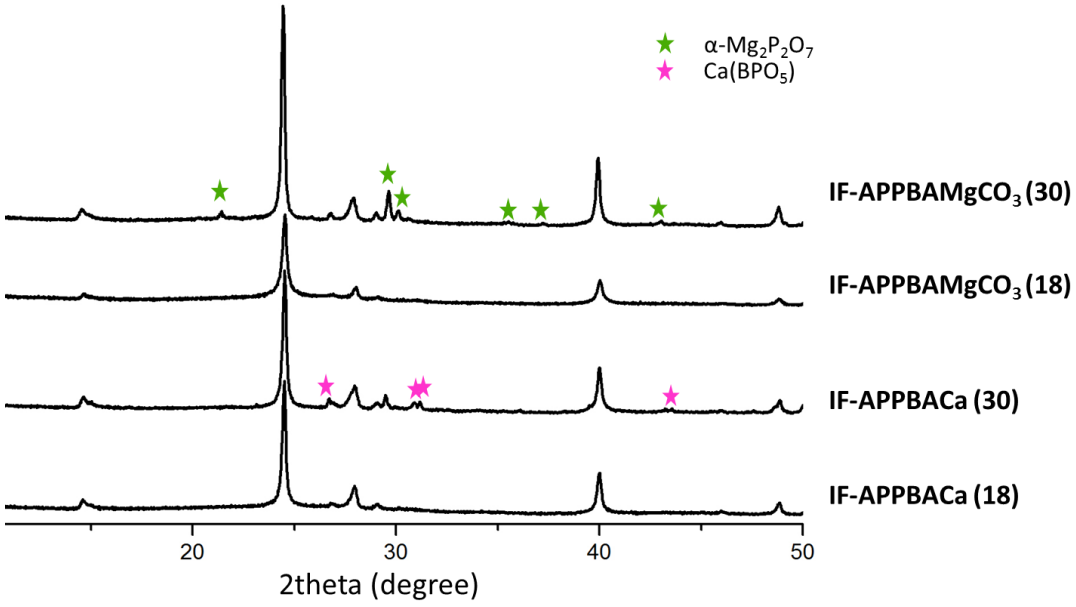

Figure 76 XRD diffractograms of IF-APPBACa and IF-APPBAMgCO₃ char residues (18 vs. 30 minutes)

To complete the results obtained by XRD, ^{31}P and ^{11}B solid state NMRs were used to characterize precisely the effects of carbonates on the modifications of phosphorous and boron structures/species in the condensed phase.

Figure 77 shows the ^{31}P NMR spectra of the five formulations. A sharp peak at -30 ppm, which is a characteristic peak of borophosphate (BPO_4) [74, 165], is found for all formulations. Regarding the peak height, BPO_4 is the main product compared to the other chemical species. It means that the formation of BPO_4 by the reaction between the degradation products of APP and of BA takes place predominantly in all cases.

For IF-APPBACa, in addition to a characteristic peak of BPO_4, there are signals appearing at -7.5, -7.9, -9.3 and -10.3 ppm (very low intensity). In this range of chemical shift, these signals can be attributed to Q^1 phosphate structure (or pyrophosphate). Calcium pyrophosphate ($Ca_2P_2O_7$), which possesses quadruple peaks can be suspected. If it is formed, it is supposed to be poorly crystalline (not identified in XRD). Additionally, a broad signal (very low density) centered at 1 ppm is also detected; it is assigned to Q^0 structure in phosphate [161, 178].

For IF-APPBAMgCO_3, four additional peaks are detected at 0, -13.2, -18.6 and -19.5 ppm. The signal at 0 ppm can be attributed to the signal of Q^0 phosphate (e.g. phosphoric acid (H_3PO_4) [74, 161]). The signals at -13.2 and -19.5 ppm are assigned to α-$Mg_2P_2O_7$ while the signal at -18.6 is assigned to β-$Mg_2P_2O_7$ [162, 207]. Nevertheless, the species identified in ^{31}P NMR (i.e. α-$Mg_2P_2O_7$, β-$Mg_2P_2O_7$) are not detected in XRD diffractograms, it could be due to the poor crystallinity or low amount of these species. Regarding the literature [184], it was mentioned that crystalline $Mg_2P_2O_7$ has a typical line width at half maximum ($LW_{1/2}$) of about 243 Hz (1.5 ppm) , whereas their amorphous counterparts normally exhibit the $LW_{1/2}$ about ten times greater. In ^{31}P NMR of IF-APPBAMgCO_3, the $LW_{1/2}$ of the signal at -13.2, -18.6 and -19.5 ppm are of 112, 194 and 154 Hz respectively. This evidences the high crystallinity of the magnesium phosphate species formed. Therefore, its low quantity is the reason why they were not identified in XRD pattern.

For IF-APPBAZnCO$_3$, apart from BPO$_4$ there is an additional sharp peak at 3.9 ppm, which is assigned to zinc orthophosphate (α-Zn$_3$(PO$_4$)$_2$) [58, 83]. Triple peaks at -16.4, -19 and -21.2 also appear with very low intensity (zoom in the red dotted line), they are assigned to zinc pyrophosphate (α-Zn$_2$P$_2$O$_7$) [58, 83].

IF-APPBANa$_2$CO$_3$ and IF-APPBAK$_2$CO$_3$ exhibit different results from the others. There is no crystalline species formed, except BPO$_4$. In the opposite, there is a broad signal lying between -10 and -25 ppm. The band is centered at about -20 ppm representing the Q^2 tetrahedral sites of metaphosphate chains. This broad signal can be assigned to amorphous forms of phosphates. Regarding the raw material of the formulations, the amorphous phosphates could be XPO$_3$ [208, 209] or amorphous phosphate containing X$_2$O (when X = Na or K).

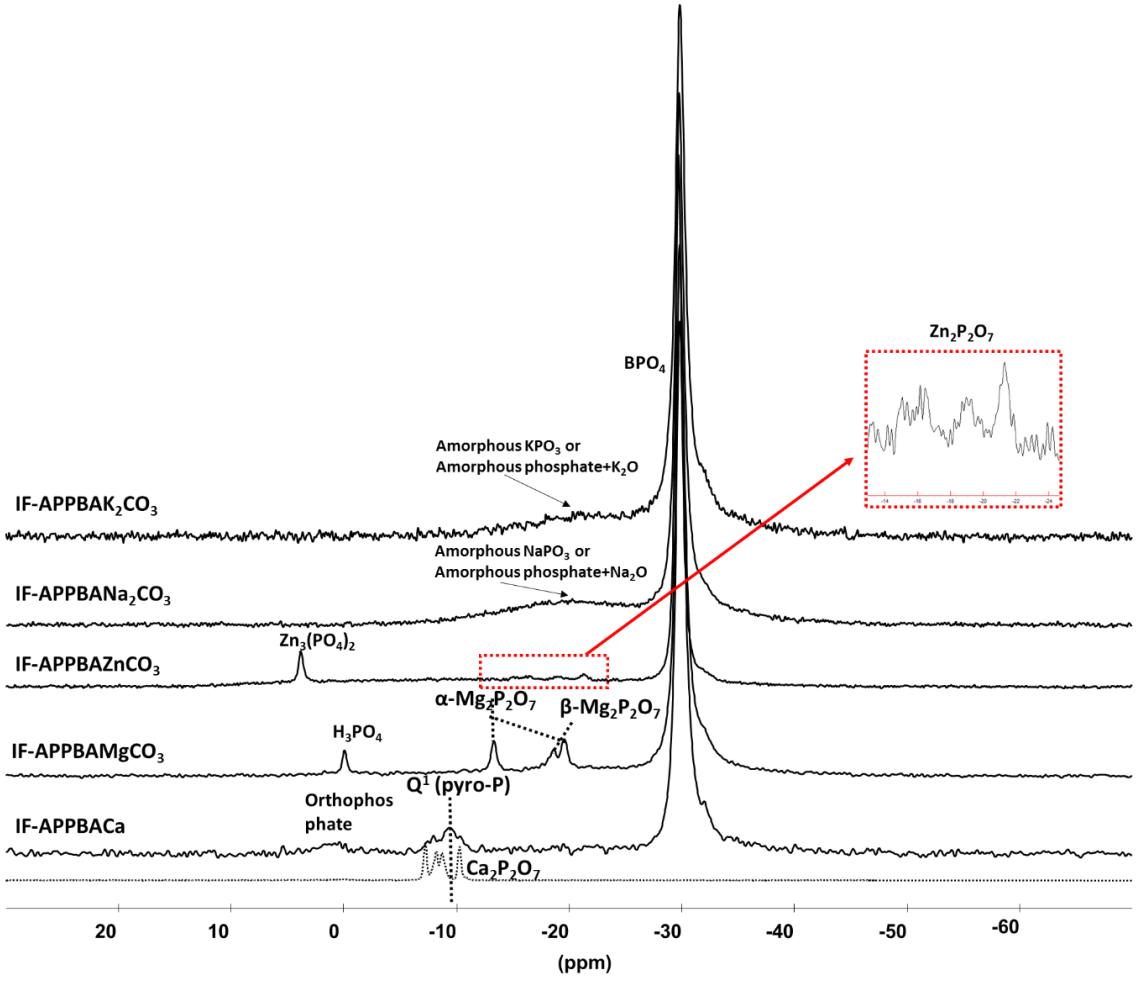

Figure 77 ^{31}P NMR spectra (9.4 T) of IF-APPBACa, IF-APPBAMgCO$_3$, IF-APPBAZnCO$_3$, IF-APPBAK$_2$CO$_3$ and IF-APPBANa$_2$CO$_3$ char residues (18 minutes)

The identification of phosphorus species in the char residues highlights that the formation of BPO_4 by the reaction between the degradation products of APP and of boric acid are predominant confirming what was observed in XRD. It makes sense since these two additives are the main components in the formulations (with high concentration). Moreover, it indicates that the reaction between APP/its degradation products and carbonates during burning leads to form different phosphate species. Nevertheless, their quantities in the condensed phase are much lower than BPO_4. Consequently, the addition of low amount of carbonate compounds affects the formation of phosphate species.

Figure 78 shows the ^{31}P NMR spectra of IF-APPBACa (a) and IF-APPBA$MgCO_3$ (b) comparing the spectra of char residues collected after 18 minutes and 30 minutes. For both cases, it demonstrated that the phosphorous species are not modified between these two points. The quantities of $CaBPO_5$ and $Mg_2P_2O_7$ (α- and β-) are supposed to increase at 30 minutes (regarding the peak intensity). This is probably the reason why these species were detected in XRD patterns at 30 minutes but not at 18 minutes.

a.

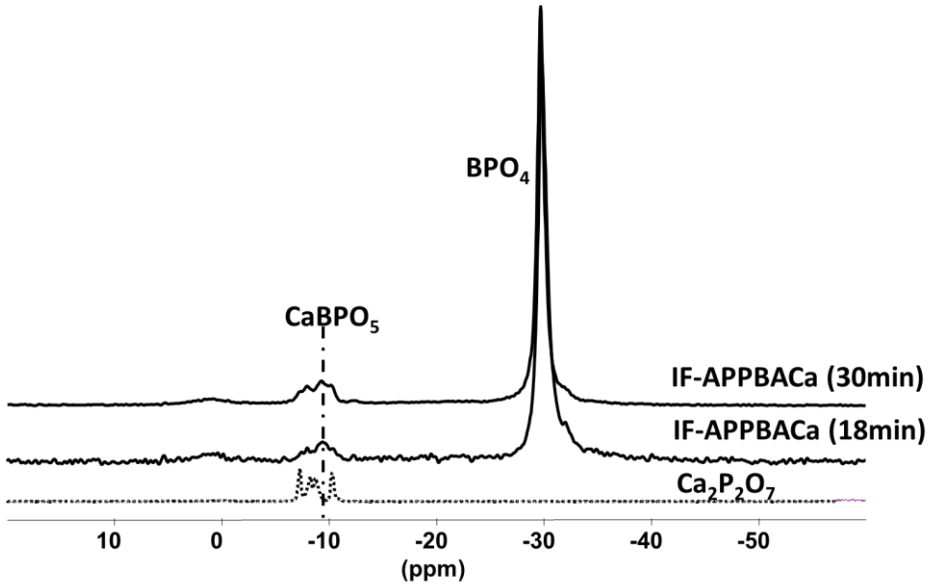

b.

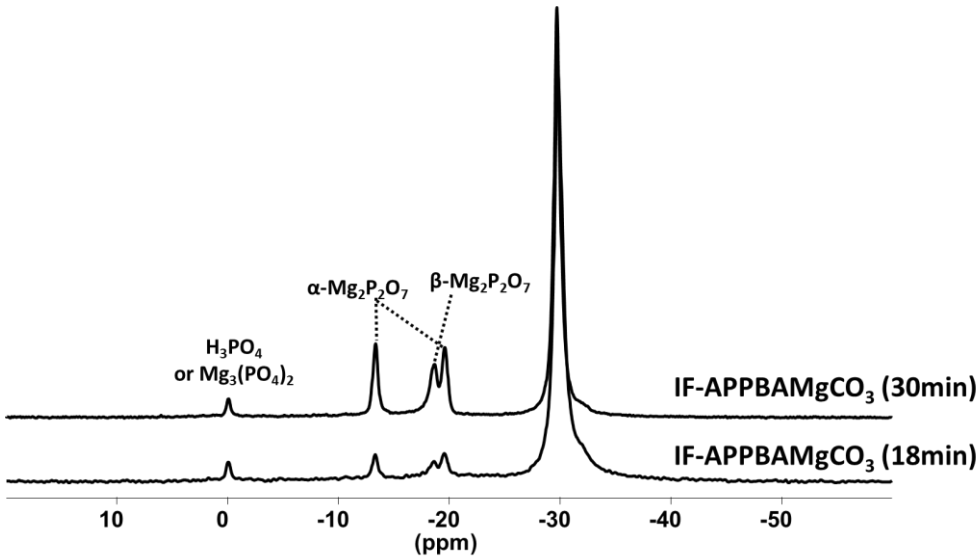

Figure 78 ^{31}P NMR spectra (9.4T) of IF-APPBACa and IF-APPBAMgCO$_3$ char residues (18 vs. 30 minutes)

These results show that the chemical species formed in the char residues of IF-APPBACa and of IF-APPBMgCO$_3$ after 18 and 30 minutes are similar. The difference is about the quantity of the species formed. Afterwards, ^{11}B NMR was carried out on the char residues collected after 18 minutes. The ^{11}B NMR spectra of the five formulations are shown in Figure 79.

For the five formulations, the formation of crystalline BPO$_4$ was evidently identified (sharp peak at -3.8 ppm) [165]. It is consistent with the results obtained by XRD and ^{31}P NMR. A low intense signal at 1 ppm is observed in IF-APPBACa and IF-APPBAMgCO$_3$ char residues, this signal can be attributed to tetrahedral boron (BO$_4$) unit. In IF-APPBANa$_2$CO$_3$ and IF-APPBAK$_2$CO$_3$ char residues, the signal of BO$_4$ is also observed but the chemical shift is different (appear at 0 ppm). A broad peak indicates the low crystallinity of this BO$_4$ unit.

For all formulations, additional signal lying between 20 and 5 ppm (broad signal) is observed: it is attributed to trigonal boron (BO$_3$) units. XRD results (Figure 75) suggested the presence of B$_2$O$_3$, which should be observed in ^{11}B NMR spectra of the samples. When compared the ^{11}B NMR spectra of the five formulations to the spectrum of B$_2$O$_3$ (green line in Figure 79), they are quite different to the one of B$_2$O$_3$. An assumption can be made that there is at least another BO$_3$ unit apart from the one of B$_2$O$_3$ superimposing in this signal.

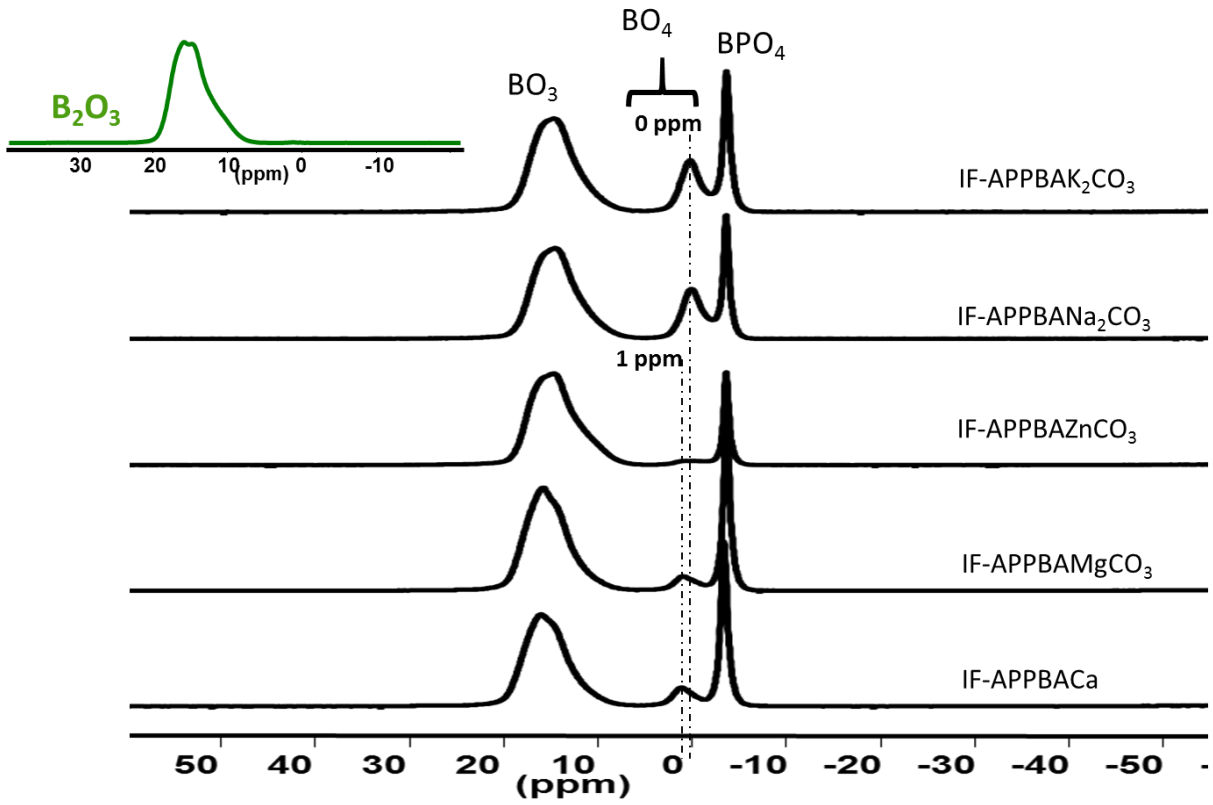

Figure 79 ^{11}B NMR spectra (18.8T) of IF-APPBACa, IF-APPBAMgCO$_3$, IF-APPBAZnCO$_3$, IF-APPBANa$_2$CO$_3$ and IF-APPBAK$_2$CO$_3$ char residues (18 minutes)

To determine the concentration of each boron species, the relative concentration of these species can be estimated by integrating the area of the corresponding signal (semi-quantitative data) as previously done. The results are shown in Figure 80. It was found that IF-APPBACa and IF-APPBAMgCO$_3$ possess higher concentration of BO$_3$ than IF-APPBANa$_2$CO$_3$ and IF-APPBAK$_2$CO$_3$ (70 - 73 vs. 65 - 66 %), while IF-APPBAZnCO$_3$ has the highest concentration of BO$_3$ (86 %). When looking at the concentration of BPO$_4$, the concentration of BPO$_4$ in IF-APPBACa and IF-APPBAMgCO$_3$ is higher than those of IF-APPBAZnCO$_3$, IF-APPBANa$_2$CO$_3$ and IF-APPBAK$_2$CO$_3$ (24 - 25 vs. 13 - 18 %) while the concentration of BO$_4$ is quite high in IF-APPBANa$_2$CO$_3$ and IF-APPBAK$_2$CO$_3$ versus other three formulations (17 - 18 vs. 1 - 5 %).

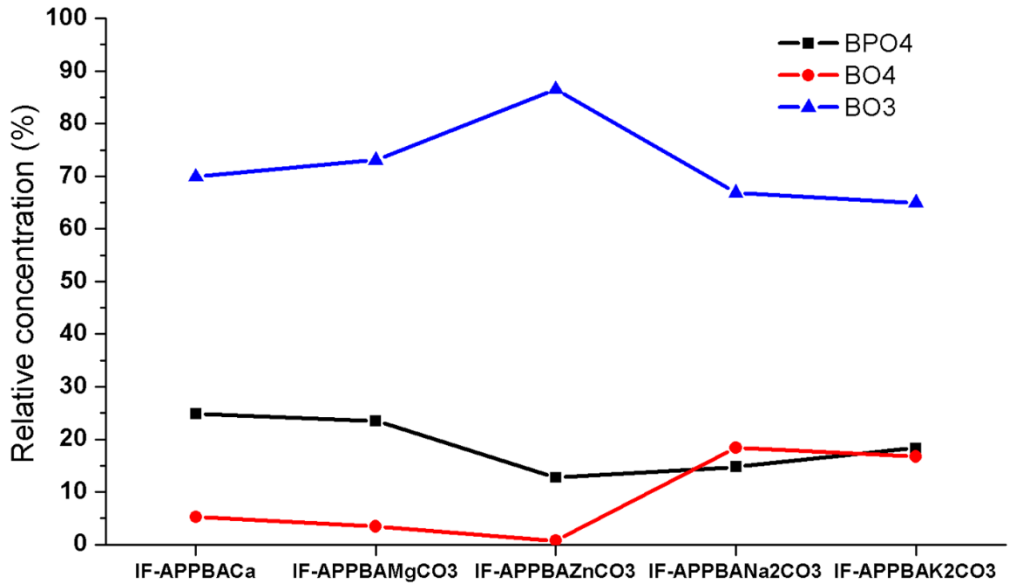

Figure 80 Relative concentration of BO_3, BO_4 and BPO_4 in the IF-APPBACa, IF-APPBAMgCO_3, IF-APPBAZnCO_3, IF-APPBANa_2CO_3 and IF-APPBAK_2CO_3 char residues

The cross characterizations of the char residues using XRD, ^{31}P NMR and ^{11}B NMR showed that the addition of different carbonates influences the chemical species formed in the condensed phase (e.g. phosphorous-based species, quantity of BPO_4). It results from the different mechanisms of reaction between borate, phosphate and carbonate during the intumescent process. Based on these results, assumptions can be made that a good fire protection obtained in the case of IF-APPBACa and IF-APPMgCO_3 formulations may be due to the stabilization of phosphorous species in the condensed phase indicating by high concentration of BPO_4 together with the formation of additional phosphorous-based compounds (e.g. $Ca_2P_2O_7$, $Mg_2P_2O_7$). These probably allow stabilizing more phosphorous in the condensed phase compared to the other formulations. As previously mentioned, the stabilization of phosphorus in the condensed phase benefits the char formation and char stabilization together with the fire protective performance of the intumescent coatings.

4.2.3 Conclusion

The effects of carbonates on the fire protective properties and on the modifications of chemical species formed in the condensed phase were studied. The graphic conclusion is shown in Figure 81. The results showed that the addition of $MgCO_3$ in the epoxy based intumescent coating containing APP and BA shows the good fire protective properties as well as that containing $CaCO_3$. Nevertheless, the char aspects and expansion of these two formulations are a bit different. The formulation with $CaCO_3$ exhibits more expansion with the presence of big holes between charred layers whereas the addition of $MgCO_3$ produces less expansion (half of what obtained in the case of $CaCO_3$) with more dense and compact char structure. $ZnCO_3$ would provide a better fire protection if the char adhesion would have been improved. Na_2CO_3 and K_2CO_3 improve the fire protective properties when compared to the reference formulation (APP+BA). The homogeneous and dense intumescent char performed when incorporated $CaCO_3$ and $MgCO_3$ are probably responsible for a good fire protection obtained. In addition to these, the incorporation of these two carbonates is supposed to stabilize more phosphorus in the condensed phase compared to the others; these could be the reason of the good fire protective performances obtained.

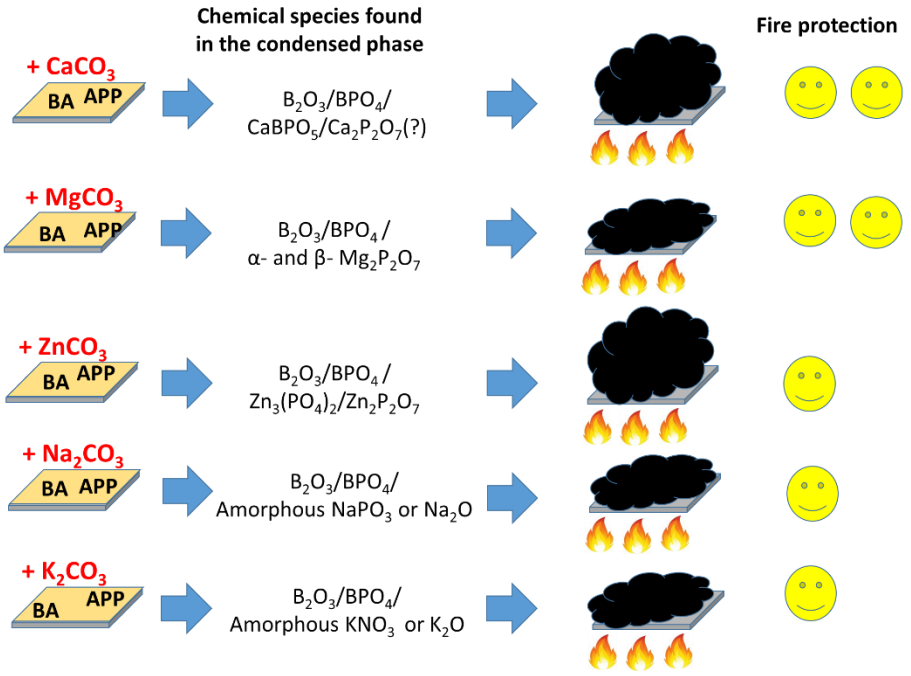

Figure 81 Graphic conclusion of the study of the effects of carbonates on intumescent behaviors

4.3 Conclusion

Chapter IV deals with the investigation of the effects of carbonates. The results showed that the addition of low amount of $CaCO_3$ into epoxy based intumescent coating, which contains phosphate and borate (e.g. APP+BA), improves the fire protective properties and adhesion/cohesion of the intumescent coating. These benefits are due to the reactivity of $CaCO_3$ in the condensed phase. It reacts with B- and P-based compounds forming various inorganic species, that could stabilize the charred structure. The decarbonation of $CaCO_3$ may enhance the expansion of intumescent char, if it occurs in the temperature range of the significant modification of viscosity (between 300 - 400 ^oC). When it occurs outside this temperature range, the role of $CaCO_3$ as a blowing agent by releasing CO_2 is not effective. The decarbonation of $CaCO_3$ can occur at different temperatures depending on its reactivity with other components of the studied systems. In this study, the lack of benefit of $CaCO_3$ in the formulation containing APP+ZB is supposed to be due to the formula itself (i.e. high weight percent of zinc borate). Consequently, this work highlights the positive effects of conventional filler $CaCO_3$ on the fire protective properties of intumescent coatings. Moreover, it was demonstrated that not only $CaCO_3$ but also $MgCO_3$ can be a favorable candidate as an ingredient of intumescent coating with improving the fire protective properties of intumescent coatings. The chemistry in the condensed phase (e.g. chemical reaction, chemical species formed) is different when different carbonate is added into the formulation; these influence the char formation, char aspect, cohesion/adhesion, expansion and fire protection obtained.

General conclusion

Playing with the chemistry of the formulation is a challenging work since it can be fine-tuned in a thousand ways. To develop the competitive and initiative formulations, a fundamental comprehension of the formulation is mandatory. This dissertation was devoted to the fundamental study of epoxy based intumescent coatings for fire protection of steel structures. It aims at providing the comprehension on the mechanisms of action of an epoxy based intumescent coating. The first goal of this work is to draw the mode of action of borates. The second goals are to examine the effects of carbonates on the fire protective properties and to elucidate its mode of action.

Four borates including boric acid, zinc borate, borax and APB were studied to have global information of borates. The incorporation of zinc borate exhibits the best fire protection among all. To get an insight of its mode of action, the formulation containing either zinc borate or boric acid were characterized in more detail examining both chemical and thermo-physical modifications during the intumescent process. It was found that the formation of homogeneous, dense and compact charred structure with high mechanical properties are responsible for a good fire protection as obtained in the case of the formulation containing zinc borate. The formation of the expanded structure occurs lately in presence of zinc borate compared to the one containing boric acid because of its relatively high dehydration temperature. These make zinc borate less competitive against boric acid at the beginning of fire test. In the case of boric acid, the potential reaction and formation of expanded char occur quickly. This provides the potential fire protection at the beginning but a fast development of expanded char in a short time (high expansion) harms the fire protective properties since the charred structure afterwards falls off form the steel.

Apart from the identification of the role of borates, the benefits of adding calcium carbonate into epoxy based intumescent coating were emphasized. It improves the fire protective properties and adhesion/cohesion of intumescent coating when it is added into the formulation containing APP and borate (work for APPBA but not for APPZB). It is opposite to what occurred in the previous part (chapter III: performance of zinc borate is better than boric acid). Note that the

formulation was simplified to examine the effects of carbonates. The additive ratio was kept to the model formulation but their percent weight in the formulation was changed. The mode of action of $CaCO_3$ was studied in detail. It was showed that $CaCO_3$ reacts with other components of the formulation forming different inorganic species, which are thermally stable compounds. These reactions favor stabilizing B and P based compounds in the condensed phase. The decarbonation of $CaCO_3$ as a blowing factor of intumescent systems can be effective in some cases: it depends on the chemical reaction of $CaCO_3$ with the components of the studied system, that makes the decarbonation occur at different temperature range. Additionally, various carbonates as an intumescent ingredient were examined. The results showed that not only $CaCO_3$ but also $MgCO_3$ provide benefits to the fire protective properties of the coating. The incorporation of other carbonates (i.e. Na_2CO_3, K_2CO_3) exhibits less protective performance compared to the two mentioned above, they however improve the fire protective performances compared to the reference formulation without carbonate.

In summary, this work provides the fundamental comprehension of epoxy based intumescent coatings. Based on these results, the possibilities to substitute borates can be pointed out. The reactivity of zinc (i.e. from zinc borate) is outstanding as shown in chapter III, it reacts with P, B and Ca based compounds playing an important role in the condensed phase. An extension of this work is the development of boron free intumescent system. In this context, some works were thus performed and the results will be discussed in the outlook.

Outlook

Based on what we learnt in this work, it suggested the important role of zinc (e.g. synergistic effect) conducting an efficient fire protection. It was observed, for example, in the formulation containing zine borate (in chapter III). From this point of view, the interest is in incorporating zinc-based compounds instead of zinc borate. Three zinc-based compounds were selected including ZnO, ZnS and $ZnSO_4.7H_2O$. ZnO and ZnS because they showed synergistic effect as a flame retardant in silicone rubber composites [210]. It was also reported that $ZnSO_4.7H_2O$ enhances the flame retardancy of polypropylene by balancing the molten viscosity and the intumescent process and strengthening the char layer [211]. The study has been applied on another formulation called ***IFZnB.*** This formulation is one of the formulations of interest formulated by the industrial partner. The composition of the formulation is presented in Table 19.

Table 19 Compositions of IFZnB

Product name	Commercial name (supplier)	Part B (% w/w)	Part A (% w/w)
Aliphatic polyamide amine	Ancamide 903 MAV (Air Products)	8.95	
2.4.6-tris(dimethylaminomethyl)phenol	Acamine K54 (Air Products)	1.77	
Melamine	Melafine (OCI Nitrogen)	15.66	
Titanium dioxide, rutile	Tronox CR-826 (Huntsman)	4.27	2.01
Modified derivative of castor oil	Thixatrol ST (Elementis Specialties)	0.27	0.61
Composite reinforcement, Man-made vitreous (silicate) fibres	Rockforce MS605-Roxul1000 (Lapinus)	2.41	9.89
Bisphenol A diglycidylether epoxy binder	Epikote 828 (Momentive)		20.97
Tris(2-chloroisopropyl)phosphate	Fyrol PCF (ICL)		6.44
Ammonium polyphosphate	Exolit AP 422 (Clariant)		18.96
zinc borate, flame retardant	Firebrake ZB (20 Mule team)		6.01
Calcium Carbonate or Dolomite	Micral 5 (Reverté)		1.72
Carbon black	Lamp Black 101 (Orion engineered carbons)		0.05
Total (% w/w)		**33.33**	**66.67**

To realize the study, zinc borate in the studied formulation (***IFZnB***) was substituted by another zinc-based compound with constant zinc molar ratio. The formulations are named IFZnO, IFZnS and IFZnSO_4 respectively. Their compositions are shown in Appendix II. Four formulations with different zinc source were carried out to the furnace test to assess their fire protective performances against hydrocarbon fire.

Time - temperature curves of four formulations are presented in Figure 82. The formulation containing zinc borate leads to the longest time to reach the failure temperature; it takes 24 minutes while IFZnS, IFZnO and IFZnSO_4 take 22, 21 and 18 minutes respectively. The incorporation of ZnO and ZnS exhibits interesting results because their times to failures are close to that of the reference formulation containing zinc borate. If the formulations containing ZnO and ZnS were fine-tuned and optimized, it could be expected to get the fire protective properties of the reference formulation.

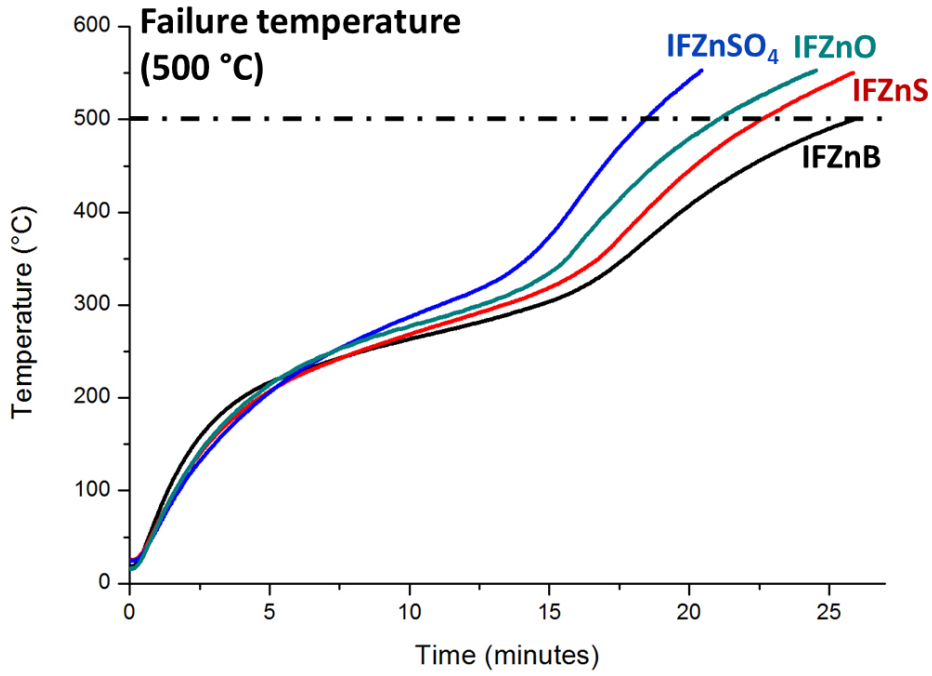

Figure 82 Time - temperature curves of IFZnB, IFZnO, IFZnS and IFZnSO_4

The char aspects and relative % of expansion of four formulations are shown in Table 20. For IFZnB, char possesses three layers: i) top layer – char is yellow and fibrous, which is quite brittle, ii) medium layer – char is grey with big size cells, they are quite homogeneous and iii) bottom layer – char is black, dense, compact and hard.

For IFZnS and IFZnO, both chars are quite similar. Three layers of char are observed. The yellow fibrous char on top layer, which is similar to IFZnB is observed. Char in medium layer builds like a multi-sheet. In the black part, there is a black sheet on the top, which is very hard and a crumbly char is found underneath.

For IFZnSO_4, expanded char can also be distinguished into three layers. The yellow fibrous char is still observed on the top. Differently, many small holes appear on the surface. It could be due to the dehydration of zinc sulfate occurring during the intumescent process. The grey layer in the middle possesses the big holes like IFZnB. Black char on the bottom is different from others (less hard than LF1-ZnO and LF1-ZnS, it is not layered but it is homogenous and crumbly).

Table 20 Char aspects and relative expansions of IFZnB, IFZnO, IFZnS and IFZnSO_4

Formulation	% Relative expansion	Global view	Cross-sectional view
IFZnB	885 ± 15		
IFZnO	843 ± 12		

IFZnS	985 ± 19		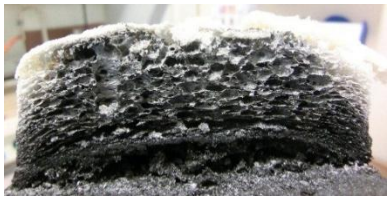
$IFZnSO_4$	1099 ± 20		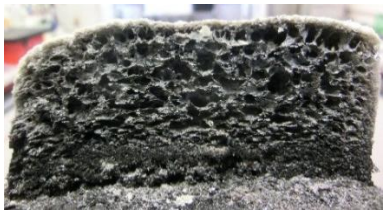

This results point out that the development of boron free intumescent coatings is possible with zinc-based compounds. Nevertheless, the formulation should be optimized to attain a longer protection time. It is also of high interest to investigate the mechanisms of action of zinc (e.g. synergistic, catalytic).

Additionally, another prospect of interest is the elucidation of the mechanisms of action of $MgCO_3$ which also exhibits promising results in fire protection. The formulation containing $MgCO_3$ provides a similar level of fire protection to $CaCO_3$ with lower expansion (-40 % of expansion). This behavior is very interesting for the fire protection against more aggressive fire such as jet fire. The incorporation of $MgCO_3$ in intumescent coating using against jet fire could be a subject of interest for future work.

List of tables and figures

List of tables

List of figures

References

1. P. Mather, *Saving lives with coatings: The essentials of passive fire protection.* European Coatings Journal, 2006. **6**: p. 48-52.
2. *World trade center collapse footage*. [cited 2017 07 March].
3. R. G. Puri and A. S. Khanna, *Intumescent coatings: A review on recent progress.* Journal of Coatings Technology and Research, 2017. **14**(1): p. 1-20.
4. T. Mariappan, *Recent developments of intumescent fire protection coatings for structural steel: A review.* Journal of Fire Sciences, 2016. **34**(2): p. 120-163.
5. M. G. Goode, *Fire protection of structural steel in high-rise buildings*, U.S.D.o.C.T. Administration, Editor 2004.
6. E. D. Weil, *Fire-Protective and Flame-Retardant Coatings - A State-of-the-Art Review.* Journal of Fire Sciences, 2011. **29**(3): p. 259-296.
7. C. Gérard, G. Fontaine, and S. Bourbigot, *New Trends in Reaction and Resistance to Fire of Fire-retardant Epoxies.* Materials, 2010. **3**(8): p. 4476-4499.
8. H. L. Vandersall, *Intumescent coating systems, their development and chemistry.* Journal of Fire Flammability, 1971. **2**: p. 97-140.
9. S. Duquesne, et al., *Influence of inorganic fillers on the fire protection of intumescent coatings.* Journal of Fire Sciences, 2012. **31**(3): p. 258-274.
10. Y. Zhou, et al., *Effect of metal oxides on fire resistance and char formation of intumescent flame retardant coating.* Journal of Inorganic Materials 2014. **29**(9): p. 972-978.
11. S. Bourbigot and S. Duquesne, *Chapter 6: Intumescent based fire retardants*, in *Fire Retardancy of Polymeric Material:*, C. A. Wilkie and A. B. Morgan, Editors. 2009, CRC Press. p. 129-163.
12. C. A. Wilkie and A. B. Morgan, *Fire Retardancy of Polymeric Materials* Second Edition ed. 2009.
13. H. Tramm, et al., *Fireproofing of wood*, 1938.
14. J. Russell, *Paint and coatings: A mature industry in transition.* Progress in Polymer Science, 1997. **22**: p. 203-245.
15. R. Moricone and A. Tugnoli, *Investigating the properties of fireproofing materials for an advanced design of equipment protection.* Chemical Engineering Transactions 2015. **43**: p. 2389-2394.
16. G. Zuccaro, *A case of choice of passive fire protection (PFP) in an Oil & Gas EPC project.* Chemical Engineering Transactions, 2012. **26**: p. 315-320.
17. *Fire protecting structural steelwork*. [cited 2017 0504]; Available from: http://www.steelconstruction.info/Fire_protecting_structural_steelwork.
18. J. Alongi, Z. Han, and S. Bourbigot, *Intumescence: Tradition versus novelty. A comprehensive review.* Progress in Polymer Science, 2015. **51**: p. 28-73.
19. K. P. Nørgaard, et al., *Investigation of char strength and expansion properties of an intumescent coating exposed to rapid heating rates.* Progress in Organic Coatings, 2013. **76**(12): p. 1851-1857.

20. S. Duquesnea, et al., *A comparative study of the mechanism of action of ammonium polyphosphate and expandable graphite in polyurethane.* Polymer Degradation and Stability, 2002. **77**: p. 333-344.
21. J. W. Hanafin and D.C. Bertrand, *Low density, light weight intumescent coating*, 2000.
22. G. C. Tesoro, *Chemical modification of polymers with flame-retardant compounds.* Journal of Polymer Science: Macromocelular Reviews, 1978. **13**: p. 283-353.
23. S. Pappalardo, *Intumescent flame retarded polypropylene systems containing sepiolite clays: properties and synergic effects*, in *Department of Chemical, Material and Industrial Production Engineering*2016, University of Naples 'Federico II'.
24. G. Camino, L. Costa, and G. Martinasso, *Intumescent Fire-retardant systems.* Polymer Degradation and Stability, 1989. **23**: p. 359-376.
25. M. Xanthos, *Functional filler for plastics*, ed. n. ed. 2010: Wiley-VCH.
26. S. Ullah, et al., *Synergistic effects of kaolin clay on intumescent fire retardant coating composition for fire protection of structural steel substrate.* Polymer Degradation and Stability, 2014. **110**: p. 91-103.
27. M. Zia-ul-Mustafa, et al., *The effect of Wollastonite filler on thermal performance of intumescent fire retardant coating.* Advanced Materials Research, 2014. **970**: p. 328-331.
28. S. Ullah and F. Ahmad, *Effects of zirconium silicate reinforcement on expandable graphite based intumescent fire retardant coating.* Polymer Degradation and Stability, 2014. **103**: p. 49-62.
29. N. Amir, F. Ahmad, and P.S.M. Megat-Yusoff, *Study on the fibre reinforced epoxy-based intumescent coating formulations and their char characteristics.* Journal of Applied Sciences 2011. **10**: p. 1678-1687.
30. B. Gardelle, et al., *Resistance to fire of silicone-based coatings: Fire protection of steel against cellulosic fire.* Journal of Fire Sciences, 2014. **32**(4): p. 374-387.
31. *UL 1709: Rapid rise fire tests of protection materails for structural steel, 1994 Underwriter Laboratories.*
32. *The protection of structural steel in hydrocarbon fires*. [cited 2015 7th, July]; Available from: http://library.ul.com/wp-content/uploads/sites/40/2015/03/144182614.pdf.
33. *Types of fire exposure*. [cited 2017 06 April]; Available from: http://www.promat-tunnel.com/en/advices/fire-protection/fire%20curves.
34. C. Beyler, et al., *Fire resistance testing for performance-based fire design of buildings*, 2007, National Institute of Standards and Technology.
35. *Higher Temperature applications* [cited 2017 7th, September]; Available from: http://www.reginaglass.com.au/fireshield/higher-temperature-applications.html.
36. J. Ciret, *Investigation of intumescent coatings for fire protection application to jet fire*, 2010, Université Lille I Sciences et Technologies
37. M. S. Deogon, *High heat resistant composition*, A.N.C. International, Editor 2012.
38. Standardization, I.O.f., *ISO 22899-1:2007 Determination of the resistance to jet fires of passive fire protection materials - Part I: General requirements* 2007. p. 1-40.
39. G. Camino, *Fire retardant polymer materials new perspectives* in *8th International Symposium on Fire Safety Science*2005, Fire safety Science Beijing, China. p. 101-110.

40. G. Camino, L. Costa, and L. Trossarelli, *Mechanism of intumescence in fire retardant additives for polymers*, in *American Chemical Society, Polymer Preprints, Division of Polymer Chemistry*1984. p. 90.
41. S. bourbigot, *Applications of intumescence for reaction and resistance to fire of materials* Materials China, 2013. **32**(3): p. 137-143.
42. S. Bourbigot, *Fireproofing polymeric materials: problems and solutions* in *Organic Materials for Sustainable Construction* 2013, John Wiley and Sons. p. 178-188.
43. S. Bourbigot, B. Gardelle, and P. Vandereecken, *Protecting substrates against damage by fire*, D.C. Corporation, Editor 2013.
44. R. J. Wade, *Intumescent composition*, A.N.C. International, Editor 2009.
45. B. Gardelle, et al., *Thermal degradation and fire performance of intumescent silicone-based coatings.* Polymers for Advanced Technologies, 2013. **24**(1): p. 62-69.
46. M. A. Boyle, C. J. Martin, and J. D. Neuner, *Epoxy Resins*, in *Composites* 2001, ASM International. p. 78-89.
47. Q. Luo, et al., *Highly effective flame retardancy of a novel DPPA-based curing agent for DGEBA epoxy resin.* Industrial and Engineering Chemistry Research, 2016. **55**(41): p. 10880-10888.
48. G. Wang and J. Yang, *Influences of molecular weight of epoxy binder on fire protection of waterborne intumescent fire resistive coating.* Surface and Coatings Technology, 2012. **206**(8-9): p. 2146-2151.
49. S. Duquesne, et al., *Thermoplastic resins for thin film intumescent coatings – towards a better understanding of their effect on intumescence efficiency.* Polymer Degradation and Stability, 2005. **88**(1): p. 63-69.
50. J. S. Wang, et al., *Metal compound-enhanced flame retardancy of intumescent epoxy resins containing ammonium polyphosphate.* Polymer Degradation and Stability, 2009. **94**(4): p. 625-631.
51. U. Sorathia, et al., *Evaluation of intumescent coatings for shipboard fire protection* Journal of Fire Sciences, 2003. **21**: p. 423-450.
52. E. D. Weil and S. Levchik, *A review of current flame retardant systems for epoxy resins.* Journal of Fire Sciences, 2004. **22**(1): p. 25-40.
53. T. A. Ward, et al., *Fire protective intumescent mastic composition and method employee same*, P. Industry, Editor 1985.
54. R. M. Nugent, et al., *Flexible intumescent coating composition* P. industries, Editor 1991.
55. M. J. Sinclair and J. E. Watts, *Fire retardant intumescent coating* C.H. Limited, Editor 2002.
56. K. J. Kittle and M. Anderson, *Intumescent composition comprising a silicate modified epoxy resin*, A.N.C. International, Editor 2016.
57. L. Herschke, et al., *Zinc phosphate as versatile material for potential biomedical applications part I.* Journal of Materials Science: Materials in Medecine, 2006. **17**: p. 81-94.
58. A. Sut, et al., *Interactions in multicomponent flame-retardant polymers: Solid-state NMR identifying the chemistry behind it.* Polymer Degradation and Stability, 2015. **121**: p. 116-125.

59. A. D. Naik, et al., *Outlining the mechanism of flame retardancy in polyamide 66 blended with melamine-poly(zinc phosphate).* Fire Safety Journal, 2014. **70**: p. 46-60.
60. G. Camino, L. Costa, and L. Trossarelli, *Study of the Mechanism of Intumescence in Fire Retardant Polymers: Part l--Thermal Degradation of Ammonium Polyphosphate-Pentaerythritol Mixtures.* Polymer Degradation and Stability, 1984. **6**: p. 243-252.
61. G. F. Levchik, et al., *Thermal behavior of ammonium polyphosphate-inorganic compound mixtures: Part 2 Manganese dioxide* Thermochimica Acta, 1995. **257**: p. 117-125.
62. S. Duquesne, et al., *Mechanism of fire retardancy of polyurethanes using ammonium polyphosphate.* Journal of Applied Polymer Science, 2001. **82**(13): p. 3262-3274.
63. G. Phillips, *National Research Development Corp*, 1974.
64. F. A. Dimanshteyn, *Fire resistant coatings* F.C. Corporation, Editor 1991.
65. R. Nugent, et al., *Flexible intumescent coating composition*, P. Industries, Editor 1992.
66. S. Ullah, F. Ahmed, and M. Yusoff, *Effect of boric acid and melemine on the intumescent fire retardant coating composition for the fire protecon of structural steel substrates.* Journal of Applied Polymer Science, 2012: p. 2983-2993.
67. F. Ahmed, et al., *Non-toxic mineral based intumescent fire retardant coating for structural applications.* International Journal of the Institue of Materials Malaysia, 2013. **1**: p. 137-156.
68. F. Zhang, et al., *Smoke suppression and synergistic flame retardancy properties of zinc borate and diantimony trioxide in epoxy-based intumescent fire-retardant coating.* Journal of Thermal Analysis and Calorimetry, 2015. **123**(2): p. 1319-1327.
69. K. K. Shen, S. H. Kochesfahani, and F. Jouffret, *Boron based flame retardants and flame retardancy*. 2 ed. 2010: CRC Press.
70. R. A Smith and R. B. McBroom, *Kirk-Othmer Encyclopedia of Chemical Technology: Boron oxides, Boric acid, and Borates* 2000.
71. A. Rotaru, *Thermal and kinetic study of hexagonal boric acid versus triclinic boric acid in air flow.* Journal of Thermal Analysis and Calorimetry, 2017. **127**(1): p. 755-763.
72. S. Taguchi, P. P. Parmentier, and T. Yamasaki, *Sassolite sublimated in a steam well at the Yunotani Geothermal Field, Aso Caldera, Kyushu.* Mineralogical Journal, 1981. **10**: p. 338-343.
73. M .Jimenez, S. Duquesne, and S. Bourbigot, *Kinetic analysis of the thermal degradation of an epoxy-based intumescent coating.* Polymer Degradation and Stability, 2009. **94**(3): p. 404-409.
74. M .Jimenez, S. Duquesne, and S. Bourbigot, *Intumescent fire protective coating: Toward a better understanding of their mechanism of action.* Thermochimica Acta, 2006. **449**(1-2): p. 16-26.
75. S. Kocakusak, et al., *Production of anhydrous, crystalline boron oxide in fluidized bed reactor.* Chemical Engineering and Processing, 1996. **35**: p. 311-317.
76. E. McCalla and R. Brüning, *Amorphization of crystalline orthoboric acid on a vitreous B2O3 substrate.* Journal of Materials Research, 2002. **17**(12): p. 3098-3104.
77. *Boric Oxides, Boric Acids, and Metal Borates*, 2016, Science Chemistry.
78. G. Ferlat, et al., *Hidden polymorphs dirve vtirification in B2O3.* Nature Materials 2012. **11**: p. 925-929.
79. L. McCulloch, *A crystalline Boric Oxide.* 1937. **59**: p. 2650-2652.

80. S.V. Berger, *The crystal structure of boron xide.* Acta Chemica Scandinavica, 1953: p. 611-622.
81. M .Jimenez, S. Duquesne, and S. Bourbigot, *Characterization of the performance of an intumescent fire protective coating.* Surface and Coatings Technology, 2006. **201**(3-4): p. 979-987.
82. S. Ullah, et al., *Effects of ammonium polyphosphate and boric acid on the thermal degradation of an intumescent fire retardant coating.* Progress in Organic Coatings, 2017. **109**: p. 70-82.
83. F. Samyn, et al., *Effect of zinc borate on the thermal degradation of ammonium polyphosphate.* Thermochimica Acta, 2007. **456**(2): p. 134-144.
84. D. M. Schubert, et al., *Structural characterization and chemistry of the industrially important zinc borate, Zn[B3O4(OH)3].* Chem mater, 2003. **15**: p. 866-871.
85. M. Sabet, A. Hassan, and C. T. Ratnam, *Effect of zinc borate on flammability/thermal properties of ethylene vinyl acetate filled with metal hydroxides.* Journal of Reinforced Plastics and Composites, 2013. **32**(15): p. 1122-1128.
86. S. Bourbigot, M. Le Bras, and S. Duquesne, *Zinc borates as synergists for flame retarded polymers.* Fire Retardancy of Polymers: New Applications of Mineral Fillers, 2003: p. 327-335.
87. A. Hermansson, T. Hjertberg, and B. Sultan, *The flame retardant mechanism of polyolefins modified with chalk and silicone elastomer.* Fire and Materials, 2003. **27**(2): p. 51-70.
88. F. S. Murakami, et al., *Physicochemical study of CaCO3 from egg shells.* Cienc. Tecnol. Aliment., 2007. **27**: p. 658-662.
89. Y. Tang, et al., *Investigation Into Poly(propylene)/Montmorillonite/Calcium Carbonate Nanocomposites.* Macromolecular Materials and Engineering, 2004. **289**(2): p. 191-197.
90. J. Z. Xu, *Zinc hydroxystannate- or zinc stannate-coated calcium carbonate as flame retardant for semirigid Poly(vinyl chloride).* Journal of Fire Sciences, 2006. **24**(2): p. 105-119.
91. L. Karlsson, et al., *Influence of melt behaviour on the flame retardant properties of ethylene copolymers modified with calcium carbonate and silicone elastomer.* Polymer Degradation and Stability, 2009. **94**(4): p. 527-532.
92. X. Almeras, et al., *Effect of fillers on fire retardancy of intumescent polypropylene blends.* Macromolecular Symposia, 2003. **198**(1): p. 435-448.
93. A. Ciudad, L. Haurie, and A. M. Lacasta, *Kinetic analysis of endothermic degradation of magnesium hydroxide, calcium hydroxide and calcium carbonate in the context of passive fire protection.* Fire and Materials, 2015. **39**(1): p. 14-25.
94. S. Deodhar, et al., *Calcium carbonate and ammonium polyphosphate-based flame retardant composition for polypropylene.* Journal of Applied Polymer Science, 2009. **120**(3): p. 1866-1873.
95. G. Bertelli, et al., *Intumescent Fire Retardant Systems - Effect of fillers on char structure.* 1989. **172**: p. 153-163.
96. A. Baykal, G. Gozel, and M. Kizilyalli, *X-ray powder diffraction and IR study of calcium borophosphate, CaBPO5.* Turk J chem, 2000. **24**: p. 381-388.

97. Q. F. Gillani, et al., *Effect of dolomite clay on thermal performance and char morphology of expandable graphite based intumescent fire retardant coatings.* Procedia Engineering, 2016. **148**: p. 146-150.
98. B. Claub, *Fibers for ceramic matrix composites.* Ceramic Matrix Composites, 2008: p. 1-20.
99. F. Ahmad, et al., *Thermal performance of glass fiber reinforced intumescent fire retardant coating for structural applications.* Proceedings of the 23rd Scientific Conference of Microsocpy Society Malaysia (SCMSM 2014), 2015: p. 1-6.
100. Z. Triantafyllidis and L. A. Bisby. *Fibre-reinforced epoxy intumescent coatings for strengthening and fire protecting steel beams*. in *7th international Conference on Fiber Reinforced Polymer (FRP) Composites in Civil Engineering (CICE 2014)*. 2014.
101. M. Morys, et al., *Variation of intumescent coatings revealing different modes of action for good protection performance.* Fire Technology, 2017. **53**(4): p. 1569-1587.
102. H. Aziz, F. Ahmad, and M. Z. Mustafa, *Effect of titanium oxide on fire performance of intumescent fire retardant coating.* Advanced Materials Research, 2014. **935**: p. 224-228.
103. H. Horacek, *Reactions of stoichiometric intumescent paints.* Journal of Applied Polymer Science, 2009. **113**(3): p. 1745-1756.
104. J. W. Gu, et al., *Study on preparation and fire-retardant mechanism analysis of intumescent flame-retardant coatings.* Surface and Coatings Technology, 2007. **201**(18): p. 7835-7841.
105. T. Mariappan, A. Agarwal, and S. Ray, *Influence of titanium dioxide on the thermal insulation of waterborne intumescent fire protective paints to structural steel.* Progress in Organic Coatings, 2017. **111**: p. 67-74.
106. C. E. Bamberger and G. M. Begun, *Synthesis and characterization of titanium phosphates, TiP2O7 and (TiO2)P2O7.* Journal of the Less Common Metals 1987: p. 201-206.
107. H. Aziz and F. Ahmad, *Effects from nano-titanium oxide on the thermal resistance of an intumescent fire retardant coating for structural applications.* Progress in Organic Coatings, 2016. **101**: p. 431-439.
108. A. Beheshti and S. Z. Heris, *Experimental investigation and characterization of an efficient nanopowder-based flame retardant coatign for atomospheric metallic substrates.* Powder Technology, 2015. **269**: p. 22-29.
109. S. Duquesne and S. Bourbigot, *Chapter 10: Char formation and characterization*, in *Fire Retardancy of Polymeric Material*, C. A. Wilkie and A. B. Morgan, Editors. 2009, CRC Press. p. 239-260.
110. F. Samyn, et al., *Crossed characterisation of polymer-layered silicate (PLS) nanocomposite morphology: TEM, X-ray diffraction, rheology and solid-state nuclear magnetic resonance measurements.* European Polymer Journal, 2008. **44**(6): p. 1642-1653.
111. B. Girardin, et al., *Characterization of thermo-physical properties of EVA/ATH: Application to gasification experiments and pyrolysis modeling.* Materials, 2015. **8**(11): p. 7837-7863.
112. J. E. J. Staggs, R. J. Crewe, and R. Butler, *A theoretical and experimental investigation of intumescent behaviour in protective coatings for structural steel.* Chemical Engineering Science, 2012. **71**: p. 239-251.

113. J. E. J. Staggs, *Thermal conductivity estimates of intumescent chars by direct numerical simulation.* Fire Safety Journal, 2010. **45**(4): p. 228-237.
114. L. Calabrese, et al., *Thermal characterization of intumescent fire retardant paints.* Journal of Physics 2014. **547**.
115. M. Muller, et al., *Investigation of the synergy in intumescent polyurethane by 3D computed tomography.* Polymer Degradation and Stability, 2013. **98**(9): p. 1638-1647.
116. S. E. Gustafsson, *Transient plane source techniques for thermal conductivity and thermal diffusivity measurements of solid materials.* Review of Scientific Instruments, 1991. **62**(3): p. 797-804.
117. P. Anna, et al., *Influence of modified rheology on the efficiency of intumescent flame retardant.* Polymer Degradation and Stability, 2001. **74**: p. 423-426.
118. P. Anna, et al., *Intumescent flame retardant systems of modified rheology.* Polymer Degradation and Stability, 2002. **77**: p. 243-247.
119. M. Bugajny, M. Le Bras, and S. Bourbigot, *Appraoch to the dynamic properties of an intumescent material.* Fire and Materials, 1999. **23**: p. 49-51.
120. S. Bourbigot, et al., *Synergistic effect of zeolite in an intumescent process: study of the interactions between the polymer and the addtives* Journal of Chemistry Society 1996. **92**(18): p. 3435-3444.
121. B. Gardelle, et al., *Characterization of the carbonization process of expandable graphite/silicone formulations in a simulated fire.* Polymer Degradation and Stability, 2013. **98**(5): p. 1052-1063.
122. S. Bourbigot, B. Gardelle, and S. Duquesne, *Intumescent silicone based coatings for the fire protection of carbon fiber reinforced composites.* Fire safety Science-draft proceedings of the 11th international symposium, 2014.
123. A. D. Naik, S. Duquesne, and S. Bourbigot, *Hydrocarbon time–temperature curve under airjet perturbation: An in situ method to probe char stability and integrity in reactive fire protection coatings.* Journal of Fire Sciences, 2016. **34**(5): p. 385-397.
124. I. S. Reshetnikov, A. N. Garashchenko, and V. L. Strakhov, *Experimental investigation into mechanical destruction of intumescent chars.* Polymer for Advanced Technologies, 2000. **11**: p. 392-397.
125. I. S. Reshetnikov, et al., *Mechanical Stability of Intumescent Chars.* Journal of Applied Polymer Science, 1998. **67**: p. 1827-1830.
126. M. Muller, et al., *Measurement and investigation of intumescent char strength: Application to polyurethanes.* Journal of Fire Sciences, 2013. **31**(4): p. 293-308.
127. Z. Wang, E. Han, and W. Ke, *Influence of nano-LDHs on char formation and fire-resistant properties of flame-retardant coating.* Progress in Organic Coatings, 2005. **53**(1): p. 29-37.
128. C. Gérard, G. Fontaine, and S. Bourbigot, *Synergistic and antagonistic effects in flame retardancy of an intumescent epoxy resin.* Polymers for Advanced Technologies, 2011. **22**(7): p. 1085-1090.
129. C. Gérard, et al., *Reaction to fire of an intumescent epoxy resin: Protection mechanisms and synergy.* Polymer Degradation and Stability, 2012. **97**(8): p. 1366-1386.

130. K. Apaydin, et al., *Layer-by-layer deposition of a TiO2-filled intumescent coating and its effect on the flame retardancy of polyamide and polyester fabrics.* Colloids and Surfaces A: Physicochemical and Engineering Aspects, 2015. **469**: p. 1-10.
131. P. Müller, et al., *Melamine poly(zinc phosphate) as flame retardant in epoxy resin: Decomposition pathways, molecular mechanisms and morphology of fire residues.* Polymer Degradation and Stability, 2016. **130**: p. 307-319.
132. A. D. Naik, et al., *Mapping the multimodal action of melamine-poly(aluminium phosphate) in the flame retardancy of polyamide 66.* RSC Advances, 2014. **4**(35): p. 18406-18418.
133. M. Morys, et al., *Revealing the inner secrets of intumescence: Advanced standard time temperature oven (STT Mufu+)-μ computed tomography approach.* Fire and Materials, 2017: p. 1-13.
134. J. Rosc, V. M. F. Hammer, and R. Brunner, *X-ray computed tomography for fast and non-destructive multiple pearl inspection.* Case Studies in Nondestructive Testing and Evaluation, 2016. **6**: p. 32-37.
135. C. Drevelle, et al., *Influence of ammonium polyphosphate on the mechanism of thermal degradation of an acrylic binder resin.* Journal of Applied Polymer Science, 2004. **94**(2): p. 717-729.
136. S. Bourbigot, M. Le Bras, and R. Delobel, *Carbonization mechanisms resulting form intumescence - part II. association with an ethylene terpolymer and the ammonium polyphosphate-pentaerythritol fir retardant system.* Carbon, 1995. **33**(3): p. 283-294.
137. S. Bourbigot, M. L. Bras, and R. Delobel, *Carbonization mechanisms resulting from intumescene association with the ammonium polyphosphate-pentaerythritol fire retardant systems.* Carbon, 1993. **31**: p. 1219-1230.
138. B. Gardelle, et al., *Resistance to fire of curable silicone/expandable graphite based coating: Effect of the catalyst.* European Polymer Journal, 2013. **49**: p. 2031-2041.
139. M. Jimenez, et al., *Comprehensive study of the influence of different aging scenarios on the fire protective behavior of an epoxy based intumescent coating.* Industrial and Engineering Chemistry Research, 2013. **52**(2): p. 729-743.
140. H. Sturm, et al., *SEM/EDX: Advanced investigation of structured fire residues and residue formation.* Polymer Testing, 2012. **31**(5): p. 606-619.
141. C. Nyambo, E. Kandare, and C. A. Wilkie, *Thermal stability and flammability characteristics of ethylene vinyl acetate (EVA) composites blended with a phenyl phosphonate-intercalated layered double hydroxide (LDH), melamine polyphosphate and/or boric acid.* Polymer Degradation and Stability, 2009. **94**(4): p. 513-520.
142. K. J. D. Mackenzie and M. E. Smith, *Multinuclear solid-state NMR of inorganic materials*. Vol. 6. 2002.
143. S. Bourbigot, et al., *Synergistic effect of zeolite in an intumescence process: study of the carbonaceous structures using solid-state NMR.* Journal of Chemistry Society, Faraday Transactions 1996. **92**: p. 149-158.
144. A. Karrasch, et al., *Solid-state NMR on thermal and fire residues of bisphenol A polycarbonate/silicone acrylate rubber/bisphenol A bis(diphenyl-phosphate)/(PC/SiR/BDP) and PC/SiR/BDP/zinc borate (PC/SiR/BDP/ZnB) – Part I: PC*

charring and the impact of BDP and ZnB. Polymer Degradation and Stability, 2010. **95**(12): p. 2525-2533.
145. M. Foldvari, *Handbook of thermogravimetric system of minerals and its use in geological practice*. Vol. 213. 2011: Geological Institute of Hungary 179.
146. N. Kanari, et al., *Thermal decomposition of zinc carbonate hydroxide.* Thermochimica Acta, 2004. **410**(1-2): p. 93-100.
147. P. Patnaik, *Handbook of inorganic chemicals*. 2001: McGraw-Hill.
148. D. Massiot, *Dmfit, Dmfit,*, 2011.
149. M. Jimenez, S. Duquesne, and S. Bourbigot, *High-throughput fire testing for intumescent coatings.* Industrial and Engineering Chemistry Research, 2006. **45**(7475-7481).
150. R. E. Myers, et al., *Ammonium pentaborate- an intumescent flame retardant for thermoplastic polyurethanes.* Journal of Fire Sciences, 1985. **3**: p. 432-449.
151. J. C. Elvira-León, et al., *Epsomite as flame retardant treatment for wood: Preliminary study.* Construction and Building Materials, 2016. **126**: p. 936-942.
152. T. Farajpour, et al., *Effect of borax on thermal and mechanical properteis of ethylene-propylene-diene terpolymer rubber-based heat insulator.* Journal of Applied Polymer Science, 2015: p. 41936-41946.
153. A. Baykal, et al., *Hydrothermal and microwave synthesis of boron phosphate, BPO4.* Turkish Journal of Chemistry, 2001. **25**: p. 425-432.
154. G. Tricot, et al., *P-O-B(3) linkages in borophosphate glasses evidenced by high field (11)B/(31)P correlation NMR.* Chemical Commununications, 2015. **51**: p. 9284-9286.
155. A-R. Grimmer, et al., *Multinuclear (11B, 31P) MAS NMR spectroscopy of borophosphates.* Fresenius J Anal Chem, 1997: p. 485-488.
156. J. D. Mackenzie, R. S. McDonald, and W. K. Murphy, *Infrared spectroscopy of melts and hygroscopic glasses.* Review of Scientific Instruments, 1961. **32**(2): p. 118-121.
157. C. J. Dileep Kumar, et al., *Sassolite formation in glass powders- A novel method to study phase seperation in alkali borosilicate glass compositions* Journal of the American Ceramic Society, 2010. **93**(10): p. 3027-3030.
158. Y. Zhang, et al., *Preparation of β-Ca3(PO4)2 bioceramic powder from calcium carbonate and phosphoric acid.* Current Applied Physics, 2005. **5**(5): p. 531-534.
159. A. Jones, et al., *Access to Chemistry*. 1999: Royal Society of Chemistry. 396.
160. J. S. Carpenter, et al., *Characterizatio of minerals, metals, and materials 2014*. 2014.
161. M. Bugajny, et al., *The origin and nature of flame retardance in ethylene-vinyl acetate copolymers containing hostaflam AP 750.* Polymer Internatioal, 1999. **48**: p. 264-270.
162. F. Fayon, et al., *31P NMR study of magnesium phosphate glass.* Journal of Non-Crystalline Solids, 2001. **283**: p. 88-94.
163. L. B. Fletcher, et al., *Femtosecond laser writing of waveguides in zinc phosphate glasses.* Optical Materials Express, 2011. **1**.
164. C. E. Smith, *The structure and properties of ternary zinc phosphate glasses for optical applications*, 2014, Missouri university.
165. K. H. Pawlowski, et al., *Flame retardancy mechanisms of bisphenol A bis(diphenyl phosphate) in combination with zinc borate in bisphenol A polycarbonate/acrylonitrile–butadiene–styrene blends.* Thermochimica Acta, 2010. **498**(1-2): p. 92-99.

166. A. K. Cheetham, et al., *Correlations between 31P NMR chemcial shifts and structural parameters in crystalline inorganic phosphates.* Journal of the Chemical Society, Chemical communications articles 1986: p. 195-197.
167. M. Roming, et al., *Characterization of noncrystalline nanomaterials: NMR of zinc phosphate as a case study.* Chemistry of Materials, 2008. **20**: p. 5787-5795.
168. F. Hammerschmidt and S. Schmidt, *The phosphonate-phosphate and phosphate-phosphonate rearrangement and their application V(1). On the reaction of s-Butyllithium/TMEDA with symmetrical trialkyl phosphates.* Monatshefte fur Chemie, 1997. **128**: p. 1173-1180.
169. B. Prieur, et al., *Phosphorylation of lignin: characterization and investigation of the thermal decomposition.* RSC Advances, 2017. **7**: p. 16866-16877.
170. A. P. Legrand, et al., *(31)P solid-state NMR study of the chemical setting process of a dual-paste injectable brushite cements.* Journal of Biomedical Materials Research Part B: Applied Biomaterials, 2009. **91**(1): p. 46-54.
171. M. R. Hansen, et al., *Refinement of borate structures from 11B MAS NMR spectroscopy and density functional theory calculations of 11B electric field gradients.* The Journal of Physical Chemistry, 2005. **109**: p. 1989-1997.
172. Y. Yang, et al., *High mechanical strength in Zn4B6O13 with an unique sodalite-cage structure.* Royal Society of Chemistry, 2017. **7**(2038-2043).
173. X. Jiang, et al., *Near-Zero Thermal Expansion and High Ultraviolet Transparency in a Borate Crystal of Zn4B6O13.* Adv Mater, 2016. **28**(36): p. 7936-7940.
174. K. P. Nørgaard, et al., *Laboratory and gas-fired furnace performance tests of epoxy primers for intumescent coatings.* Progress in Organic Coatings, 2014. **77**(10): p. 1577-1584.
175. S. Bourbigot, et al., *PA-6 clay nanocomposite hybrid as char forming agent in intumescent formulations.* Fire and Materials, 2000. **24**: p. 201-208.
176. J. W. E. Weiss and D. L. Bryce, *A solid state 11B NMR and computation study of boron electric field gradient and chemical shift tensors in boronic acids and boronic esters.* Journal of Physical Chemistry A, 2010. **114**(15): p. 5119-5131.
177. S. V. Levchik, et al., *Mechanism of Action of phosphorus based flame retardants in Nylon 6. II Ammonium polyphospahte/Talc* journal of fire sciens, 1995. **13**: p. 43-58.
178. M. Casetta, et al., *Influence of the Recycling Process on the Fire-Retardant Properties of PP/EPR Blends.* Macromolecular Materials and Engineering, 2011. **296**(6): p. 494-505.
179. M. Villa and K. R. Carduner, *A 31P-NMR study of borophosphate glasses.* Journal of Solid State Chemistry 1987. **69**: p. 19-23.
180. K. Sasaki, et al., *Characteristic Sorption of H3BO3/B(OH)4- on Magnesium Oxide.* Materials Transactions, 2013. **54**(9): p. 1809-1817.
181. J. Brus, et al., *Efficient strategy of 2D 11B-11B solid-state NMR spectroscopy for monitoring covalent self-assembly of boronic acid-derived compounds: Transformation and unique architecture of bortezomib molecules in solid state.* Physical Chemistry Chemical Physics, 2016: p. 1-21.
182. G. Tricot, et al., *The D-HMQC MAS NMR technique: An efficient tool for the editing of through-space correlation spectra between quadrupolar and spin-1/2 (31P, 29Si, 1H, 13C) nuclei.* Annual Reports on NMR spectroscopy, 2014. **81**: p. 145-184.

183. L. Urbanczyk, et al., *Preparation of fire-resistant poly(styrene-co-acrylonitrile) foams using supercritical CO2 technology.* Journal of Materials Chemistry, 2010. **20**(8): p. 1567.
184. M. A. Fichera, et al., *Solid-state NMR investigations of the pyrolysis and thermo-oxidative decomposition products of a polystyrene/red phosphorus/magnesium hydroxide system.* Journal of Analytical and Applied Pyrolysis, 2007. **78**(2): p. 378-386.
185. K. P. Nørgaard, et al., *Engineering model for intumescent coating behavior in a pilot-scale gas-fired furnace.* American Institute of Chemical Engineers Journal, 2016. **62**(11): p. 3947-3962.
186. J. H. Ramos, et al., *Hydrothermal Synthesis and Characterization of Bio-Sourced Macroporous Zinc Phosphates Prepared with Casein Protein.* Crystal Growth & Design, 2016. **16**(9): p. 4897-4904.
187. M. L. Bras, et al., *Use of polyurethanes as cha-forming agents in polypropylene intumescent formulations* Polymer internatioal, 2000. **49**: p. 1115-1124.
188. *The engineering toolbox,* http://www.engineeringtoolbox.com/thermal-conductivity-d_429.html.
189. F. Samyn and S. Bourbigot, *Protection mechanism of a flame-retarded polyamide 6 nanocomposite.* Journal of Fire Sciences, 2014. **32**(3): p. 241-256.
190. A. Yoshihiro, *Kinetic studies on crystallization of calcium metaphosphate glass.* Journal of the Ceramic Society of Japan, 1973. **81**(11): p. 471-476.
191. Y. K. Jeng and B. K. Ryu, *Effect of CeO2 content on the crystalline growth and hydrophobic properties of borophosphate glass enamel.* Journal of the Ceramic Society of Japan, 2016. **124**(9): p. 920-925.
192. G. Ç. Gul and F. Kurtulus, *Rietveld refinement, optical and photoluminescence properties of blue emitting phosphors RE (Y, Er, Gd, La, Nd)-doped CaBPO 5.* Optik - International Journal for Light and Electron Optics, 2016. **127**(24): p. 11674-11680.
193. R. Kniep, et al., *Borophosphate - A neglected class of compounds: Crystal structure of Mii(BPO5) (Mii = Ca, Sr) and Ba3(BP3O12).* Angewandte Chemie International Edition in English, 1994. **33**(7): p. 749-751.
194. D. Zielniok, C. Cramer, and H. Eckert, *Structure-property correlations in ion-conducting mixed network former glasses- solid state NMR studies of the system Na2O-B2O3-P2O5.* Chemistry of Materials, 2007. **19**: p. 3162-3170.
195. G. Tricot, A. Saitoh, and H. Takebe, *Intermeditate length scale organisation in tin borophosphate glasses- new insights from high field correlation NMR.* Physical Chemistry Chemical Physics, 2015. **17**: p. 29531-29540.
196. N. H. Ray, *The structure and properties of inorganic polymeric phosphates*, in *Inorganic Source of Polymeric Materials Symposium*1979, The british polymer journal. p. 163-177.
197. R. J. B. Jakeman and A. K. Cheetham, *Combiend single crystal X-ray diffraction and magic angle spining NMR study of α-CaZn2(PO4)2.* Journal of the American Chemical Society, 1988. **110**: p. 1140-1143.
198. J. S. Knyrim, *Synthetic investigations into main group and transition metal borates at extreme conditions*, 2008, Ludwig-Maximilians-Universitat Munchen.
199. R. Kaindl, G. Sohr, and H. Huppertz, *Experimental determinations and quantum-chemical calculations of the vibrational spectra of B-ZnB4O7 and B-CaB4O7.* Spectrochimica Acta Part A: Molecular and Biomolecular Spectroscopy, 2013. **116**: p. 408-417.

200. N. Grassie and M. I. Guy, *Degradation of epoxy polymers: Part I - Products of thermal degradation of bisphenol A diglycidyl ether.* Polymer Degradation and Stability, 1985. **12**(1): p. 65-91.
201. H. Qu, et al., *The synergism of MgCO3 and 2ZnCO3.3ZnO.4H2O as flame retardants and smoke suppressants for flexible poly(vinyl chloride)PVC.* e-Polymers, 2011. **85**: p. 1-9.
202. M. Rigolo and R. T. Woodhams, *Basic magmesium carbonate flame retardants for polypropylene.* Polymer Engineering & Science, 1992. **32**: p. 327-334.
203. G. F. Levchik, S. V. Levchik, and A. I. Lesnikovich, *Mechanisms of action in flame retardant reinforced nylon 6.* Polymer Degradation and Stability, 1996. **54**: p. 361-363.
204. Y. T. Pan and D. Y. Wang, *One-step hydrothermal systhesis of nano zinc carbonate and its use as a promising substitute for antimony trioxide in flame retardant flexible poly(vinyl chloride).* The Royal Society of Chemistry 2015. **5**: p. 27837-27843.
205. J. W. Gilman, et al., *Fire retardant additives for polymeric materials - I. char formation from silica gel-potassium carbonate.* Fire and Materials, 1997. **21**: p. 23-32.
206. M. A. Hassan, et al., *Thermal analysis techniques as a primary sign for fire retardancy of new textile back-coating formulations.* Journal of Industrial Textiles, 2010. **39**(4): p. 357-376.
207. C. Jager and D. Ehrt, *Investigation of solid state reactions of binary polyphosphate - fluoride systems by means of thermal analysis, X-ray diffraction and NMR spectroscopy.* 1988. **159**: p. 103-112.
208. R. O. Omrani, et al., *Structural and thermochemical properties of sodium magnesium phosphate glasses.* Journal of Alloys and Compounds, 2015. **632**: p. 766-771.
209. L. Montagne, G. Palavit, and R. Delaval, *31P NMR in (100-x)(NaPO3)-xZnO glasses.* Journal of Non-Crystalline Solids, 1997. **215**: p. 1-10.
210. C. Jiao, J. Zhuo, and X. Chen, *Synergistic effects of zinc oxide in intumescent flame retardant silicone rubber composites* Plastics, Rubber and Composites 2013. **42**(9): p. 374-378.
211. N. Wu, c. Ding, and R. Yang, *Effects of zinc and nickel salts in intumescent flame-retardant polypropylene.* Polymer Degradation and Stability, 2010. **95**(12): p. 2589-2595.

Appendix

Appendix I: Compositions of IF(ZB)m, IF(borax)m, IF(APB)m and IF(ZB)wt intumescent coatings

Table 21 Compositions of IF(ZB)m

Description	Commercial name (supplier)	Part B (% w/w)	Part A (% w/w)
Aliphatic polyamide amine	Ancamide 903 MAV (Air Products)	17.03	
Calcium Carbonate or Dolomite	Micral 5 (Reverté)	1.85	
Based on amonium polyphosphate	Exolit AP 755 (Clariant)	2.13	8.26
Titanium dioxide, rutile	Tronox CR-826 (Huntsman)	0.36	
Natural, expanded silicate	Rotocell 0,5 mm (Rotec)	1.04	0.55
Composite reinforcement, Man-made vitreous (silicate) fibres	Rockforce MS603-Roxul1000 (Lapinus)	2.55	1.24
Composite reinforcement, Man-made vitreous (silicate) fibres	Rockforce MS605-Roxul1000 (Lapinus)	3.06	1.24
Bisphenol A diglycidylether epoxy	Epikote 828 (Momentive)		30.20
Tris(2-chloroisopropyl)phosphate (TCPP)	Fyrol PCF (ICL)		7.77
Carbon black	Lamp Black 101 (Orion engineered carbons)		0.06
Fumed silica	AEROSIL R 8200 (Evonik)		0.82
Zinc borate, flame retardant	***Firebrake ZB (20 Mule team)***		***21.83***
Total (% w/w)		**28.02**	**71.98**

Table 22 Compositions of IF(borax)m

Description	Commercial name (supplier)	Part B (% w/w)	Part A (% w/w)
Aliphatic polyamide amine	Ancamide 903 MAV (Air Products)	15.93	
Calcium Carbonate or Dolomite	Micral 5 (Reverté)	1.73	
Based on amonium polyphosphate	Exolit AP 755 (Clariant)	1.99	7.73
Titanium dioxide, rutile	Tronox CR-826 (Huntsman)	0.33	
Natural, expanded silicate	Rotocell 0,5 mm (Rotec)	0.97	0.52
Composite reinforcement, Man-made vitreous (silicate) fibres	Rockforce MS603-Roxul1000 (Lapinus)	2.39	1.16
Composite reinforcement, Man-made vitreous (silicate) fibres	Rockforce MS605-Roxul1000 (Lapinus)	2.86	1.16
Bisphenol A diglycidylether epoxy	Epikote 828 (Momentive)		28.25
Tris(2-chloroisopropyl)phosphate (TCPP)	Fyrol PCF (ICL)		7.27
Carbon black	Lamp Black 101 (Orion engineered carbons)		0.05
Fumed silica	AEROSIL R 8200 (Evonik)		0.77
Borax	***Borax***		***26.88***
Total (% w/w)		**26.21**	**73.79**

Table 23 Compositions of IF(APB)m

Description	Commercial name (supplier)	Part B (% w/w)	Part A (% w/w)
Aliphatic polyamide amine	Ancamide 903 MAV (Air Products)	18.01	
Calcium Carbonate or Dolomite	Micral 5 (Reverté)	1.95	
Based on amonium polyphosphate	Exolit AP 755 (Clariant)	2.25	8.74
Titanium dioxide, rutile	Tronox CR-826 (Huntsman)	0.38	
Natural, expanded silicate	Rotocell 0,5 mm (Rotec)	1.10	0.58
Composite reinforcement, Man-made vitreous (silicate) fibres	Rockforce MS603-Roxul1000 (Lapinus)	2.70	1.31
Composite reinforcement, Man-made vitreous (silicate) fibres	Rockforce MS605-Roxul1000 (Lapinus)	3.23	1.31
Bisphenol A diglycidylether epoxy	Epikote 828 (Momentive)		31.94
Tris(2-chloroisopropyl)phosphate (TCPP)	Fyrol PCF (ICL)		8.22
Carbon black	Lamp Black 101 (Orion engineered carbons)		0.06
Fumed silica	AEROSIL R 8200 (Evonik)		0.87
Ammonium pentaborate	***Riedel doha***		***17.34***
Total (% w/w)		**29.63**	**70.37**

Table 24 Compositions of IF(ZB)wt

Description	Commercial name and supplier	Part B (% w/w)	Part A (% w/w)
Aliphatic polyamide amine	Ancamide 903 MAV (Air Products)	17.59	
Calcium Carbonate or Dolomite	Micral 5 (Reverté)	1.91	
Based on amonium polyphosphate	Exolit AP 755 (Clariant)	2.20	8.54
Titanium dioxide, rutile	Tronox CR-826 (Huntsman)	0.37	
Natural, expanded silicate	Rotocell 0,5 mm (Rotec)	1.07	0.57
Composite reinforcement, Man-made vitreous (silicate) fibres	Rockforce MS603-Roxul1000 (Lapinus)	2.64	1.28
Composite reinforcement, Man-made vitreous (silicate) fibres	Rockforce MS605-Roxul1000 (Lapinus)	3.16	1.28
Bisphenol A diglycidylether epoxy	Epikote 828 (Momentive)		31.20
Tris(2-chloroisopropyl)phosphate (TCPP)	Fyrol PCF (ICL)		8.03
Carbon black	Lamp Black 101 (Orion engineered carbons)		0.06
Fumed silica	AEROSIL R 8200 (Evonik)		0.85
Zinc borate, flame retardant	***Firebrake ZB (20 Mule team)***		***19.25***
Total (% w/w)		**28.94**	**71.06**

Appendix II: Compositions of IFZnO, IFZnS and IFZnSO$_4$ intumescent coatings

Table 25 Compositions of IFZnO

Description	Commercial name (supplier)	Part B (% w/w)	Part A (% w/w)
Aliphatic polyamide amine	Ancamide 903 MAV (Air Products)	9.30	
2.4.6-tris(dimethylaminomethyl)phenol	Acamine K54 (Air Products)	1.84	
Melamine	Melafine (OCI Nitrogen)	16.27	
Titanium dioxide, rutile	Tronox CR-826 (Huntsman)	4.44	2.09
Modified derivative of castor oil	Thixatrol ST (Elementis Specialties)	0.28	0.63
Composite reinforcement, Man-made vitreous (silicate) fibres	Rockforce MS605-Roxul1000 (Lapinus)	2.50	10.28
Bisphenol A diglycidylether epoxy	Epikote 828 (Momentive)		21.79
Tris(2-chloroisopropyl)phosphate (TCPP)	Fyrol PCF (ICL)		6.69
Amonium polyphosphate	Exolit AP 422 ex Clariant		19.70
ZnO	***Sigma Aldrich***		***2.34***
Calcium Carbonate or Dolomite	Micral 5 (Reverté)		1.79
Carbon black	Lamp Black 101 (Orion engineered carbons)		0.05
Total (% w/w)		**34.64**	**65.36**

Table 26 Compositions of IFZnS

Description	Commercial name (supplier)	Part B (% w/w)	Part A (% w/w)
Aliphatic polyamide amine	Ancamide 903 MAV (Air Products)	9.26	
2.4.6-tris(dimethylaminomethyl)phenol	Acamine K54 (Air Products)	1.83	
Melamine	Melafine (OCI Nitrogen)	16.20	
Titanium dioxide, rutile	Tronox CR-826 (Huntsman)	4.42	2.08
Modified derivative of castor oil	Thixatrol ST (Elementis Specialties)	0.28	0.63
Composite reinforcement, Man-made vitreous (silicate) fibres	Rockforce MS605-Roxul1000 (Lapinus)	2.49	10.23
Bisphenol A diglycidylether epoxy	Epikote 828 (Momentive)		21.69
Tris(2-chloroisopropyl)phosphate (TCPP)	Fyrol PCF (ICL)		6.66
Amonium polyphosphate	Exolit AP 422 ex Clariant		19.61
ZnS	***Sigma Aldrich***		***2.79***
Calcium Carbonate or Dolomite	Micral 5 (Reverté)		1.78
Carbon black	Lamp Black 101 (Orion engineered carbons)		0.05
Total (% w/w)		**34.48**	**65.52**

Table 27 Compositions of IFZnSO$_4$

Description	Commercial name (supplier)	Part B (% w/w)	Part A (% w/w)
Aliphatic polyamide amine	Ancamide 903 MAV (Air Products)	8.78	
2.4.6-tris(dimethylaminomethyl)phenol	Acamine K54 (Air Products)	1.74	
Melamine	Melafine (OCI Nitrogen)	15.36	
Titanium dioxide, rutile	Tronox CR-826 (Huntsman)	4.19	1.97
Modified derivative of castor oil	Thixatrol ST (Elementis Specialties)	0.26	0.60
Composite reinforcement, Man-made vitreous (silicate) fibres	Rockforce MS605-Roxul1000 (Lapinus)	2.36	9.70
Bisphenol A diglycidylether epoxy	Epikote 828 (Momentive)		20.57
Tris(2-chloroisopropyl)phosphate (TCPP)	Fyrol PCF (ICL)		6.32
Amonium polyphosphate	Exolit AP 422 ex Clariant		18.60
ZnSO$_4$.7H$_2$O	***Normapor***		***7.80***
Calcium Carbonate or Dolomite	Micral 5 (Reverté)		1.69
Carbon black	Lamp Black 101 (Orion engineered carbons)		0.05
Total (% w/w)		**32.70**	**67.30**

Appendix III: Potential interactions between $CaCO_3$ and BA

Figure 83 shows the experimental, calculated and difference weight loss curves of BA/$CaCO_3$. The mixture ratio of BA and $CaCO_3$ is 91/9 % w/w, which is respected to that present in IF(BA) formulation. The difference weight loss gives an evidence on the interactions between the additives (the details were described in chapter II).

The stabilization and destabilization are a bit remarkable in two points: i) between 100 °C and 200 °C and ii) after 700 °C. It was found that the difference weight loss is between 0 and -2. The difference weight loss approaches zero (non-significant value) pointing out the absence of reaction between the two additives. It can be concluded that there is no reaction between BA and $CaCO_3$ up to 800 °C.

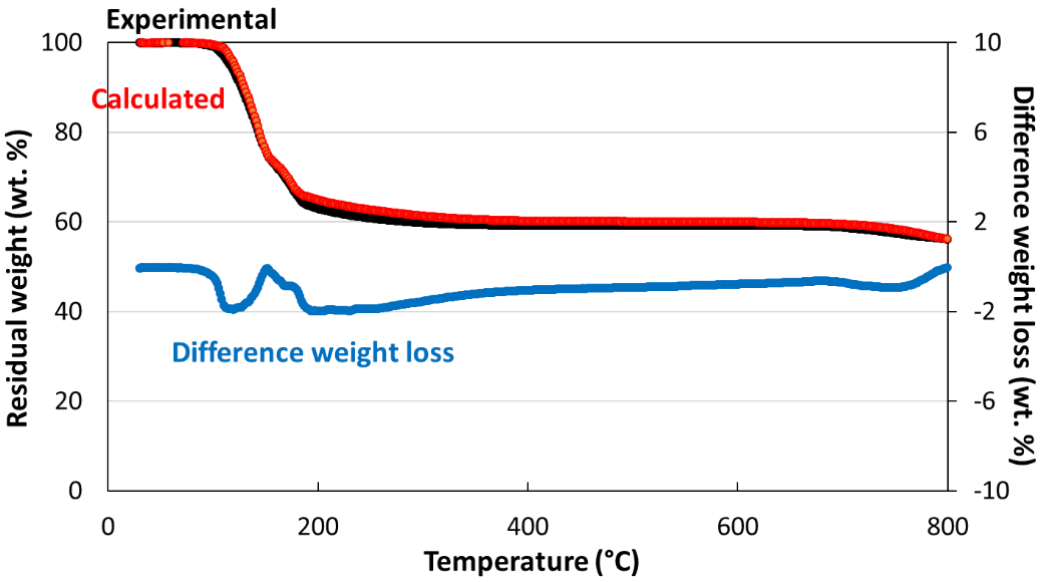

Figure 83 Experimental, calculated residual weight and difference weight loss of BA/$CaCO_3$ (91/9 % w/w)

Appendix IV: Complex viscosity and expansion of IF-APPZB and IF-APPZBCa

The complex viscosity, relative expansion and TG curve of IF - APPZB and IF - APPZBCa are shown in Figure 84. The modifications of viscosity in the temperature range 100 ^{o}C - 500 ^{o}C are almost superimposed. It confirms the previous observation (in 4.1.2.2) that the addition of low amount of $CaCO_3$ (3.45 wt. %) into the reference formulations (APP + borate) does not change their viscosity during melting (up to 500 ^{o}C). The viscosity is steady from the beginning of the measurement up to about 300 ^{o}C. This phenomenon is well consistent with TG curves of the samples. TG curves indicate that these formulations do not decompose up to 300 ^{o}C. Between 300 ^{o}C and 340 ^{o}C, the viscosity increases a bit (1 - 3 x 10^5 Pa.s). It then increases sharply up to 500 ^{o}C. High viscosity value and no drop of viscosity (even if in the critical point) are particular phenomena observed only for the formulations containing zinc borate. It was stated [91] that, at high temperature, a material degrades evolving gases, it causes the material to swell. A high melt viscosity is required since it can trap the evolved products reducing the volatiles transported through the material. However, a too high viscosity could reduce the ability of the material to swell. This can be explained the reason why these two formulations did not expand in the furnace test and it highlights the significant effect of boric acid and zinc borate on the viscosity of the intumescent matrix during burning.

For the expansion, IF-APPZB and IF-APPZBCa have no expansion from the beginning up to about 350 ^{o}C. It is noticeable that the expansion starts at higher temperature than the beginning of the decomposition (350 ^{o}C vs. 300 ^{o}C) and they reach the maximum values of 35 and 87 relative % of expansion. It shows the same tendency to the formulations containing boric acid, the addition of $CaCO_3$ into IF-APPZB has no significant modification of expansion.

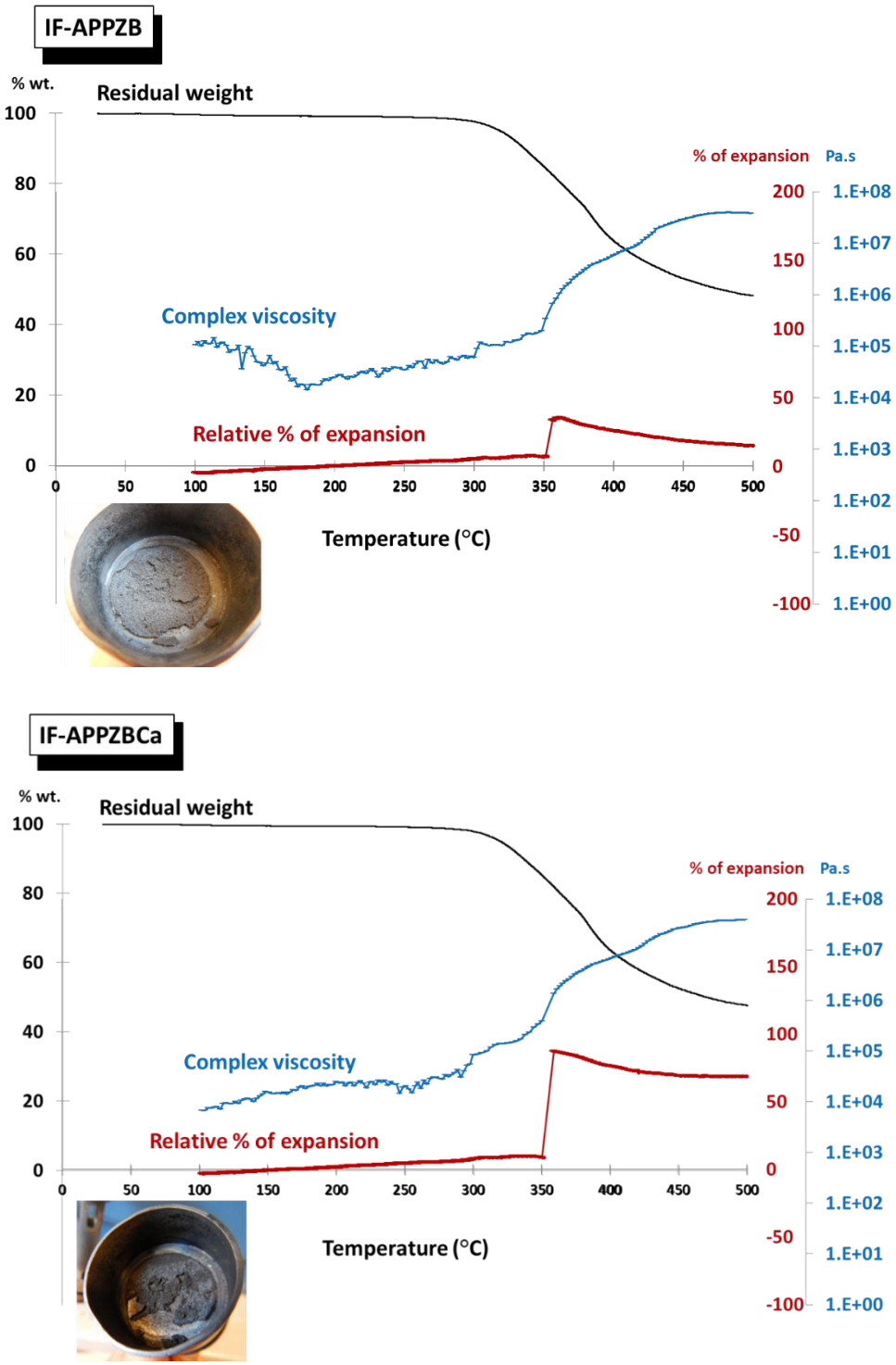

Figure 84 Complex viscosity, relative expansion and TG curves of IF-APPZB and IF-APPZBCa

Appendix V: Publication

Getting a better insight into the chemistry of decomposition of complex flame retarded formulations: Highlights of using solid state NMR

N. Hansupo,[a] G. Tricot,[b] S. Bellayer,[a] F. Samyn,[a] S. Duquesne,[a] M. Jimenez,[a] M. Hollman,[c] P. Catala,[c] S. Bourbigot[a*]

[a] Univ. Lille, ENSCL, UMR 8207, UMET, Unité Matériaux et Transformation, F59652 Lille, France

[b] LASIR UMR-CNRS 8516, Université de Lille, Sciences and Technologies, F59655 Villeneuve d'Ascq, France

[c] Hempel, S.A.U. Carretera de Sentmenat 108, E-08213 Polinya, Barcelona, Spain

*Corresponding author: S. Bourbigot
Tel: +33 3 20 43 48 88, E-mail address: serge.bourbigot@ensc-lille.fr

Abstract

The aim of this study is to characterize the char residue of an intumescent coating obtained after a UL1709 furnace test. The formulation deals with an epoxy based intumescent coating containing numerous additives and among them are zinc borate, ammonium polyphosphate and silicate fibers. In this case, numerous reaction products are formed upon burning. The study was carried out using various characterization methods including Electron Probe Micro-Analysis (EPMA), X-ray diffraction (XRD) and solid-state Nuclear Magnetic Resonance (NMR). It particularly highlights the potential of the recent developed NMR technique called two-dimensional Dipolar Heteronuclear Multiple Quantum Correlation (2D D-HMQC) NMR. As a result, EPMA evidenced that B/P and B/Si are located in the same region suggesting the formation of boron-phosphorus and/or boron-silicone containing compounds on the sample surface. On the XRD pattern, H_3BO_3, B_2O_3 and TiO_2 can be identified as crystalline species. The chemical species containing boron, silicone and phosphorous were then characterized using 1D NMR but definitive assignments could be not given. To specify the latter species, 2D D-HMQC NMR was performed and it evidenced the formation of amorphous borophosphates and borosilicate. These species allow reinforcing the char and improving fire protective properties of the coatings. This cross characterization provides clear information on the chemical reactivity between the intumescent additives. The work highlights the particular interest of the advanced NMR technique, which is the promising characterization tool and the technique of choice for intumescent char analyses.

Keywords: solid state NMR, characterization, intumescent char residue, amorphous borosilicate and borophosphate species